Head Office: Università degli Studi di Padova

Department of Chemical Sciences

Ph.D. COURSE IN: MOLECULAR SCIENCES
CURRICULUM: CHEMICAL SCIENCES
SERIES 35° CYCLE

NOVEL APPROACHES TO SELECTIVE CATALYTIC SYSTEMS FOR THE DIRECT SYNTHESIS OF HYDROGEN PEROXIDE

Thesis written with the financial contribution of Università degli Studi di Padova

Coordinator: Prof. Leonard Prins
Supervisor: Prof. Paolo Centomo

Ph.D. student : Francesco Sandri

Index

Chapter 1: Analysis of hydrogen peroxide in methanol solutions

Chapter 2: Starting point of the project and preliminary investigation

Chapter 3: Coordinating solvents as selectivity enhancers: preliminary investigations with acetonitrile

Chapter 4: Effect of acetonitrile on zeolite supported palladium catalysts

Chapter 5: Coordinating solvents as selectivity enhancers: beyond acetonitrile

Chapter 6: Correlation between amount of co-solvent and promotion effect

Chapter 7: Investigation with the Trickle Bed Reactor

ABSTRACT OF THE THESIS

This Thesis is focused on the investigation of supported palladium catalysts for the direct synthesis of hydrogen peroxide, with particular attention to a novel material based on a mesoporous ion-exchange resin as the support. The main topic of this Thesis is the investigation of coordinating solvents, mainly acetonitrile and N,N-dimethylformamide, as novel corrosion-free promoters, to replace halides, commonly exploited as selectivity enhancers but leading to corrosion issues. The addition of coordinating solvents to the reaction mixture, i.e. methanol, remarkably increases not only the selectivity but also the production of hydrogen peroxide. This effect can be obtained only for catalysts supported on ion-exchange materials, suggesting that the key of the promotion effect is in the formation of Pd(II) complexes and their subsequent interaction with the support. This phenomenon is described in details and defined by using a semi-batch reactor working under very mild condition. Finally, preliminary investigations have been performed to make possible the exploitation of the most promising catalysts in an experimental setup suitable for the industrial application, such as a continuous flow reactor.

RIASSUNTO DELLA TESI

In questa Tesi sono stati studiati catalizzatori di palladio supportati per la sintesi diretta del perossido di idrogeno, con particolare attenzione ad un supporto catalitico innovativo, basato su una resina a scambio ionico mesoporoso. Il principale oggetto di ricerca di questa Tesi è lo studio di solventi coordinanti, soprattutto acetonitrile e N,N-dimetilformammide, usati come promotori innovativi, per sostituire gli alogenuri. Questi ultimi, infatti, sono tipicamente usati come promotori della selettività, ma causano però anche problemi di corrosione. L’aggiunta di solventi coordinanti alla miscela di reazione, composta da metanolo puro, aumenta non solo la selettività, ma anche la produzione di perossido di idrogeno. Poiché questa reattività può essere ottenuta solo per catalizzatori supportati su materiali in grado di dare scambio ionico, la chiave dell’effetto promotore è probabilmente la formazione di complessi di Pd(II) e la loro successiva interazione con il supporto catalitico. Questo fenomeno è stato descritto in dettaglio e definito utilizzando un reattore semi-batch operante in condizioni molto blande. Infine, è stato svolto uno studio preliminare per rendere possibile l’impiego del catalizzatore più promettente in un reattore a flusso continuo, che risulta particolarmente interessante nell’ottica di un impiego tecnologico.

Part 1

INTRODUCTION

1.1 Introduction to hydrogen peroxide

Hydrogen peroxide (HP) is an almost colourless liquid, with a pale blue colour, completely miscible in water. Some of its physical properties are similar to those of water, due to the formation of hydrogen bonds, such as the melting point (-0.43° C) and the boiling point (150.2° C). In particular, the higher melting point when compared to water is due to the formation of stronger hydrogen bonds. The presence of the lone pairs on the oxygen atoms makes the dihedral angle between the H–O–O bonds dependent on the extent of the hydrogen bonding and therefore on the aggregation state, being maximal in the gas phase (111°) and minimal in the solid state (90°). It can be ionized by deprotonation of the O–H bond, to form $[HO_2]^-$ and $[H_3O]^+$ in water solutions (pK_a=12.38 at 298 K). It can be obtained with a 100% purity by fractional crystallization from a water solution, although it has no practical applications. It is an unstable compound, as it decomposes with the following equation:

$$H_2O_2(l) \rightarrow H_2O_{(l)} + O_2(g)$$

This reaction is enhanced in the presence of solubilized ions of transition metals (mainly Fe, Cu, Mn or Cr) or their oxides and hydroxides and therefore commercial solutions are stabilized with complexing agents. The decomposition reaction in the presence of cations of transition metals involves the formation of hydroxyl radicals, that are very reactive species, and this reaction is known since long time ago as the Fenton process.[1] Moreover, an alkaline pH promotes the decomposition reaction, as well as some metal catalyst such as platinum or silver. Noticeably, HP is a strong oxidant, not only at low pH like the most common oxidants, but also under alkaline conditions, according to the following semi-reactions:

$$H_2O_2 + 2H^+ + 2e^- \rightarrow 2H_2O \quad \text{at pH=0 (2)}$$

$$H_2O_2 + 2e^- \rightarrow 2OH^- \quad \text{at pH=14 (3)}$$

The standard potentials of reactions (2) and (3) are $E^0=+1.76$ V and $E^0=+0.87$ V, respectively. Hydrogen peroxide can also behave as reductant (reactions 4 and 5):

$$O_2 + 2H^+ + 2e^- \rightarrow H_2O_2 \quad \text{at pH=0 (4)}$$

$$O_2 + 2H_2O + 2e^- \rightarrow H_2O_2 + 2OH^- \quad \text{at pH=14 (5)}$$

In this case, the standard potential are $E^0=-0.66$ V and $E^0=+0.08$ V, for reaction (4) and (5), respectively. Moreover, hydrogen peroxide can give substitution reactions with alkyl or acyl functionalities, to form mainly hydroperoxides (R–O–O–H), peroxides (R–O–O–R) or percarboxylic acids (R–(C=O)–O–O–H). Thanks to the large variety of reactions it can give, hydrogen peroxide is largely employed in several industrial fields. The general overview on HP given on this Paragraph is according to references.[2,3]

1.2 Applications of hydrogen peroxide

The most important features of hydrogen peroxide are its high redox potential and the formation of water as the reduction by-product. Moreover, the content of active oxygen is very high, second only to dioxygen.[4] This makes HP a strong and green oxidant and therefore its exploitation increased continuously over years, as well as its production. According to literature the steadily increasing annual HP production is shown in Table 1.

Table 1: annual production of hydrogen peroxide over years.

Year	**Annual production**	**Reference**
mid-1990s	1.5 Mt/a	Ciriminna et al.[5]
2006	2.2 Mt/a	Hage et al.[6]
2015	3 Mt/y	Ciriminna et al.[5]
2018	6.5 Mt/y	Gao et al.[7]

The most relevant employment involves HP as bleaching agent, mainly for cellulose pulp and paper, to remove lignin and coloured compounds such as ink in the recycled paper. This reaction is carried out under alkali conditions to form HOO^- as the reactive species. In recent years its consumption in this field has consistently risen, mainly to replace chlorine based oxidants.[4,8–10] The bleaching properties of HP are also exploited in the whitening of textiles, in substitution of sodium hypochlorite. Hydrogen peroxide replaced this chemical also in the formulation of laundry bleaches: to this regard, it can be directly added to the detergent, in the case of liquid formulations, or used to produce components of powder formulations, such as sodium perborate or percarbonate, releasing HP under washing conditions. This bleaching system is particularly efficient as it preserves the colours of the clothes when compared to the hypochlorite. Hydrogen peroxide can be efficiently used for environmental applications such as purification of municipal or industrial wastewater, especially in the abatement of cianide anion.[11,12] The mining sector involves HP in the extraction, separation, etching and passivation of a large number of metals,[13,14] while dealing with semiconductors, HP is used to clean and remove impurities from germanium and silicon. This chemical can be employed as disinfectant[15,16] and in concentration above 90% is used as rocket propellent, in combination with hydrazine or with metal catalyst to produce dioxygen.[2,3]

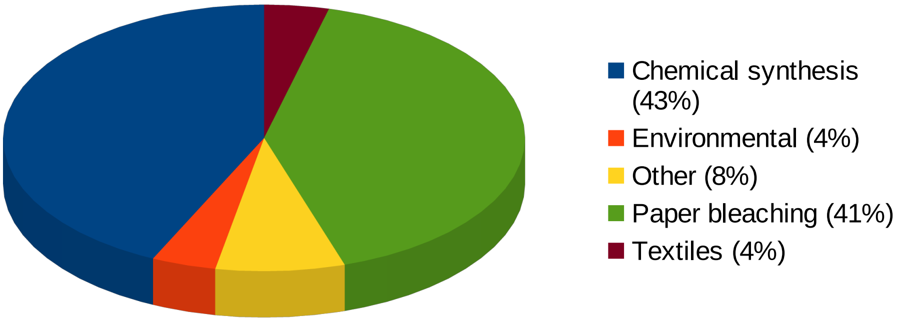

Figure 1: hydrogen peroxide consumption in Europe, according to the reference.[4]

However, the highest demand of HP comes from the chemical synthesis (Figure 1), as the consequence of the discovery of the activation over TS-1 or other titanosilicalites of hydrogen peroxide in plenty of oxidation reactions. The most exploited reactions, catalysed by TS-1, are the epoxidations of olefins,[17,18] mainly propylene to obtain propylene oxide (PO).[19–21] In 2008 the first plant for the production of PO from HP (namely HPPO process) was built, defining a turning point in the industrial exploitation of HP.[5] Again, the HPPO process aims to replace chlorine-based processes, more expensive both in terms of capital and energetic costs and with a higher production of wastewater.[22] Another important topic is the production of adipic acid via oxidation of cyclohexene in substitution of nitric acid, thus avoiding the release of noxious nitric oxides. The reaction is catalysed by Na_2WO_4 and leads initially to the formation of an epoxide, hence the oxidation is performed by opening the ring with the formation of two carboxylic functions.[23] Further employments in chemical synthesis are the reaction of cyclohexanone in the presence of ammonia, to produce cyclohexanone oxime that rearranges to ε-lactam, to be subsequently polymerized to Nylon-6.[24,25] TS-1 is involved in the catalytic hydroxilations of aromatic rings with HP, with a particular interest in the synthesis of phenol from benzene.[26,27] Furthermore, HP can oxidize alkanes to produce alcohols and ketones,[28,29] therefore achieving the functionalization of organic compounds with no reactive groups, without using harsh reaction conditions. Finally, hydrogen peroxide is used in addition reactions (Paragraph 1.1) to produce percarboxylic acids and other organic and inorganic peroxides.[4] The increases of HP production as well as the green nature of this oxidizing agent are boosting the development of novel technologies in innovative fields. A few examples are the removal of pesticides and other pollutants with HP combined with a hydrodynamic cavitation and a Fenton-like system with iron salts.[30] The formation of highly reactive radical species can be promoted with UV light and turns out to be very effective in the disinfection from bacteria resistant to the sole UV radiation.[31,32] Recently hydrogen peroxide is gradually replacing other chemicals, mainly chlorine based oxidants, due to the lower environmental impact combined to better performance. However, the exploitation of HP is strongly connected to its availability, that depends on the production process. In Paragraphs 1.3-1.4 are presented the obsolete and current production processes, which is by far the most important source of HP. Finally, the limitations of this process as well as the needs for the development of possible alternatives are also discussed.

1.3 Production of hydrogen peroxide: an historical overview

Depending on the industrial process, the production of HP can be divided in three phases.[3] The first synthetic procedure to obtain HP was patented in 1818 by Thenard, who reported the production of a water solution of HP by treating barium peroxide with a nitric acid solution. On these bases, the first industrial processes was developed, by treating barium peroxide with acids (H_2SO_4 or HCl) to produce HP and barium sulfate. In the case of HCl, sulfuric acid was later added to the solution, to precipitate barium cations. The process allows the production of a 3% HP solution and was employed until 1920, but it was suddenly replaced by a novel process since it is economically disadvantageous due to the side-production of $BaSO_4$.[3] The second phase came therefore with the production of HP by electrolysis of sulfuric acid or ammonium sulfate solution, that completely replaced the production from barium peroxide. Peroxosulfuric acid is produced in the reaction and is subsequently hydrolysed to sulfuric acid and hydrogen peroxide.

$$2H_2SO_4 \rightarrow H_2S_2O_8 + H_2$$
$$H_2S_2O_8 + H_2O \rightarrow H_2SO_5 + H_2SO_4$$
$$H_2SO_5 \rightarrow H_2SO_4 + H_2O_2$$

Thanks to this process the worldwide HP production increased from $2 \cdot 10^3$ t/y to $30\text{-}35 \cdot 10^3$ t/y.[3] However, the biggest breakthrough in the industrial production came with the development of the auto-oxidation (AO) reactions of some organic compounds, such as hydroquinones, to produce the related anthraquinone and hydrogen peroxide. The following reduction of the quinone, typically a catalytic hydrogenation with dihydrogen, allows to restore the starting compound, that can be further oxidized (Figure 2).

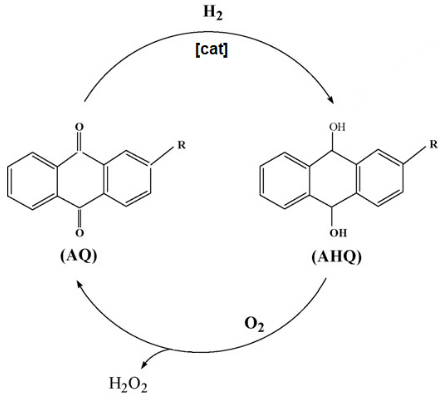

Figure 2: production route of HP by AO of quinones.

This forms a cycle of oxidation and reduction reactions, mediated by an organic compound, that makes possible to obtain HP from hydrogen and oxygen in a very efficient way without a direct contact of the gases. In the 50s a similar process was developed by Shell (Figure 3), with 2-propanol as the organic substrate that was involved to form a hydroperoxide, but the efficiency of the process was much more limited when compared to quinones.

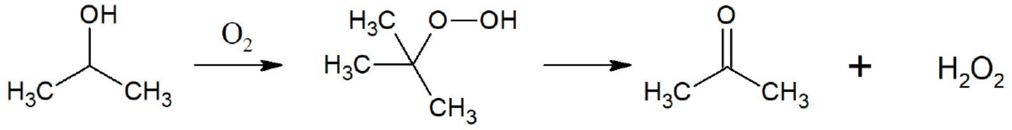

Figure 3: production route of HP by oxidation of 2-propanol.

Therefore, the production of HP by AO reaction of quinones, in particular anthraquinone and its derivates (Figure 2), almost completely replaced any other industrial process and is nowadays the source of more than 95% of the worldwide production of this chemical.[33]

1.4 The anthraquinone auto-oxidation process

As mentioned before, the anthraquinone AO process, namely Riedl-Pfleiderer process, replaced any other HP production route due to its very high efficiency. This process was designed in 40s but its core remained unchanged over years and can be divided in fours steps (Figure 4).

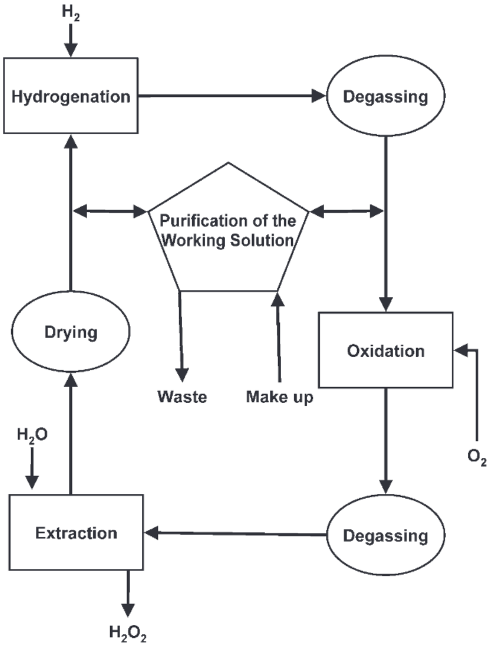

Figure 4: scheme of the Riedl-Pfleiderer process.[4]

In the first step an organic solution of an anthraquinone derivative is catalytically reduced with hydrogen in the presence of a heterogeneous catalyst to produce the corresponding hydroanthraquinone. The catalyst originally involved was Raney nickel, but more recently are used palladium catalysts supported on inorganic supports, such as alumina, silica or other aluminosilicates. Moreover, lanthanides or boron can be used as dopants to increase the performance of the material.[4,34] The reaction conditions are typically mild (T=30-45° C, p= 2-4 atm), in order to keep the conversion as low as possible, to avoid the formation of by-products from the hydrogenation of anthraquinone.[4] This is one of the main issues related to the AO process, as the consumption of the anthraquinone needs a regeneration by purification of by-products and reintegration of the quinone. Moreover, the purification procedure is done by physisorption over activated alumina and generates great amount of solid wastes.[7] Particular attention should be given to the reactor technology, as it is very important to remove the catalyst from the reaction mixture since metal contaminations in the final product decompose HP into water and oxygen. Therefore, past technologies were based on slurry reactors and filtration systems to completely remove the catalyst, whereas a more recent approach involves a fixed-bed catalyst, avoiding the filtration procedures.[35] The working solution containing the diol is treated with air under condition of temperature and pressure similar to those of the hydrogenation step, to oxidize the hydroquinone and produce HP in concentration in the range of 1-2 % w/w. No catalysts are needed in the oxidation step. The final product is extracted with water, purified and distilled with steam to obtain an HP concentration up to 70%: such a high concentration is required mainly as it is suitable for shipping the product, although most of the applications need lower concentrations.[5] The working solution, upon purification from water and by-product, can be reused in the hydrogenation plant.

1.4.1 Needs for an alternative to the AO process and possible options

The Riedl-Pfleiderer process has been very well optimized over time and is particularly advantageous and safe, since the direct contact of the reaction gases is avoided. However, there are several concerns about the formation of hydrogenation products that are contaminating the reaction mixture and several purification steps of the working solution and the final product are needed. These issues are increasing the cost of the process as the consequence of the high energy consumption and therefore, together with the high capital costs of the plant, making this process sustainable only on large scale production.[4,7,14] Taking also into the account the hazard related to the shipping of concentrated HP solutions, this oxidant is generally produced in the vicinity of industries with a high demand of HP, such as paper mill or HPPO facilities. The exploitation of hydrogen peroxide is limited in medium and small industries, where other highly polluting oxidants are still used, as a delocalized production of HP is needed. The development of a technology that allows the in-situ production of an HP solution in a sustainable way could be coupled with plenty of industrial processes. This would likely almost completely replace the use of chlorine based compounds leading to a switch towards a more “green” and environment friendly approach to the industrial oxidation processes. For example, only taking into the account the production of propylene oxide, which is partially produced by the HPPO process, a complete substitution of the current production route with that involving HP would represent a remarkable improvement. In fact, the HPPO process produces 75% less wastewater with also a reduction of 35% of the energetic consumption.[22] Similar improvements can be also obtained in several other processes, by replacing polluting and “less green” chemicals with hydrogen peroxide. Moreover, an alternative way to produce HP would further boost the development of novel technologies, exploiting this chemical in novel fields.[5] As this issue has been taken into account since a long time, several alternative methods for the production of HP were proposed over years. However, some of these suffer from serious issues related to the scale up, such as the synthesis from plasma, the production mediated by enzymes or the photocatalysis with semi-conductors. Among these, the plasma approach is the most investigated and looks one of the most promising. This method involves the production of radicals from a dielectric discharge that take place in a H_2/O_2 gas mixture and the consequent formation of a plasma generates radicals, which eventually evolve to hydrogen peroxide. Nevertheless, the employment of this process on relatively large scale is still hindered by safety issues and the high energy demand.[15] A more promising approach in the production of HP consist in the electrochemical reduction of oxygen with homogeneous metal complexes or metal complexes supported on electrodes acting as the catalyst.[36] This approach allows to avoid the use of organic solvent to produce HP water solutions and its exploitation became more advisable with the development of metal free electrodes.[37,38] However, this approach for the production of hydrogen peroxide requires a supply of electric energy which is not sustainable by now, but looks very promising for the future, when this process can be coupled with a photovoltaic system.[5] Nowadays the best choice as an alternative to the AO process is the direct synthesis of HP from H_2 and O_2, representing the topic of this project.

1.5 The direct synthesis of hydrogen peroxide

1.5.1 First steps towards the direct synthesis of hydrogen peroxide

The direct synthesis (DS) of hydrogen peroxide, namely the reaction between hydrogen and oxygen to form hydrogen peroxide, is catalysed by transition metals and was patented in 1914, long time before many others production routes, by Henkel and Weber.[39] As several efficient production processes were developed, the DS was set aside for long time, until an alternative to the AO process was needed. In particular, this occurred during the 60s, when the cost of HP from the AO process was still high enough to make this chemical sustainable. As a consequence, several patents were filed, using metals of the tenth group as the catalyst, the bases of the DS research. One of the first patents reports on the production of HP from the elements in an alkali aqueous media containing borate, to produce HP, that eventually is converted *in-situ* in perborate anions.[40] Since the first investigations, it was clear that HP should be stabilizes and accordingly mineral acids and chelating agents, to lower the pH, and scavenging metal ions, respectively, were added to the solution.[41] Further investigations showed that a remarkable promotion effect for the DS can be obtained with the addition of hydrobromic acid or halides, [42,43] or by using palladium catalyst alloyed with further noble metals such as platinum.[44] Many efforts were spent in the choice of the catalyst support: whereas the first patent involves porous clay impregnated with palladium,[39] several inorganic supports were also employed. Moreover, activated carbon was also proposed and showed the best performances in the DS, specially after a suitable fluorination treatment, aimed to increase its hydrophobicity.[43] Particularly relevant for this Thesis is the patent by Kim and Schoenthal (Shell company),[45] reporting for the first time the exploitation of ion exchange palladium catalysts as well as the addition of organic nitrogen containing compound as promoters for the DS reaction.

This reaction obtained further interest in the 90s due to the aforementioned findings on TS-1 and other titanium silicalites as the catalyst for oxidation with HP. In fact, several investigations were published, aiming to couple the DS with the epoxidation of olefins with the *in-situ* HP produced by DS.[46–48] Thanks to these investigations, the DS gained more and more importance within the scientific community and became deeply investigated as a possible alternative to the AO process. At this point, the fundamental parameters affecting the performances of the catalyst in the DS were already unravelled. The metal of choice for the DS is palladium, that gives better HP production than other transition metals[49] and the performances of which can be improved in the alloyed form. Further important features of the catalytic system are the nature of the support and the composition of the liquid phase, in terms of both the solvent and promoters (such as acids, halides or HP stabilizers). Several additional parameters influencing the DS were pointed out by further investigations and will be discussed later on. However, the two main issues related on the DS are the safety precautions due to the explosiveness of H_2/O_2 gas mixtures in a wide range of molar ratios and the selectivity of the reaction.[12] Being water the thermodynamic product of the reaction (Figure 5), the issue of the selectivity is the main concern making this reaction uncompetitive with respect the Riedl-Pfleiderer process.

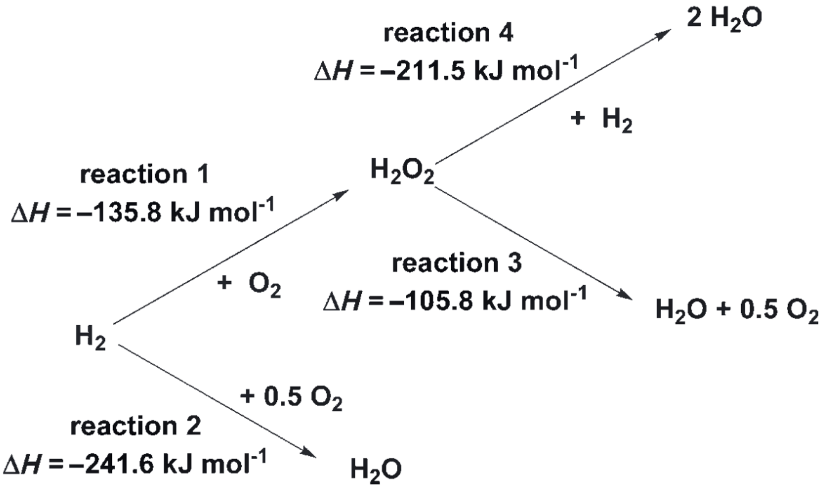

Figure 5: reaction scheme of the DS.[4]

1.5.2 The mechanism of formation of hydrogen peroxide in the direct synthesis reaction

Hydrogen and oxygen can give several reactions, leading to different products (Figure 5). On the one hand, the DS of hydrogen peroxide is the desired reaction. On the other hand, there are further hydrogenation reactions, such as the direct synthesis of water and the hydrogenation of HP, leading to water and wasting hydrogen, the most expensive reagent. All the possible reactions involved in the DS are thermodynamically favoured ($\Delta G^0 < 0$), with the formation of water being the most favoured ($\Delta G^0 = -354.3$ kJ/mol), when compared to the formation of HP ($\Delta G^0 = -120.4$ kJ/mol). Moreover, the dismutation of HP to form water and oxygen is also a parasite reaction consuming the produced HP ($\Delta G^0 = -105.8$ kJ/mol). This whole system turns out to be extremely complex and challenging, from both the technological and scientific point of view. For the practical exploitation of this process, which is still not implemented nowadays, high selectivity and high productivity must be achieved, in order to obtain a high production of HP with no waste of hydrogen. Although not yet fully rationalized, the reaction mechanism is of utmost importance in understanding the DS and for the design of a catalyst. Early studies using mixtures of $^{18}O_2$ and $^{16}O_2$ shown that the O–O bond must remain uncleaved to obtain HP, and the dissociation of dioxygen eventually leads to the formation of water.[50] Nevertheless, the mechanism of oxygen reduction is still not clarified and is assumed to depend on the solvent and the presence of promoters.[51] The first mechanism proposed involves a Langmuir-Hinshelwood model, in which the O_2 is absorbed in a non dissociative way, whereas hydrogen dissociates to form hydrogen atoms, by reacting with the adjacent oxygen atom to form absorbed hydroperoxide and finally H_2O_2.[52,53] However, more recent investigations evaluating the influence of the gas pressures on the steady state rate of formation of HP proposed a model corresponding substantially to the mechanism of oxygen reduction (ORR) reported for electrochemical processes.[54] The mechanism (Figure 5) claims that H_2 acts only as the electron donor towards the Pd nanoparticles to reduce oxygen to O_2^{2-}, that is later protonated by the solvent to produce H_2O_2. This mechanism better fits with the experimental data, that cannot be described by the Langmuir-Hinshelwood model and explain also the advantage of exploiting an acid media for the DS.[55]

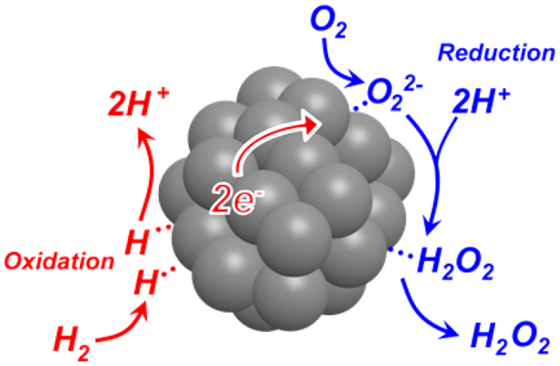

Figure 6: proposed mechanism for the formation of HP by ORR-like mechanism.[55]

Although the model fits the reported catalytic results, the mechanisms of reduction and proton transfer are still unclear. Nevertheless, XAS studies pointed out the formation, under reaction conditions, of hydride species dissolved into the Pd lattice that could act as the actual reducing agent towards oxygen. These results provide an alternative explanation for the incompatibility of the Langmuir-Hinshelwood mechanism [56,57] and are also supported by computational calculations.[58] However, the ORR mechanism is in agreement with the well established effect of the solvent on the DS reaction. In fact, the presence of a protic solvent is mandatory: in particular, only traces of hydrogen peroxides are produced in pure aprotic solvents such as acetonitrile, dimethylsulfoxide or propylene carbonate,[55,59] whereas alcohols lead to a high production of HP.[12,60] On the basis of the proposed mechanisms, protic solvents can improve the HP production by protonation of the absorbed oxygen species, but could also act as a source of hydrogen for the formation of hydrides, or stabilize charged intermediates of the DS.[51] To this regard, although promising in view of a technological application, water is not the best solvent in the DS[61–63] due to the limited gas solubility with respect organic solvents and therefore HP can be obtained only with the addition of additives in solution.[12,60,64] Nevertheless, more recent investigations are suggesting that the organic solvent takes part on the reaction mechanism as redox mediator, especially when alcohols are involved. In fact, they can be oxidized to intermediates that eventually evolve to HP[65] or they can form carboxylic species which enhance the selectivity of the catalyst by partial coverage of the metal nanoparticles.[62] In the presence of promoters such as hydrohalic acids further mechanisms should be considered for the DS, as palladium can form soluble palladium complexes that are later reduced to colloidal palladium. Those Pd species are claimed to be the active species in the formation of HP[66,67] or can alternatively act as reservoir for soluble palladium species.[61] This kind of reactivity is well established for palladium catalysts for cross-coupling processes, such as the Heck reaction.[68,69] Summing up, the nature of the solvent, as well as the presence of acids and halides are likely influencing the formation of HP. Moreover, further parameters such as the partial pressure of hydrogen, could influence the nature of the catalyst and therefore the mechanism of reaction, making the DS reaction particularly complex. The lack of knowledge on the very basis of the formation of hydrogen peroxide from gases still represents a crucial obstacle in the design of catalysts for the production of HP.

1.5.3 The effect of the second metal

A common approach to increase the selectivity of the DS is alloying palladium with a further metal, particularly platinum and gold. Platinum was the first metal used for this purpose:[44] when used in small amount (Pt/Pd ratio of 0.1) can increase both productivity and selectivity of the DS, whereas larger contents negatively affect the selectivity.[70,71] The effect of platinum is partially due to the modification of the electronic density of palladium, that hinders the formation of metal peroxides, leading to HP.[72] The effect of gold in the DS was deeply investigated by Hutchings et al.,[73,74] by evaluating the effect of support[75,76] and halides[77,78] on gold bimetallic catalysts. The same research group also pointed out the improvement of the performance of PdAu catalysts with the addition, beside gold, of a further metal, such as Pt[79] or Ni, Cu and Zn.[78] As a general trend, the Pt leads to a remarkable increase of the catalyst activity (i. e. hydrogen consumption), and, when present in proper amount, of HP productivity as well. Conversely, gold is much more effective in the selectivity enhancement due to the inhibition O–O cleavage and of H_2O_2 hydrogenation.[80] This effect, similarly to Pt is assumed to be generated by an electron withdrawal effect of Au on Pd atoms.[81] However, the higher the amount of Au, the higher the selectivity and the lower the conversion, therefore a very accurate choice of the Pd/Au ratio is needed to optimize the catalytic performance.[82] Similar effects on the performances of the catalyst can be obtained by alloying Pd with less noble metals, as reported by Wang et al. about the effect of Ni, Ga, In, Sn,[83–85] whereas the effect of Zn was independently studied by Wilson et al.[59] and Freakley et al.[86] Finally, the effect of Sn has been studied by Freakley[87] and Li,[88] and that of Te was evaluated by Tian et al.[89] Several publications reported the same effect in the DS for several further transition metals, with the exception of Ru and Rh that promote the formation of water.[90] The effect of the second metal in alloy with Pd can be generally described as the isolation and the partial oxidation of Pd atoms, enhancing the formation of peroxo species and therefore of HP, no matter what is the metal involved (Figure 7).[91,92]

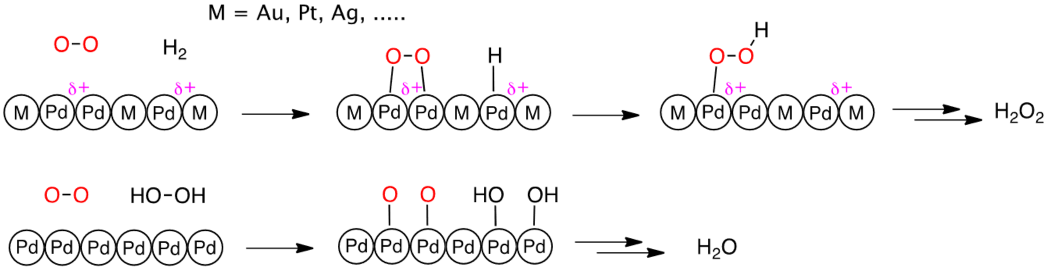

Figure 7: schematic representation of the effect of the second metal on the DS.[91]

However, it is interesting to underline how the issue of the selectivity has always been a crucial point in sequential hydrogenation reaction, typically catalysed by Pd. The partial poisoning of the catalyst, on the basis of the well known Lindlar catalyst,[93] has nothing new with catalysts designed for the DS, though represents an adjustment for this reaction of the strategy already adopted or the selective hydrogenation of alkynes.

1.5.4 Effect of promoters

As long as the mechanism of the formation of HP is not clarified, it becomes very tough to define the effect of halides and acids as promoters in the DS. Many efforts were spent by the research group of Lunsford, trying to rationalize the effect of hydrohalic acids, mainly HCl. It is reported that with high concentration of HCl (<0.1M) the catalytic activity turn out to be the same either by adding Pd/SiO_2 or dissolving $PdCl_2$ in the reaction mixture. Moreover, in the case of Pd/SiO_2 the liquid phase is still catalytically active and produces HP when the solid part is removed. Palladium can be present in solution either in colloidal form or as $PdCl_4^{2-}$, the latter becoming favoured by increasing the O_2/H_2 ratio of the gas feed (Figure 8).[52,61,66]

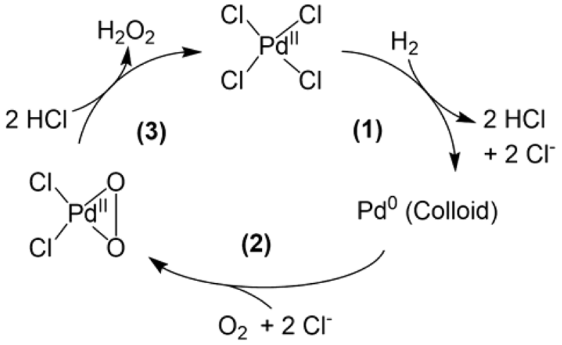

Figure 8: proposed catalytic cycle for HP formation by Pd within acidified water.[61]

Under such conditions, the solid catalyst has a very small stability and behaves only as a "palladium reservoir", being the active form in the liquid phase as soluble complexes or colloids. Nevertheless, this is far from being convenient in view of a practical application.[12] The addition of smaller amounts of halides still leads to a promotion effect on the DS, without a massive leaching of the metal. The selectivity enhancement of the halides is proposed to rely on the selective poisoning of the most active catalytic sites, that are responsible for the breaking of the O–O bond. This was proven both experimentally [51,94] and theoretically.[95] This is valid in the case of Cl^- and Br^-, whereas F^- increase the rates of HP hydrogenation and formation of water and I^- completely poisons the catalyst.[96] As the site-blocking can also inhibit HP production, the extent of the deactivation can be tuned by changing the pH of the reaction mixture, in order to obtain a lower production of water, without completely poisoning the catalyst.[94,97] The interaction between halides and palladium nanoparticles is more complex than a mere selective blocking of the catalytic sites, as the halides are affecting the electronic structure of the metal,[98] inhibiting the dissociation of the O-O bond, likely by reducing the electronic donation to the anti-bonding orbital of the dioxygen. Other investigations of Centomo et al. showed a further level of complexity of interaction. In fact, thanks to *in-operando* XAFS characterizations it was possible to investigate the catalyst under duty, revealing modification of the metal phase induced by bromide ions during the DS. Therefore, Br^- is able to bind to the more active Pd(II) centres leading to a reconstruction of the active metal, to obtain a structure with a lower amount of over-active atoms responsible of water synthesis.[99,100] By considering that hydrogen peroxide and oxygen are present in the reaction mixture of the DS reaction and both are strong oxidant, it is surprisingly never considered in literature the possibility of formation of oxidized derivatives of halides. Those could interact in the mechanism of formation of HP with still unexplored ways, further increasing the complexity of the system.

1.5.5 Effect of Pd oxidation state

A fundamental parameter affecting the selectivity of the catalyst is the oxidation state of Pd. This aspect is highly controversial and often discussed in literature reports and appears very difficult to be evaluated, as the catalyst can evolve during the DS reaction and may remarkably differ from the form it assumes before and after the catalytic experiment. Among the factors influencing the oxidation state of palladium the most important are the composition of the gas mixture, the solvent, the promoters possibly present in solution, the presence of second metal beside palladium and interactions of the active phase, gases and H_2O_2 with the catalytic support. The first detailed investigation on the effect of the oxidation state of palladium by using XPS comes from Blanco-Brieva et al.[101] and claims that Pd^{II} is necessary to achieve high selectivity. On the other hand, Burato et al., by applying a reduction treatment to a very similar catalyst, reached better performances due to the presence of metal Pd.[102] This is consistent with the report of Liu et al., pointing out that Pd^0 is the active phase in the HP production, while a PdO is easily reduced under duty to form the most active metal phase.[51,103] However, any XPS analysis, as well as TEM and XRD characterizations cannot rule out the presence of a thin layer of PdO on the surface of the metal nanoparticles that could strongly affect the production of HP. A more sophisticated evaluation is obtained by EXAFS using synchrotron light, giving a value of the Pd^0/Pd^{II} ratio under duty: this makes possible to measure the fraction of Pd^{II} present in reduced catalysts and to verify that it does not change significantly during the DS in the absence of promoters. Conversely, when Br^- is present in solution a decrease in the Pd^{II} signal is observed: this is consistent with the removal of a significant amount of PdO phase and leads to the promotion of the selectivity towards HP, typically observed with halides.[100] The removal of Pd^{II} by bromide ions is also reported by Biasi et al., but the conclusive statement is somehow surprising, as they pointed out that Pd^0/Pd^{II} ratio does not affect the selectivity of the catalyst and the effect of Br^- is to be attributed only to the selective site blocking.[104] Conversely, other works suggest that oxidized palladium is much more efficient in the production of hydrogen peroxide,[105,106] according also to computational investigations.[107] Furthermore, recent results conclude the debate on the higher selectivity of metal palladium rather than its oxide phase pointing out that HP is formed on the interfaces between Pd/PdO phases.[108] In this connection, it is important to notice that, in some cases, the catalytic support also plays a key role, promoting the formation of PdO domains, thus increasing the extent of the boundary between Pd and PdO phases.[109,110]

1.5.6 Effect of the catalytic support

The choice of the support is of fundamental importance for the performance of a catalyst in the DS reaction, as it determines many parameters of the metal nanoparticles such as electronic structure, shape and dimension of the metal catalyst.[12] Several inorganic supports were investigated over time, mainly silica, alumina or other metal oxides, as well as active carbon. Among these it is reported that catalyst supported over active carbon are more active in the production of HP.[76] This can be related to the higher surface area of carbon supports, even though it was also reported that the surface area is less important than the morphology of the porous system.[111] One of the features of the support that has to be taken into account is the hydrophobicity, as early investigations demonstrate the increase of this parameter brings to an improvement of the selectivity.[112,113] This is supposed to be the consequence of the more efficient back-diffusion of the HP from the catalytic sites to the bulk solution, hindering the decomposition of hydrogen peroxide.[91] However, the most important parameters belonging the catalytic support are its isoelectric point and the presence of acid functionalities (both Brønsted or Lewis type). In fact, it is widely proven that acidic supports, such as factionalized silica[114,115] or zirconia,[116] can improve the selectivity of the catalyst. The same effect can be obtained with acid pretreatment of the support, while this has a more detrimental effect on the overall activity of the catalyst.[117] The role of the acidic sites can be explained both with an electronic withdrawal effect over the metal nanoparticles,[118] or by the participation of protons in the mechanism of HP formation similarly to homogeneous H^+ ions.[119] For this reason, several material bearing ion-exchange groups able to exchange cations, such as zeolites or polymer based ion-exchange resins were successfully used as the catalytic support in the DS reaction. Several works report the use of zeolites, mainly the ZSM-5 type, claiming good performances in the DS, even without the use of promoters.[49,120,121] However, zeolites typically present a microporous structure with very narrow pores, that can represent a strong limitation on the performances of the catalysts, as it is also demonstrated in this work. As for ion-exchange resins, by tuning the synthetic procedure it is possible to obtain polymers with different morphologies, from microporous to macroporous, and several different functionalities,[122,123] that can be later sulfonated to introduce ion-exchange groups. This makes ion-exchange resins very interesting supports for metal catalysts in the DS reaction. The first time these class of catalysts were applied in the DS in 1977, in the aforementioned patent,[45] and after this work several other publications are reported.[80,101,124,125] The main issue related to these material is the thermal stability, but in this case is not representing a drawback as the DS reaction is held a low temperature (room temperature or lower). For these reasons ion-exchange resins are chosen as the catalytic support of main interest on this work, in particular the novel mesoporous poly-divinylbenzene, that is deeply described later on.

1.6 Ion-exchange resins

1.6.1 Morphology of crosslinked polymers

At the solid state, the chains of linear polymers, such as polystyrene, are collapsed in a glassy (or semi-crystalline) structure. These materials can be dissolved in a suitable solvent, able to interact with the polymer chains. When a bi-functional monomer (crosslinking agent) is also polymerized, the polymer chains are connected and the resulting material, commonly known as “resin”, appears insoluble, although it can be swollen in suitable solvents. As for the dissolution of uncross-linked polymers, the swelling is the result of the solvation of the polymer chains that, in case of resins, is interrupted by the elastic forces developing when the solvent molecules enter the polymer framework. The polymer morphology is directly determined by the synthetic approach and essentially depends on two parameters, such as the crosslinking degree and the exploitation of a nonsolvent (or precipitating solvent), i.e. a “bad” solvent, unable to swell the polymer. Initially, the polymerization leads to a gel phase and with low amount of crosslinker (typically below 10% mol) and without nonsolvents, the reaction continues until a high degree. At this point the liquid phase is partially expelled by the gel phase and by removing the solvent a glassy solid is obtained. This mechanism is called microsyneresis and produces a material with very low surface area (<10 m^2/g). This resin, namely gel-type resins, can be completely swollen to obtain a homogeneous polymer having a porous system (up to a few nm in size) formed by the distancing of the polymer chains. In the presence of a nonsolvent and with a high crosslinking degree, the macrosyneresis mechanism occurs. The amount of crosslinking to obtain the macrosyneresis depends on the nature and amount of the precipitating solvent, but is typically higher than 12%. When this mechanism occurs, the initially formed nuclei of gel phase become insoluble and expel the liquid phase. The polymerization continues around these nuclei, forming a gel phase surrounding inaccessible polymer spheres, that become connected each other. This generates a permanent porous system (size of 20-60 nm) that are formed by the empty spaces created by the stacking of the polymer spheres (Figure 9).

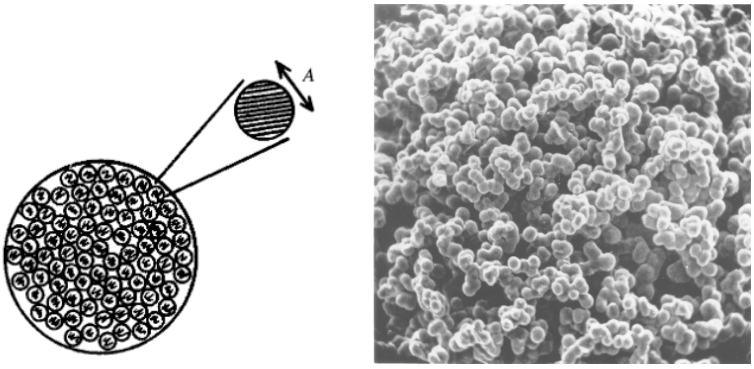

Figure 9: enlarged macroporous resin bead showing individual microgel particles (A = 100 nm) and SEM image of a macroporous resin.[126]

This kind of cross-linked polymers is called macroporous resins. The nuclei of these spheres have a high degree of crosslinking that makes them unswellable, even in the presence of a good solvent: this makes part of the polymer inaccessible, as only the shell of the nuclei can be swollen as a gel-type phase. The permanent porosity of macroporous resins develop a limited surface area at the dry state (50-1000 m^2/g). Moreover, are much more resistant to shear stress or osmotic pressure that can occur during the swelling and de-swelling of the material and are more tolerant to oxidizing agents that can damage gel-type resins with a consequent decrease of the crosslinking degree (Figure 10).

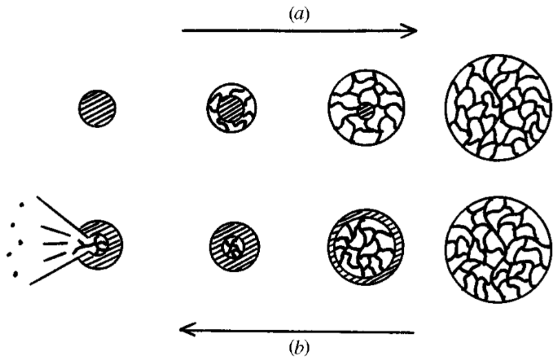

Figure 10: solvent response of gel-type resins: (a) shrinking glassy core to form an expanded gel in a good solvent; (b) contraction of swollen gel on addition to a bad solvent with bursting of resin due to osmotic shock.[126]

The general overview on crosslinked polymers given on this Paragraph is according to references.[126–128]

1.6.2 Application of ion-exchange resins

The ion-exchange resins are functionalized crosslinked polymer bearing groups able to exchange ions, in the swollen state. Ion-exchange resins can be classified as cation and anion exchangers, according to their ability to exchange anions or cations. The latter is the only typology involved in the DS, therefore only these are introduced in this Paragraph. In general, cation exchangers are styrene-divinylbenzene co-polymers, that are functionalized to introduce -SO_3H groups which are able to exchange cations. The main purpose of these materials is the exchange of cations in aqueous solutions and they are accordingly exploited, for example, to replace Ca^{2+} with Na^{+} in the sweetening of water, or to complete deionize the water, by coupling a cation exchanger with an anionic one.[127] However, the presence of strong acid groups allows the use of these materials as acid catalysts. In this frame, one of the most important reaction catalysed by ion-exchange resins is the synthesis of methyl *tert*-buthyl ether.[129] Further applications are in the alkylation, condensation, and hydration reactions.[130] Moreover, there is an interest in the use of ion-exchange catalysts for esterification reactions, in the frame of biodiesel production. In fact, as biodiesel is produced by transesterification of triglycerides by base catalyst, free fatty acids (FFA) must be completely removed to avoid catalyst consumption and the formation of foam. To this end, FFA are esterified with methanol by acid catalysis.[131] Replacing concentrated sulfuric acid with ion-exchange resins avoids expensive separation steps as well as corrosion issues related to the use of the homogeneous catalyst.[132,133]

The use of polymers as templating agents to control the growth of inorganic materials is a well established strategy in the design of novel nano-materials.[134] To this regard ion-exchange resins are suitable for the preparation of palladium catalysts for the DS reaction. To produce the catalyst, a cationic Pd precursor can be easily introduced in the resin by ion-exchange and then reduced to form metal palladium that aggregates to form nanostructured metal particles. The size of the nanoparticles is strongly related to the morphology of the porous system of the polymer, that acts as a template, particularly effective in the case of gel-type resins,[135,136] even though macroporous resins can control the growth of the metal nanoparticles inside the gel phase surrounding the highly crosslinked nuclei.[137] With this approach is possible to obtain bifunctional materials bearing both acid sites and metal nanoparticles, that are used in several reactions, mainly the industrial production of methyl isobutyl ketone from acetone and hydrogen,[138] but also alcohol oxidation[139] or the hydroxylation of benzene to phenol.[140] As for the DS, the use of ion-exchange resin as support is convenient to exploit acid functionalities able to increase the selectivity of the reaction and are already extensively employed for this purpose (Paragraph 1.5.6). Among the novel palladium catalysts supported on ion-exchange resin, the material reported by Frison et al.[141] turns out to be particularly interesting, due to the peculiar morphology of the catalytic support, namely sulfonated polydivinylbenzene, that is deeply discussed in Paragraph 1.6.3.

1.6.3 Polydivinilbenzene and its application in the DS

In 2009 a novel mesoporous superhydrophobic material, namely polydivinylbenzene (pDVB) was obtained by Zhang et al. from the radical polymerization of the sole divinylbenzene.[142] The key to obtain this polymer with very peculiar characteristics is the use of divinylbenzene as the only monomer, under solvothermal conditions in a closed vessel under autogenic pressure, a method typically involved in the synthesis of zeolites. Particularly important is the choice of the solvent, that must be a good solvent able to solubilize the monomer, therefore acting as a porogenic agent in the same way as for the synthesis of gel-type resins. The solvent can be chosen by evaluating its capability of solubilize polystyrene and in this case the solvents of choice is tetrahydrofuran (THF). Finally, the dilution ratio must be high enough to ensure the formation of the porous system. Similarly, the reaction time has to be enough to allow the complete polymerization and the formation of the porous system. Moreover, the addition of a small amount of water increases the diameter of the mesopores. Further investigations pointed out that the increase of the solvent/monomer ratio allows to turn from glassy non-porous solid, to mesoporous materials up to polymers with a macroporous morphology (Figure 11).[143]

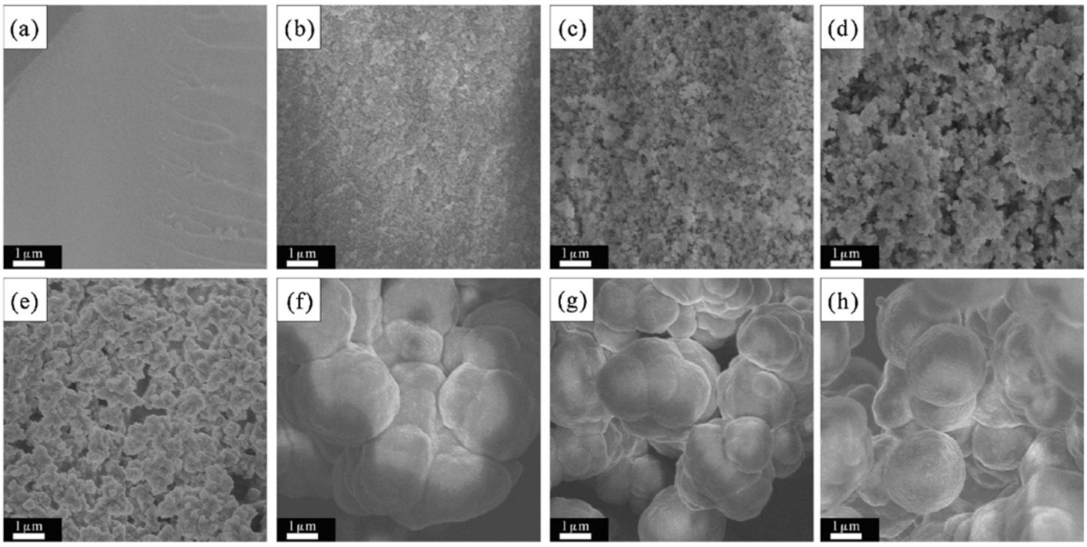

Figure 11: SEM images of pDVB synthesised with different amount of porogenic solvent. The amount of solvent increases from image a to image h. The mesoporous morphology is obtained in the materials reported in images d and e.

Therefore the investigation of the swollen state morphology of the material is of the utmost importance and can be obtained with Inverse Size Exclusion Chromatography (ISEC), that allows to determine the pore size distribution. Basically, this technique uses the swollen polymer as the stationary phase of a chromatographic column and solutions of standard solutes with different and well known hydrodynamic sizes are eluted. On the basis of the retention times of the standards it is possible to determine the pore size distribution of the material in the swollen state.[144] By coupling this technique with the standard nitrogen physisorption that provides information about the dry state of the material, it is possible to fully describe the morphology of the material, synthesized with THF as the porogenic solvent, used in the 10:1 vol ratio respect to the monomer (Table 2).[145]

Table 2: characterizations of pDVB obtained by the polymerization of 6 g of divinylbenzene in 60 mL of THF, with 6 mL of water.

Dry state characterizations				
BET surface area [m^2/g]	External surface area from t-plot slope [m^2/g]	Micropore volume [cm^3/g]	Cumulative surface area in pores >4nm [m^2/g]	Total pore volume [cm^3/g]
1096	1091	0.008	436	2.07
Swollen state characterizations				
Pore diameter [nm]	Pore volume [cm^3/g]		Pore wall surface area [m^2/g]	
600	0.62		4.1	
300	0		0	
150	0		0	
80	6.78		339	
40	0.7		70	
20	0		0	
10	0		0	
Total	8.1		413	

These characterizations show for pDVB a dry state surface area comparable to that of active carbon, remarkably without micropores, as almost half of the surface area is developed by pores bigger than 4 nm. In the swollen state the porous system expands and almost all the pores are in the range 40-80 nm. As for other crosslinked polymers, the morphology of the porous system depends on the mechanism of polymerization. Initially, thanks to the high dilution of the monomer in the porogen solvent, the polymer chains grow and form a gel phase similarly to the polymerization of gel type resins. However, when the microsyneresis happens and the phase separation starts, the polymerization and thus the crosslinking degree are high. Therefore, the phase separation occurs with the expulsion of small liquid droplets from the polymer phase, that act as the template for the growing polymer. The resulting morphology of the material can be described as a solid foam with very thick polymer walls and plenty of mesopores connected each others (Figure 12).[146]

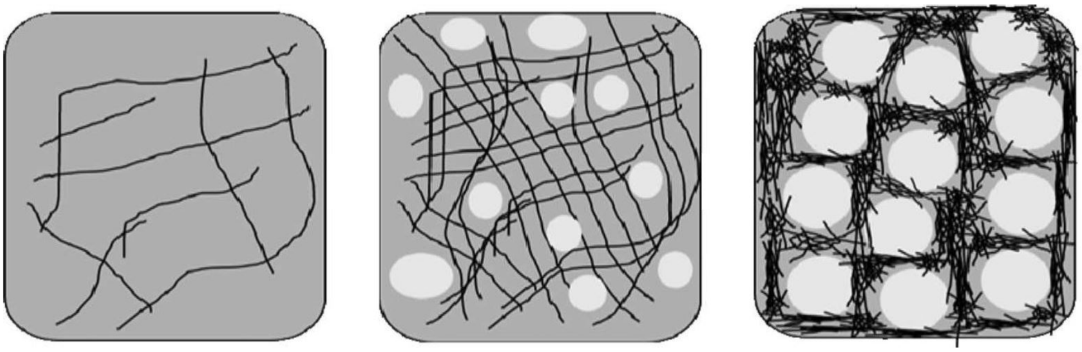

Figure 12: pore formation by microsyneresis in pDVB.

The structure of the solid collapses once the porogen solvent is removed, but can be almost completely restored by the addition of a suitable solvent. Consequently, for pDVB the swelling is not related to the solvation of the polymer chains, as a gel phase is absent, but is simply the filling of the pores, increasing in size due to the removal of capillary forces that otherwise keep the structure in the collapsed form. Although, this material was designed for the selective absorption of pollutant and its superhydrophobic properties,[147] it was later functionalized and turned into catalysts as well as catalytic support. The introduction of quaternary ammonium functionalities by co-polymerization with vinylimidazolate was adopted to develop a base catalyst for the transesterification reaction to produce biodiesel. The open mesoporous morphology allows a very efficient diffusion of the reagents inside the catalysts and ensures remarkable catalytic performances.[148,149] Mesoporous pDVB was also used to produce acid catalysts, by introducing sulfonic groups with sulfonation using chlorosulfonic acid or by co-polymerization with sodium *p*-styrene sulfonate, exploited in the esterification of FFA.[150,151] The very promising performance shown by this kind of catalysts is partially due to the hydrophobic nature of the polymer framework causing an efficiently expulsion of water that otherwise deactivates the catalytic sites.[150] In 2019 Frison et al. exploited Pd nanoparticles supported sulfonated pDVB (SpDVB) to promote the DS.[141] The fast removal of polar molecules is a very important feature as it allows an efficient back-diffusion of the HP produced to the bulk reaction mixture, avoiding its further reduction to water. In this frame, the mesoporous morphology is highly beneficial for this process, as the catalyst supported on SpDVB (namely Pd/SpDVB) is much more selective than palladium catalysts supported on active carbon or gel-type resins.

1.7 Introduction to this project and state of the art

Palladium catalysts supported on ion-exchange resins are very promising catalysts in the DS reaction and are widely investigated since the first report by Kim and Schoental[45] in 1977. The tunable morphology of the polymer supports as well as the possible functionalization of the polymer matrix makes possible the design of catalysts with tailor made features to increase the selectivity of the reaction. In fact, the results obtained by Frison et al. with a semi-batch reactor operating under mild conditions in the absence of promoters are already very promising. Therefore, this work starts as the continuation of the preliminary investigations made with the Pd/SpDVB catalyst, by using the same experimental setup. Some later optimizations, mainly in the quantification of the HP produced, granted higher quality on the experimental data and the performances of the catalyst. A crucial improvement of great importance on the reactor allows to do catalytic experiments with long catalytic runs (more than 24 hours, technically there is no upper limit in the length of the experiment). In literature, most of the investigations are based on batch or semi-batch reactors and temporally limited from 30 minutes to some hours, with very few examples over 24 hours or even just 4 hours. As it is well established that the selectivity is high in the first minutes of reaction and then drop with time,[12] limiting the investigation of catalysts to short time could be misleading. The first part of the work deals with the effect of the polymerization procedure on the polymer support and the consequent effects on the performance of the corresponding Pd catalysts on the DS. This part of the project started before the PhD project and was continued in this work mainly with the characterizations of the catalysts. Then, the less active catalyst in HP production among those synthesised during the Thesis was chosen for further investigations, to better appreciate the optimization of the catalytic system.

The main focus of the work is the investigation of alternative promoters for the selectivity of the reaction, as the use of acids or halides in solution makes not feasible the DS process for technological applications, due to the corrosion issues of the plant,[12,152,153] along with the enhancement of the leaching of the active metal.[52,153] Some investigations were made on this purpose, by using organic halides as non-corrosive promoters.[154] However, the enhancer showing the best performance is *tert*-butyl bromide and exert his promotion effect likely due to its hydrolysis that produces Br^- ions (even though some good results were obtained with phenyl bromide, without any release of bromide in solution). An important feature of halides, particularly bromides and chlorides, is their ligand behaviour towards Pd(II) to form $[PdX_4]^{2-}$ complexes.[155] Starting from this, a number of ligands for Pd(II), to be used as novel selectivity enhancers for the DS, was investigated. Ideally, to be suitable for technological application, these promoters should not leach the metal components of both the reactor and the catalysts in solution and should be cheap and non toxic. In 2013, Abate et al. reported the positive effect of coating Pd nanoparticles by polyvinyl alcohol on the selectivity, allegedly due to the stabilization of the metal nanoparticles towards the aggregation.[156] However, polyvinyl alcohol could also coordinate Pd(II) and this might contribute as well to the selectivity enhancement. Starting from this work, palladium ligands with S, P or O as donor atoms were used to functionalize Pd nanoparticles, in order to promote the formation of hydrogen peroxide (Figure 13).[157,158]

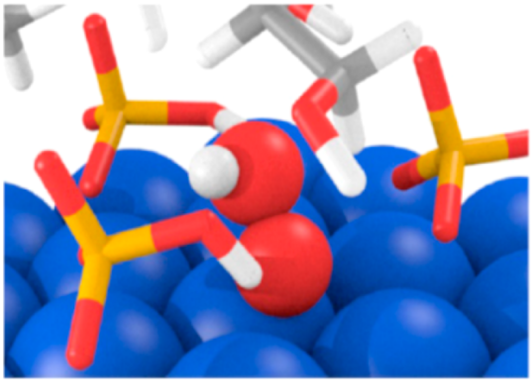

Figure 13: long-chain alkyl ammonium phosphates coadsorbed on Pd increase HP selectivity and are predicted to increase barriers for O−O bond rupture during the DS.[157]

Thanks to this approach a selectivity increase is reported, although the presented results cannot be considered fully reliable due to the permanganometric method used to measure HP in the reaction mixture (Chapter 1). Interestingly, during the development of this work, the treatment of Pd nanoparticles with NHC carbene behaving as Pd(II) ligands was reported to promote the selectivity of DS in a very efficient way.[159] Whereas in the literature investigation a rather complicate kind of promoter was exploited, in this work the choice of the ligand is based on the simplicity, in order to potentially scale up this enhancement approach to technological applications. To this regard, some of the most common organic solvents, such as nitriles, amides or sulfones, can behave as ligands for Pd(II). In particular, the investigation on innovative promoters for DS started from very common solvents like acetonitrile (ACN), N,N-dimethylformamide (DMF) and dimethylsulfoxide (DMSO). Among these, ACN is the only ligand already considered as the solvent for this reaction. In fact, a positive effect in the use of ACN as solvent was reported by Kim and Schoental[45] in their patent, the same that is also describing for the first time the use of ion-exchange resins as catalytic support. Nevertheless, no explanation about the enhancement effect of ACN is reported in the patent. The first report about the use of ACN in the open literature is published in 2003 by Burch and Ellis,[160] but the results should be carefully evaluated, as the method used for the quantification of HP was not reliable (Chapter 1). In 2015, Paunovic et al.

reported on the effect of several co-solvents in addition to methanol on PdAu bimetallic catalysts.[161] It was found a positive effect on the selectivity of the reaction, as ACN can inhibit O–O cleavage by partially coating the metal nanoparticles. This explanation is very similar to that proposed to rationalize the effect of halides. Nevertheless, these studies were made in the presence of both sulfuric acid and hydrobromic acid, making the reaction conditions very corrosive and particularly complicate to identify the effect of the co-solvent. The main focus of this investigation is the effect of coordinating solvents on monometallic palladium catalysts for the DS of HP, supported on several materials, such as ion-exchange resins (mainly SpDVB), alumina, silica, different kinds of zeolites and activated carbon. This study was carried out with both a semi-batch reactor (SBR), operating under very mild conditions, and a continuous trickle-bed reactor (TBR) operating under pressure. Some of the key points of this work are the investigation of the performance of the catalysts over very long time (with SBR) and the use of a halides- and acid-free reaction mixture.

Part 2

RESULTS AND DISCUSSION

Chapter 1: Analysis of hydrogen peroxide in methanol solutions

2.1 Titration of hydrogen peroxide in organic solutions: an underestimated issue

The production of HP with the DS is widely investigated since 90s and in most of the cases methanol is used as the solvent (or co-solvent), since it is protic[51] and ensures a good solubility of the reaction gases. A key point on the first part of this project is the validation of a reliable method for the quantification of the amount of HP produced during a catalytic test: this is a fundamental starting point for the evaluation of the performance of the catalyst. Based on literature, four main methods are used for this purpose (Figure 14), i. e. volumetric titrations (iodometry, cerimetry and permanganometry) and the detection with UV-Vis spectrophotometry of a coloured peroxidic complex, obtained by reaction between HP and $TiOSO_4$. Nevertheless, these methods were developed for the determination of HP concentration in pure water and the reliability of these in methanol solution is almost no discussed in literature. Therefore, the starting point of this investigation is the evaluation of the reliability of these four methods for methanol solutions of HP, to identify the most suitable for the analysis of DS reaction mixtures.

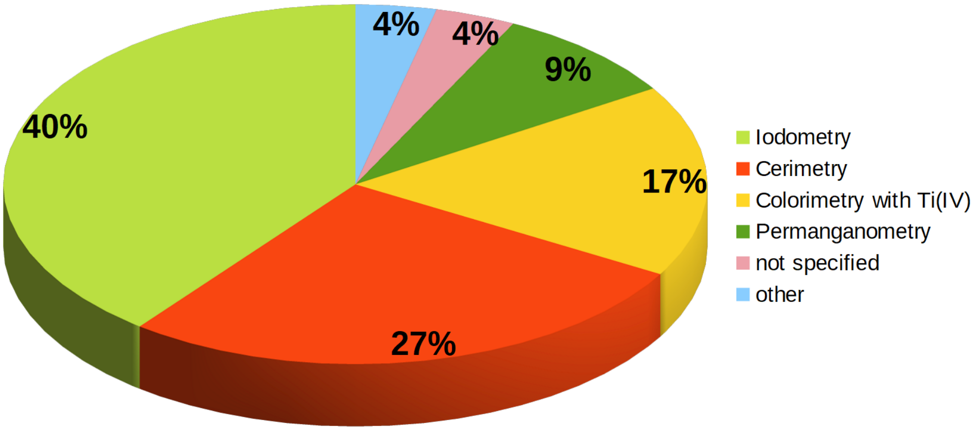

Figure 14: methodologies for the assessment of the HP concentration in catalytic studies of direct synthesis.

To this regard, the concentration of HP of several standard methanol solutions was determined with the four above mentioned methods and compared with the expected value. For each titration, only 1 mL of standard solution was analysed, as it is the amount of a typical sample of the catalytic experiments (Paragraph 4.4.2.2). Nevertheless, the results of this investigation can be safely generalized to any typical laboratory DS experiment, as the volume of the samples of the liquid mixture, specially in batch or semi-batch experiments, are generally small to limit the perturbation of the reaction environment. The solutions used in this work and their concentrations are reported in Table 3. The Stock Solution consists in a water solution of HP and its titration after the addition of methanol is helpful to understand the interfering effect of the organic solvent.

Table 3: HP solutions used for the evaluation of the analysis methods.

Solution	**Concentration [mM]**
Titr1	0.0933 ± 0.0029
Titr2	0.187 ± 0.005
Titr3	0.467 ± 0.010
Titr4	0.933 ± 0.021
Titr5	1.87 ± 0.04
Stock Solution	9.33 ± 0.14

2.1.1 Iodometric titration

The iodometric titration is a back titration with sodium thiosulfate of the triiodide that is formed by addition of potassium iodide to a HP solution. The reaction involved are the following:

$$H_2O_2 + 3I^- + 2H^+ \rightarrow I_3^- + 2H_2O$$

$$I_3^- + 2S_2O_3^{2-} \rightarrow 3I^- + S_4O_6^{4-}$$

This method is strongly influenced by the pH. On the one hand in basic environment iodide ions catalyse the dismutation of HP to water and oxygen[162–165] and iodine can dismutate to I^- and IO_3^-.[2] On the other hand, a low pH atmospheric oxygen can oxidize iodide ions to iodine. Beside these drawbacks this method is widely exploited as it is slightly affected by organic solvents and stabilizers which are typically present in HP solutions.[166] As the reaction of oxidation of iodide with HP is slow, acid is needed to promote the reaction and a high oxidation state transition metal salt can be added as the catalyst. Hence, to better understand the reliability of this method, in this work the oxidation of iodide with HP has been alternatively with a slightly acidic (10^{-3} M sulphuric acid) and a strongly acidic (5 M sulfuric acid) solution of sodium molybdate(VI). With the addition of 5M sulfuric acid, the final acid concentration in the titrated samples is ca 1M, close to the value reported in the literature procedure.[166] Figure 15 shows the results of the titrations of the Stock Solution as such and after 1:1 dilution with methanol.

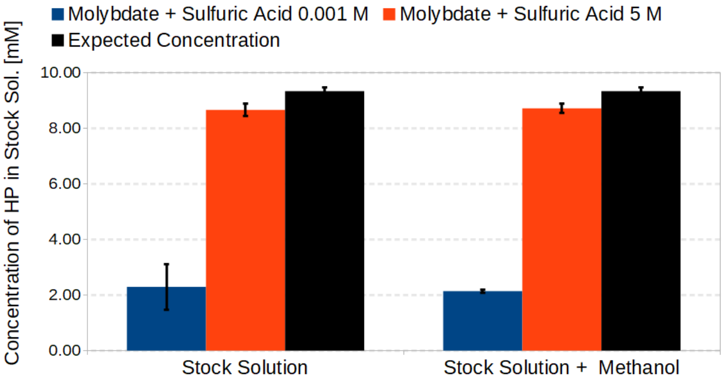

Figure 15: iodometric titration under mildly and strongly acidic conditions (1 mM and 5 M H_2SO_4 solutions of Na_2MoO_4, respectively) of 1 mL of the aqueous Stock Solution as such (left) and after the addition of 1 mL methanol (right). All the concentrations are referred to the volume of Stock Solution used for the analysis and compared to the corresponding known reference concentration (black bar).

Both at low and high H^+ concentration the iodometric titration underestimated the HP concentration, with a very large gap (ca 80%) between the expected value at low H^+ concentration and a much smaller one (ca 10%) at high H^+ concentration. The results obtained for the aqueous stock solution and for the 1:1 hydro-alcoholic solution are strictly comparable, suggesting that HP is not consumed in the oxidation of methanol. In addition, no consumption of thiosulfate was observed in the titration of pure methanol, excluding possible interferences from the alcohol or its impurities (Figure 16). Although these results suggest that a highly acidic environment is recommended, different outcomes are observed in the analysis of the even more diluted solutions Titr1-Titr5. The experimental values are reported in Figure 16.

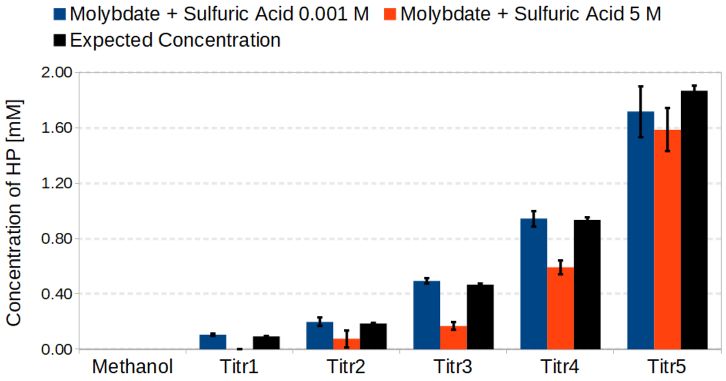

Figure 16: concentrations of HP in the standard HP solutions Titr1-Titr5 from Iodometric titration using mildly (blue bars) and strongly (red bars) acidic solutions of Na_2MoO_4 (1 mM and 5 M in H_2SO_4, respectively). All the concentrations are referred only to the volume of Titr1-Titr5 solutions used for the analyses and are compared to the values expected from the respective dilution ratios of the Stock Solution (black bars).

In this case, for concentrations up to 2 mM a low concentration of H^+ is much more appropriate. In fact, only for Titr5 (1. 86 mM), the results of the titrations in both mildly or strongly acidic environment are not too far. For Titr1-Titr4 the concentration of HP is largely underestimated in strongly acidic solutions, with a systematic decrease of the accuracy with increasing dilution of the analyte. No I_2 in Titr1 and only 41% of the expected amount in Titr2 were found. This supports the hypothesis that a too high H^+ concentration promotes reactions of HP which compete with I^- oxidation so effectively to suppress it completely in very diluted solutions. Nevertheless, a complete description of the nature of these side reaction is out of the scope of this work. However, even in a slightly acidic environment the accuracy of the titration depends on the HP concentration, but in this case it changes in the opposite way. Whereas a slight overestimation of HP concentration is present in Titr1-Titr4, in Titr5 (1.86 mM) it was underestimated by 8% (which became ca 80% in the 9.33 mM solution shown in Figure 16). Looking at the molar ratio between HP and H^+, in the titrations under strongly acidic conditions this is very low (10^{-6} – 10^{-4}), whereas in the titration under mild acidic conditions the HP/H^+ ratio is much higher, from $4.6 \cdot 10^{-2}$ to 0.93 for solutions Titr1-Titr5 and in the Stock Solution turns out to be 4.65. As two moles of H^+ are consumed per mol of HP in the reaction with iodide, a sufficient amount of acid must be provided. The amount of I_3^- produced in the reaction would be otherwise lower than the actual amount of HP in the solution. In addition, in a H^+ depleted solution the excess of HP could react in a catalytic way with iodide to form dioxygen. In both cases the amount of HP detected by the titration would be underestimated. This could explain why the underestimation of the concentration of HP is so severe for the Stock Solution. To summarize, this investigation shows that methanol does not imply any sensible interference and that the pH of the solution should be carefully adjusted to achieve the best conditions of reliability. A further critical issue of the iodometric analysis of HP methanol solutions obtained from DS is the colour returning of the I_2-starch complex at the end of the titration due to atmospheric oxygen, severely affecting the determination of the end-point. It was found that the higher the HP concentration the higher the extend of this phenomena, making the detection of the end-point somewhat arbitrary. As a matter of fact, the titrations of the most concentrated solutions, Stock Solution and Titr5, for which this issue is qualitatively clearer, seem to be also affected by a higher uncertainty, both at high and low HP/H^+ ratio. In this context, the effect of bromide ions, commonly used in the DS reaction as HBr as promoters, was also assessed. For this purpose the Stock Solution was titrated after the addition of an equal volume of a solution of HBr in methanol (200 ppm). In view of the relatively high HP concentration, in this case a high concentration of H^+ was also applied. The production of I_2 after the end-point was remarkable and this phenomenon, which was relatively faster at the beginning, went on for more than one hour. This suggests that in the presence of HBr and, possibly, of oxidized bromine species (aged HBr can contain some Br_2, easily recognized from its yellow-red colour) enhances the rate of oxidation of I^- by O_2. Upon addition of the same solutions used for the iodometric titration of HP (Na_2MoO_4, H_2SO_4, KI) to a few mL of the 200 ppm HBr solution in methanol the formation of I_2 was clearly observed without any addition of HP. This qualitative observation supports the conclusion that HBr remarkably enhances the oxidation of iodide by atmospheric oxygen. Accordingly, HBr can cause the over-production of I_2 by air oxidation, which could lead to the overestimation of the concentration of HP and therefore to an apparent increase on the selectivity. In conclusion, to reliably assess the concentration of HP in real samples of DS reaction mixtures upon iodometric titration, the conditions for the analysis should be carefully adjusted.

2.1.2 Permanganometric titration

With this method HP is oxidized to dioxygen with a standard solution of potassium permanganate, under strongly acidic conditions.

$$5H_2O_2 + 2MnO_4^- + 6H^+ \rightarrow 5O_2 + 2Mn^{2+} + 8H_2O$$

pH must be low to prevent the formation of solid MnO_2, the favoured reduction product under neutral or moderately basic environment, that catalyse HP disproportionation. At low pH, the reduction of MnO_4^- yields the Mn^{2+} aquo-ion, almost colourless, hence permanganate acts as auto-indicator due to its own intense violet colour. This method is known to be very accurate for the titration of aqueous solution of HP.[167] Organic substances are known to interfere with permanganometric titrations and their presence (and those of other reducing species) is spotted by the fading of the end point. For this reason the iodometric titration is considered more reliable when oxidizable organic substances are present.[166] Nevertheless, the permanganometric titration is often employed for the analysis of reaction mixtures obtained from the DS, even when the solvent (or co-solvent) is an alcohol. Therefore, the accuracy of this analytical method for the DS mixture was evaluated by titrating the Titr1-Titr5 solutions (Table 3) and the Stock Solution with a standard aqueous solution of potassium permanganate 0.2 mM. The Stock Solution was again analysed as prepared and after 1:1 dilution with methanol. Low pH was ensured by the addition of 5 M sulfuric acid. The results are illustrated in Figure 17.

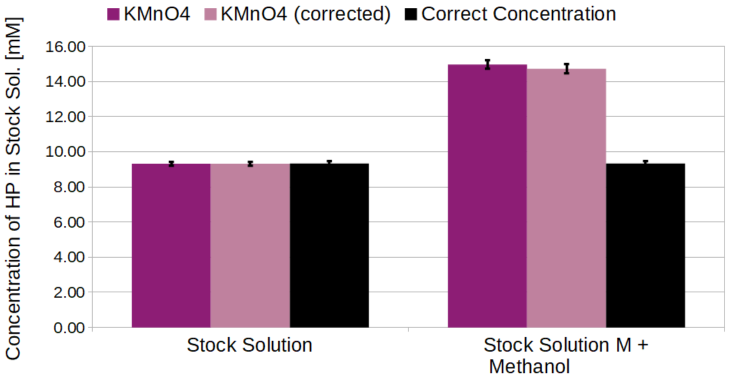

Figure 17: titration with 0.2 mM $KMnO_4$ of a standard 1 mL M HP aqueous solution (left) and after the addition of 1 mL of methanol (right). The concentration estimated with the titration, after the correction by $KMnO_4$ consumption of the pure solvent and the expected value are reported in purple, pink and black colours, respectively.

Unlike the iodometric titration, the amount of titrant consumed by the solvent itself is not negligible, even when HP is not present in solution. Accordingly, to take into account the MnO_4^- consumption by the solvent, a blank experiment was performed by measuring the titrant consumed by 1 mL of methanol. The results of the permanganometric titrations, both the raw ones and those including the blank corrections, are summarized in Figure 18.

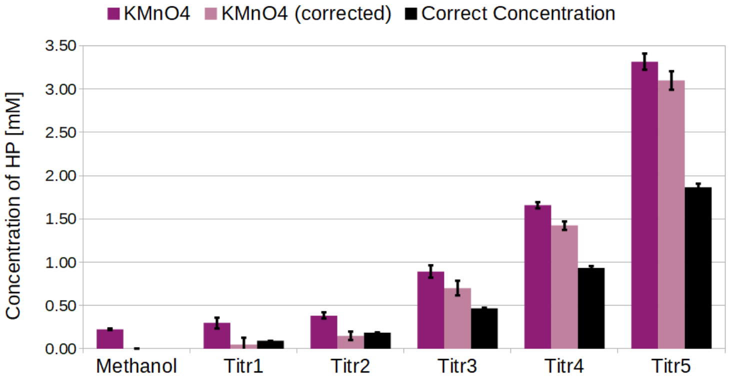

Figure 18: titration of Titr1-Titr5 with standard aqueous $KMnO_4$, 0.2 mM (purple bars). All the concentrations are referred only to the volume of Titr1-Titr5 solutions used for the analyses and are compared to the values expected from the respective dilution ratios of the stock solution (black bars). Pink bars represent concentrations corrected taking into account over-consumption of $KMnO_4$ due to methanol oxidation.

On these grounds, the evaluation of the performance of the DS catalysts requires great care when the reaction is carried out in hydro-alcoholic solution and the HP concentration is assessed by permanganometry. Under these circumstances over-estimation of the HP concentration has to be expected, from large (a few tens %) for relatively concentrated mixtures to severe (several hundreds %) for the relatively diluted ones and more in general this method must be avoided in the titration of HP in methanol solution.

2.1.3 Cerimetric titration

In cerimetric titrations, HP is oxidized to O_2 by a standard solution of cerium (IV) sulfate under acidic conditions, with ferroin as the indicator.[166,168] After the end point excess cerium (IV) oxidizes the indicator turning the solution to colourless.

$$H_2O_2 + 2Ce^{4+} \rightarrow O_2 + Ce^{3+} + 2H^+$$

To ensure the reliability of the method the five methanol solutions of HP, as well as the Stock Solution as prepared and with the addition of methanol, were analysed with cerimetric titration. The small size of the samples (and of the amounts of HP to be titrated) is more relevant here, because the colour change of the indicator requires the consumption of additional cerium(IV), and for very diluted samples this could be the cause of inaccuracy. In this work one drop of ferroin was used per mL of solution to be titrated. Hence, the amount of cerium(IV) needed to oxidize one drop of ferroin in 1 mL of either methanol or water was measured, in order to evaluate the extent of the possible interferences, if any. Unfortunately ferroin is not very deeply coloured and appreciating its colour change with only one drop of indicator per mL of solution of the analyte is hard. On the other hand, a bigger amount is not recommended to avoid further errors in the measurement. In fact, the titration of this small amount of the indicator in blank solution consumed, both in water and methanol, an amount of cerium(IV) sulfate corresponding to an apparent HP concentration of ca 0.2 mM. Moreover, HP can be slowly consumed by ferroin: this was qualitatively confirmed by the complete fading, in 1h under magnetic stirring, of 5 mL of the solution Titr5 to which five drops of ferroin had been added. In view of these circumstances, cerimetric titration of very diluted HP solutions could be particularly challenging, if not even little reliable. The results of the titrations of the five hydro-alcoholic HP solutions (Titr1-Titr5, Table 3) and of a blank sample in methanol (only indicator, no HP) are illustrated in Figure 19.

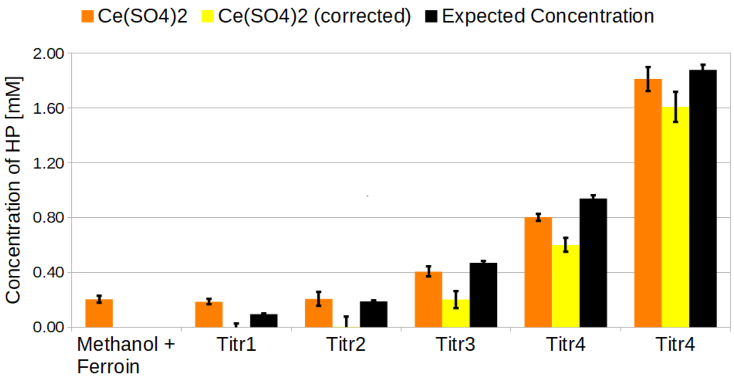

Figure 19: results of cerimetric titrations of HP methanol solutions. The result of the titration of the indicator is reported as the reference. The raw results of the titrations (orange bar) are reported along with those corrected by the amount of titrant consumed by the indicator (yellow bar) and those expected from the dilution ratio (black bar)

The orange bars in Figure 19 represent the raw results of the titrations. For the most diluted solutions (Titr1, 0.093 mM; Titr2, 0.186 mM) the results are higher than the expected ones, but somewhat smaller than the blank. In these two cases the effect of the oxidation of the indicator is quite apparent. If this is taken into account by subtracting the blank from the raw results of all the samples (yellow bars) a systematic underestimation of HP is apparent. It should be appreciated that also the raw results for Titr3-Titr5 gave concentrations somewhat lower than the known ones. The extent of under-estimation becomes relatively smaller as the HP concentration increases and amounts to “only” 15% for Titr5 (1.86 mM), but for Titr4 it already approaches 35%. The results of the titrations of the Stock Solution are illustrated in Figure 20.

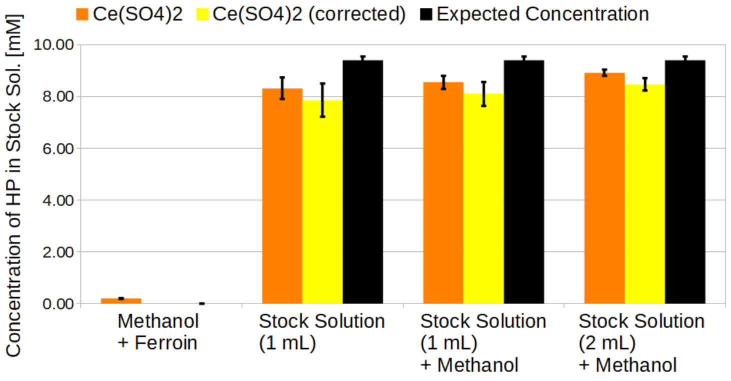

Figure 20: results of cerimetric titrations of the HP aqueous Stock Solution, as prepared and after addition of methanol (1 mL). The result of the titration of the indicator is reported as the reference. The raw results of the titrations (orange bar) are reported along with those corrected by the amount of titrant consumed by the indicator (yellow bar) and those expected from the dilution ratio (black bar).

In this case the Stock Solution was analysed not only as described above (1 mL as such and after the addition of 1 mL of methanol), but also after the addition of the alcohol to 2 mL of the solution. The latter titration confirmed that the higher the amount of HP to be titrated the more accurate is the result. In fact, the cerimetric method still underestimates the HP concentration, but with a double volume of stock solution titrated the gap was 7%, the smallest achieved in these investigations. For the titration of 1 mL of the as prepared Stock Solution and after the addition of 1 mL of methanol, the results are almost the same, showing that methanol oxidation by cerium(IV) does not significantly interfere. In conclusion, the cerimetric titration appears suitable for the quantitative analysis of HP methanol solutions, provided their concentration is higher than 2 mM or large amounts are available. In any case some underestimation should be expected.

2.1.4 Spectrophotometric analysis with titanium oxysulfate

The fourth method commonly reported in the literature for the analysis of reaction mixtures of the DS[169,170] is the indirect measure of the concentration of HP by the spectrophotometric analysis of the peroxidic complex $[Ti(O_2)OH(H_2O)_3]^+_{(aq)}$.[171,172]

This is obtained upon reacting HP with an aqueous solution of $TiOSO_4$.[173]

$$H_2O_2 + TiO^{2+} + H_2O \rightarrow Ti(O_2)(OH)_2 + 2H^+$$

For the evaluation of the method, alcoholic solutions with different HP concentration and containing the same amount of methanol and of an acidic solution of titanium oxysulfate were analysed. These solutions (Vis1-Vis9) were prepared by dilution of the proper amount of solutions Titr1-Titr5 (Table 4).

Table 4: HP solutions for the spectrophotometric analysis. 0.5 mL of $TiOSO_4$ solution have been added to each samples, prepared according to the reported information, before dilution to 10 mL with water. Concentrations refer to the final 10 mL solution, determined with spectrophotometric analysis at 409 nm.

Solution	**Concentration [mM]**	**Preparation**
Vis1	0.00467±0.00016	0.3967 g of Solution Titr1
Vis2	0.0093±0.0005	1 mL of Solution Titr1
Vis3	0.0187±0.0008	1 mL of Solution Titr2
Vis4	0.0467±0.0018	1 mL of Solution Titr3
Vis5	0.093±0.004	1 mL of Solution Titr4
Vis6	0.187±0.007	1 mL of Solution Titr5
Vis7	0.467±0.014	5 mL of Solution Titr4
Vis8	0.933±0.019	1 mL of Stock Solution + 1 mL MeOH
Vis9	1.87±0.05	2 mL of Stock Solution + 1 mL MeOH

The water/methanol ratio is important because the position of the absorption peak of $[Ti(O_2)OH(H_2O)_3]_{+(aq)}$ depends on the solvent. In this work the maximum of absorbance occurred at 409 nm.

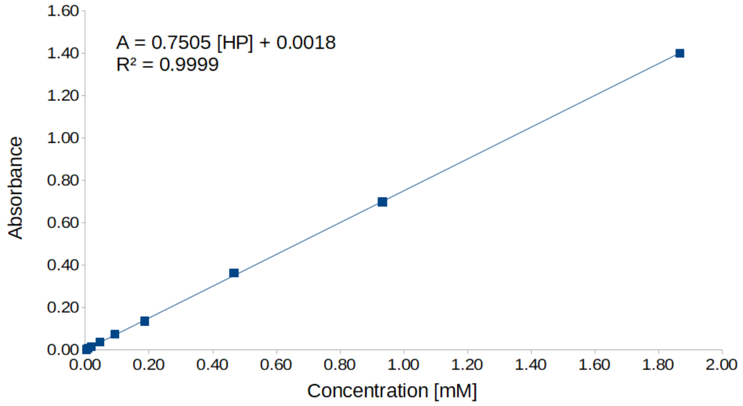

Figure 21: absorbance at 409 nm of the Vis1-Vis9 solutions (Table 4), with linear fit of the data and equation of the curve.

The absorbance (A) at this wavelength was measured for hydro-alcoholic solutions of known concentration (Vis1-Vis9, Table 4) ranging from 4.675 µM (Vis1) to 1.866 mM (Vis9). A linear dependence of the absorbance on the HP concentration was observed in this range (Figure 21). With a further point from a 4.6 mM solution included (A=3.24) the linear fit was still excellent (R^2=0.9989), meaning intermolecular interaction of the chromophore in solution are weak. Accordingly, this method could be suitable for the analysis of HP solutions in a concentration range wider than three orders of magnitude (more concentrated solutions can be simply diluted to achieve measurable absorbance values). Interestingly, in this work no modification of the UV-Vis spectra or precipitation of titanium dioxide was observed in solutions of $[Ti(O_2)OH(H_2O)_3]^+_{(aq)}$ stored at 4°C for 24 hours or more. The precipitation of TiO_2 is matter of concern not only because it would decrease the concentration of $[Ti(O_2)OH(H_2O)_3]^+_{(aq)}$, but also because suspended solids would scatter the radiation and interfere with the spectrophotometric measure. Although Ti(IV) hydrolysis does not appear to be an issue, suspended solids could be present in the DS reaction mixtures as the result of mechanical erosion of the catalyst, depending on its nature and on the design of the experimental set-up. As the fines more effectively scatter light when their size is comparable to the radiation wavelength, their presence cannot be appreciated simply at glance.

Figure 22: samples of reaction mixture at different reaction time, after the addition of $TiOSO_4$ solution, as collected (4, 8 and 12) and after filtration on Teflon syringe filters (4x, 8x and 12x).

Figure 22 shows the pictures of three different DS reaction mixtures, after addition of $TiOSO_4$ solution, collected at different times during a real catalytic run in the semi-batch reactor described later (Paragraph 4.4.2.2). Each of them was syringe-filtered with a Teflon filter (cut-off 450 µm), but nevertheless to the naked eye they appear the same as before filtration. In spite of this, the results of their spectrophotometric analyses are different and clearly affected by light scattering (Figure 23). Due to the overestimation of the absorbance at 409 nm of the unfiltered solutions, the measured amount of HP produced in the reaction (Figure 23, blue line) was overestimated as well, by about 40%, in comparison with the filtered solution (Figure 23, yellow line).

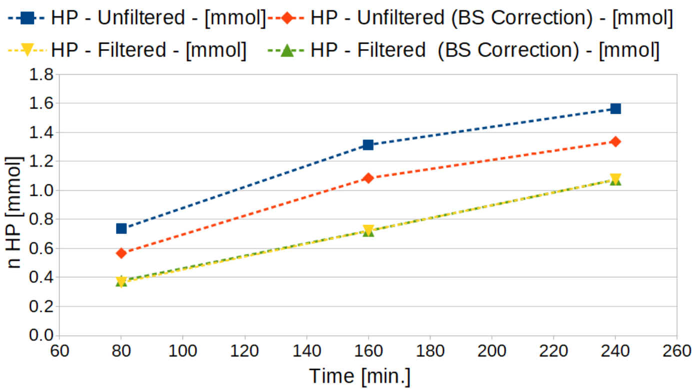

Figure 23: moles of HP determined with spectrophotometric analysis at 409 nm of the as collected samples of reaction mixture (blue curve) and after correction with the absorbance at 800 nm (red curve, see text). As the reference, the results of the spectrophotometric analysis of the samples after filtration are also presented (yellow and green curves).

The red line of Figure 23 was obtained upon subtraction of the absorbance of the $[Ti(O_2)OH(H_2O)_3]^+_{(aq)}$ solutions at 800 nm from the absorbance at 409 nm. This correction would work if the effect of light scattering were the same at every wavelength. This is apparently not the case and the filtration of the solutions is recommended prior the spectrophotometric analysis. If the same subtraction is made on the spectrum of the filtered solution no change in the values of HP as a function of the time reaction is observed (Figure 23, green and yellow lines). This implies that the filtration is enough to completely remove from the solution scattering particles so that the apparent absorbance at 800 nm is practically equal to zero. Moreover, by measuring solution Vis6 in methanol and in a methanol solution containing 94.3 ppm of HBr no difference in the absorbance at 409 nm were recognized, revealing that HBr does not interfere with the spectrophotometric method.

2.1.5 Conclusive remarks on the titration of hydrogen peroxide

In conclusion, spectrophotometric analysis appears a very reliable method for the quantification of alcohol solutions of HP. It can be applied in a large range of HP concentrations and is not affected by interferences arising from the presence of methanol. However, when the design of the experimental set-up or the mechanical properties of the catalyst allow the formation of suspended fines, filtration of the samples to be analysed is recommended to prevent light scattering. Since this method turns out to be the most efficient among those investigated, it was chosen to analyse the HP produced in the DS reaction in this work. Moreover, this investigation allows to better evaluate and to asses the reliability of the literature results, as discussed on Paragraph 1.7. As for the other methods, iodometric titration turns out to be difficult since the amount of acid is fundamental to ensure the reliability of the method, but it should be adjusted knowing a priori the range of HP concentration to be titrated. Conversely, permanganometry must be avoided, as it leads to high overestimation of the analyte concentration. Finally, cerimetric titration is reliable only when a high amount of HP solution is available, which is not the case of the large majority of DS experiments reported in literature.

Chapter 2: Starting point of the project and preliminary investigation

2.2 Introduction of the Chapter

2.2.1 Overview on the preparation of ion-exchange supported catalysts

In this work several catalysts are investigated in the DS, both with the SBR and TBR setups. Some commercially available catalysts, such as Pd/C (1% with eggshell distribution of the metal nanoparticles, Alfa-Aesar) and Pd/Al_2O_3 (1% Alfa-Aesar), were used as benchmarks, whereas different kind of catalysts supported on inorganic materials were provided by co-workers. The palladium catalysts supported on ion-exchange resins represent the main focus of the investigation and are synthesized in our laboratory. The catalysts based on polydivinylbenzene and its derivatives have been syntheses from the polymerization of the support, whereas other ion-exchange supported catalysts were prepared by using commercial ion-exchange resins (Lewatit K2621 ad K1221). The pDVB polymer is synthesized according to literature,[145] by using a solvent-monomer volume ratio of 10:1. The polymerization under solvothermal conditions has been performed by using an autoclave with a Teflon inlet to obtain a monolith, that has been grossly broken and dried under a fume hood for 14 days, with an evident decrease in the volume due to the de-swelling of the material (Figure 24).

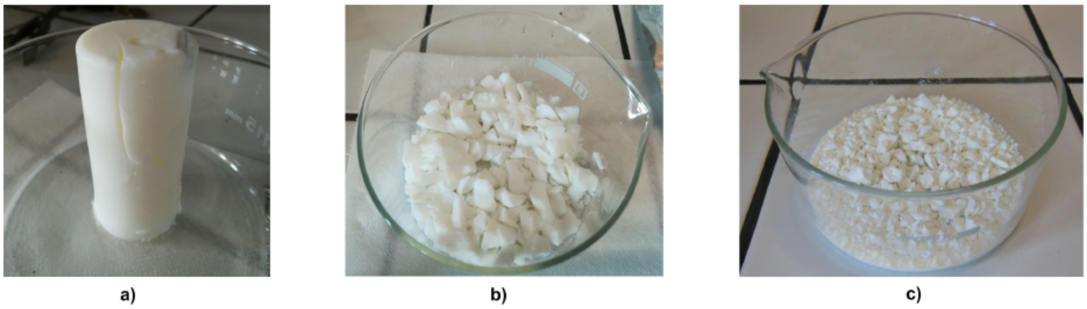

Figure 24: pDVB a) as synthesized, in the form of a monolith, b) ground and swollen, c) ground and dried.

This material has been sulfonated with concentrated sulfuric acid (95-98%), as alternative methods involving chlorosulfonic acid or oleum would form sulfone bridges that crosslink the polymer chains and change the morphology of the material.[174] Before the sulfonation, the polymer is swollen with an excess of 1,2-dichloroethane (15 mL per gram of polymer, Figure 25). In this investigation, this standard procedure has been modified in order to evaluate the effect of the sulfonation procedure on the performance of the resulting catalysts (see Chapter 2).

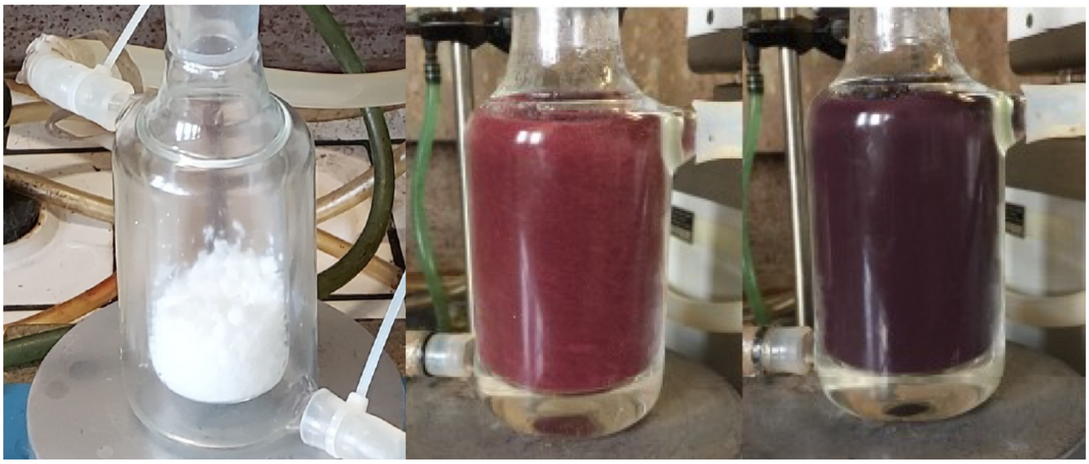

Figure 25: pDVB swollen with 1,2-dichloroethane (left), after the addition of H_2SO_4 (centre) and at the end of the sulfonation procedure.

The palladium precursor, typically $[Pd(NH_3)_4]SO_4$, was introduced into the sulfonated pDVB (SpDVB), as well as the commercial ion-exchangers, by ion-exchange with the sulfonic groups. Then, the materials were reduced with hydrogen in an autoclave. After loading a slurry of the catalyst in THF, the reactor was pressurized at 5 bars and heated at 65°C for 5 hours. This allows to reduce the metal precursor, without neutralizing the acid functionalities, as it occurs when basic reductants, such as sodium borohydride, are used. After reduction, palladium atoms aggregate to form metal nanoparticles, according to past literature (Figure 26).

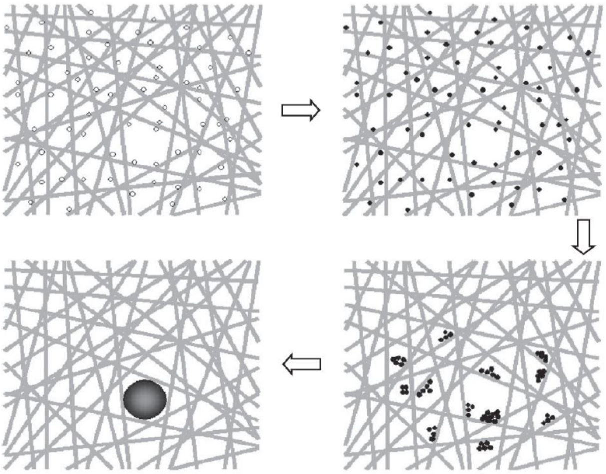

Figure 26: formation of palladium nanoparticles in the polymer framework.[135]

The unfunctionalized pDVB was also used to prepare Pd catalysts impregnation, in order to better evaluate the effect of sulfonic groups in the DS. All these experimental procedures were found to be very reproducible, by evaluating the performances of several batches of catalysts. Further details on the experimental procedures for the syntheses of the catalysts are reported in Paragraph 4.1.

2.2.2 Performances of the benchmark Pd/C catalyst under semi-batch conditions

Most of the outcomes reported in this Thesis were obtained using the SBR setup under very mild conditions (T=25° C and P=1 atm), allowing the investigation of the catalysts in long term experiments. The gas mixture is fed into the reactor by using two different mass-flow controller, ensuring constant flow rates of 1 mL/min and 24 mL/min, for H_2 and O_2. Therefore, the resulting gaseous mixture is not explosive and hydrogen is the limiting reagent. The total volume of the reaction mixture is kept constant to 300 mL for all the experiment and before any experiment the catalyst is swollen with a small amount of the reaction mixture (2-3 mL). This setup makes possible to evaluate the hydrogen consumption almost continuously over time, by periodically sampling the exhausted gas mixture with a micro-gaschromatograph (μ-gc). Further details on the experimental setup are described in Paragraph 4.4. The commercial Pd/C catalyst is used as the reference for the synthesized catalyst. The results of a catalytic experiment with 100 mg of Pd/C are presented in Figure 27, as an example of a typical catalytic experiment reported in this Thesis.

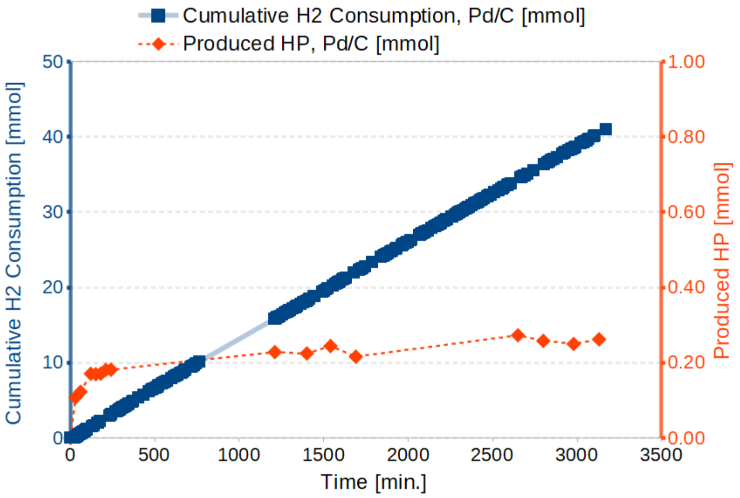

Figure 27: DS catalytic tests with Pd/C in methanol (Blue squares: cumulative hydrogen consumption; red diamonds: HP production).

In the case of Pd/C the cumulative consumption (blue squares) increases linearly over time, thus the catalyst presents a constant conversion of the gas, with no deactivation in the considered range of time. Only a short induction time (about 15 min.) can be observed. More details on the calculation of the consumption of hydrogen are reported on Paragraph 4.4.2.3. The amount of produced hydrogen peroxide (orange diamonds) is determined from the analysis of samples of the reaction mixture. For sake of convenience, the absolute amount of produced HP is reported, instead of the concentration, in order to make easy to qualitatively evaluate the selectivity of the catalyst, by comparing the mole of produced HP with the cumulative consumption of hydrogen. From these data, further parameters defining the performances of a catalyst, such as the H_2 conversion, the HP selectivity and the HP productivity, expressed as mmol of HP produced per gram of Pd, can be obtained. These parameters are obtained according to the following equations:

$$C(\%)=\frac{n_{H_2,cons}}{n_{H_2,\mathrm{FED}}}\cdot 100$$

$$S(\%)=\frac{n_{H_2O_2}}{n_{H_2\mathrm{cons}}}\cdot 100$$

$$P=\frac{n_{H_2O_2}}{m_{Pd}\cdot\Delta t}$$

With $n_{H_2,cons}$ the total moles of H_2 consumed by the catalyst, $n_{H_2,FED}$ the total moles of H_2 fed to the reactor, $n_{H_2O_2}$ the moles of produced HP, m_{Pd} the metal loading in grams and Δt the reaction time; the derivation of the total moles of hydrogen consumed is reported on Paragraph 4.4.2.3. These equations make possible to calculate the parameters defining the performances of Pd/C (Figure 28).

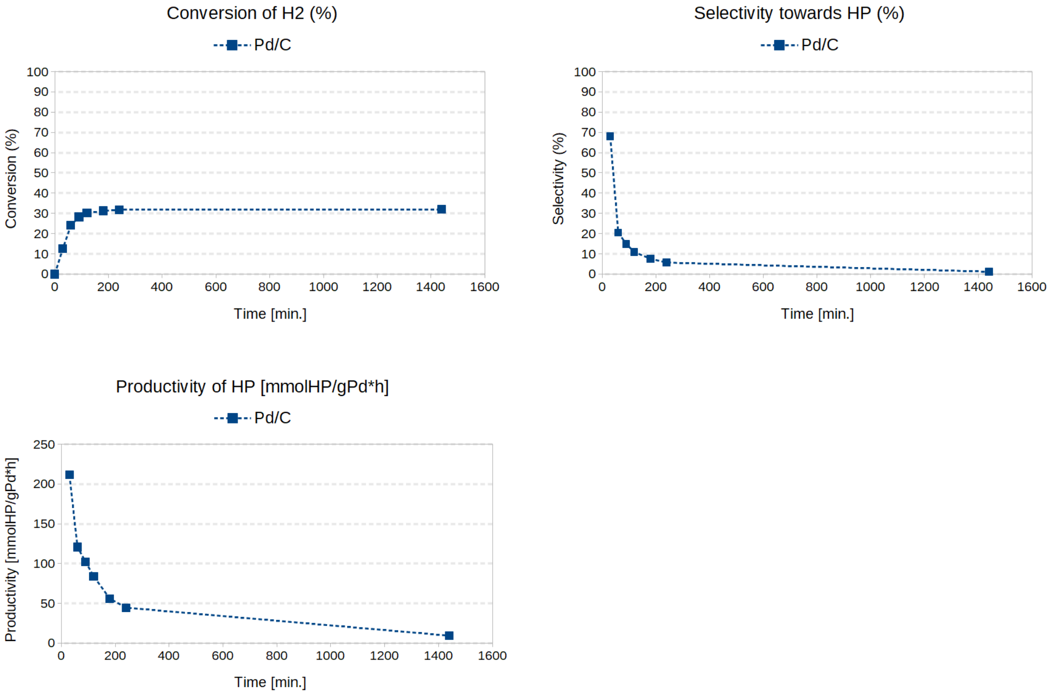

Figure 28: performance of the catalysts (H_2 conversion, upper left; selectivity towards HP, upper right; HP productivity, lower left).

The conversion, selectivity and productivity as defined with the previous equations are cumulative and consider the total amount of hydrogen consumed and hydrogen peroxide produced until a certain time, thus are not instantaneous values. As the consequence, when the consumption of hydrogen is constant over time, a linear trend in the kinetic plot of the cumulative consumption can be observed (Figure 27). Therefore, the conversion reaches a plateau value, slightly below 32% for Pd/C. The selectivity is decreasing over time, as a consequence of the design of the reactor. In fact, as HP is produced, it accumulates in solution and consequently its hydrogenation is more and more probable. Hence, the HP concentration reaches a plateau and the selectivity lowers over time, as the conversion of hydrogen is constant. This behaviour is generally observed in any catalytic experiment with SBR setup.

2.2.3 Summary of the previous investigations

2.2.3.1 Synthesis and characterizations of the polymer supports

Previous unpublished investigations on Pd/SpDVB catalyst were focused on the tuning of the sulfonation procedure and the consequent effect on the performance of the catalyst. The first step of the sulfonation procedure is the swelling with an excess of 1,2-dichloroethane (DCE), to reduce the osmotic stress that develops during the reaction. In fact, pDVB poorly swells in sulfuric acid due to its hydrophobicity, conversely the sulfonated more polar resin can swell in H_2SO_4. Therefore, the osmotic stress can occur during the sulfonation of pDVB, as the consequence of the gradual change in hydrophilicity of the material and of the presence of a very polar sulfonating agent and the consequent extent of the swelling of the material. The preventive swelling of the material in an inert solvent reduces this effect. As long as the sulfonation occurs, the inert solvent, which initially swells the hydrophobic polymer, is displaced by sulfuric acid, solvating the sulfonated domains. As the sulfonation occurs from outside to inside the polymer particles, the formation of sulfonated domains allows the diffusion of sulfuric acid and the counter-flow expulsion of the inert solvent, that poorly interacts with sulfonated polymer. The aforementioned osmotic stress stems from the local mismatch between the different swelling degrees of different fractions of the polymer. In fact, the polymer can be swollen by sulfuric acid in the sulfonated domain, by the swelling solvent in the unfunctionalized domains or can be not swollen in the case the amount of swelling solvent is not enough to completely swell the material. This generates an osmotic stress in the material and can damage the structure of the polymer.[126,175] In the previous work, the osmotic stress on the polymer was intentionally induced by carrying out the sulfonation under conditions of partial swelling. This was made by using amounts of DCE, insufficient to completely swell the pDVB matrix, and by exploiting a solvent that boils below the temperature used in the sulfonation procedure (namely dichloromethane, DCM) in order to enhance the de-swelling of the polymer, Moreover, the highest possible osmotic stress has been exerted by carrying on the sulfonation process without any swelling solvent. These catalysts were characterized in this Thesis, with particular attention both to the nanostructured metal phase and the polymer support. The Specific Absorbed Volume (SAV) values of pDVB in DCE and DCM are summarized in Table 6. By considering 2 g of pDVB were usually exploited for the sulfonation, 30 mL of DCE are enough to ensure the complete swelling of the material, whereas 10 mL is almost half of the volume required to the polymer sample. The batches of the sulfonic pDVB (SpDVB) synthesized by changing kind and amount of swelling solvent during the sulfonation and characterized in this Thesis are described in Table 5.

Table 5: sulfonated pDVB characterized in this work [a].

#	**Label**	**Specific Ion-exchange capacity (SIEC) [mmolH$^+$/g] [b]**	**Description**
1	E30SpDVB	2.15 -2.30 (34-37%)	Sulfonated after swelling with 30 mL of DCE
2	E10SpDVB	2.10-2.19 (33-35%)	Sulfonated after swelling with 10 mL of DCE
3	M10SpDVB	1.78 -1.97 (27-30%)	Sulfonated after swelling with 10 mL of DCM
4	SA100SpDVB	1.96-2.29 (30-37%)	Sulfonated with 100 mL of H_2SO_4 and no swelling

a: the two values reported are referred to different synthetic batches, produced to ensure the reproducibility of the synthesis; b: in parentheses the fraction of sulfonated aromatic rings, assuming one sulfonic group per ring.

The standard sulfonation procedure provided the material, E30SpDVB, with the highest value of the specific ion-exchange capacity (SIEC), although less than half of the aromatic rings were singularly sulfonated. Although the difference is limited (less than 5%), the reduction of the amount of DCE from 30 to 10 mL leads to a slight reduction of the IEC in E10SpDVB. This might be due to the incomplete swelling of pDVB during the sulfonation. It can be supposed that as long as the sulfonation occurs, the DCE moves from the sulfonated (hydrophilic) fraction of the material towards the unswollen (hydrophobic), hence reducing the damage caused by the osmotic stress. A clearly lower sulfonation degree is achieved when DCM is used as swelling agent instead of DCE, to prepare M10SpDVB, the ion-exchange capacity of which is lowered by about 18%. Not only the amount of DCM is lower than needed to obtain the full swelling of the resin sample, but it is also very volatile. As the sulfonation reaction is performed at 80°C, some DCM is expelled not only upon displacement by H_2SO_4 from the sulfonated domains of the polymer framework, but arguably also upon evaporation from unsulfonated regions, leaving a larger portion of the pore system unavailable for the functionalization. When the sulfonation is performed without the organic swelling solvents, the resulting material (SA100SpDVB) is a brown powder spotted by dark, seemingly charred regions which are more tough than the remaining material. This heterogeneous appearance suggests a poorly controlled reaction, which is in line with the relatively poor reproducibility of the SIEC (Table 5) and SAV values (Table 6) for two different batches of SA100SpDVB obtained by sulfonation of the same material. The latter ones not only show relatively high difference to each other, but also a loss of porosity in comparison with the other materials.

Table 6: Specific Absorbed Volume (SAV) of pDVB and different batches of SpDVB.[a]

#	Polymer	DCE	DCM	MeOH
1	pDVB	9.2 mL/g	8.8 mL/g	–
2	E30SpDVB	–	–	3.5-3.6
3	E10SpDVB	–	–	3.7-3.8
4	M10SpDVB	–	–	3.5-3.5
5	SA100SpDVB	–	–	2.2-2.8

a: different values were taken from batches of the same sample prepared independently from one another.

The dry-state specific surface areas (A_g) of the materials were also measured upon nitrogen physisorption (Table 7).

Table 7: BET characterization of pDVB and different batches of SpDVB.[a]

#	Polymer	A_g [BET, m^2/g]		$\overline{A}_g$ [BET, m^2/g]		Percent change of the $\overline{A}_g$	
		Batch 1	Batch 2	Batch 1	Batch 2	Batch 1	Batch 2
1	pDVB	1223		1223		–	
2	E30SpDVB	717	745	881	904	-28	-26
3	E10SpDVB	667	689	803	837	-34	-28
4	M10SpDVB	643	689	764	820	-37	-33
5	SA100SpDVB	658	868	807	1062	-37	-13

a: different values were taken from batches of the same sample prepared independently from one another.

According to the literature, the unfunctionalized polymer (pDVB) presents a very high specific surface area (A_g), that appears higher than the reference value (1092 m^2/g).[145] As a general trend, the sulfonation reaction causes the reduction of A_g. This is in part only apparent, because the formal addition of SO_3 to some monomeric units implies the increase of their average formula weight, thus for the proper assessment of the differences between one material and another the A_g values are better referred to the mass of unfunctionalized pDVB which they contain, hereafter labelled as $\overline{A}_g$ and which can be readily calculated from the values of the respective SIECs and the “gross” specific surface area. For each sulfonic resin the couples of $\overline{A}_g$ values obtained from independently prepared batches are comparable, which suggests that the sulfonation procedures are well reproducible. $\overline{A}_g$ for E30SpDVB, E10SpDVB and M10SpDVB are anyway much lower than for pDVB. This suggests a real decrease of A_g in the sulfonated samples of pDVB, which can be attributed to the physical damage to the resin, due to the osmotic stress during the sulfonation. The data of Table 7 also show that $\overline{A}_g$ decreases in the order E30SpDVB> E10SpDVB> M10SpDVB, so that the extent of the osmotic stress arguably goes the other way round, as expected. The $\overline{A}_g$ values obtained for the two samples of SA100SpDVB are ambiguous, because they correspond to the highest and the smallest osmotic stress level observed in our experiments. This highlights the little reproducibility of the sulfonation without any swelling solvent, which is reason why SA100SpDVB was discarded for further testing, whereas all the other materials were used to produce Pd catalyst with 1% w/w metal loading.

Table 8: features of the palladium catalysts for the DS of HP employed in this work.

Catalyst	**Catalytic support**	**Preparation procedure**
Pd/E30SpDVB	Ion-exchange resin	Ion-exchange+H_2 reduction
Pd/E10SpDVB	Ion-exchange resin	Ion-exchange+H_2 reduction
Pd/ M10SpDVB	Ion-exchange resin	Ion-exchange+H_2 reduction
Pd/pDVB	Non-sulfonated pDVB	Impregnation+reduction with $NaBH_4$

a: this catalyst is the only already investigated by Frison et al.[141] *However, according to Chapter 1, the results reported could be affected by errors connected to the determination of* H_2O_2 *with iodometric titration.*

2.2.3.2 Synthesis and characterizations of the metal nanoparticles

The particles size distribution obtained by TEM characterization of the first Pd/SpDVB catalyst, i.e. Pd/E30SpDVB, were already reported by Frison et al.[141] and are summarized in Figure 29, together with the TEM characterization of the Pd/C catalyst used in this work.

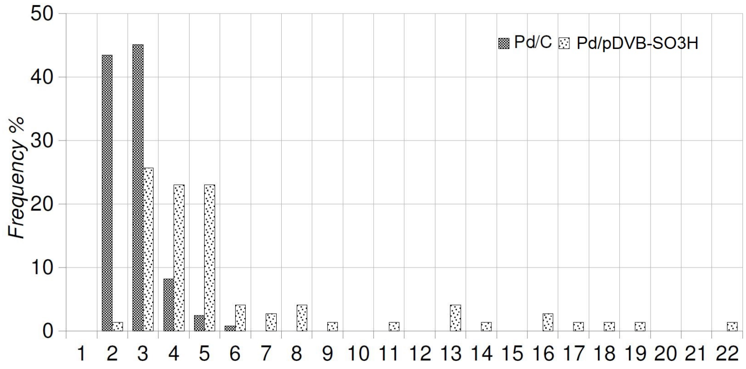

Figure 29: dimensional distribution of Pd/E30SpDVB (labelled as Pd/pDVB-SO3H) and Pd/C, obtained from TEM characterization of the catalysts.[141]

The XRD characterization of the SpDVB supported catalysts synthesized in this work is reported in Figure 30 and Table 9.

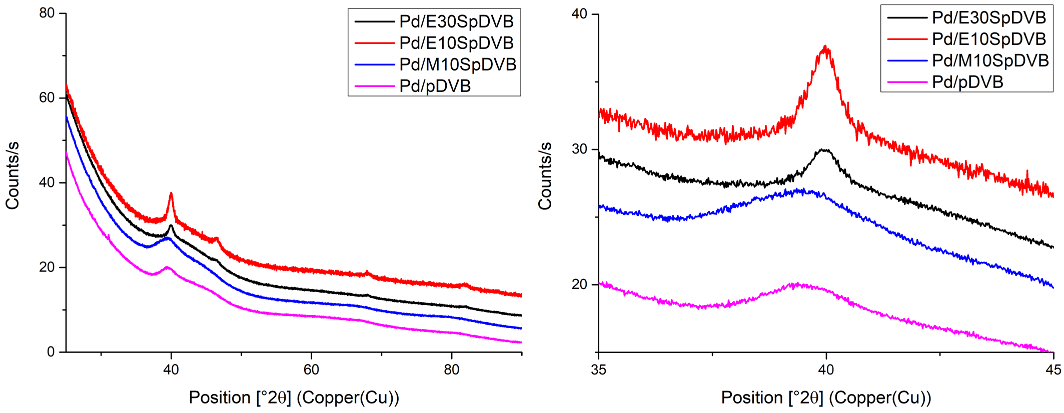

Figure 30: XRD characterization of the catalysts before the catalytic experiment.

Table 9: average nanoparticle size calculated with the Scherrer equation from the half-width of the peaks at 2θ ≈ 40° in the XRD powder spectra of Pd/E30SpDVB, Pd/E10SpDVB, PdM10/SpDVB and Pd/pDVB.

Catalyst	**FWHM**	**Average Pd dimension [nm]** [a]
1 – Pd/E30SpDVB	0.786	12 (4-6, average value not specified)
2 – Pd/E10SpDVB	0.727	13
3 – Pd/M10SpDVB	2.87	3 (4.7)
4 – Pd/pDVB	2.19	3.9 (5.7)

a: nanoparticle size from TEM in parentheses, where available.

The Scherrer analysis of the half-width of the peaks (Table 9) shows that within each pair of catalysts the palladium nanoparticles are more or less equally sized (1, 2 and 3, 4), but for the first pair they are larger (12-13 nm) than for the second one (3-4 nm). In addition the small, but clearly appreciable, shift to lower 2θ values of the most intense reflection of Pd/M10SpDVB and Pd/pDVB suggests that in their small nanoparticles the interatomic distances are somewhat higher than in Pd/E30SpDVB and Pd/E10SpDVB.

This expansion is counter-intuitive because in nanostructured metals the surface atoms are pulled inwards by bonding with the lattice atoms and this generally brings out the contraction of the lattice parameters. The relaxation observed herein could be explained either by the interaction of the metal surface with the support, strong enough to off-set the pulling action of the inner bonds, or by the presence of guest atoms in its interior. The supports of Pd/M10SpDVB and Pd/pDVB are the least sulfonated ones (pDVB in fact not at all). This suggests that if any metal-support interaction takes place, the relatively electron-rich, non substituted aromatic rings could be responsible of the nanoparticle relaxation. However, taking into account literature data on the adsorption of benzene on the Pd(111) surface, this seems very unlikely.[176] The strongest interaction is observed for adsorbed C_6H_6 molecules laying flat on the surface, which implies saturation at $\Theta=0.13$. For flat adsorbate molecule the desorption heat was estimated in 95 $KJ\cdot mol^{-1}$ for $0.09<\Theta<0.13$ (β-state) and in 130 $KJ\cdot mol^{-1}$ when $0.05<\Theta<0.09$ (γ-state). As the sublimation heat of benzene is 44 $KJ\cdot mol^{-1}$, its heat of adsorption on Pd(111) is only 2-3 times larger. Moreover, in our case the aromatic rings are embedded into the stereochemically rigid polymer framework and this of course should strongly restrict their ability to be adsorbed parallel to the metal surface. In fact also the adsorption of tilted benzene molecules was detected by Tysoe and co-workers (α-state), and cannot be therefore ruled out, but their interaction with the metal surface is much weaker. Although for the α-state of adsorbed benzene Tysoe and co-workers did not report any value of the heat of desorption, they found that its desorption peak was centred around 280 K much lower than the maxima for the β-state (380 K) and of the γ-state (520 K).[176]

Accordingly, it can be argued that the nanoparticle expansion observed for PdM10/SpDVB and Pd/pDVB is rather brought out by an interstitial guest element in the lattice. Hydrogen is the best candidate, because all the XRD data and the TEM data (see below) rule out the presence of any PdO phase. Moreover, the catalysts are prepared with a final reduction step in which the slurries of the catalysts precursors in THF are treated with H_2 at 304 KPa whereby the formation of PdH_x phases is feasible.[56,177] The TEM characterization of Pd/pDVB and of PdM10/SpDVB (Figure 31) is in agreement with the XRD data. The assessment of their nanoparticle size yields larger values which than the Scherrer analysis, but still in the correct order (Pd/pDVB > Pd/M10SpDVB) and smaller than in Pd/E30SpDVB and in Pd/E10SpDVB. However, in Pd/E30SpDVB it is reported a small number of nanoparticles with diameter up to 22 nm that can more significantly contribute to the peak width rather than a larger number of smaller particles, due to the bigger dimension of the crystallite. Finally, A more detailed analysis for Pd/M10SpDVB supports the occurrence of the nanoparticle expansion and is compatible with the formation of α-PdH_x (Figure 32 and Table 10).

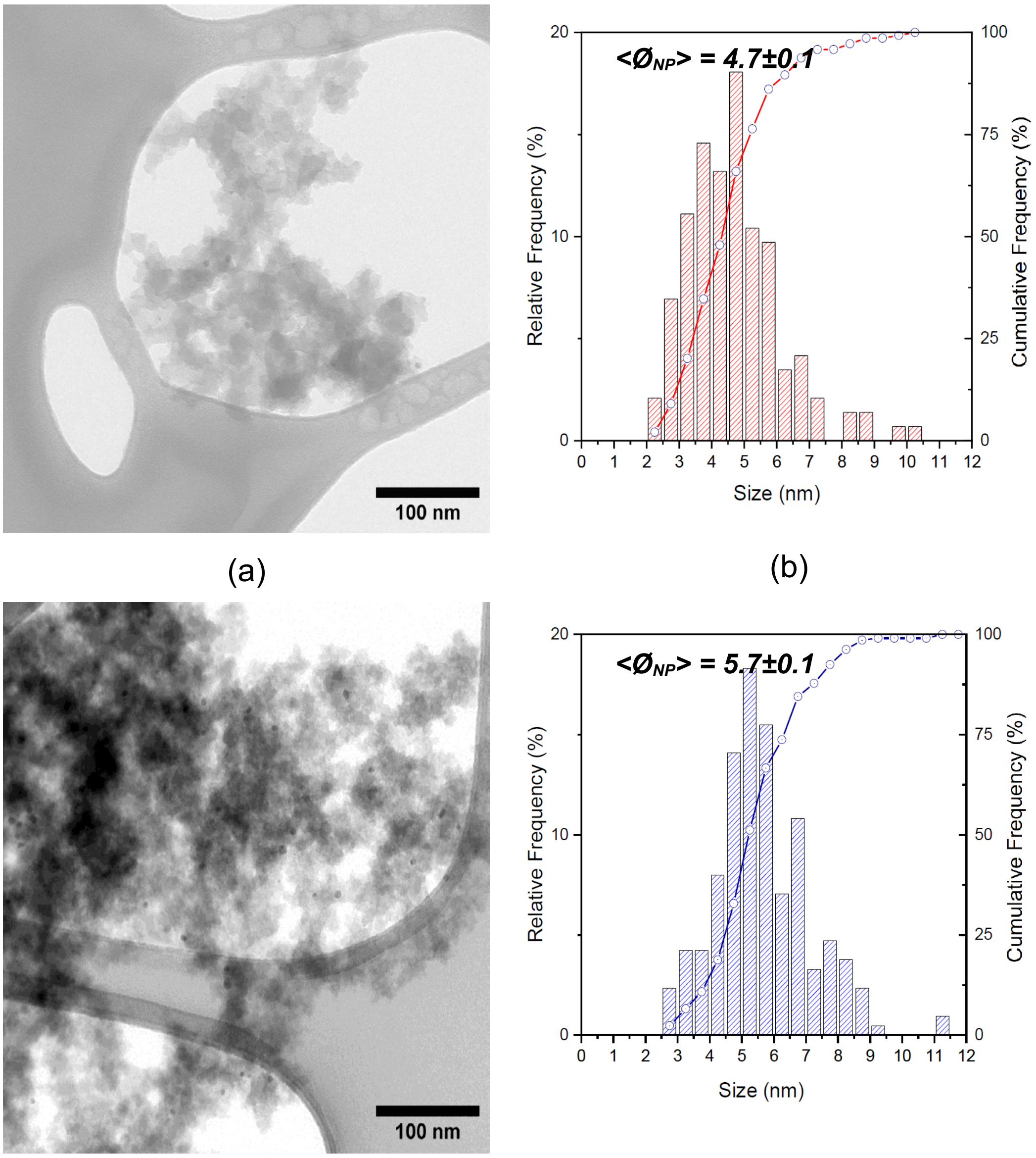

(a) (b)

(c) (d)

Figure 31. low resolution TEM micrographs and nanoparticle size statistics of Pd/pDVB (a, b) and PdM10/SpDVB (c, d).

The selected area electron diffraction (SAED) of Pd/M10SpDVB from an image field of roughly $6.4 \cdot 10^4$ nm^2 (more or less 50 % covered by the sample, Figure 3) shows a consistent increase of the d-spacings for all the detectable planes approaching the values of the β-PdH$_x$ phase. The observed expansion was 2.3 % in the 111 and 002 directions and 1.7 % for the 222 planes, which is comparable to, but not as high as, the values very recently reported by Zhao et al. for β-PdH$_x$ embedded in CuO matrices.[178] On the one hand this fully confirms the absence of any PdO phase and on the other one it suggests that α-PdH_x was formed, which features an almost unaltered metal lattice hosting H atoms.[56,179] Grundwaldt and co-workers were able to distinguish between α- and β-PdH_x from subtle features of the XANES spectra of some palladium catalysts of theirs.[56] On date we have no XANES data available, but the combination of the XRD and TEM characterization of PdM10/SpDVB nevertheless rules out other possible explanations. We also attempted the FFT analysis on a portion of a HR-TEM image of a single nanoparticle of Pd/M10SpDVB. In the above reported case of Zhao et al.,[178] this analysis was in line with SAED of the same sample. This was not the case for Pd/M10SpDVB for which a contraction of 1.7 % with respect to palladium was recorded. Even though one of the largest particle of this catalyst was selected, it is much smaller and apparently less crystalline than those obtained and observed by Zhao et al. in much more defined HR-images than it was possible to obtain in our case. In this context we were not able to extract d-spacing valued directly from the distance of atomic rows in the TEM micrograph. Thus we believe that in present case the results from the analysis of single particles are less reliable than data recorded for a large collection (XRD, SAED), which militate for the presence of a PdH_x. In this context further work is needed in order to provide further and possibly ultimate support to this conclusion.

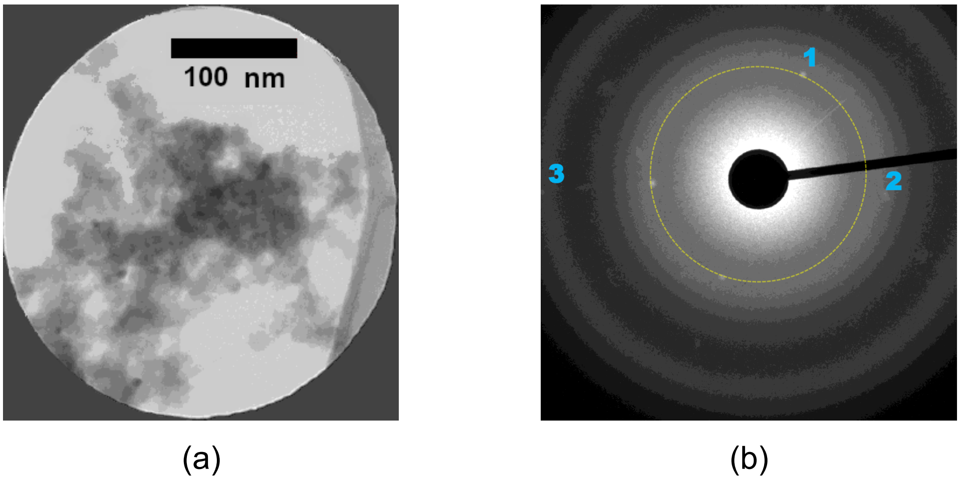

(a) (b)

Figure 32. SAED analysis of Pd/M10SpDVB.

Table 10: results of SAED analysis of Pd/M10SpDVB.

Spot	D-spacing [nm]		
	Pd	PdH_x	exp.
1	0.2246 (111)	0.2321 (111)	0.2299
2	0.1945 (002)	0.2010 (022)	0.1996
3	0.1123 (222)	0.1160 (222)	0.1143

2.2.3.3 Results of the catalytic experiments – *effect of the sulfonation procedure*

The performances in the DS reaction of the catalysts produced by tuning the sulfonation procedure were tested before the characterization implemented with this work. In Figure 33 are reported the results of the catalytic experiments, together with those of the reference catalyst, Pd/C.

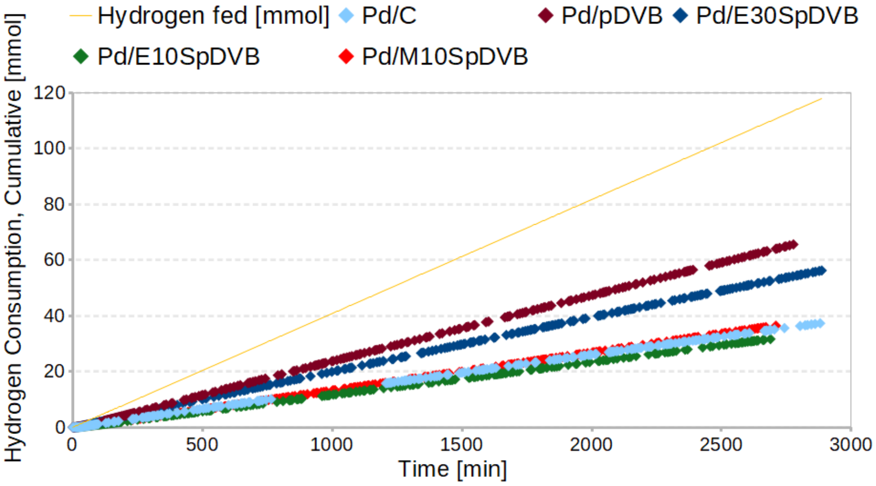

Figure 33: cumulative hydrogen consumption of catalysts on several polymer supports, prepared with different sulfonation procedures.

All the catalytic experiments were carried at least 2650 min, since these “long-runs” are particularly useful to appreciate the evolution of the catalysts with time and the changes, if any, of their performances.

Figure 33 illustrates the cumulative hydrogen consumption with Pd/E30SpDVB, Pd/E10SpDVB, Pd/M10SpDVB, Pd/pDVB and Pd/C and these plots are extremely useful to appreciate at a glance the differences of catalytic activity from their slopes. They are all almost perfectly linear with time, indicating a constant rate of H_2 consumption, i.e. a steady conversion, although for Pd/pDVB and Pd/E30SpDVB a slight increase of the slope is observed. The cumulative production of HP is illustrated in Figure 34 (full test, upper panel; up to 240 min, lower panel).

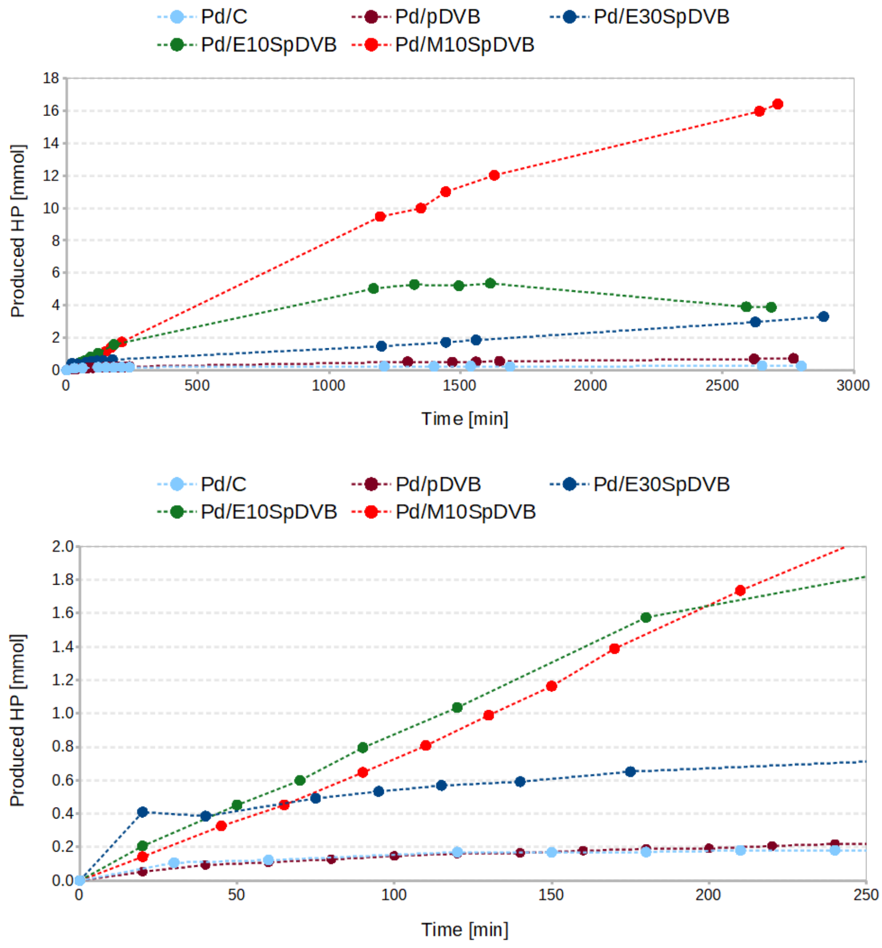

Figure 34: cumulative hydrogen peroxide production for different catalysts at the end of the test (upper panel) and after 240 min (lower panel).

In spite of consuming H_2 much faster than the other catalysts, Pd/pDVB shows the lowest production of HP, hence it is by far the least selective of the set investigated here. The parameters that better describe the catalysts performance are reported in Figure 35.

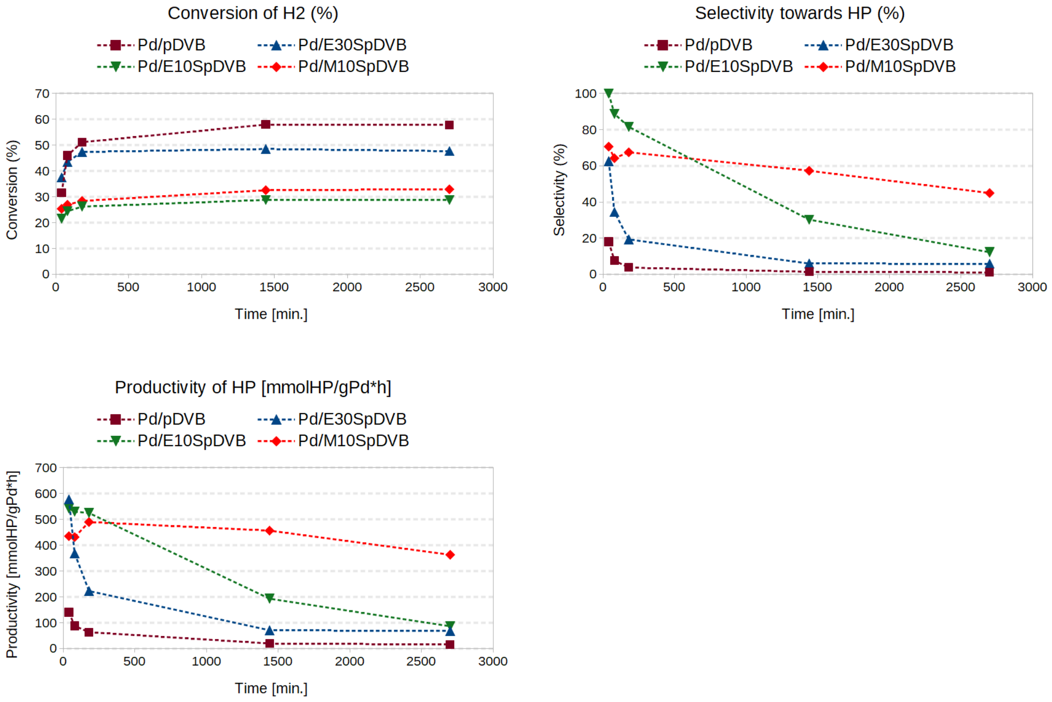

Figure 35: performance of the catalysts (H_2 conversion, upper left; selectivity towards HP, upper right; HP productivity, lower left).

In spite of their lower activity the catalysts based on sulfonated pDVB presents higher selectivity and yields in HP (Figure 7). Although both these parameters decline with time for all the catalysts, the sulfonated ones are consistently more selective and productive from the beginning to the end of the reaction. In general this shows the beneficial role of the sulfonic groups, but there are differences from one catalyst to another. In particular Pd/E10SpDVB and Pd/M10SpDVB, which are based on the supports sulfonated under the conditions of highest osmotic stress, have similar activity and selectivity towards HP in the first four hours of reaction and clearly outperform Pd/E30SpDVB, featured by a somewhat higher sulfonation degree. This suggests that the degree of sulfonation, provided it is high enough, is not the only key parameter for controlling the catalytic performance.

In fact Pd/M10SpDVB and Pd/E10SpDVB have similar sulfonation degrees, but their behaviour is different. Whereas the former is still productive at the end of the test (2770 min, Figure 34) only a moderate decrease of actual selectivity after about 1200 min and an averaged final value of about 50 %, the latter stops producing HP after about 1200 min (Figure 5). The XRD characterization of these two catalysts (Figure 30) shows that the active phase is different in the fresh materials, with Pd/M10SpDVB featured by the presence of PdH_x, most likely of the α-type. However, the relatively high selectivity and productivity of Pd/M10SpDVB cannot be attributed to the presence of PdH_x, or not completely. In fact XRD spectrum of Pd/pDVB shows that they are present also in this catalyst, which is very poor as far HP production is concerned. Therefore a good performance cannot be given for granted only by the initial presence of PdH_x in the catalyst. This is also supported by the comparison of Pd/M10SpDVB and Pd/E10SpDVB at the beginning of the reaction, with the latter better behaving up to 180 min.

2.2.3.4 Ex-situ characterization of the exhausted catalysts

The XRD spectra of exhausted Pd/M10SpDVB and Pd/pDVB are almost superimposable to those of the fresh samples, which suggests that the α-PdH_x phase is still present (Figure 36).

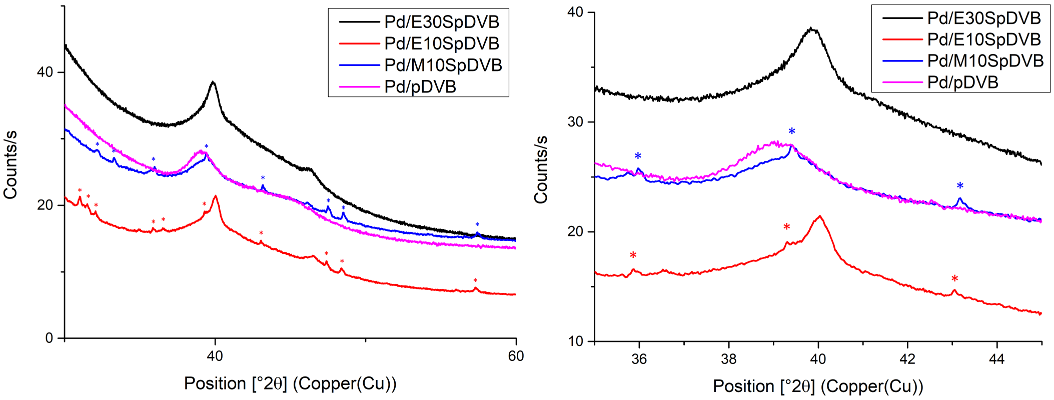

*Figure 36: XRD characterization of the catalysts after the catalytic test. Small peaks marked with a * in the blue and red spectra are due to calcite contaminations during the preparation of the samples.*

The existence of PdH_x species in catalysts for the DS with lean H_2/O_2 mixtures is somewhat counter-intuitive in that there is plenty of O_2 to oxidize them. However, under H_2 lean conditions Grünwaldt and co-workers were able to track with operando XAS the formation of α-PdH$_x$ in the bulk of palladium nanoparticles during the DS,[56] with some oxygen found only on the surface of the metal. In the investigations presented later on in this Thesis, some evidence of increasing Pd$^{(II)}$/Pd$^{(0)}$ from XPS spectra of exhausted catalysts were gathered. However, the TEM characterization did not show any hint of the presence of oxidized palladium phases (see Paragraph 2.3.2.4). This was attributed to the different regions of the materials probed by XPS (a surface technique) and TEM and to the circumstance that some oxidation can take place only in a small fraction of the catalysts involving an as well small fraction of the metal. This is in agreement with the above mentioned finding by Grünwaldt and co-workers of only small amounts of oxygen on the surface of the active nanoparticles of DS palladium catalysts.

Whereas differences, if any, between the XRD spectra of fresh and exhausted Pd/M10SpDVB and Pd/pDVB are negligible, the main peak (2θ ≈ 40°) of the XRD spectra of exhausted Pd/E30SpDVB and Pd/E10SpDVB show some broadening in comparison with the fresh catalysts (Figure 36). This suggests the presence of some overlap with a component at smaller 2θ values.

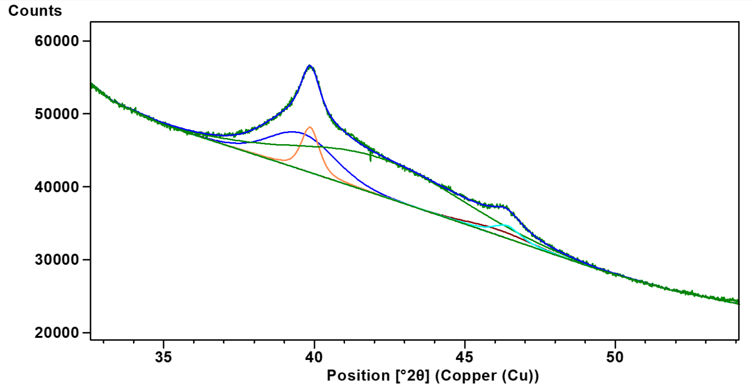

Figure 37: fit of diffraction peaks of Pd/E30SpDVB (green line: experimental data; light green background diffraction from the support; blue and brown lines: components from expanded Pd lattice; orange and light blue lines: components from metallic Pd; blue line: sum of the components of the fit).

The analysis of this peak for exhausted Pd/E30SpDVB (Figure 37) shows a broad contribution where the main peak is observed for Pd/M10SpDVB and Pd/pDVB overlapping with a sharper contribution in the same position of the signal from the fresh catalyst and with a very broad contribution attributed to the background diffraction of the support. The quantitative estimation of these contributions is not reliable at all, but it can be concluded that both Pd/E30SpDVB and Pd/E10SpDVB undergo a partial reconstruction of the metal phase under duty, which leads to the formation of smaller, more expanded nanoparticles likely containing hydrogen guest atoms. The reconstruction of the Pd/E30SpDVB catalyst under DS are deeply discussed below (Paragraph 2.3.2.1), presenting more extensive investigations of this catalyst.

2.2.3.5 Formation of peroxides on ion-exchange resins by auto-oxidation reaction.

Literature investigations report on the poly-styrene degradation by dioxygen from air to form hydroperoxy groups bound to the benzylic positions of the polymer chains. It was pointed out that this mechanism of degradation can occur under very harsh condition (100° C for 270 hours), or in the presence of UV radiation.[180] In this context the benzylic C-H bonds are particularly reactive because of the relative stability of the benzylic radicals, which are the intermediate of the auto-oxidation (AO) reaction. This kind of reactivity is on the basis of the production of phenol and acetone with the cumene process (Hock process).[181] Not only the formation of benzyl hydroperoxide could occur also in the sulfonic poly-styrene resins largely employed as ion-exchangers, but it was also for ion-exchange membranes, after degradation by radicals and HP.[182] From this, the issue on a possible degradation of the polymer support during the DS has risen, since in the oxidative environment the polymer support could both get damaged or produce HP as by-product of its degradation. With the investigations preceding this work this circumstance was confirmed, as it was discovered that, by the simple suspension in a protic solvent under air at atmospheric pressure, ion-exchange resins can form small amounts of HP. Although this behaviour is more evident with alcohols, such as methanol or ethanol, it can occur to a smaller extent also in water. This phenomenon, that is related to the presence of atmospheric oxygen, is much more consistent with SpDVB than with other commercial ion-exchange resins, as in 72 hours about 0.6 mmol of HP are formed per gram of material. For sake of comparison, with the commercial macroporous sulfonic resin K2621 only 0.1 mmol of HP per gram of material are formed. This is likely due to the more strained and therefore stressed structure of the polymer chains, making the material more reactive.[183] Some EPR investigations of E30SpDVB and the corresponding Pd catalyst before and after a catalytic experiment showed the presence of radicals in the polymer matrix, even before the DS, and formation of new radical species under duty. In this sense, the catalytic support could contribute to the overall production of HP, with a mechanism likely similar to that of formation of hydroperoxides in the Hock process by auto-oxidation reaction (Figure 38), that eventually leads to the formation of HP.

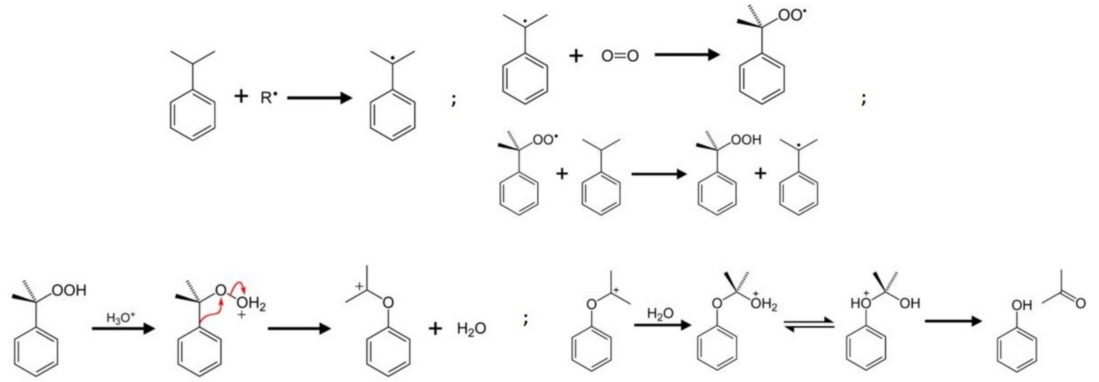

Figure 38: reaction mechanism of the Hock process for the production of phenol and acetone.

The g factor of the radical species detected on the pristine material and on the catalyst after a DS test are compatible with a carbon radical and an oxygen radical, precursor of hydroperoxyl species, respectively. The evolution of those species towards hydrogen peroxide is not yet unravelled, nevertheless the supported hydroperoxides are the most suitable precursors of HP. This mechanism of production of HP is pretty interesting and could have very important outcomes in the frame of the application of ion-exchangers. However, in the case of the DS the production of HP by the support is of a very small extent and since there are no direct proof of the mechanism to be catalytic, this can slightly contribute to the overall synthesis of hydrogen peroxide.

2.2.3.6 Conclusions remarks on the preliminary investigations

In former investigations the effect of the sulfonation procedure on the morphology of the catalytic support and on the performance of the corresponding Pd catalysts in the DS were studied. The damages of the polymer structure, induced by the osmotic stress during the synthesis, make the supported catalyst to be more active in the production of HP. However, the stability of the most damaged support needs to be deeply investigated and is out of the scope of this project. As to the investigations on novel selectivity enhancers, Pd/E30SpDVB was selected, due to its high stability (and reproducibility), resulting from the absence of osmotic stress damages. Moreover, as this catalyst is the less performant in the production of HP among the series of SpDVB supported catalysts, a potentially positive effect of selectivity enhancers is more evident. Hence, in investigation on the effect of coordinating solvents on the DS the catalyst Pd/E30SpDVB, for sake of simplicity coded as Pd/SpDVB, is used. The XRD and SAED characterizations of the materials show the probable presence of a PdH_x phase in some catalysts, but on the basis of the current evidences there is no correlation between the presence of this peculiar Pd form and the performance of the catalyst. However, thanks to these investigations, a first evidence on the reconstruction of the metal phase was obtained. The formation of HP from the catalytic support, although quite surprising, appears poorly relevant to the overall catalytic behaviour of the materials. In fact, with the SBR setup HP concentration typically reaches a steady state, clearly indicating that the HP production and consumption rates are equal. These rates are much higher than the HP production by the polymer, that takes days to be appreciable. Therefore, in the case the HP production rate on the polymer support is particularly slow, the productivity is mainly due to the metal phase of the catalyst.

Chapter 3: Coordinating solvents as selectivity enhancers: preliminary investigations with acetonitrile

2.3 Introduction to the promotion effect of acetonitrile

As briefly discussed in Paragraph 1.7 the effect of acetonitrile (ACN) on the DS is investigated with this work, as it shares the ligand properties of the most common selectivity enhancers, namely halides, without presenting the drawbacks of corrosion and leaching. Its effect was evaluated by using the selected enhancer as a co-solvent together with methanol, as a protic solvent is needed in the reaction and water is not suitable due to the low solubility of the reagent gases. Several monometallic palladium catalysts, supported on cationic commercial ion-exchange resins and pDVB were tested, along commercial Pd/C and Pd/Al_2O_3 catalysts, considered as the reference. The catalysts were investigated in long catalytic experiments (t ≥ 48 h) with the SBR setup.

2.3.1 Effect of acetonitrile of Pd/C

In the previous work of Frison et al.[141] the commercial Pd/C catalyst (1% w/w of palladium, with egg-shell metal distribution) was already tested in the DS with a 4 hours catalytic experiment. The catalyst showed a good H_2 conversion but a poor selectivity towards HP, under conditions strictly comparable to those employed herein, apart from the absence of acetonitrile. The results of the catalytic experiment with Pd/C with pure methanol or methanol with 10% of ACN as the co-solvent are reported in Figure 39. Moreover, to compare these experiments with the results obtained with palladium supported on ion-exchangers in acid form, a further catalytic test in the presence of 0.6 M H_2SO_4 was carried. The acid concentration chosen for this experiment is representative of the concentration of H^+ (about 2.5 mmol·g^{-1}) inside the resin (developing a specific volume of about 4.5 mL·g^{-1} when swollen with methanol).

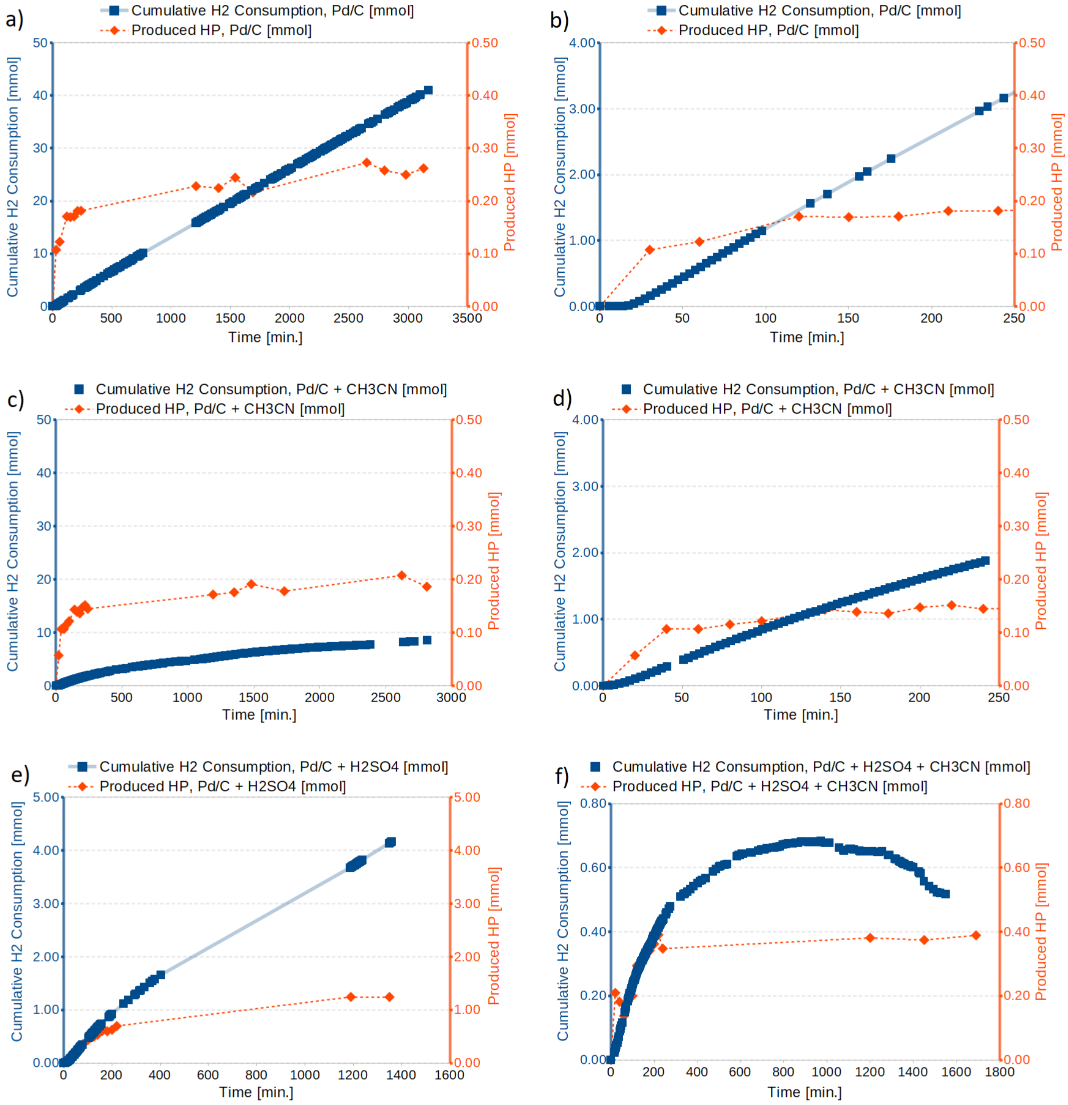

Figure 39: DS catalytic tests with Pd/C in methanol (a, b), in methanol:acetonitrile 9:1 vol (c, d), in methanol with 0.6 M of H_2SO_4 (e) and in methanol:acetonitrile 9:1 vol and 0.6 M H_2SO_4 (f) (Blue squares: cumulative hydrogen consumption; red diamonds: HP production).

In the case of pure methanol as the solvent, during the first 240 min the conversion of H_2 (i.e. its consumption rate) steadily increases and stabilizes at a constant value. Conversely, when acetonitrile is present, Pd/C clearly undergoes to a deactivation. At the beginning, acetonitrile reduces the conversion of hydrogen at any time lower, although steadily increasing (Figure 40).

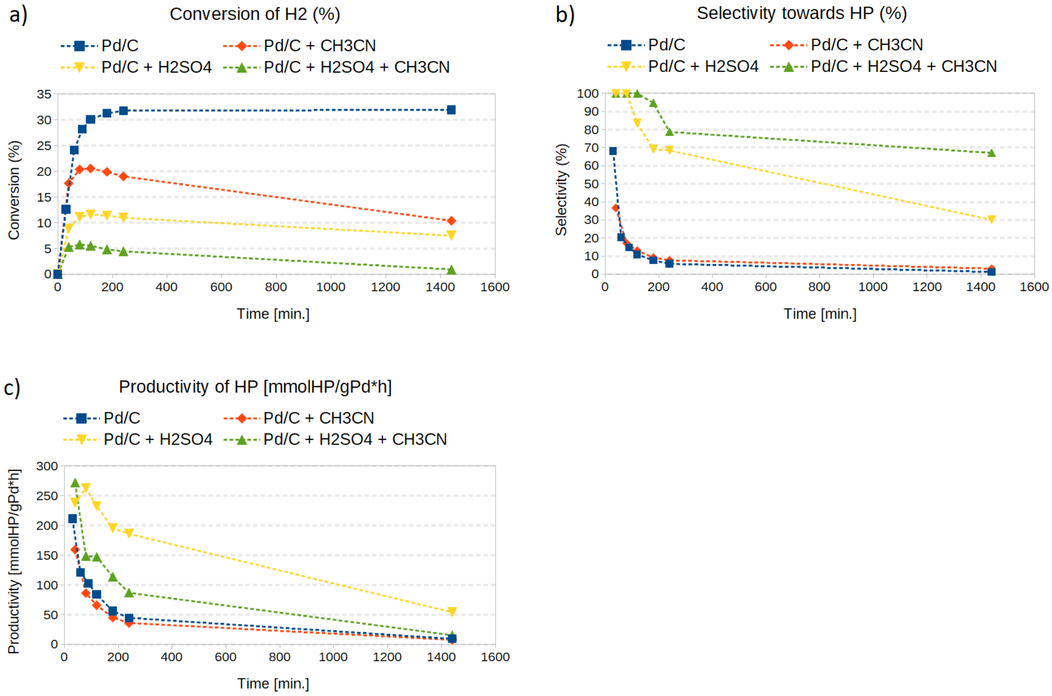

Figure 40: conversion (a), selectivity (b) and productivity (c) of Pd/C in methanol (blue squares), in methanol:acetonitrile 9:1 vol (red diamonds), acidified methanol (yellow triangles) and in acidified methanol:acetonitrile 9:1 vol (green triangles).

After reaching the maximum of conversion at 120 min, it starts to steadily decline, until achieving about 25 % of its top value at the end of the experiment (t > 2500 min). Independently on the presence of acetonitrile, the rate of production of HP is relatively fast only at the beginning of the reaction and dramatically drops shortly after the stabilization of the hydrogen conversion. After about 250 min a very small further increase, if any, of the concentration of HP is observed. In the presence of acetonitrile the final amount of produced HP is 0.20 mmol (0.65 mM), to be compared with 0.26 mmol (0.9 mM) obtained without the co-solvent (Figure 39). However, Pd/C is much more selective with acetonitrile, as the result of a faster decrease of the H_2 consumption than the decrease of the amount of produced HP. However, the selectivity of Pd/C after 1440 min is only 2.2%. The selectivity values more or less compare in the same way as above at any time (Figure 40), but they are in general better for shorter times as shown for example by the data at 1440 min (Figure 41).

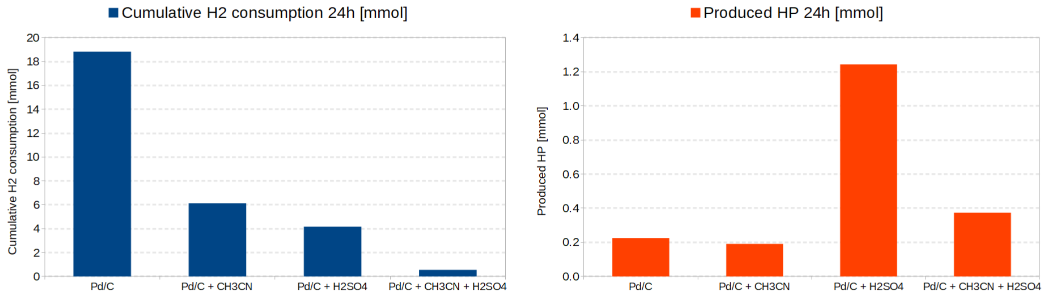

Figure 41: total consumption of hydrogen at 24 h (left) and production of H_2O_2 *(right) after 24 h.*

The decrease of the selectivity with time is readily accounted for by the building-up of HP, which starts to be hydrogenated or decomposed faster and faster until it is consumed at the same rate of its production. In this moment the instant selectivity is zero and a plateau of the HP concentration is observed, as long as this is the steady state of the system. As ion-exchange resins bear acid -SO_3H groups and acid is a well established selectivity enhancer, a suitable amount of sulfuric acid was introduced in the reaction mixture during tests with Pd/C, for sake of comparison.

In acid medium the hydrogen consumption and the HP productivity appreciably decrease and increase, respectively (Figures 39e and 39f), according to literature.[12,77,184] Although H_2SO_4 is effective as enhancer, Pd/C is poorly selective, when acetonitrile is not present. Interestingly, in acid medium the initial selectivity is very close to 100%, independently on the presence of acetonitrile. However, when acetonitrile is used, such a high selectivity is maintained for a longer time (up to 180 min) and remains 78% and 68% after 240 min and 1440 min, respectively (Figure 40). Conversely, in the presence of acid, H_2 conversion is relatively low, being lower than 12% and 5%, without acetonitrile and in the presence of the co-solvent, respectively. In the latter case, after about 1000 min a decrease of the cumulative H_2 consumption, corresponding to an apparent increase of the total amount of hydrogen after the reactor, starts to be observed (Figure 39f). Some small instability of the gas chromatographic response in the analysis of the off-gas, which would be otherwise negligible, could significantly affect the measurement of the low amounts of H_2 consumed by poorly active catalysts.

This makes the hydrogen signal slightly higher than the value at the beginning of the experiment, therefore leading to an apparent negative consumption, resulting as a decrease of the cumulative H_2 consumption.

In conclusion, for Pd/C the increase of the selectivity towards HP in the presence of acetonitrile is essentially the result of the suppression of the catalytic activity. The addition of H_2SO_4 leads to an appreciable increase of the HP productivity.

2.3.2 Pd supported on cross-linked organic polymers (resins)

Three resin-supported Pd catalysts (1%, w/w) were prepared using different co-{polystryene-divinylbenzene} based cross-linked polymers. Pd/SpDVB (Paragraph 2.2.1) was used to investigate the effect of ACN on the catalytic behaviour. The catalyst supported on the corresponding unfunctionalized polymer, Pd/pDVB, was tested in the presence of ACN, to assess the possible effect of the sulfonic groups. Further catalysts, Pd/K2621 and Pd/K1221, were prepared with the very same procedure exploited for the preparation of Pd/SpDVB, using the commercial ion-exchange resins Lewatit K2621 and K1221, with macroporous and gel type morphology, respectively. The investigation of these catalysts is useful to evaluate the role of the morphology of the support on the catalytic properties.[128]

2.3.2.1 Pd supported on polydivinylbenzene derived materials

Using pure methanol as the solvent, the apparent H_2 consumption rates over Pd/pDVB and Pd/SpDVB are closely comparable (Figure 42), with about 60 mmol of H_2 converted in 2500 min (average TOF ≈ $150 \cdot \mathrm{mmol}_{H_2} \cdot \mathrm{mmol}_{Pd} \cdot h^{-1}$). The similar mesoporous open texture of these catalysts suggests that the dissolved gases diffuse towards the metal nanoparticles at comparable rates.

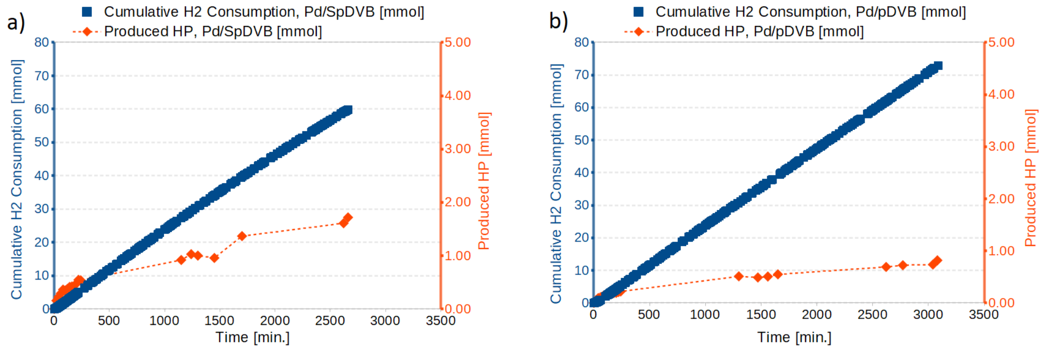

Figure 42: DS catalytic tests with Pd/SpDVB(a) and Pd/pDVB (b) in methanol (Blue squares: cumulative hydrogen consumption; red diamonds: HP production).

As reported in Paragraph 2.2.3.3, Pd/SpDVB is clearly more selective than Pd/pDVB, whereas Pd/pDVB is appreciably more selective than Pd/C (Figure 34), due to the open pore system. After an 180-240 min of induction period the rate of hydrogen consumption become constant and a stable conversion is reached for both catalysts.

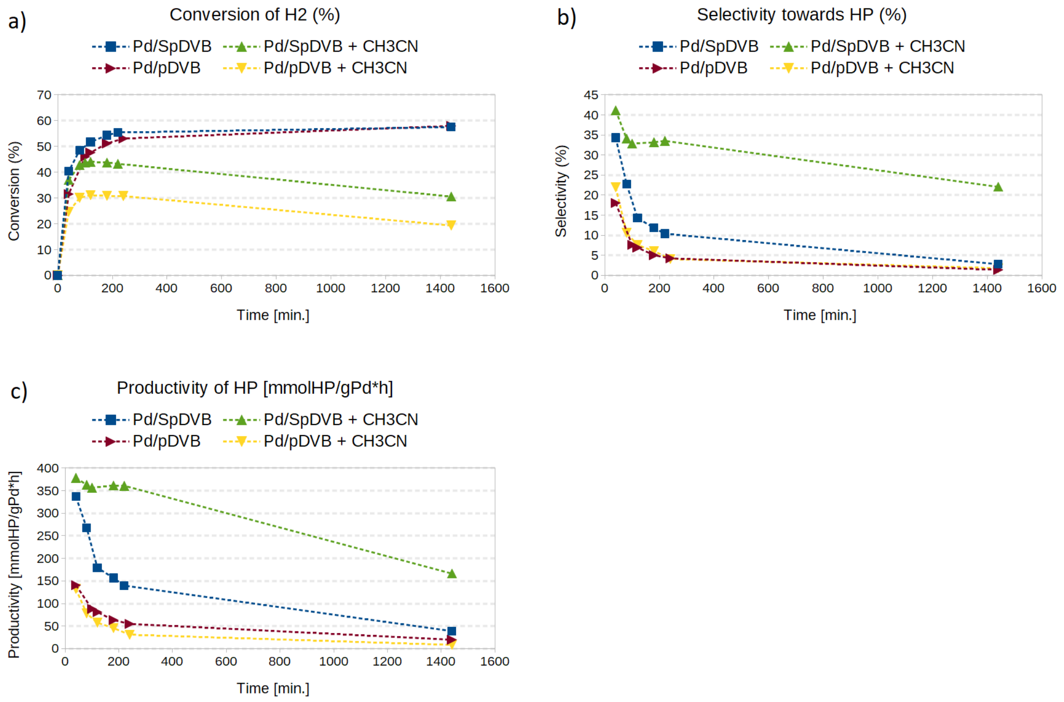

Figure 43: conversion (a), selectivity (b) and productivity (c) of Pd/SpDVB in methanol (blue squares), of Pd/SpDVB in methanol:acetonitrile 9:1 vol (red diamonds), of Pd/pDVB in methanol (yellow triangles) and of Pd/pDVB methanol:acetonitrile 9:1 vol (green triangles).

In spite of the presence of the protonated sulfonic groups in Pd/SpDVB, no appreciable difference with Pd/pDVB is observed in the conversion of H_2 (Figure 43). Taking into the account that the concentration of H^+ introduced as H_2SO_4 for the test with Pd/C is comparable to the local concentration of -SO_3H groups within Pd/SpDVB catalyst, the introduction of the sulfonic groups into pDVB has a different effect with respect the addition of H_2SO_4 to Pd/C, leading to a ten-fold reduction of the rate of H_2 consumption (Figure 39). In some cases the interaction of the active metal surface with the anions introduced with a homogeneous acid promoter HX was reported to be negligible.[55] However, it should be considered that the -SO_3^- groups of SpDVB are fixed and their mobility and ability to interact with the metal surface are therefore limited.

One of the most interesting features of Pd/SpDVB is its relatively high resistance to the deactivation. Not only there is a negligible change, if any, in the hydrogen consumption rate after 240 min, but also the HP production never stops. Even after 2500 min H_2O_2 concentration still increases, although at a lower rate in comparison with the beginning of the experiment, and never reaches a plateau value. In the case of Pd/C the plateau value occurred just after about 250 min. The effects of the addition of acetonitrile to the reaction mixture are larger for Pd/SpDVB than for Pd/pDVB. For Pd/pDVB a very small selectivity enhancement is observed at the beginning of the reaction (Figure 43), but after 120 min it is practically the same as in methanol. On the other hand, at any time acetonitrile decreases the H_2 conversion and increases the HP productivity of Pd/SpDVB, with respect to pure methanol, so that the catalyst is remarkably more selective (Figure 43).

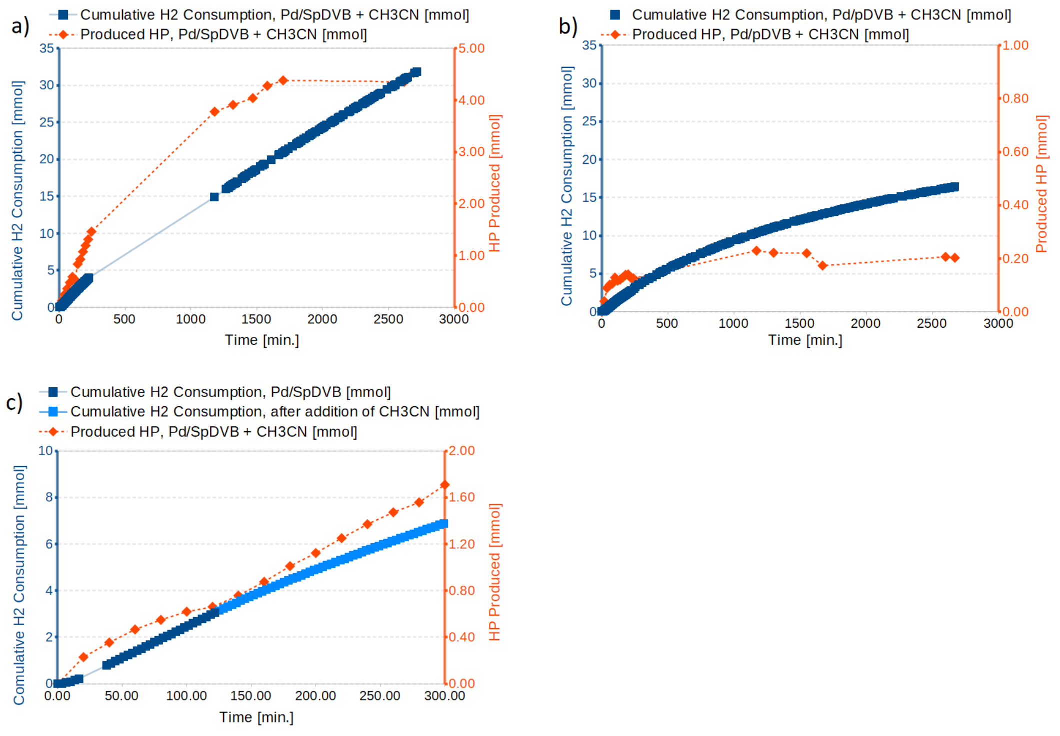

Figure 44: DS catalytic tests of Pd/SpDVB (a) and Pd/pDVB (b) methanol:acetonitrile 9:1 vol. Cumulative hydrogen consumption is reported on blue squares, the produced HP is reported on red diamonds. In panel (c) is reported the effect of ACN when introduced at 120 min in the reaction mixture.

Interestingly, the effect of acetonitrile is observed also when it is introduced after 120 min from the beginning of the experiment (Figure 44c). After the addition, the rate of hydrogen consumption starts to (slowly) decline and a clear sudden increase of the HP productivity can be observed. This behaviour supports the conclusion that the main action of acetonitrile is simply the partial inhibition of these catalysts. The different effect of the addition of acetonitrile as the co-solvent on the rate of H_2 consumption of Pd/pDVB and Pd/SpDVB catalysts rules out the hypothesis that the reacting gases are less soluble in the methanol/acetonitrile mixture than in pure methanol. In this context also Paunovic et al. came to the conclusion that in mixed water/organic solvent mixtures (including acetonitrile) the solubility of the gases is not a key factor in the direct synthesis of HP.[161] The most remarkable feature of resin catalysts is rather the effectiveness of the fixed -SO_3H groups of Pd/SpDVB in keeping a relatively high selectivity for longer time, in comparison with homogeneous acids. In fact, the selectivity of

Pd/SpDVB undergoes a modest decrease from the initial 41% value to 33% after 80 min, but it does not change any longer up to 240 min. In this period HP is produced at the rate of 360 $mmol_{HP} \cdot g_{Pd}^{-1} \cdot h^{-1}$. This is the first time in which a *selectivity plateau* is observed, i.e. a selectivity value practically independent of time. The final selectivity at 1440 min is lower, but when the decrease starts to occur is not known at the moment, because the experimental set-up available for this investigation prevented the overnight collection of data. At any rate, the final 25% selectivity is five times higher than the second best value achieved herein, at the same reaction time. A possible explanation about the enhancement effect of ACN could be in the inhibition of the O-O splitting with the consequent formation of water, as suggested by Paunovic et al.[161] In order to evaluate this hypothesis, experiments on the degradation of HP were made (Paragraph 2.3.2.2).

2.3.2.2 Effect of ACN on HP degradation with Pd/SpDVB catalyst

The HP degradation experiment were designed in order to evaluate the consumption of hydrogen peroxide by dismutation over Pd catalysts, mimicking the conditions involved in a typical DS test. In particular, as the catalyst changes during a DS experiment, due to the modification of the composition of the reaction mixture, the addition of a “fresh” catalyst on a pre-built HP solution could lead to a misleading evaluation of the degradation behaviour. Nonetheless, this latter approach is typically reported in literature to evaluate the activity of a catalyst in the degradation of HP.[78,108,185] Conversely, here a different approach is used: a standard DS catalytic experiment has been carried out for 1200 min to generate HP in the liquid phase and subsequently the H_2 feed has been interrupted, by maintaining the O_2 flow rate to 24 mL/min, in order to completely remove hydrogen from the reactor and the reaction mixture. In Figure 45 the negative time represent the catalytic experiment before the interruption of the hydrogen flow, where the build up of the concentration of HP is still visible for the experiment in the presence of ACN.

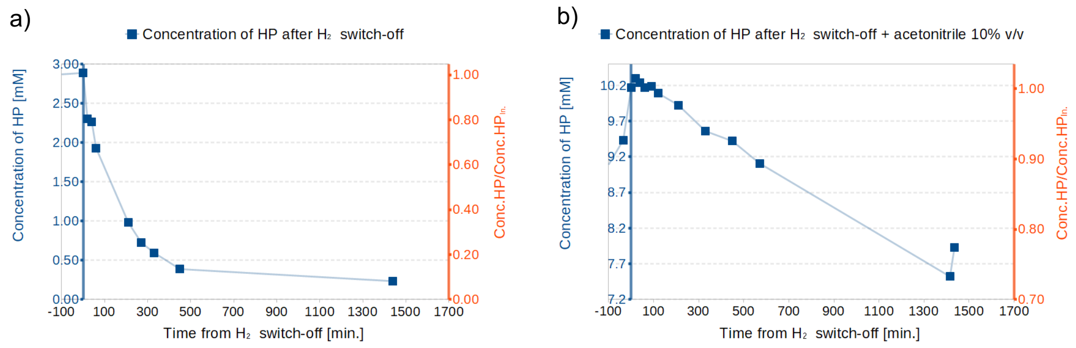

Figure 45: degradation of HP with Pd/SpDVB in pure methanol (a) and in methanol:acetonitrile 9:1 vol (b). The moment in which H_2 feed has been switched off is considered the zero point of the experiment.

In the absence of acetonitrile the drop of HP concentration is clearly exponential (Figure 45), indicating a first order reaction with respect the reagent with a value of $t_{½}$ of 156 min. In the presence of acetonitrile, the amount of HP at the time of the switch-off (3.0 mmol; $[H_2O_2]$≈10 mM) was about three times higher than with pure methanol (0.95 mmol; $[H_2O_2]$≈3.2 mM), in line with the higher productivity of the promoted catalyst. The subsequent drop of the HP amount over the promoted catalyst was one order of magnitude slower. As almost equally good regressions can be obtained by fitting the experimental data with both linear and an exponential functions (Figure 46), the reaction order with respect HP cannot be unambiguously assessed. However, the values of $t_{½}$ determined for a zero order and a first order reactions are comparable (2600 and 3100 min) and turn out to be one order of magnitude larger than the value observed for the reaction in pure methanol.

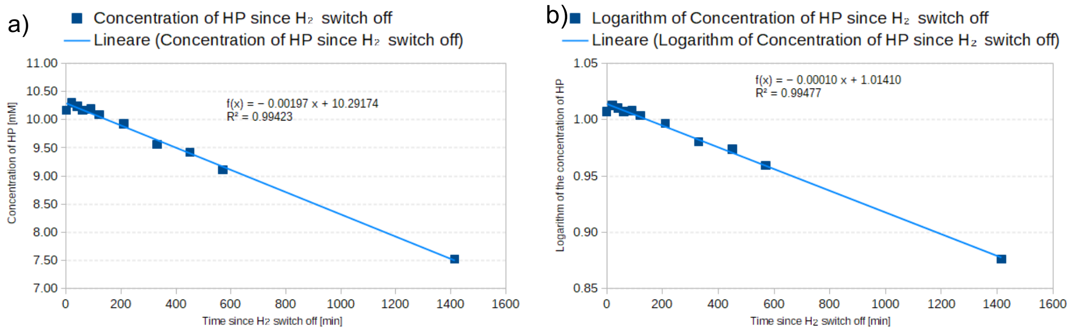

Figure 46: fitting of HP degradation curve, (a) fit considering a zero order kinetic, (b) fit considering a first order kinetic.

2.3.2.3 X-ray photoelectron spectroscopy characterization

According to some literature reports, the selective inhibition of the hydrogenation and/or dismutation of HP in the presence of mineral acids and halides is connected to the increase of the Pd(II)/Pd(0) ratio.[89,110,186] The higher activity of the metal Pd surfaces in the production of water is also supported by computational investigation.[107] Being a good ligand towards Pd(II), acetonitrile is expected to stabilize, upon adsorption, the oxidized form of palladium on the metal surface and also to lead to the formation of soluble complexes, such as $[Pd(N\equiv C\text{-}CH_3)_4]^{2+}$, upon the oxidative erosion of the metal nanoparticles.[69,187]

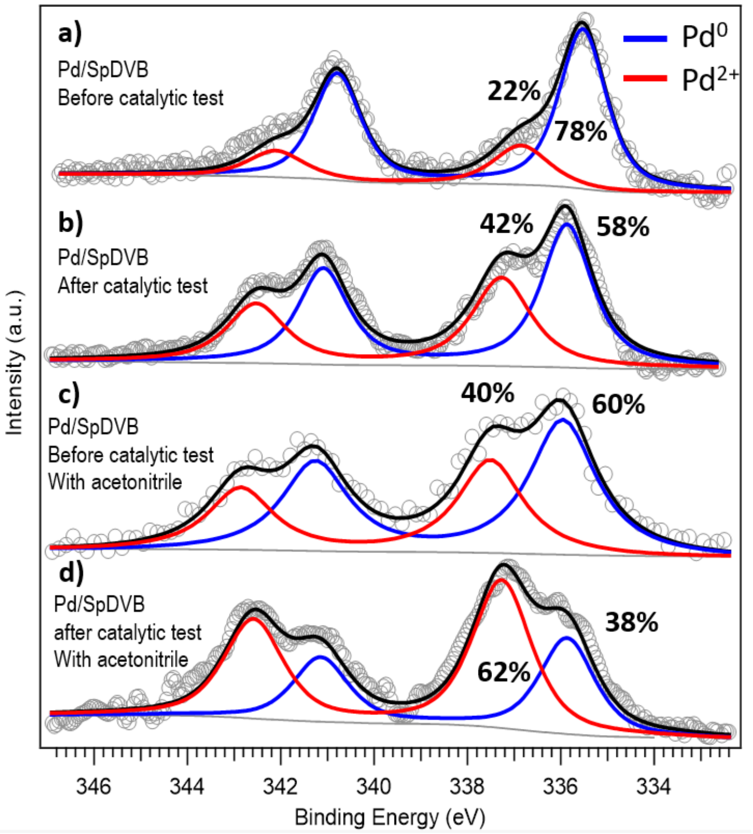

Figure 47: 3d$_{5/2}$ XPS characterizations of Pd/SpDVB. Void circles: experimental data; black line: fit; deconvolved lines: blue, Pd(0); red, Pd(II).

In this context, we investigated on the oxidation state of palladium in Pd/SpDVB by means of XPS. The characterization shows that the fresh catalyst contains both Pd(II) and Pd(0) (Figure 47a and Table 11), with most palladium in the reduced form (78%; Table 12). The binding energy (BE) for the $3d_{5/2}$ levels of Pd(II) and Pd(0) are in good agreement with values previously reported for supported palladium catalyst.

Table 11: binding energies (eV) of Pd(0) and Pd(II) of Pd/SpDVB compared to literature values.

	Ji et al.[186]	Gemo et al. [188]	Fresh Pd/SpDVB	Exhausted Pd/SpDVB	
				unpromoted	*promoted*
Pd(0) 3d5/2	335.6 – 336.1	336.0	335.6	335.9	335.9
Pd(II) 3d5/2	337.8 – 338.3	337.8	336.9	337.2	337.3

The fraction of Pd(0) at the end of catalytic experiment without ACN decreased to 58%, with no changes of the BE (Table 12). Thus in the regions of the material sampled by XPS an overall partial oxidation of palladium is detected, likely due to the large excess amount of O_2 used during the catalytic test and to the accumulation of H_2O_2 in solution. The presence of acetonitrile strongly favours the oxidation of Pd(0) even in the catalyst simply suspended and swollen in the methanol/acetonitrile mixture for 24 h, under air conditions, before the introduction into the reactor (Panel c of Figure 47). Although the partial pressure of O_2 in air is much lower than in the gas mixture used for the DS, it was enough to lower the Pd(0) fraction to 60%, more or less the same observed in Pd/SpDVB recovered from the DS without acetonitrile. When Pd/SpDVB was recovered from the DS test with ACN, the fraction of Pd(0) was as low as 39%, with final Pd(II) amounting to 61% (Table 12). This might be favoured by the potential presence of cationic complexes, like $[Pd(NCMe)_4]^{2+}$ or related species, as counterions of the fixed $-SO_3^-$ groups of the support.

Table 12: relative abundance of Pd(0) and Pd(II) in Pd/SpDVB before the catalytic experiment, after the catalytic experiment in methanol and after the catalytic experiment in methanol:acetonitrile 9:1 vol.

	Pd/SpDVB		
	Fresh	*Unpromoted exhausted*	*Promoted exhausted*
Pd(0) 3d5/2	78%	58%	38%
Pd(II) 3d5/2	22%	42%	62%

The presence of acetonitrile in the exhausted catalyst is indicated by a weak, but clearly detectable (1% at/at), nitrogen 1s signal in the XPS spectrum (Figure 48), which is absent in the characterization of the catalyst recovered after a test without acetonitrile.

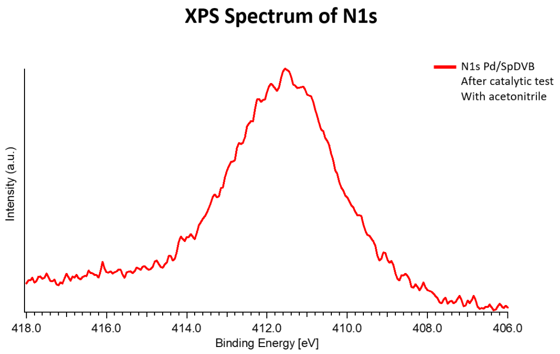

Figure 48: XPS signal of nitrogen in Pd/SpDVB after the catalytic experiment in the presence of ACN.

The presence of absorbed or physisorbed acetonitrile can be ruled out because it is expectedly removed under the ultra-high vacuum conditions in the XPS chamber. However, the N/Pd ratio in the XPS is much higher than possible for palladium-bound acetonitrile as the only nitrogen source. In principle, products of the hydrolysis of acetonitrile could contribute to the relatively large proportion of nitrogen detected by XPS. However, no such hydrolysis products can be detected with ^{1}H-NMR characterization of the reaction mixture. In fact, quantitative NMR analysis with 1,4-dioxane as the internal standard, reveal that the amount of ACN remains unchanged after the reaction and no by-products are found in solution (Figure 49-50 and Table

13). Nevertheless, species like ammonium ions could be retained inside of the support by their ionic interaction with the fixed -SO_3^- groups of the support.

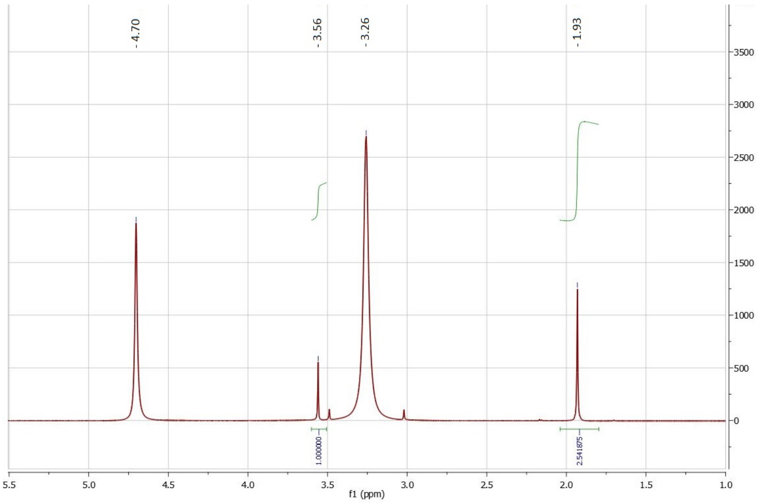

Figure 49: NMR spectra of the methanol solution with 10% v/v of acetonitrile. Peaks of methanol can be detected at 3.26 ppm and 4.70 ppm. Acetonitrile signal is observed at 1.93 ppm. The signal of the methyl groups of the internal standard is present at 3.56 ppm.

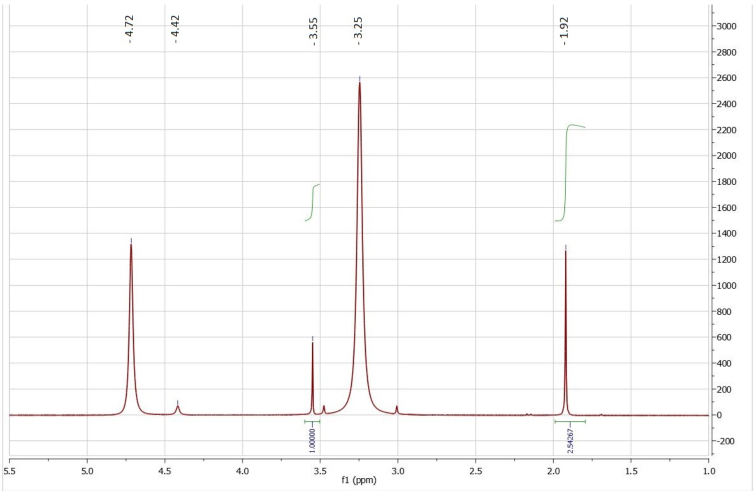

Figure 50: NMR spectra of the reaction mixture after the catalytic experiment. Peaks of methanol, acetonitrile and 1,4-dioxane are observed at the same ppm of the previous spectrum. At 4.42 ppm the signal of the protons of HP can be detected.

Table 13: integrals of the peaks of the internal standard (set to 1) and acetonitrile.

	Reaction mixture before the catalytic experiment	Reaction mixture after the catalytic experiment
1,4-dioxane	1.00000	1.00000
Acetonitrile	2.54187	2.54267

Even though no other nitrogen species than acetonitrile are detected in solution by ^{1}H-NMR, a strong palladium depletion in the regions of the catalysts measured by XPS could be compatible with the high N/Pd ratios observed with this technique. Assuming that the beads of the exhausted Pd/SpDVB are more or less spheres with 1 μm of diameter and that XPS detects the atoms in a 5 nm thick external layer, it follows that only a spheric crown representing 3% of the volume of the catalyst responds to this analysis. A very small amount of nitrogen, hardly detectable in solution, could be enough for their accumulation in an external layer of the catalyst bead and therefore can be detected in the XPS analysis.

2.3.2.4 Transmission electron microscopy characterization

The TEM characterization of a fresh sample of Pd/SpDVB has been already done by Frison et al (Paragraph 2.2.3.2 and ref[141]). After a catalytic experiment with acetonitrile, HR-TEM (Figure 51) shows that the nanoparticles are mainly comprised of metal palladium, in that the observed d-spacing (0.22 nm) compares well with the distance of 111 planes in metal Pd.[183] This finding does not seem consistent with XPS characterization (Paragraph 2.3.2.3), showing Pd(II) as the main component of the metal phase. However, the direct comparison between the results of TEM and XPS could be misleading. In fact, both techniques measure only a limited fraction of the materials and TEM is not sensible to molecular palladium species, such as $[Pd(N{\equiv}C\text{-}CH_3)_4]^{2+}$ which might significantly contribute to XPS signals.

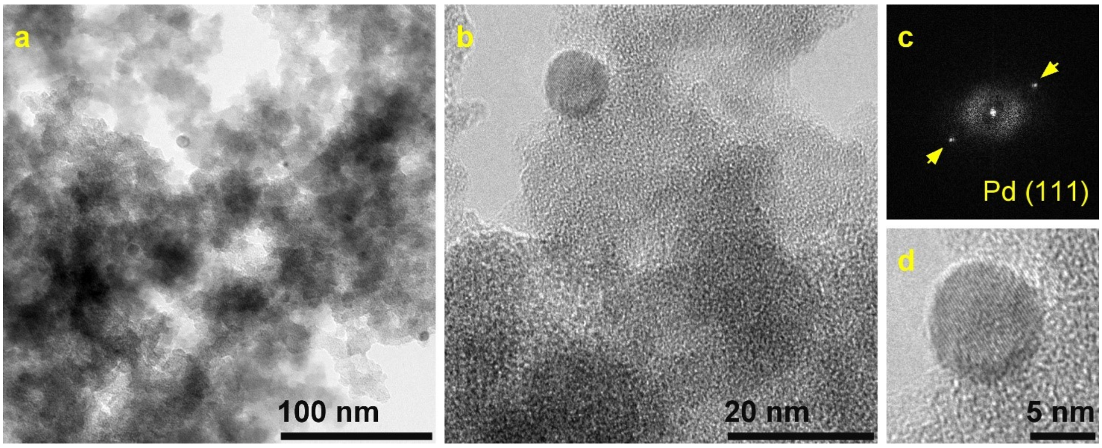

Figure 51: a-b) Representative (HR)TEM of Pd/SpDVB and c) FFt analysis of d) selected Pd NP.

Low-resolution TEM microphotographs of the exhausted catalyst show a significant change of the nanoparticle size distribution (Figure 52), which becomes bimodal.

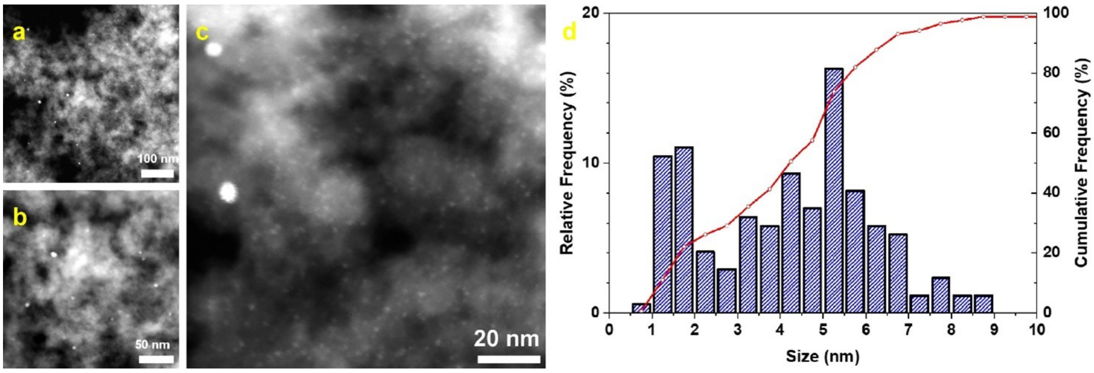

Figure 52: a-c) representative STEM images of Pd/SpDVB at different magnification and related d) size distribution of the Pd NPs in the sample recovered from a catalytic experiment in the presence of ACN.

The 4-6 nm fraction is the most abundant (ca 60% of the nanoparticles), but the fraction of the nanoparticles larger than 6 nm decreased to ca 10% and a small-sized fraction, centred at 1-2 nm (ca 25-30% of the nanoparticles) appeared. The nanoparticle size redistribution in a supported catalyst during a reaction under liquid-solid conditions can be associated to a release-and-capture mechanism, which can be favoured by oxidative conditions and the presence of good ligands for the oxidized metal.[68,189] In catalysts supported by thermally stable inorganic solids this problem can be mitigated by the calcination of the material, which fosters the evolution of molecular species into the nanostructured active phase. However, Pd/SpDVB cannot withstand this treatment because the support undergoes de-sulfonation at 120°C in the presence of water (back aromatic electrophilic substitution)[190] or at 275°C in the dry material, and decomposition at 450°C. This was evaluated by DSC–TGA characterisation of the SpDVB support under N_2, non oxidative conditions (Figure 53).

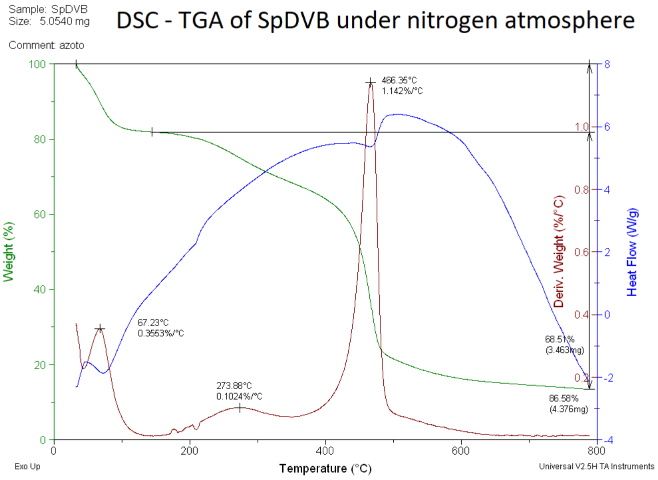

Figure 53: DSC and TGA characterisation of SpDVB. Mass loss is represented by the green line, DSC signal is represented by the blue line. The brown curve is the derivative of weight with respect to temperature. A 10 °C/min heating ramp from 30° C to 800° C was applied, under nitrogen atmosphere

More in details, at 67° C the loss of solvent present in the material, likely a residual small amount of methanol present after the sulfonation, is detected. At 273° C the de-sulfonation reaction happens, with a consequent loss of SO_3. At 466° C the carbonization of the polymer backbone occurs. The results of TGA clearly indicate that any calcination process is unfeasible for this kind of catalyst. Hence, without calcination the metal phase of Pd/SpDVB can be expected to be comparatively little stable. On the one hand, this would make it more susceptible to the release of cationic molecular species of Pd(II), favoured by the presence of acetonitrile. On the other hand the ion-exchange ability of the support could favour their capture by retaining the cationic ones close to the supported metal nanoparticles.

Most often the final result of the reconstruction of nanoparticles is the thermodynamically favoured increase of their size. By contrast Pd/SpDVB undergoes the decrease of the nanoparticle size during the DS. As this is an up-hill process its mechanism must involve high energy intermediates such as molecular leached palladium(II) species. With Pd/SpDVB a limited metal leaching is observed (0.78%, 1.80% and 2.85% at 60, 120 and 2500 min, respectively) when the reaction is carried out in the presence of ACN. Strictly comparable levels are observed with pure methanol as the solvent (1.83% at 120 min, 2.86% at 2500 min, see Paragraph 4.6.1). Taking into account the large time on stream, the leaching level can be considered relatively low, with much of palladium released during the catalyst stabilization. In general, this highlights the ability ion-exchanging supports to limit the transfer of the leached metal into the bulk liquid phase, in spite of the fact that the catalyst was not calcined, and to effectively self-remediate to the relatively little stability of the catalyst. The most straightforward explanation of this particular ability of sulfonic ion-exchange resins to retain the metal inside the polymer network is the ionic interaction of cationic soluble palladium species with the fixed negative charges of the polymer framework. In the presence of acetonitrile these species are most likely $[Pd(N{\equiv}C\text{-}CH_3)_4]^{2+}$ or related ones. Under these circumstances the capture of the leached species could make their concentration inside the catalysts high enough as to have a fast nucleation, competing with the deposition of palladium on existing nanoparticles (growth) and thus favouring the formation of new, small nanoparticles. A similar reconstruction of the nanostructured metal was obtained when the catalyst was used without acetonitrile. In view of the similar leaching levels observed with and without methanol, this finding supports the hypothesis that the leached species are the intermediates of a nucleation-controlled reconstruction. However further work is needed to assess the mechanism of the nanoparticles reconstruction, such the investigation of the role of palladium scavengers.

The effect of this reconstruction process, if any, on the selectivity is not clear at the moment. At the end of the DS in pure methanol, the proportion of small nanoparticles in the recovered catalyst seems even somewhat higher (almost

40%, Figure 54) than in the case of the promoted catalyst. However, when comparing TEM images of different materials, the extent to which they represent the whole samples is always a problem and the populations of the smallest nanoparticles in the two exhausted catalysts samples could be closer than they appear from TEM.

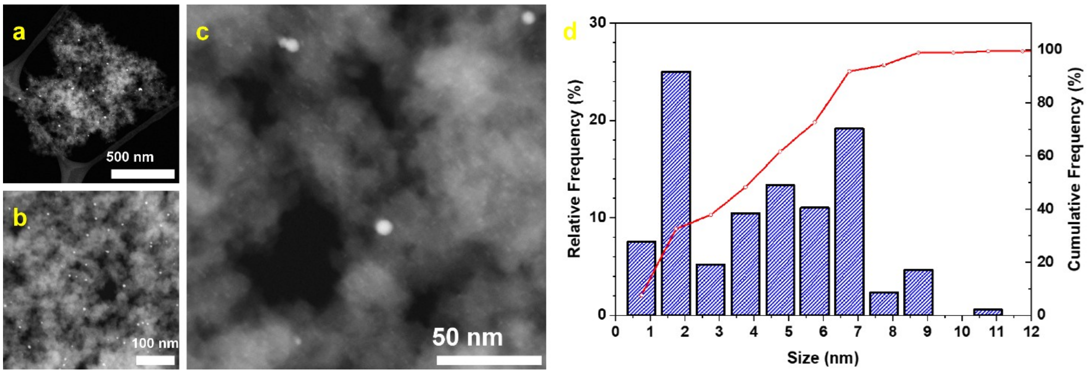

Figure 54: a-c) representative STEM images of Pd/SpDVB at different magnification and d) related size distribution of the Pd NPs in the sample recovered from a catalytic experiment with no addition of acetonitrile.

The relationship between particles size and selectivity towards HP is deeply discussed on literature.[12,91] However, also in this case there are controversial opinions on the effect of the size and shape of the metal phase in the DS reaction. In a recent paper, Tian et al.[191] investigated the DS of HP using a semi-batch reactor not too much different from that used in this work, concluding that smaller NPs are more selective in the production of HP, excluding single site Pd catalysts which are not active at all. On the other hand, Sterchele et al.[192] found that with ion-exchange resins as the supports palladium DS catalysts are more active and selective when the metal nanoparticles are relatively large and similar findings were also reported by Flaherty and co-workers in their extensive study of the DS mechanism.[59] This suggests that not only the size of the palladium nanoparticles is affecting the selectivity of Pd/SpDVB, but also that the promotion effect is more complex. In fact, although a comparable reconstruction of the metal phases of Pd/SpDVB both in the absence and in the presence of acetonitrile is observed, different selectivity values are obtained under these two conditions.

2.3.2.5 Effect of the release of acid from the SpDVB support

The TEM and XPS characterizations of the spent catalysts suggest that in the presence of acetonitrile in the reaction mixture the formation of Pd(II) cationic ACN complexes as the ligand occurs. Those dicationic complexes could easily give ion-exchange reaction with the -SO_3H groups leading to the release of acid in solution, as the exchange of a monocation with a dication is thermodynamically favoured.[193] Even though the amount of acid that can be released is small, it is necessary to rule out that the effect of acetonitrile is not based just on the formation of homogeneous H^+, acting as a selectivity enhancers. As a rough estimation, the highest amount of acid released happens with the total dissolution of the Pd nanoparticles into dicationic complexes. As in a typical catalytic experiment the total amount of Pd is 1 mg, corresponding to $9.4 \cdot 10^{-3}$ mmol, the highest amount of acid that can be released is $18.8 \cdot 10^{-3}$ mmol. This amount, in 300 mL of methanol is not easily detectable with the most common analytic techniques. To rule out that the release of such a small amount of acid leads to the selectivity enhancement, specific catalytic experiments focused on the release of acid from the sulfonic groups into the solution and on the exploitation of a neutralized catalyst were designed.

In detail, an excess of a salt of a divalent cation was added in solution to prompt the complete release of H^+ from the support. The compound of choice is magnesium nitrate as it is soluble in methanol and is not expected to promote neither acid-base or redox side reactions and does not contain halides. These features should ensure that the selected compound does not interfere with the DS process. The amount of $Mg(NO_3)_2$, introduced into the reactor during the conditioning of the catalytic before the experiment, is 60 mg (0.40 mmol), almost twice the moles of -SO_3H groups present in 100 mg of catalyst SIEC= 2.30 mmolH^+/g). The result of the catalytic experiment in the presence of $Mg(NO_3)_2$ is reported on Figure 55.

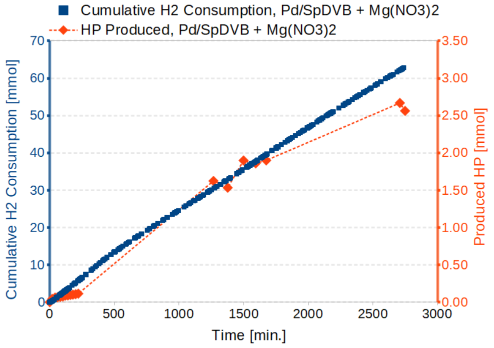

Figure 55: DS catalytic tests of Pd/SpDVB in methanol with the addition of 60 mg of Mg(NO_3)$_2$. Cumulative hydrogen consumption is reported on blue squares, the produced HP is reported on red diamonds.

As a qualitative estimation, the hydrogen consumption slightly decreases after about 500 min from the beginning of the catalytic experiment. On the other hand, the production of HP is limited in the first 240 min of reaction, when compared to the performances in pure methanol, never exceeding the value of 0.12 mmol. This is assumed to occur before the ion-exchange reaction, therefore having a negative effect on the HP production by the dissolved magnesium. The reason of the negative effect of magnesium nitrate on HP production is not fully understood and is out of the scope of this work, but could rely on the increased ionic strength of the reaction mixture. After about 500 min, the ion-exchange is completed and the acid is released in solution, with the consequent decrease of the hydrogen consumption coupled with the enhancement of the HP production, as observed for Pd/C in the presence of H_2SO_4 (Paragraph 2.3.1). Interestingly, when the magnesium salt is added in the whole reaction mixture (300 mL), the small amount of reaction mixture used to swell the catalyst for 2 hours before the experiment contains Mg. This leads to the same result presented in Figure 55, with the only difference that the decrease of the rate of hydrogen consumption is brought 120 min forward. This confirms that this effect is due to the ion-exchange process, which in this case starts during the swelling of the catalyst. However, even though the release of acid in solution brings to an increase of both the production of HP and the H_2 selectivity, the extent of this effect is not as high as in the presence of ACN. When ACN is present in the reaction mixture, some Pd can form cationic complexes that undergo to ion-exchange, with the consequent release of H^+ in solution. However, due to the limited amount of Pd loaded into the catalysts (usually 1% w/w), this effect is remarkably limited with respect that obtained in the experiment in the presence of Mg^{2+} even if all the Pd is oxidized and completely dissolves. Hence, only a small part of the supported H^+ is likely released in solution during a catalytic test with acetonitrile and this small amount cannot explain the observed productivity and selectivity enhancement.

To better investigate on the role of the release of acid in solution, the corresponding catalyst in the neutralized form was prepared. The sulfonic groups of the support were converted into sodium form by neutralization with a with a NaOH solution before the synthesis of the metal nanoparticles. The catalysts supported on neutralized ion exchangers are expected to be less active in the DS, due to the lack of acidic functionalities that are promoting the formation of HP. The neutralized catalyst, namely Pd/SpDVB(Na), has been tested both with methanol and with methanol:acetonitrile 9:1 as the reaction mixture (Figure 56).

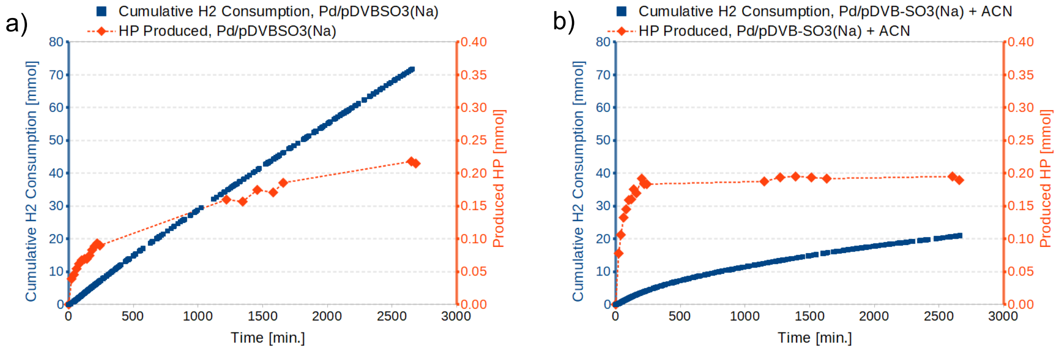

Figure 56: results of catalytic tests of Pd/SpDVB(Na) in methanol (a) and in methanol:acetonitrile 9:1 vol (b). Cumulative hydrogen consumption is reported on blue squares, the produced HP is reported on red diamonds.

The Pd/SpDVB(Na) catalyst presents a high cumulative hydrogen consumption, being even higher of that achieved by Pd/SpDVB and comparable to that of Pd/pDVB. Conversely, the production of HP is very low, being the lowest obtained with Pd catalysts supported on pDVB based materials. In fact, the HP productivity is quite low: after 240 min only 0.09 mmol of HP have been produced, increasing up to 0.22 mmol after more than

2650 min. Therefore the catalyst presents a very low selectivity towards HP, that starts from 5.3% after 40 min and drops to 1.3% at 240 min. When ACN is present in solution, the conversion is much lower, as it drops form 70% in methanol to 25% at the steady state (<1440 min), with a continuous decrease over time. The HP production is almost unchanged (0.19 mmol) but this value is reached after 240 min. As the consequence, the selectivity decreases from 16.9% at 40 min to 4.6% at 240 min and is significantly higher than in pure methanol. In this case the effect of ACN is evident only during the first four hours of reaction, increasing the HP production of the catalyst. However, after reaching a plateau value, which is independent on the solvent, the HP concentration stops increasing. Hence, the effect of ACN on the performance of the catalyst is positive, as it leads to a selectivity and productivity enhancement, even though, differently from Pd/SpDVB, this is valid only in the first four hours of reaction. The reason of the interruption of the increase of the HP production over Pd/SpDVB(Na) is unclear and further characterizations of this catalyst are needed to assess important features, such as the isoelectric point, that could determine the catalytic performances (Paragraph 1.5.6). However, the positive effect in the DS obtained by the addition of ACN in solution confirms once more that the release of acid cannot explain the selectivity enhancement, as the case of neutralized supports only Na^+ are released in solution. Interestingly, the addition of $Mg(NO_3)_2$, changes very little the performance of Pd/SpDVB(Na) catalyst in methanol and, unlike Pd/SpDVB, the rate of hydrogen consumption does not change over time (Figure 57). This further confirms that the changes of the rate of hydrogen consumption and HP production curves are connected to the ion-exchange reaction and the consequent release of the acid in solution.

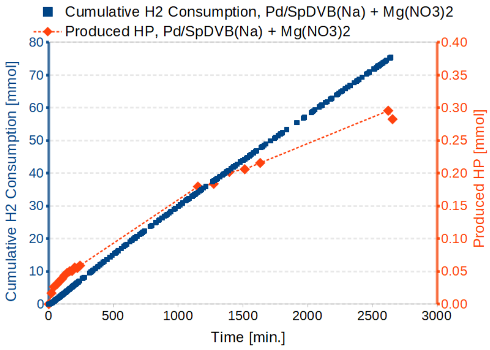

Figure 57: results of catalytic tests of Pd/SpDVB(Na) in methanol with the addition of 60 mg of Mg(NO_3)$_2$. Cumulative hydrogen consumption is reported on blue squares, the produced HP is reported on red diamonds.

2.3.2.6 Pd/K2621 catalyst

The commercial macroporous ion-exchange resin Lewatit K2621 was used to prepare a Pd catalyst with the same experimental procedure reported for Pd/SpDVB (Paragraph 2.2.1). Nanostructured palladium and palladium-alloys catalysts supported on this polymer were deeply studied in the DS of HP.[80,101,104,124,194] The reported TEM characterization of fresh Pd/K2621, prepared with the very same protocol exploited in this work, showed a unimodal gaussian distribution of the metal nanoparticle size, with the highest frequency at 5 nm and an average value of 4.8 nm.[195] The average size of the nanoparticles of fresh Pd/K2621 is larger than that of fresh Pd/SpDVB. The effect of the addition of ACN to the catalytic behaviour of Pd/K2621 in the DS, are reported in Figure 58.

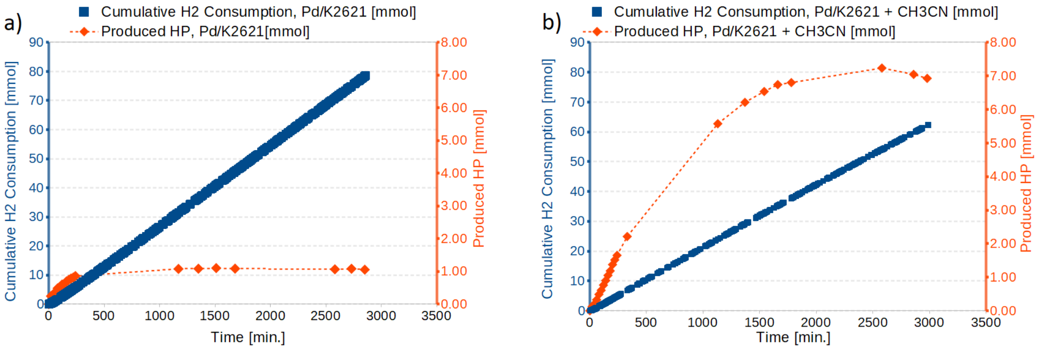

Figure 58: results of catalytic tests of Pd/K2621 in methanol (a) and in methanol:acetonitrile 9:1 vol (b). Cumulative hydrogen consumption is reported on blue squares, the produced HP is reported on red diamonds.

Under the reaction conditions of this work, Pd/K2621 is slightly more active than Pd/SpDVB (Figure 59; after 1440 min the H_2 conversion is stable at 66%). During the first 240 min, Pd/K2621 is both more selective and productive towards HP than Pd/SpDVB (Figure 59) and produces 1.00 mmol of HP in 240 min. However, at 1440 min the amount of produced HP increased only to 1.10 mmol (ca 3.7 mM) and, differently from Pd/SpDVB, for longer reaction times the production of HP practically stopped (Figure 58).

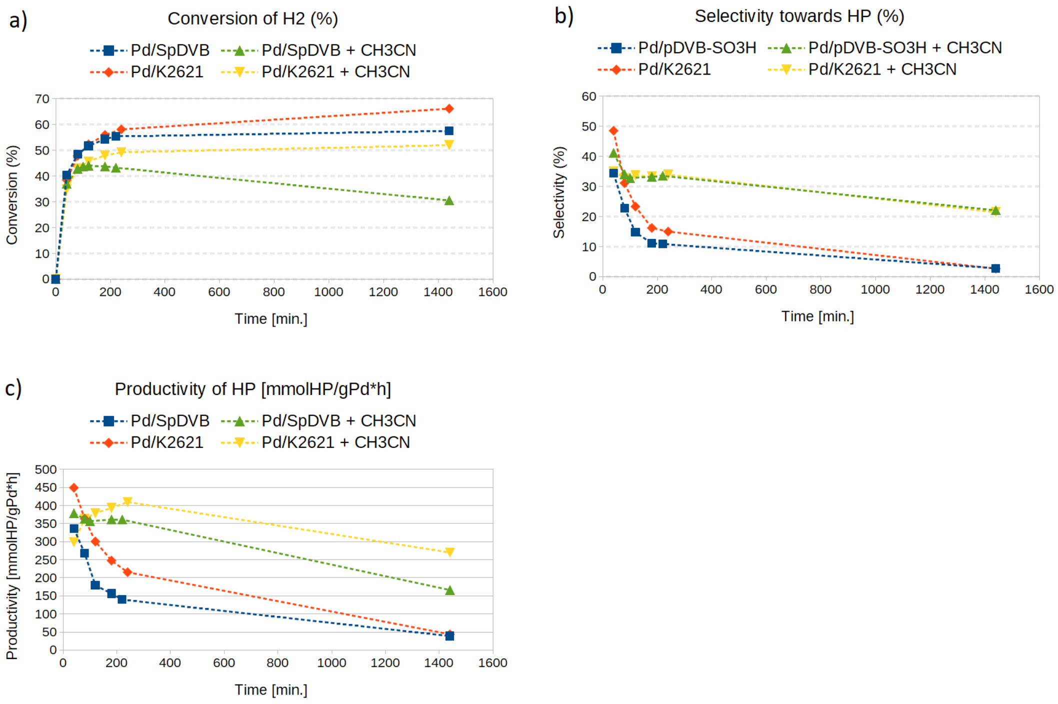

Figure 59: conversion (a), selectivity (b) and productivity (c) of Pd/SpDVB in methanol (blue squares), of Pd/K2621 in methanol (red diamonds), of Pd/K2621 in methanol:acetonitrile 9:1 vol (yellow triangles) and of Pd/SpDVB in methanol:acetonitrile 9:1 vol (green triangles).

According to the XPS characterization of fresh and exhausted Pd/K2621, the metal undergoes a net oxidation during the reaction, similarly to Pd/SpDVB, with the amount of Pd(0) decreasing from the initial 62% to the final 37% (Figure 60, Table 14). The experimentally observed final leaching level is 4.46 % with respect the initial Pd content and appears higher than for Pd/SpDVB (2.85%), albeit comparable.

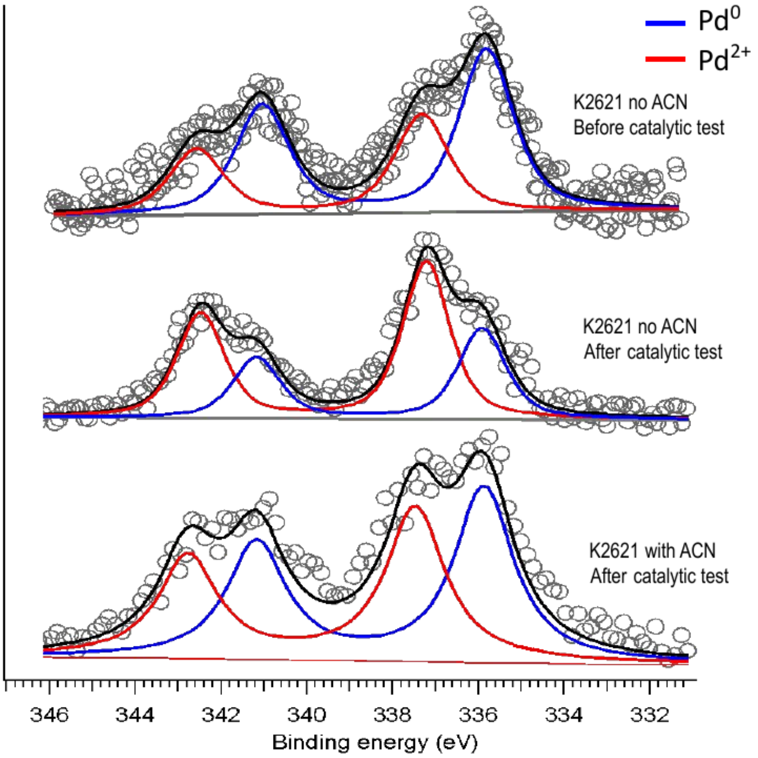

Figure 60: 3d$_{5/2}$ XPS characterizations of Pd/K2621. Void circles: experimental data; black line: fit; deconvolved lines: blue, Pd(0); red, Pd(II).

Table 14: relative abundance of Pd(0) and Pd(II) in Pd/SpDVB and in Pd/K2621 before the catalytic experiment, after the catalytic experiment in methanol and after the catalytic experiment in methanol:acetonitrile 9:1 vol.

	Pd/K2621		
	Fresh	*Unpromoted exhausted*	*Promoted exhausted*
Pd(0) 3d5/2	62%	37%	55%
Pd(II) 3d5/2	38%	63%	45%

The TEM characterization of Pd/K2621 recovered at the end of the catalytic experiment (Figure 61) shows a small decrease of the average size of the metal nanoparticles, from 4.8 to 4.3 nm. The size distribution is not clearly bimodal as observed for Pd/SpDVB after the catalytic test, but it appears no longer gaussian. Similarly to Pd/SpDVB (Paragraph 2.3.2.4) this is apparently compatible with a reconstruction of the metal phase based on a release-and-capture mechanism.

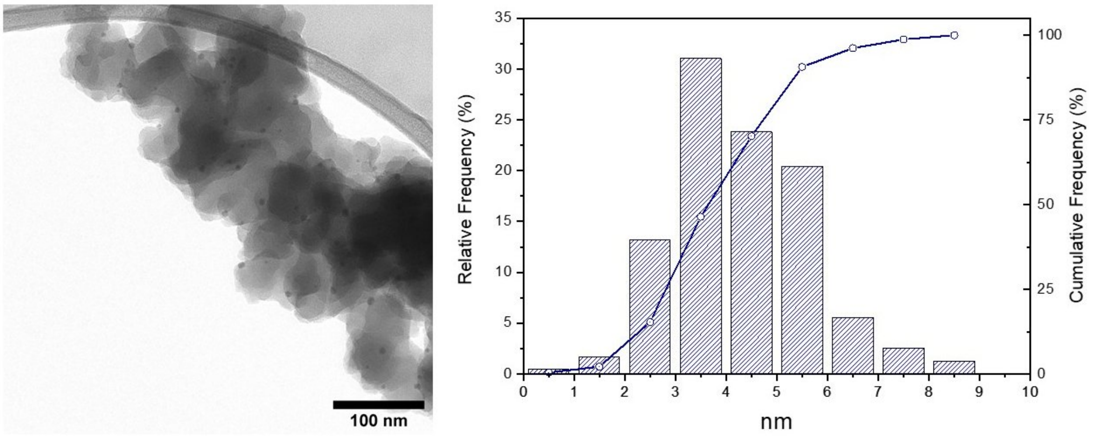

Figure 61: TEM micrograph of Pd/K2621 and related size distribution of the Pd NPs in the sample recovered from a catalytic experiment with no addition of acetonitrile.

However, some differences can be recognized between Pd/K2621 and Pd/SpDVB, particularly the relatively little change of the nanoparticles size of Pd/K2621 after the reaction. This might reasonably depend on the different morphology of K2621 and of SpDVB. In the former, the “working arena” for the formation of the nanoparticles and the catalytic action is, at least partially, the swollen gel-phase layer decorating the pore walls of the support (Figure 62, right). Conversely, in the SpDVB, the formation of a gel-phase, if any, is negligible (Figure 62, right).[145] Under these circumstances the metal nanoparticles of Pd/K2621 are closer and more protected by the polymer chains of the support (Figure 62, left) than in Pd/SpDVB (Figure 62, right) and this could explain why they are reconstructed to a smaller extent[135] and confirms that our catalysts are not directly comparable with Pd/HAp investigated by Tian et al. as discussed above.

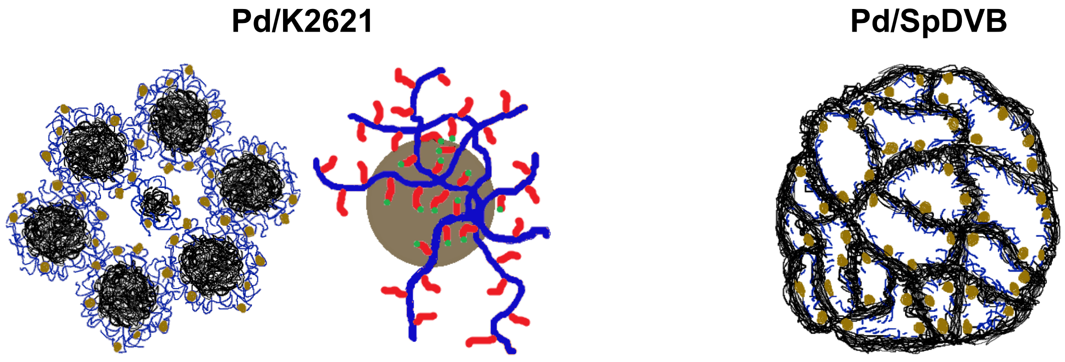

Pd/K2621

Pd/SpDVB

Figure 62: palladium nanoparticles (light-brown circles) in the polymer framework of Pd/K2621 (left panels) and Pd/SpDVB (right panels). Blue lines represent the polymer chains in the swollen gel-phase; green spots and red lines represent the side sulfonic groups, respectively interacting and not interacting with the metal surface.

However, Pd/K2621 produces HP for a remarkably shorter time than Pd/SpDVB and is eventually much less productive. With Pd/K2621, HP must first leave from the gel-phase swollen by the solvent and, if this process is relatively slow, HP can start to be transformed into water when its concentration is still relatively low. Conversely, with its relatively very open morphology, featured by highly accessible mesopores, the support of Pd/SpDVB apparently allows the efficient removal of HP from the catalyst, thus retarding the onset of its hydrogenation and/or dismutation.

With ACN as the co-solvent Pd/K2621 is also promoted: its selectivity and productivity are both increased in comparison with the unpromoted catalyst. HP concentration increases for 1440 min, up to 7.1 mmol (23.6 mM) with a seven-fold increase with respect to unpromoted Pd/K2621 (Figure 58). As the result, the productivity of the catalyst tops 410 $mmol_{HP}\cdot g_{Pd}^{-1}\cdot h^{-1}$ after 240 min and is still 270 $mmol_{HP}\cdot g_{Pd}^{-1}\cdot h^{-1}$ after 1440 min (Figure 59). Remarkably, the selectivity of promoted Pd/K2621 in the first 1440 min changes in a very similar way as that of Pd/SpDVB (Figure 43) and also in this case a stable selectivity is observed for at least 240 min. K2621 is also a sulfonic ion-exchange resin, hence these results support the hypothesis that Pd(II) cationic soluble species stabilized by acetonitrile and interacting with the sulfonic groups of the ion-exchanger are involved in the promoting action of the co-solvent. In this case, the effect of acetonitrile is even stronger, which seems in line with the morphology of the polymer support, the polymer chains of which are in a closer contact with the metal nanoparticles.

When Pd/K2621 is used in the presence of acetonitrile as the co-solvent (and promoter), the final metal leaching is lowered to 3.3%, the proportion of Pd(II) is increased to 45% only from the initial 38% (Figure 60, lower panel and Table 14) and the reconstruction of the metal nanoparticles is even more limited in comparison to unpromoted Pd/K2621. In fact, their average diameter in the exhausted promoted catalyst is 4.7 nm, much closer to the value of fresh Pd/K2621 (Figure 61).

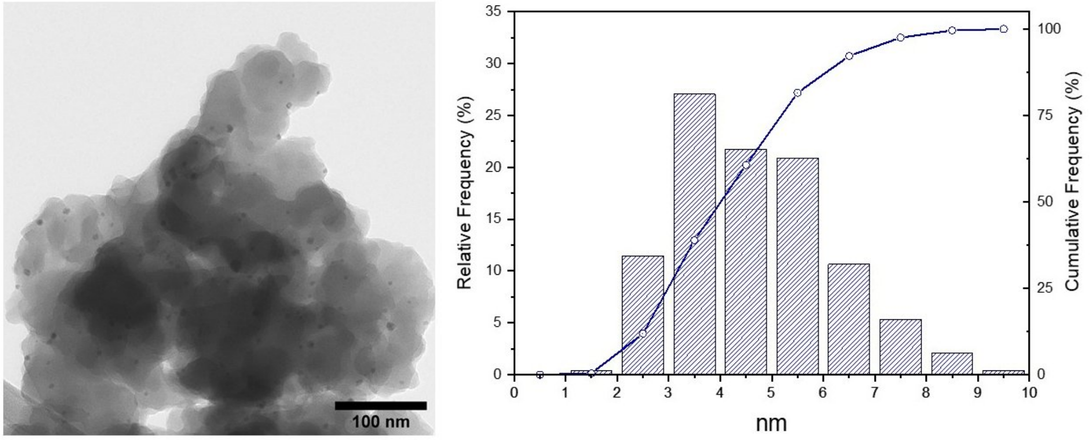

Figure 63: TEM micrograph of Pd/K2621 and related size distribution of the Pd NPs in the sample recovered from a catalytic experiment in the presence of acetonitrile.

All these findings point to a higher level of protection of the metal phase inside the gel-phase swollen by the mixture of methanol and acetonitrile in comparison with pure methanol. This can be readily explained by the different ability of the two media to swell K2621, as highlighted by their specific volumes in pure methanol (1.33 $cm^3 \cdot g^{-1}$) and in methanol:acetonitrile, 9:1, v/v (1.00 $cm^3 \cdot g^{-1}$). With a lower swelling degree of the gel-phase in the presence of acetonitrile,[196] the oxidative reconstruction of the metal phase, favoured by the stabilization of Pd(II) by acetonitrile, apparently occurs to a lower extent. In fact, the dependence of the behaviour of cross-linked polymers supported catalysts on the swelling degree is well documented. [123,137] As in pDVB based materials there is no gel-phase, or it is formed in negligible amount, their swelling properties depend to a lesser extent on the nature of the swelling solvent. Accordingly, the metal nanoparticles of Pd/SpDVB are not as protected as in Pd/K2621 and are more susceptible of reconstruction.

In summary, the effect of acetonitrile is qualitatively similar in Pd/SpDVB and in Pd/K2621, with an apparent net oxidation of the metal phase and reconstruction of the metal nanoparticles. Due to the different morphology of the supports, the effect is smaller in Pd/K2621 and even more so when acetonitrile is present, as it affects the swelling behaviour of the supports. In the case of Pd/SpDVB the reverse is true, because the metal nanoparticles are not protected by the presence of a gel-phase and are more exposed to the action of acetonitrile. In the unpromoted catalysts (DS in pure methanol), Pd/K2621 is somewhat more selective than Pd/SpDVB, likely because the size of the nanoparticles is only slightly lower and this seems to be beneficial for this kind of catalysts. In the presence of acetonitrile, the behaviour of these two catalysts is levelled at least as far as the selectivity is concerned. Their plots of selectivity as the function of the time are practically superimposable in the first 1440 min, implying that under these conditions the selectivity of the catalysts is not size-dependent. The common feature of these two catalysts in action is the reconstruction of the metal phase and it can be argued that the selectivity is controlled by this dynamic process based on the release-and-capture. Its mechanism could involve the control of the oxidation state of the metal, the formation of soluble molecular Pd(II) species stabilized by acetonitrile and their interplay with the surface of the nanoparticles.

2.3.2.7 Pd/K1221 catalyst

Commercial gel-type ion-exchange resin Lewatit K1221 was used to prepare a Pd catalyst with the same procedure exploited for the synthesis of Pd/SpDVB and Pd/K2621. According to Frison et al.,[141] catalysts supported on gel-type resins are not very active in the DS due to the high diffusive restrictions generated by the gel polymer matrix in which the palladium NPs are embedded. On the other hand, taking into the account the experiments with Pd/K2621 in the presence of ACN, the stronger the interaction between the polymer framework and the metal nanoparticles the higher the expected promotion effect of ACN. The results of the catalytic experiments of DS with Pd/K1221 catalyst in methanol and in the presence of acetonitrile are reported in Figure 64.

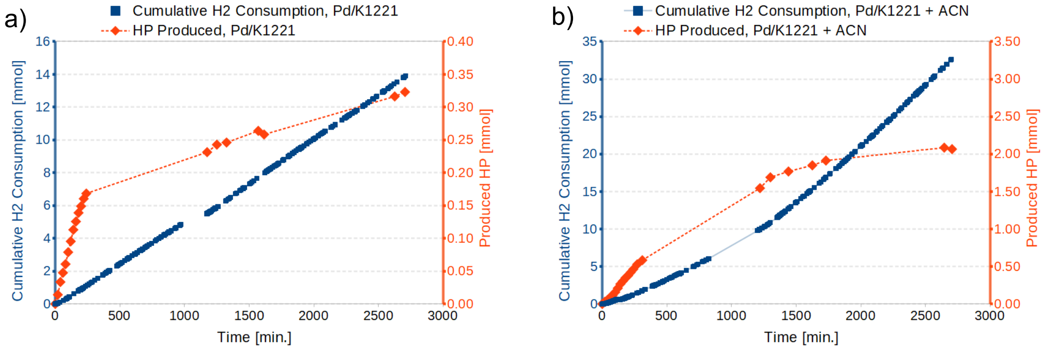

Figure 64: results of catalytic tests of Pd/K1221 in methanol (a) and in methanol:acetonitrile 9:1 vol (b). Cumulative hydrogen consumption is reported on blue squares, the produced HP is reported on red diamonds.

In line with the results obtained with Pd/pDVB, Pd/SpDVB and Pd/K2621, the catalytic activity of Pd/K1221 is limited, being not only the lowest among the polymer supported catalysts studied in this Thesis, but also lower than that of Pd/C. When acetonitrile is present in solution, the catalyst shows higher H_2 consumption and HP production. For sake of comparison, the catalytic performance of Pd/K1221 is reported along with that of Pd/SpDVB in Figure 65.

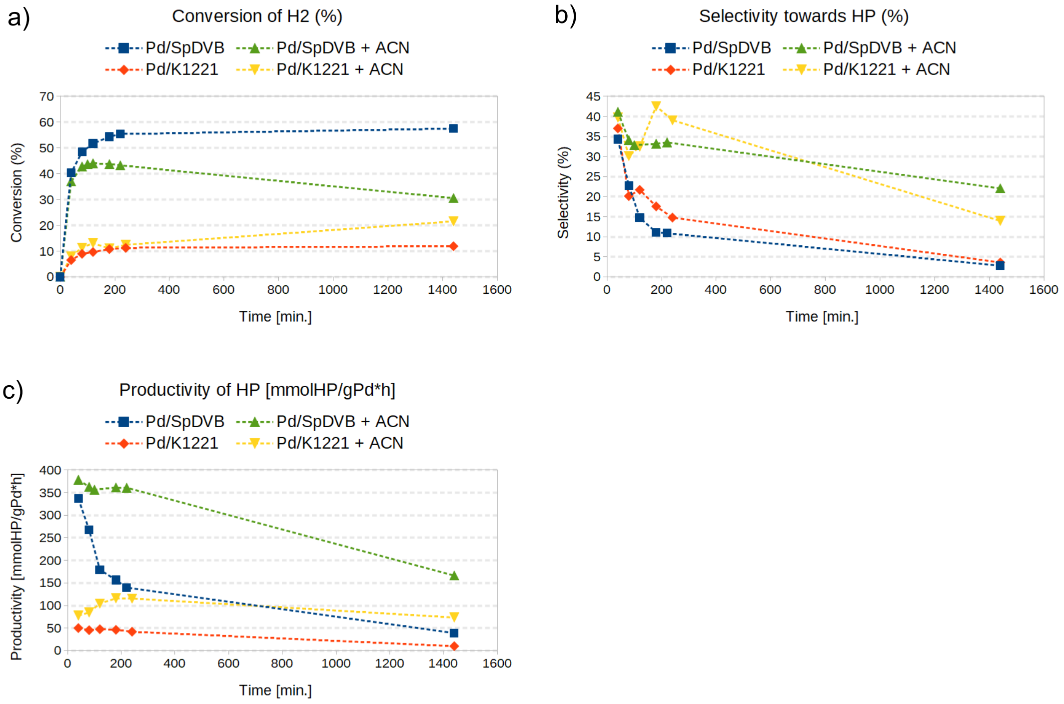

Figure 65: conversion (a), selectivity (b) and productivity (c) of Pd/SpDVB in methanol (blue squares), of Pd/K1221 in methanol (red diamonds), of Pd/K1221 in methanol:acetonitrile 9:1 vol (yellow triangles) and of Pd/SpDVB in methanol:acetonitrile 9:1 vol (green triangles).

These findings further confirm that in presence of ACN the stronger the interaction between the polymer matrix and Pd nanoparticles the higher is the enhancement effect. In this case, due to the gel-type morphology, featured by small mesopores and micropores in the swollen state, the interactions are so strong, that the formation of more active species leads not only to a productivity enhancement but also to the promotion of the conversion. Not only this is the first time this effect is observed, but also Pd/K1221 is the only catalyst investigated in this work showing this particular enhancement behaviour in the presence of ACN. Unfortunately, no XPS or TEM characterisations of the Pd/K1221 (fresh or spent) are available at the moment, even though an increase of the Pd(II)/Pd(0) ratio is expected also in this case. More interesting would be the TEM characterisation, as it makes possible to evaluate the reconstruction of the metal phase, that is expected to be particularly significant considering the strong trapping effect of the gel-type polymer matrix with respect to the metal NPs.

2.3.3 Conclusive remarks on the effect of acetonitrile

Acetonitrile is a novel corrosion-free selectivity enhancer, but its effect strongly relies on the nature of the catalytic support. With unfunctionalized supports, acetonitrile mainly behaves as a poison. In fact, it inhibits the hydrogen consumption over Pd/C and Pd/pDVB, making them very little productive and in the presence of H_2SO_4 the poison effect is even more pronounced. By contrast, with catalysts supported on ion-exchange resins, such as Pd/SpDVB, Pd/K2621 and Pd/K1221, acetonitrile leads to a remarkable improvement of both selectivity and productivity. Interestingly, the extent of the enhancement depends on the morphology of the ion-exchange support. In particular, in the presence of acetonitrile, the selectivity at 240 min of the Pd catalyst supported on a mesoporous ion-exchanger (Pd/SpDVB) is 3.5 times higher than that of the unpromoted catalyst, whereas it appears and double and 2.5 times higher than that of the catalysts supported on macroporous (Pd/K1221) and gel-type (Pd/K2621) sulfonic resins, respectively. Moreover, from 90 to 240 min the selectivity changes very little with time, with the exception of Pd/K1221, for which an increase is even observed. For longer reaction times, the selectivity declines, but much less than for the unpromoted catalysts: for Pd/SpDVB and Pd/K2621 the selectivity at 1440 min is 8 times higher in the presence of acetonitrile, whereas with Pd/K1221 is “only” 4 times higher than the value of the unpromoted catalyst.

The detection of nitrogen and enhanced Pd(II) signals in the XPS spectrum of the catalysts recovered from the catalytic experiments with acetonitrile shows that the promoter can strongly interact with the catalyst, favouring the oxidation of the metal. In spite of this, the level of leaching is practically unaffected. This can be readily attributed to the ability of the resins to retain the leached species within the support, through their ionic interactions with the sulfonic groups. In this context, a relatively high concentration of *cationic* acetonitrile complexes of Pd(II), such as $[Pd(N{\equiv}C\text{-}CH_3)_4]^{2+}$ or related ones, can be envisaged inside the catalyst. These species are very likely involved in the reconstruction of the metal nanoparticles showed by TEM of the exhausted catalysts. Nanoparticles smaller than the original ones are formed in a thermodynamically up-hill process, which requires a fast nucleation step. This implies the release of molecular species of palladium in the liquid phase (leaching) and a relatively high concentration thereof inside the catalyst. However, the size distributions of the nanoparticles observed at the end of the catalytic experiments with and without acetonitrile are quite similar, indicating that the promoter do not simply mediate the reconstruction of the nanoparticles and that the different catalytic behaviours cannot be accounted for by the different in the nanoparticle sizes. Finally, some XRD characterizations show no difference from the fresh catalyst and the catalysts after the DS experiment in pure methanol or in the presence of ACN. The formation of the fraction of smaller nanoparticles is allegedly not seen due to their very low dimension. In this context, it is quite clear that acetonitrile is an effective inhibitor of the splitting of O-O bonds, as observed herein and by Paunovic and co-worker[161] in the decomposition of HP, but still this does not explain the effect or the ion-exchange catalytic support, turning ACN from poison to promoter.

To shed a light on the possible role of an ion-exchange material on the catalytic performance in the DS in the presence of acetonitrile, the investigation has been extended to zeolite supported Pd catalysts.

Chapter 4: Effect of acetonitrile on zeolite supported palladium catalysts

2.4 Introduction to the effect of acetonitrile on zeolite supported catalysts

Zeolite are deeply investigated as catalytic supports for metal nanoparticles for the DS (Paragraph 1.5.6). The main positive features of these materials for the DS are the high resistance to the degradation in oxidative environment and the presence of acid groups, the amount of which can be tuned by changing the Si/Al ratio. On the other hand, zeolites are featured by micropores, leading to diffusive restrictions that can negatively affect the performance of the catalysts. In this Chapter, several zeolite supports produced by the research group of Prof. Peirong Chen (South China University of Technology, Guangzhou, China) were used for the preparation of palladium catalysts, to extend the investigation of the promotion effect of ACN to further ion-exchange materials. More in details, three different types of zeolites, namely LTA, SSZ-13(1Al) and SSZ-13(2Al), were included in the investigation. The former is one of the most common zeolite used in the water treatment or separation of gas mixtures,[197] and its structure is composed by sodalitic cages connected via cubic units[198] whereas SSZ-13 zeolites are belonging to the chabazite-structured zeolites and are exploited in the purification of gases.[198–200] The structure of LTA and SSZ-13 zeolites is reported in Figure 66.

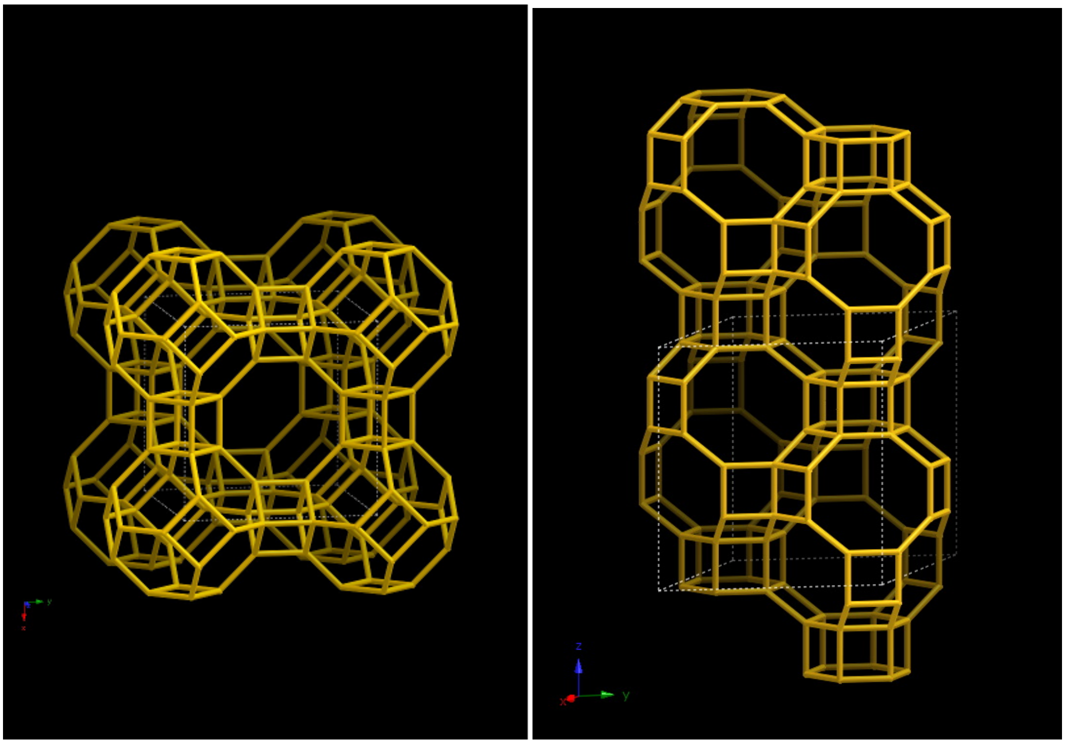

Figure 66: structures of LTA (left) and SSZ-13 (right) zeolites.[201]

The structural difference between SSZ-13(1Al) and SSZ-13(2Al) zeolites is the presence of one (1Al) or two (2Al) aluminium arrangements in the six member rings of the structure. In Figure 67 are reported the XRD characterizations of the three zeolites, that are in agreement with the literature (black lines).

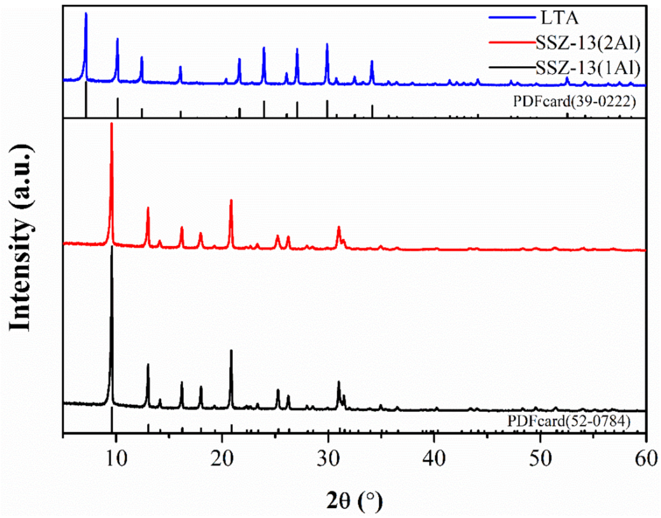

Figure 67: XRD characterization of LTA (blue spectra), SSZ-13(1Al) (red spectra) and SSZ-13(2Al) (black spectra), together with the literature spectrum (black line).

The zeolites were used to prepare catalysts with two different synthetic approaches, such as ion-exchange (IE) and wet impregnation (WI), always using palladium nitrate as the metal precursor. The ion-exchange procedure is substantially similar to that exploited for the synthesis of part of the polymer supported catalysts (Chapter 3). The wet impregnation approach consists in the treatment of a slurry of the support with the metal precursor followed by the solvent removal by evaporation. The results of the Si/Al ratios and surface area characterisations of the catalysts are summarized in Table 15 and Table 16.

Table 15: characterization of the zeolite supports.

Sample	**Si/Al ratio**	**S_{BET} (m^2g^{-1})**
SSZ-13(1Al)	11.50	550
SSZ-13(1Al)	10.29	569
LTA	1.50	2.51

Table 16: characterization of the zeolite catalysts.

Sample	**Si/Al ratio**	**Pd content (% w/w)**
Pd/SSZ-13(1Al) WI	11.60	1.01
Pd/SSZ-13(1Al) IE	10.29	1.01
Pd/SSZ-13(2Al) WI	10.40	1.00
Pd/SSZ-13(2Al) IE	10.17	1.22

The palladium content of the zeolite catalysts is very close to 1% w/w, with Pd/SSZ-13(2Al) IE being slightly higher. The Si/Al ratio of SSZ-13 zeolites is in the range 10.17-11.60, whereas it appears remarkably lower for LTA (1.50). Thanks to its higher acidity, the LTA-supported catalysts are expected to be more active towards the DS, although the surface area of LTA is much lower than expected for a microporous material. This suggests a hindered porous system, poorly accessible to the metal precursor and the reaction gases during the synthesis of the catalyst and the DS, respectively. On the basis of the available characterization it is not possible to explain the very limited surface area of the provided LTA zeolite, that is expected to be similar to that of SSZ-13,[202] All the palladium catalyst were testes in the DS as received, that is after the introduction of the metal precursor by IE or WI and the subsequent calcination. Moreover, all the palladium containing zeolite materials were reduced with the same experimental procedure developed for resin catalysts. The reduced catalysts were studied in the DS reaction both in methanol and in the 9:1 vol methanol:acetonitrile mixture. The reduced catalysts are coded with the suffix Pd(R)/ before the name of the zeolite support.

Unfortunately, as XPS, TEM and EXAFS characterizations of the fresh and spent catalyst are still ongoing, information on the active metal phase and its modification after the catalytic experiments are not yet available. Therefore, for zeolite catalysts the effect of the co-solvent, catalytic support and synthetic procedure can be mainly obtained only from the results of the catalytic experiment. For sake of comparison, the commercial 1% w/w Pd/Al_2O_3 was used as the reference catalyst.

2.4.1 Pd/Al_2O_3 reference catalyst

The commercial 1% w/w Pd/Al_2O_3 catalyst has been used as the reference for zeolite catalyst instead of Pd/C. In fact, this catalyst is useful for the evaluation of the effect of ACN as the support is more similar to zeolites than active carbon, without bearing ion-exchange groups. In Figure 68 are reported the catalytic experiments of Pd/Al_2O_3 with methanol and a 10% vol ACN solution in methanol reaction mixtures.

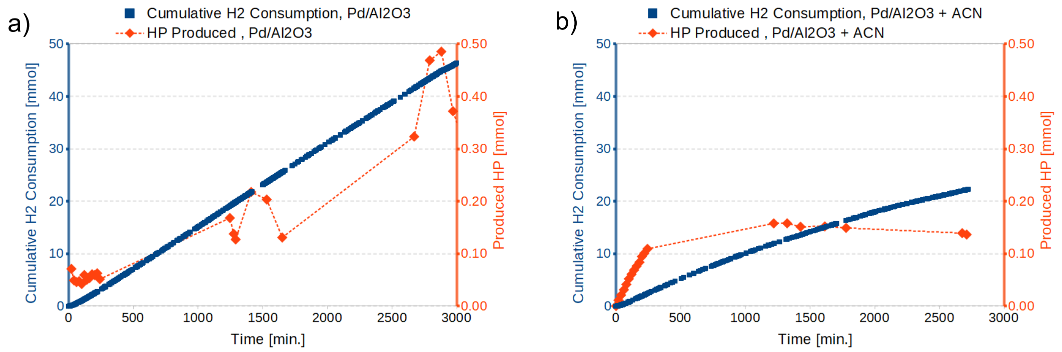

Figure 68: results of catalytic tests of Pd/Al_2O_3 in methanol (a) and in methanol:acetonitrile 9:1 vol (b). Cumulative hydrogen consumption is reported on blue squares, the produced HP is reported on red diamonds.

Although the results of produced HP suffer from a high dispersion in pure methanol, the effect of ACN appears strictly comparable to that of Pd/C catalyst. The Pd/Al_2O_3 catalyst is active in the consumption of hydrogen, with a conversion at the steady state of 37%, slightly higher than Pd/C. However, the catalyst produces very little hydrogen peroxide, being the selectivity at 10% after 40 min and steadily decreasing over time. Therefore, the Pd/Al_2O_3 catalyst turns out to be the less selective and productive than Pd/C and the palladium catalysts supported on resins. When ACN is present in the reaction mixture, the consumption of hydrogen is lower, with the conversion of 23% at 1440 min, decreasing to 20% at the end of the catalytic experiment. This kind of deactivation has been also observed for any resin catalyst (Paragraphs 2.3.2.1 and 2.3.2.6), with the exception of Pd/K1221. In the presence of ACN, the selectivity of Pd/C remains almost unchanged. Since the selectivity is not significantly affected by the presence of acetonitrile, the deactivation of the catalyst leads to the decrease of the production of HP, similarly Pd/C and Pd/pDVB. These results further confirm that the use of acetonitrile as the co-solvent with catalysts supported on materials lacking of ion-exchange functions does not enhance the performance, but rather leads to poor H_2 conversion and HP production.

2.4.2 LTA supported catalysts

Taking into account the peculiar features of LTA zeolite (Paragraph 2.4), the rationalization of the catalytic outcomes of the catalysts supported on this material is particularly difficult. The as prepared IE catalyst (Figure 69, green profile) shows a very low conversion of H_2 (only 0.21 mmol in 240 min) and the complete selectivity towards HP during the first four hours of reaction. After about 400 min the catalyst activates and the production of HP almost stops, with the consequent drop of the selectivity. As Pd/LTA IE catalyst is prepared without applying any reduction treatment after the calcination, the palladium phase is largely oxidized and is expected to be partially reduced by the H_2 under DS conditions. According to literature reports suggesting higher selectivity for catalysts with higher Pd(II) content (Paragraph 1.5.5), the catalyst at the beginning of the test is very poorly active and very highly selective, whereas as soon as the reduction of the metal phase starts the activation of the catalyst and the decrease of the selectivity can be observed. This hypothesis is further confirmed by the reactivity of the corresponding reduced catalyst, Pd(R)/LTA IE (Figure 69, blue profile). In fact, the treatment with hydrogen before the catalytic experiment increases the activity during the first hours of reaction, with a HP production comparable to that of unreduced Pd/LTA IE. With respect the form Pd/LTA IE catalyst assumes after 400 min under DS conditions, Pd(R)/LTA IE shows lower activity and HP production after one day of reaction (1440 min). When ACN is added in solution, both the production of hydrogen peroxide and the conversion of hydrogen increase, and Pd(R)/LTA IE appear more productive than Pd/LTA IE in the first four hours of reaction (Figure 69). The detailed rationalization of LTA catalysts produced by IE is complicate as they are very little active, with the highest conversions of 20% and 15% in the presence of ACN and in pure methanol respectively, rapidly decreasing over time during the catalytic experiment. Moreover, the productivity values are very low, reaching the highest value of 60 $mmol_{HP}/g_{Pd}h$ in the presence of ACN, after 40 min.

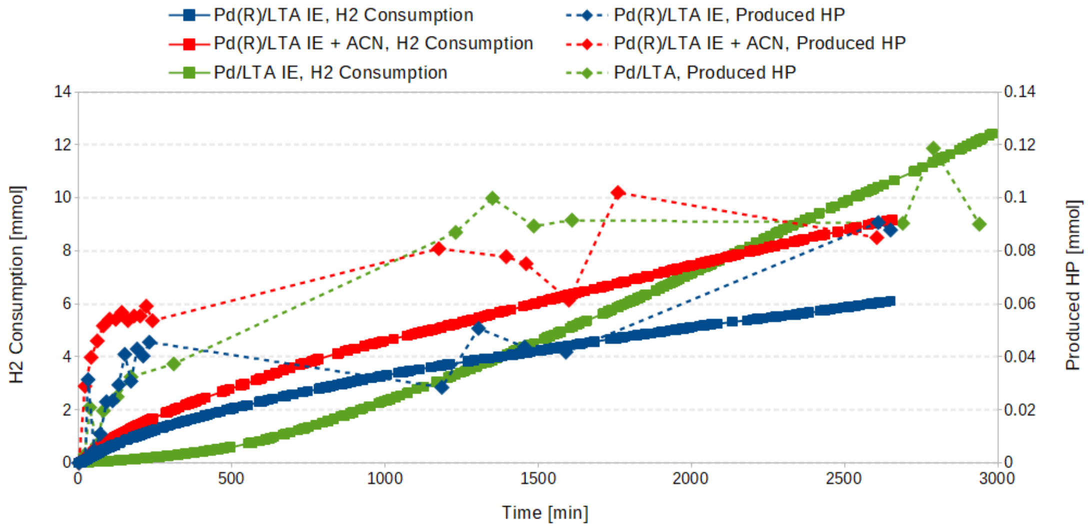

Figure 69: results of catalytic tests of Pd supported on LTA, prepared by IE method. In blue Pd(R)/LTA IE cumulative H_2 consumption (squares) and produced HP (diamonds) in methanol, in red Pd(R)/LTA IE cumulative H_2 consumption (squares) and produced HP (diamonds) in methanol:acetonitrile 9:1 vol and in green Pd/LTA IE cumulative H_2 consumption (squares) and produced HP (diamonds) in methanol.

The reactivity of LTA catalyst produced by WI is particularly different, from Pd/LTA IE. In this case, similarly to the test with Pd/C in the presence of both ACN and H_2SO_4 (Paragraph 2.3.1), the hydrogen consumption is very low and the experimental error becomes relevant, leading to an apparent negative consumption. In this case, differently from Pd/LTA IE, the expected reduction of Pd(II) of the unreduced catalyst does not seem to occur, as no significant activation of the catalyst can be observed. The production of HP of Pd/LTA WI is also very limited and results only 0.04 mmol higher than with Pd/LTA IE. Although the absolute values remain limited, the reduction of the catalyst, to produce Pd(R)/LTA WI, significantly increases the catalytic performance, with an overall three times higher hydrogen consumption at the end of the experiment (18 mmol vs 6 mmol) and the double amount of produces HP (0.18 mmol over 0.09 mmol). The reduced catalyst does not show any deactivation over time and the consumption of H_2 (0.36 mmol/h) is almost equal to that of Pd(R)/LTA IE (0.34 mmol/h).

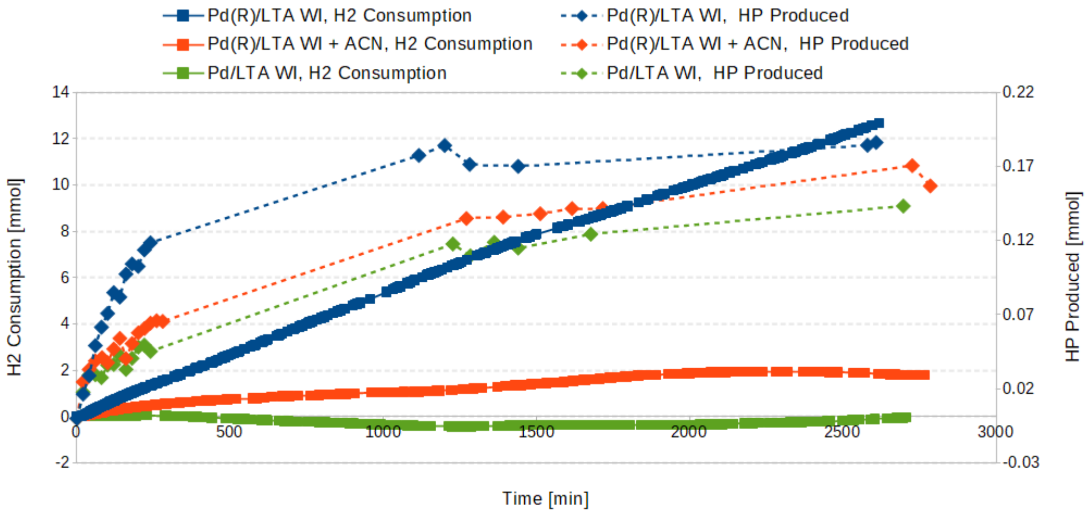

Figure 70: results of catalytic tests of Pd supported on LTA, prepared by WI methods. In blue Pd(R)/LTA WI cumulative H_2 consumption (squares) and produced HP (diamonds) in methanol, in red Pd(R)/LTA WI cumulative H_2 consumption (squares) and produced HP (diamonds) in methanol:acetonitrile 9:1 vol and in green Pd/LTA WI cumulative H_2 consumption (squares) and produced HP (diamonds) in methanol.

These results suggest that the Pd(R)/LTA WI catalyst is probably more stable than Pd(R)/LTA IE during the reaction. In fact, both un-reduced and reduced LTA WI catalysts maintain over the whole test their performances, corresponding to those shown by IE catalysts only at the beginning of the catalytic experiments. Similarly to the reference catalyst, the addition of acetonitrile (Figure 70, red profile) leads both to the deactivation of the catalyst and to the reduction of the production of HP, resulting in a negligible increase of the selectivity (1-2%). The lack of enhancement for Pd(R)/LTA WI could be connected to the particular stability of the catalyst, suggested by the observed reactivity of the as prepared and reduced materials and hindering the formation of cationic species, responsible of the promotion effect (Paragraph 2.3.3). As a general overview, LTA supported catalysts are very little active and show a very limited production of hydrogen peroxide, when compared to the reference catalyst (Pd/Al_2O_3). This outcome is not affected by the synthetic approach used for the preparation of the catalysts and can be explained by very low surface area of the support.

2.4.3 SSZ-13(1Al) supported catalysts

As the Si/Al ratio is lower for SSZ-13(1Al) zeolite than for LTA, the derived catalysts are expected to be less active in the production of HP, in the same way Pd/SpDVB outperforms the corresponding Pd/pDVB catalyst (Paragraph 2.3.2.1). On the other hand, this catalyst presents a much larger surface area that could positively effect the activity in the DS. The catalytic experiment of DS with Pd/SSZ-13(1Al) IE catalyst are reported in Figure 71.

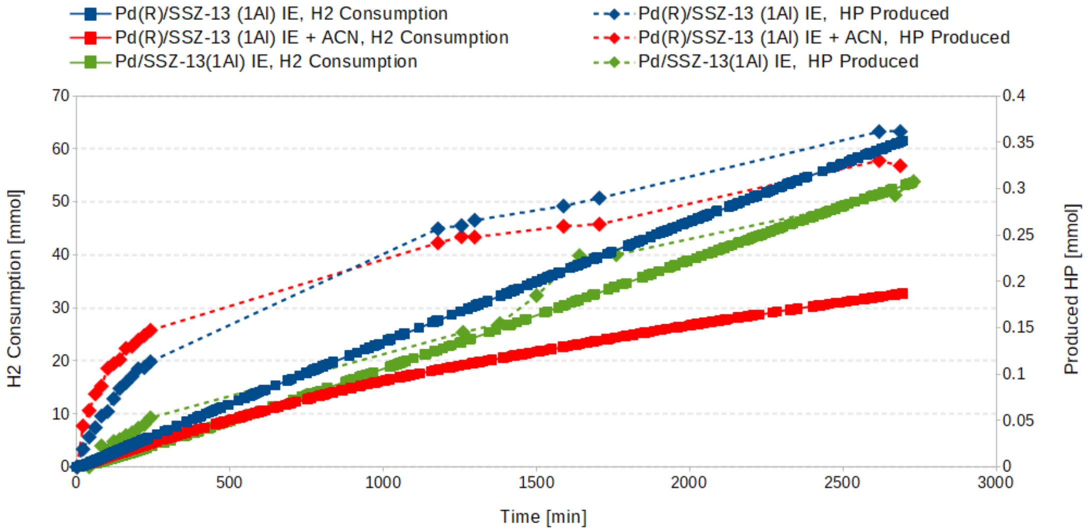

Figure 71: results of catalytic tests of Pd supported on SSZ-13(1Al), prepared by IE methods. In blue Pd(R)/SSZ-13(1Al) IE cumulative H_2 consumption (squares) and produced HP (diamonds) in methanol, in red Pd(R)/SSZ-13(1Al) IE cumulative H_2 consumption (squares) and produced HP (diamonds) in methanol:acetonitrile 9:1 vol and in green Pd/SSZ-13(1Al) IE cumulative H_2 consumption (squares) and produced HP (diamonds) in methanol.

With methanol as the reaction solvent, Pd/SSZ-13(1Al) IE presents a cumulative hydrogen consumption comparable to that of Pd/Al_2O_3 and much higher than that of Pd/LTA catalysts. In case of the unreduced catalyst (Pd/SSZ-13(1Al) IE), the conversion increases from 21% at 40 min to 46% at 1440 min, with a very short induction time, whereas, differently from Pd/LTA IE catalyst, the conversion of hydrogen is already high after less than one hour of catalytic experiment. With the reduced catalyst Pd(R)/SSZ-13(1Al) IE the conversion is even higher, increasing from 44% at 40 min to 57% at 1440 min. Also in this case the reduction treatment is increasing the activity of the catalyst, although the unreduced one is already active. Nevertheless, the production of hydrogen peroxide is very low for both Pd/SSZ-13(1Al) IE and Pd(R)/SSZ-13(1Al) IE and appears higher for the reduced catalyst, especially in the first four hours of reaction. However, these catalysts turn out to be also highly productive in the formation of water, with the selectivity never overcoming 4.5% and 2.5% for the unreduced and reduced catalysts, respectively. Similarly to polymer catalysts (Chapter 2 and 3), this can be explained once more by taking into account the microporous morphology, typical of zeolites. In contrast to pDVB based catalysts, the back diffusion of the produced HP towards the bulk solution is hindered, increasing the probability of the further hydrogenation of HP to be water. The presence of ACN in the reaction mixture lowers the hydrogen consumption when compared to pure methanol as the reaction mixture. Under these conditions, the deactivation continues over time, with a conversion of 35% and 30% at at 1440 min and at the end of the catalytic experiment, respectively. With Pd(R)/SSZ-13(1Al) IE the production of HP increases in the first four hours of reaction in the presence of ACN, with respect to pure methanol as the reaction mixture. This leads to a selectivity increase of about 5% at 40 min and 1.5% at 240 min when compared to the experiment in pure methanol. After 1440 min the HP production is higher in pure methanol, but the lower H_2 consumption still grants an overall selectivity enhancement. Also in this case the effect of ACN as the promoter for ion-exchange catalysts is evident, even though the overall performance of Pd(R)/SSZ-13(1Al) IE in the DS is limited: in fact, the unpromoted system mainly produces water and the addition of ACN is not enough to remarkably improve the catalytic results.

Almost the same trend can be recognized for further catalysts prepared by WI (Figure 72). In fact, the reduced catalyst (Pd(R)/SSZ-13(1Al) WI) is the more active in the consumption of H_2, and the corresponding unreduced material (Pd/SSZ-13(1Al) WI) appears less active, with a conversion only about 10% lower at any time. Also in the experiment with the reduced catalyst in the presence of ACN, a decrease of the conversion occurs. Hence, the hydrogen consumption profiles of the SSZ-13(1Al) catalysts prepared by IE and WI are almost superimposable. However, this trend cannot be observed for the production of HP, as both Pd/SSZ-13(1Al) WI and Pd(R)/SSZ-13(1Al) WI are much less selective than the corresponding catalysts prepared by IE method.

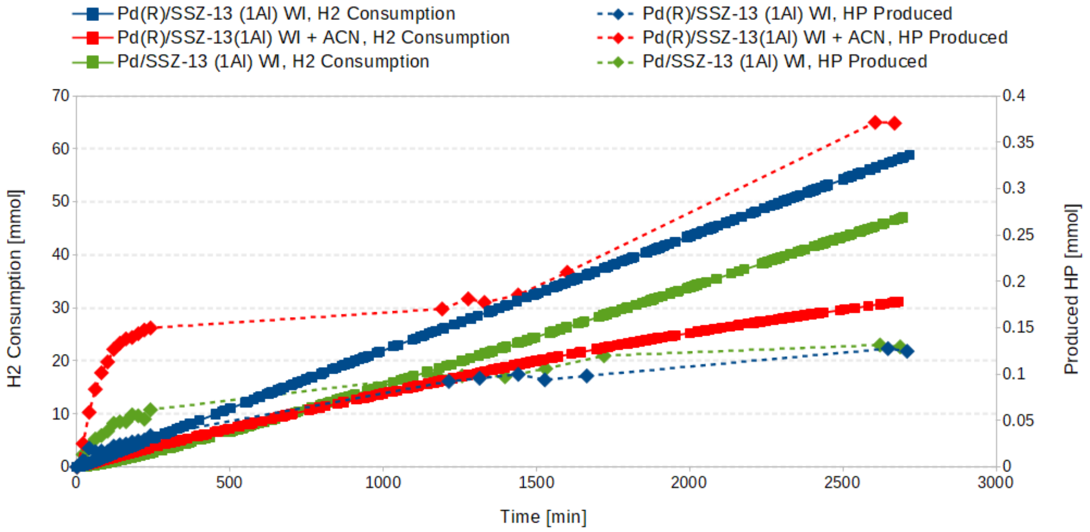

Figure 72: results of catalytic tests of Pd supported on SSZ-13(1Al), prepared by WI methods. In blue Pd(R)/SSZ-13(1Al) WI cumulative H_2 consumption (squares) and produced HP (diamonds) in methanol, in red Pd(R)/SSZ-13(1Al) WI cumulative H_2 consumption (squares) and produced HP (diamonds) in methanol:acetonitrile 9:1 vol and in green Pd/SSZ-13(1Al) WI cumulative H_2 consumption (squares) and produced HP (diamonds) in methanol.

However, when acetonitrile is used as enhancer, the profile of the production of HP for IE and WI is almost comparable at the end of the test, only differing after one day of reaction. In particular, after one day of reaction, the production of HP almost stops and starts to slowly increase again after 1500 min. In summary, Although substantially different from the outcomes of SSZ-13(1Al) IE materials, the results of the SSZ-13(1Al) supported catalysts prepared by WI confirm once more the promotion effect of ACN. Additional information about the metal phases of the catalysts prepared by WI and IE is needed to identify possible structural or chemical features (in particular nanoparticles size and oxidation state) to rationalize the different reactivity. Furthermore, the consumption of hydrogen of the unreduced catalysts supported on Pd/SSZ-13(1Al) is comparable to that of Pd/Al_2O_3, whereas the corresponding reduced catalysts significantly outperform the reference catalyst. Conversely, the production of hydrogen peroxide is always lower then the reference, with the exception of Pd(R)/SSZ-13(1Al) IE, that shows a productivity close to that of the reference catalyst.

2.4.4 SSZ-13(2Al) supported catalysts

The SSZ-13(2Al) support presents the same structural properties of the (1Al) material and only differs in the presence of two Al units in the six member rings (namely 6MR, d6r in Figure 73).

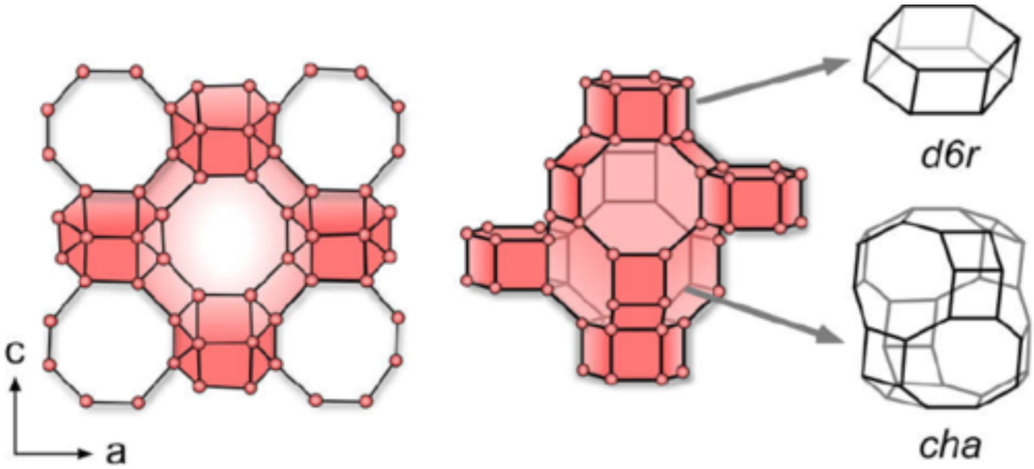

Figure 73: schematization of the structure of SSZ-13 catalyst.[203]

In Figure 74 are reported the results of the DS experiments with the catalysts supported on SSZ-13(2Al) produced by IE method.

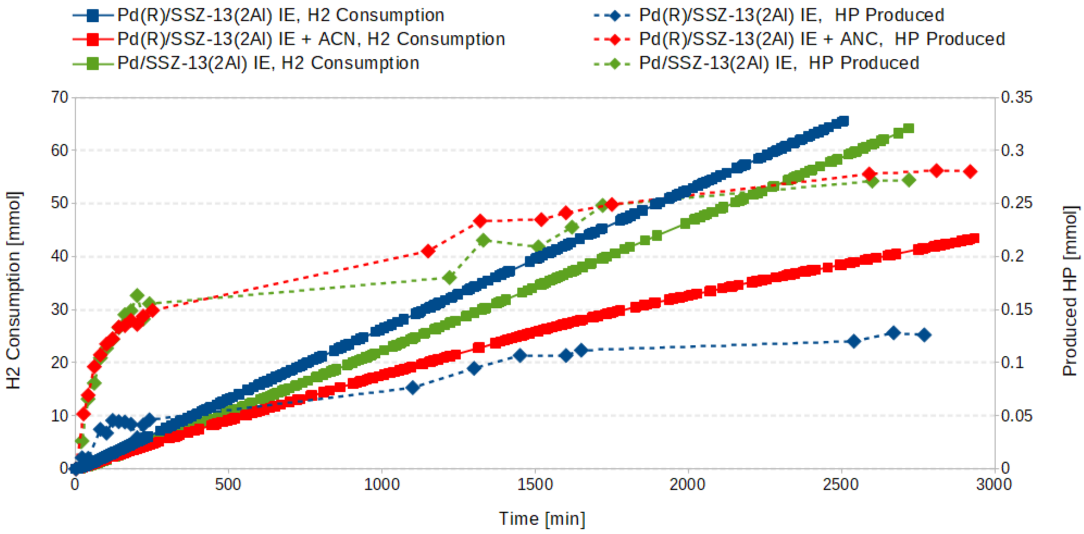

Figure 72: results of catalytic tests of Pd supported on SSZ-13(2Al), prepared by IE methods. In blue Pd(R)/SSZ-13(2Al) IE cumulative H_2 consumption (squares) and produced HP (diamonds) in methanol, in red Pd(R)/SSZ-13(2Al) IE cumulative H_2 consumption (squares) and produced HP (diamonds) in methanol:acetonitrile 9:1 vol and in green Pd/SSZ-13(1Al) IE cumulative H_2 consumption (squares) and produced HP (diamonds) in methanol.

The reduced catalyst Pd(R)/SSZ-13(2Al) IE shows a hydrogen consumption comparable to that of both the corresponding catalyst of the (1Al) series and the reference catalyst. On the other hand, the production of HP is lower, resulting at any reaction time almost one third of the amount produced by the corresponding catalyst of the (1Al) series. When ACN is added to the reaction mixture the conversion lowers from 65% for the unpromoted catalyst to 36% at the end of the catalytic experiment. At the same time, the promotion effect due to the combination of ion-exchange groups and ACN leads to a higher production of HP. The selectivity of the unpromoted catalyst never overcomes 2%, whereas in the presence of ACN starts from 11% to steadily decrease, as observed in almost any experiment with the SBR setup. Moreover, the addition of ACN induces for Pd(R)/SSZ-13(2Al) IE catalyst one of the highest increase of HP production, equal to 0.280 mmol at the end of the catalytic experiment, with respect 0.126 mmol in pure methanol. By assuming for zeolite catalyst the same enhancement model proposed for sulfonic materials (Paragraph 2.3.3), the presence of two ion-exchange functions in a 6MR allows a stronger interaction of the dicationic Pd(II) complexes with the support. The higher activity of the unreduced Pd/SSZ-13(2Al) IE catalyst with respect to Pd/SSZ-13(1Al) IE could be also explained by the stronger interaction with Pd(II), considered as the metal phase more active in the production of HP.

The presence of more active catalytic species in the unreduced catalysts of the (2Al) series is even more evident in the catalyst prepared by WI (Figure 73).

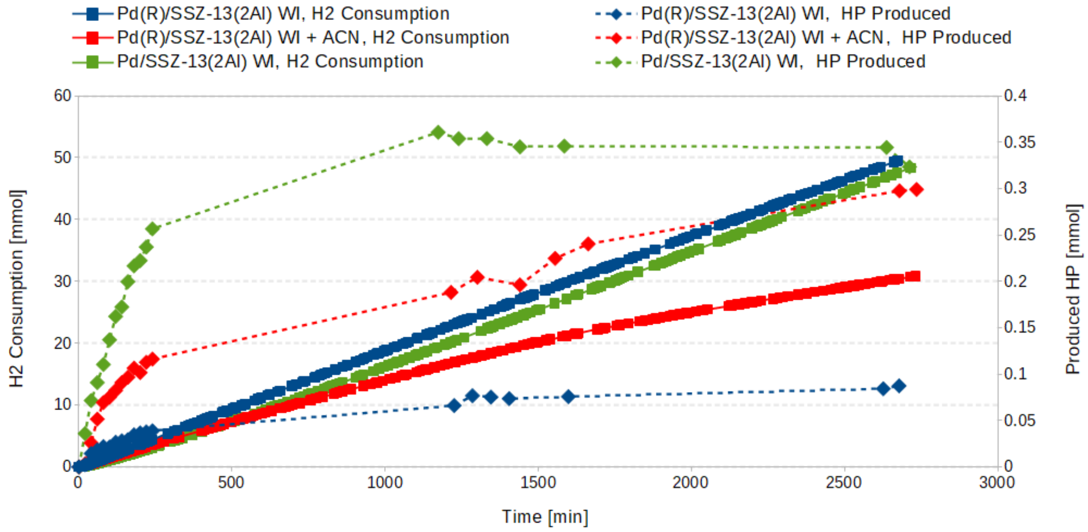

Figure 73: results of catalytic tests of Pd supported on SSZ-13(2Al), prepared by WI methods. In blue Pd(R)/SSZ-13(2Al) WI cumulative H_2 consumption (squares) and produced HP (diamonds) in methanol, in red Pd(R)/SSZ-13(2Al) IE cumulative H_2 consumption (squares) and produced HP (diamonds) in methanol:acetonitrile 9:1 vol and in green Pd/SSZ-13(1Al) WI cumulative H_2 consumption (squares) and produced HP (diamonds) in methanol.

In this case, the Pd/SSZ-13(2Al) WI catalyst shows a very high HP production, mainly in the first 240 min of reaction. By reducing the catalyst, ACN remarkably promotes the selectivity and the productivity still increases until the end of the test and is higher than that of the corresponding (1Al) catalyst (especially before 1500 min). In this case, the reduced catalyst Pd(R)/SSZ-13(2Al) WI shows a lower consumption of hydrogen with respect to the catalyst produced by IE. Although further investigations are needed to fully rationalize the reactivity, the most important results obtained from the catalysts supported on SSZ-13(2Al) is the further confirmation of the positive effect of ACN on both the production of HP and the selectivity of the reaction. The outcomes confirm that ion-exchange groups in the catalytic support are needed to ensure the enhancement effect of ACN, and suggest that the proximity of 2 Al moieties in the six members rings enhances the more the promotion effect.

2.4.5 Conclusions on the investigation with zeolite supported catalysts

Although the results of the zeolite supported catalysts cannot be fully rationalized due to the lack of characterisations, some important conclusions can be drawn from this investigation. First, it should be noticed that all the catalysts supported on zeolites, both as prepared (i.e. calcined) or reduced, are in the best cases as good as the reference catalyst, in terms of production of HP. Some of them, mainly the reduced catalysts supported on SSZ-13, show a conversion of hydrogen higher than Pd/Al_2O_3, but the production of hydrogen peroxide is never higher than the reference. LTA based catalysts result poorly active as the result of the particularly limited specific surface area. As to SSZ-13 supported catalysts, the reduced catalyst is more active but less selective than the corresponding unreduced material, with the exception of Pd/SSZ-13(1Al).

The most important finding of this investigation deals with the effect of ACN, that always leads to an increase of the selectivity and most of the time of the productivity as well. Finally, ACN exerts the strongest enhancement for the catalysts supported on SSZ-13(2Al), probably due to the more efficient interaction of the support with the Pd dicationic species.

Although minor differences in the performances can be recognized, the performance of palladium catalysts supported on zeolites in the DS are not comparable to that of Pd catalysts supported on resins, or even on active carbon.

The main achievement of this section is the experimental demonstration that acetonitrile can work as a promoter in the DS not only with catalysts supported on ion-exchange resins, but more in general with any support bearing ion-exchange functionalities. This outcome makes possible to extend the scope of this investigation from polymer materials to further classes of catalysts. In Chapter 5 the promotion effect is further investigated to demonstrate that it is not specifically connected to acetonitrile, but it represents a more general phenomenon, achievable, in principle, with any coordinating solvent.

Chapter 5: Coordinating solvents as selectivity enhancers: beyond acetonitrile

2.5 Introduction to the general effect of coordinating solvents

In Chapter 3 a selectivity enhancement of the DS with acetonitrile, similar to that of halides, has been presented. From the chemical point of view, the choice of ACN as selectivity promoter relies, similarly to halides, on its coordinating properties towards Pd(II). This preliminary investigation pointed out that the selectivity enhancement can be achieved with the synergetic effect of ACN and of a catalytic support with specific chemical features. In fact, the presence of ion-exchange sulfonic groups in the support material enhances the release-and-capture mechanism promoted by ACN, with an increase of the HP productivity and the consequent remarkable selectivity enhancement. This has been demonstrated for Pd nanoparticles supported on ion-exchange resins (Chapter 3) and zeolites (Chapter 4). In this Paragraph the promotion of the selectivity in the DS of HP was extended, by investigating the effect of further coordinating solvents on the selectivity of palladium catalysts supported on SpDVB, being the most promising resin catalyst. In particular, this investigation takes into the account benzonitrile (PhCN), to further verify and extend the effect of nitriles, N,N-dimethylformamide (DMF) and dimethylsulfoxide (DMSO). This study aims to demonstrate that the selectivity enhancement of the DS can be obtained with coordinating solvents of different nature. Thanks to DFT calculations it was possible to correlate the performance of the catalysts with the ligand properties of the selected enhancer. This represents a further confirmation of the previously reported release-and-capture mechanism, at the basis of the selectivity enhancement. The catalytic experiments reported in Chapter 5 have been carried out with Pd/SpDVB and Pd/C as the reference. The details of the catalysts and of their characterization before the catalytic tests are presented in Chapters 3 and 4.

2.5.1 Effect of benzonitrile on Pd/SpDVB

The first part of the investigation is focused on the effect on the DS of nitriles with alkyl substituents more hindering than methyl. As the mechanism of promotion proposed for ACN in Chapter 3, is based on the ligand properties of the functional group, the selectivity enhancement is expected to be recognized, in principle, for any nitrile, reasonably with differences depending on steric hindrance and electronic properties of the molecule. For this purpose, benzonitrile (PhCN) was selected and the performance in the DS of Pd/SpDVB was evaluated using a 10% vol methanol solution of this solvent. The cumulative H_2 consumption and the production of HP profiles showed by the resin catalyst are reported in Figure 74, along with those obtained with the unpromoted catalyst. For sake of comparison, the catalytic performance of the same catalyst in the presence of ACN are presented.

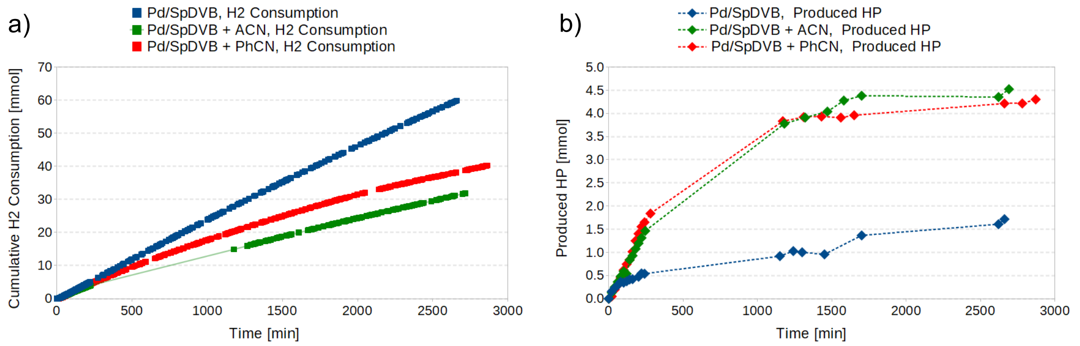

Figure 74: catalytic tests with Pd/SpDVB in pure methanol (blue), in methanol:acetonitrile 9:1 (green) and in methanol:benzonitrile 9:1 (red). The cumulative H_2 consumption and the production of HP are reported in panels a) and b), respectively.

According to the results obtained with ACN, PhCN partially reduces the hydrogen consumption (Figure 74a), although the effect is less evident when compared to ACN. However, the increase in HP production with respect to the unpromoted catalyst is almost the same for both solvents, being only slightly higher in the presence of PhCN (Figure 74b). The effect of nitriles can be also clearly recognized by considering H_2 conversion, HP selectivity and HP hour productivity of the catalyst (Figure 75).

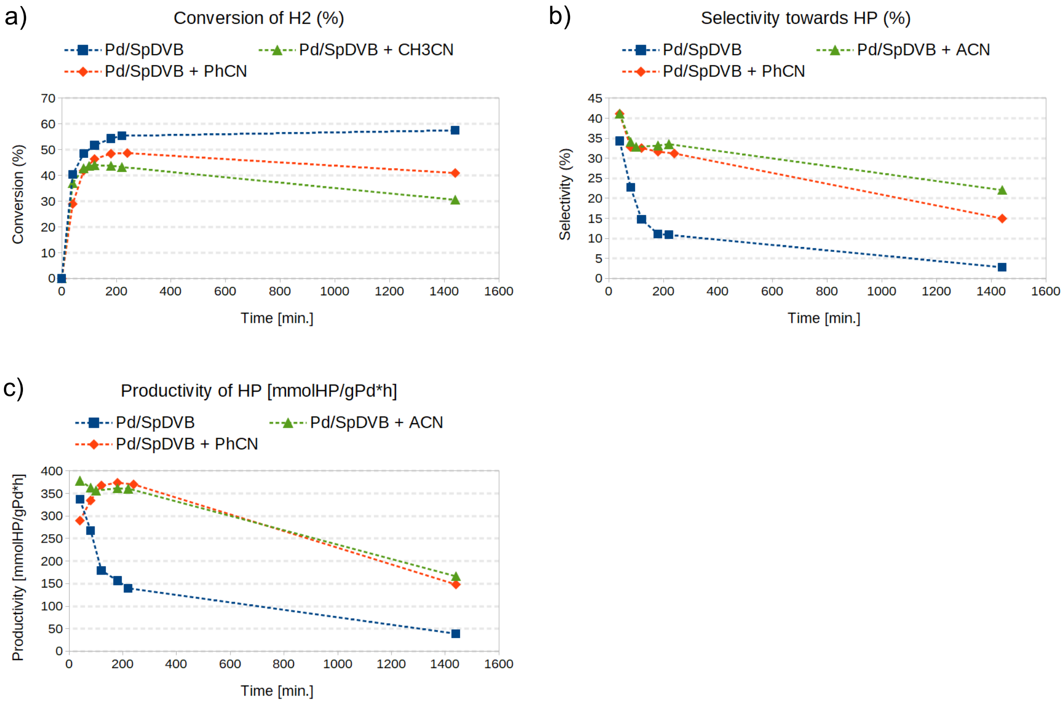

Figure 75: catalytic experiments of Pd/SpDVB in methanol (blue), methanol with 10% vol. of ACN (green) and methanol with 10% vol. of PhCN (red). The three sections illustrates; a) conversion of H_2; b) selectivity towards HP; c) hour productivity of HP.

H_2 conversion of Pd/SpDVB (Figure 75a) increases over time during the first 240 min of reaction to reach a plateau at about 55%. In the presence of ACN the induction time is quite lower, as the deactivation occurs, leading to a decrease in H_2 conversion (-15% of conversion after 24 hours, compared to the unpromoted catalyst). With PhCN the effect is similar, but slightly weaker (-10% after 24 hours). The HP productivity (Figure 75c) after 120' of reaction reaches a plateau with both ACN and PhCN, corresponding to 360 mmolHP/g_{Pd}·h and 370 mmolHP/g_{Pd}·h for ACN and PhCN. Similarly to the productivity, the selectivity (Figure 75b) in the presence of both nitriles reaches a plateau almost at the same values (slightly above 30%), which is somewhat higher in the presence of ACN, but mostly due to the lower values of conversion. After 1440 min (24 hours) the productivity decreases to a value which is about 150 mmolHP/g_{Pd}·h for both the co-solvents, whereas the selectivity is higher in the presence of PhCN, but this is more related to the different conversion than to the different amount of produced HP. By assuming the coordination of nitrile groups via π orbitals, the aromatic rings are closer to the surface, blocking a high fraction catalytic sites and allegedly lowering the H_2 conversion. However, experimental results show the opposite trend. This suggest that the nitriles are coordinated via N atoms: in this case, the aromatic rings are not efficiently packed on the surface of the nanoparticles, due to the steric hindrance. As the result, a lower fraction of catalytic sites is saturated, leading to a less pronounced deactivation of the catalyst (Figure 76).

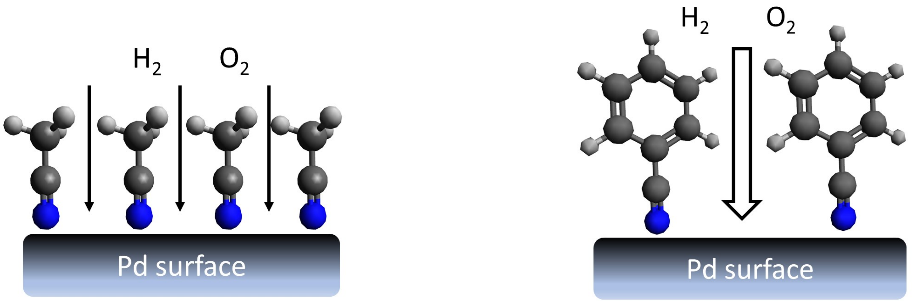

Figure 76: hypothesized coverage distribution of nitriles in correlation with the steric hindrance. On left coverage of a metal nanoparticle by ACN, on right coverage of a metal nanoparticle by PhCN.

Interestingly, this investigation shows the effect of the coordination of the nitrile groups on the surface of the Pd nanoparticles only affects the hydrogen conversion. The mechanism of selectivity enhancement seems related not only to absorption phenomena, but also, and more significantly, to the interaction of Pd(II) cationic complexes with the sulfonic functionalities.

For sake of comparison, the effect of PhCN as the co-solvent was also investigated on the reference catalyst (Pd/C). However, differently from ACN, on the one hand no change of selectivity was observed, on the other hand the hydrogen consumption was significantly lowered by the presence of PhCN. This is a further confirmation that nitriles act as a poisons for catalysts supported on materials lacking of ion-exchange groups, as the consequence of the coverage of the metallic nanoparticles.

2.5.2 Effect of DMSO and DMF on Pd/SpDVB

The effect of further coordinating co-solvents, potentially acting as ligands for Pd(II), were investigated. More in detail, dimethylsulfoxide (DMSO) was used as the co-solvent to exploit the σ-donor ligand properties of both sulfur and oxygen atoms. Moreover, N,N-dimethylformamide (DMF) was also included in the investigation, to further study the coordinating effect of the oxygen atom of the carbonyl group. The catalytic tests with Pd/SpDVB in the presence of DMSO or DMF (10% vol in methanol) are reported in Figure 77, along with the test with Pd/SpDVB and Pd/SpDVB in the presence of ACN (10% vol. in methanol), for sake of comparison.

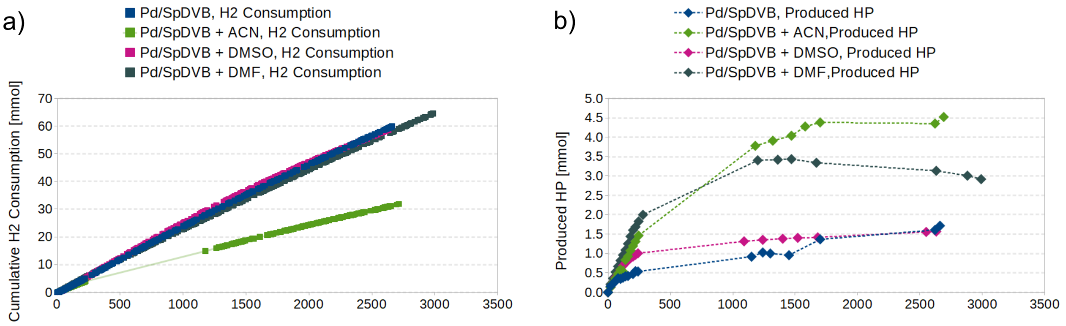

Figure 77: results of catalytic tests with Pd/SpDVB in methanol (blue), methanol with 10% vol. of ACN (green), methanol with 10% vol. of DMSO (purple) and methanol with 10% vol. of DMF (grey). In a) the cumulative H_2 consumption, and in b) the production of HP.

Differently from nitriles (Figure 74), DMSO and DMF are not deactivating the catalyst. In fact, no considerable decrease in the H_2 consumption is observed (Figure 77a) and only in the presence of DMSO a very small decrease in activity can be recognized after 24 hours of reaction. Differently from ACN, the passivation effect of DMSO or DMF on the Pd nanoparticles active in the DS is not reported in literature. This could explain the very little influence of DMSO and DMF on the conversion of the catalyst, when compared to ACN. However, the production of HP is strongly affected by the presence of a co-solvent (Figure 77b). On the one hand DMSO leads to an increase of HP production in the first 240 min of reaction (from 0.54 mmol to 1.01 mmol for the unpromoted catalyst and in the presence of DMSO, respectively), but after 2880 min (48 hours) of reaction, the amount of HP produced is almost the same of the unpromoted one. On the other hand, in the first 240 min of reaction, DMF remarkably enhances the HP production, which is higher than ACN (1.83 mmol and 1.46 mmol in the presence of DMF and ACN, respectively). Nevertheless, the HP productivity of the catalyst decreases during the test. This leads the concentration of HP to reaches a plateau after one day of reaction, whereas after two days the HP concentration starts to decrease (from 11.4 mM to 10.0 mM, corresponding 3.44 mmol and 2.92 mmol of HP produced, respectively).

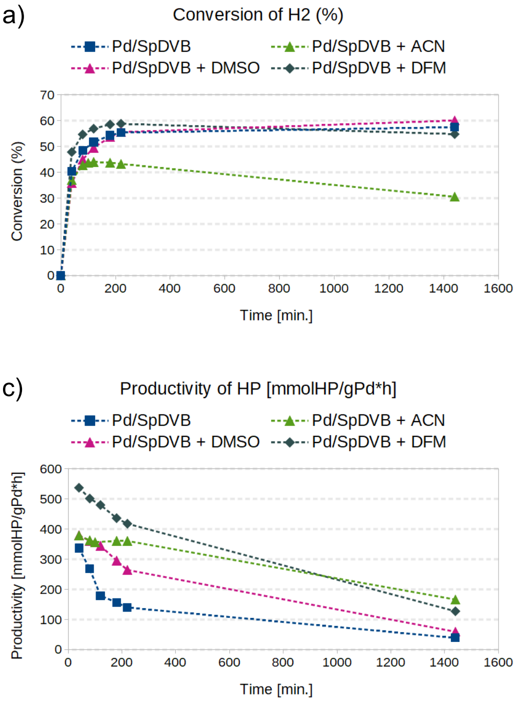

Figure 78: Pd/SpDVB in methanol (blue), methanol with 10% vol. of ACN (green) methanol with 10% vol. of DMSO (purple) and methanol with 10% vol. of DMF (grey). The three sections illustrates; a) conversion of H_2; b) selectivity towards HP; c) productivity of HP.

As reported before, the H_2 conversion (Figure 78a) is slightly affected by DMSO, whereas in the presence of DMF a slight increase is observed for the first four hours of reaction. As to the selectivity (Figure 78b), both solvents lead to an increase. With DMSO the increase is about 10% for the first four hours. However, after 1440 minutes no changes in selectivity are observed, when compared to the unpromoted catalyst. DMF turn out to be the most effective co-solvent in the promotion of the selectivity in the first 120 min of reaction, nevertheless a plateau value for the selectivity is not observed neither for DMF or DMSO. This effect can be obtained only with nitriles and allows to reach higher selectivity even for long-term reactions (>24 hours). Nonetheless, in the presence of DMF the selectivity reaches 47% after 40 min, which represents the highest value achieved with Pd/SpDVB in the presence of any co-solvent, under these reactions conditions.

The leaching of palladium at the end of the catalytic test was investigated, to evaluate the stability of Pd/SpDVB in the presence of a coordinating co-solvent. This can be achieved by determining with ICP-OES the amount of palladium present in the reaction mixture, after solvent evaporation and dissolution of the residual with aqua regia (Paragraph 4.6.1). Interestingly, during the evaporation of the reaction mixture initially containing DMSO, a white crystalline solid was recovered. This compound was identified as dimethyl sulfone, by single crystal XRD (cell parameters; a= 7.292, b=8.035, c= 7.290).

Table 17: leaching of palladium after a catalytic experiment in the presence of a co-solvent.

Co-solvent	**% of leaching**[a]		
Time [min]	**60**	**120**	**End of experiment**
None	0.78	1.80	2.85
ACN	-	1.83	2.86
DMSO	-	-	15.26[b]
DMF	-	-	3.11

[a]: the value is referred to 1 mg of palladium, corresponding to the amount of metal present in 100 mg of catalyst, used for a catalytic experiment.

[b]: the value is underestimated as part of the dimethyl sulfone was used for the characterisations. Pd contaminations in the dimethyl sulfone have been recognized by mass spectroscopy.

As to the reference catalyst Pd/C, the presence of DMSO and DMF deactivates the catalyst and reduces the HP production (Figure 79). This is once more in agreement to the results obtained with ACN, showing that the presence of sulfonic groups is mandatory to reach the selectivity enhancement with coordinating co-solvents. Only with DMF a small increase in the selectivity is observed (up to 6% from 40 min to 240 min), but it is not coupled with an increase of the production of HP. Therefore, this selectivity enhancement is related to the suppression of the overall activity of the catalyst, as observed when ACN is used as the co-solvent. Interestingly, with DMSO the catalysts does not produce HP in the first 4 hours of catalytic test, in agreement with the findings of Wilson et al.[55] for Pd/SiO_2 catalyst. However, after 500' the catalyst increases H_2 consumption and a small amount of HP is detected (up to 0.30 mmol). Further investigations are needed to explain the activation of the catalyst for long reaction time.

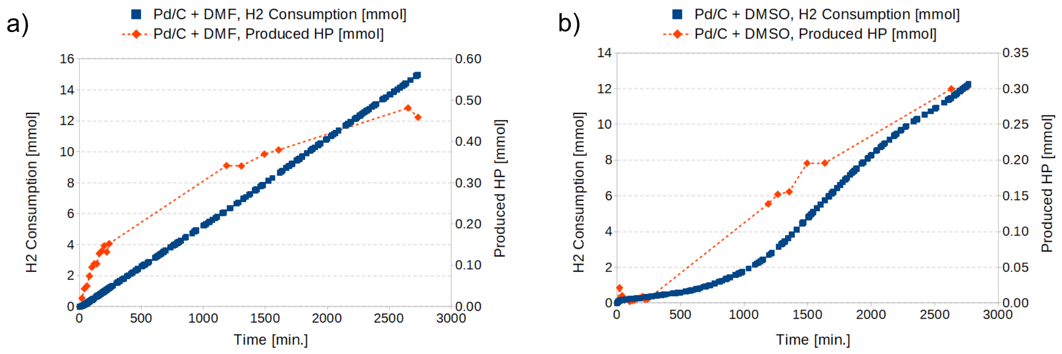

Figure 79: results of catalytic tests of Pd/C in methanol:DMF 9:1 (a) and in methanol:DMSO 9:1 vol (b). Cumulative hydrogen consumption is reported on blue squares, the produced HP is reported on red diamonds.

In conclusion, the selectivity enhancement can be obtained with solvents bearing coordinating groups different from nitriles (Figure 78b), such as DMF and DMSO. In this case, different kind of functionality lead to different increases of HP production, differently evolving over time (Figure 77b). Interestingly, these further coordinating solvents do not reduce the H_2 consumption differently from nitriles, for which a continuous deactivation of the catalyst over the test is observed (Figure 74). Several investigations reported on the interaction between Pd nanoparticles and DMSO,[204] and DMF.[205,206] In these works the stabilizing effect of these coordinating solvents has been studied under conditions that differ from those typically employed in the DS. Therefore, is not so straightforward to predict a decrease of the H_2 consumption, even though the experimental results suggest a weak coating of the metal nanoparticles, leading to a decrease of the conversion. As to ACN, the formation of new active species, more selective towards the production of HP, and their interaction with the support enhance the HP productivity of the catalyst. A more complete summary of the catalytic performance in the presence of the co-solvents is presented in Paragraph 2.5.3, together with the results of the computational investigations.

2.5.3 Computational investigations on the formation of Pd(II) complexes

The first step of the release-and-capture mechanism in the presence of a coordinating solvent, which is on the basis of the selectivity enhancement, can be divided in two steps. The former is the oxidation of the metallic palladium by oxygen or HP, while the latter is the formation of a palladium(II) complex with general formula PdL_4^{2-} (where L is the coordinating solvent in the reaction mixture). Hence, it can be assumed that the influence of the co-solvent belongs the second step of the mechanism, as the contribution of the co-solvent in the oxidation of palladium can be typically ignored. Starting from this assumption, a computational investigation has been developed, in order to identify a possible correlation between the selectivity enhancement given by a co-solvent and its capability to form a PdL_4^{2-} complex. This was performed by evaluating the energetic gain that occurs when an uncoordinated Pd^{2+} ion react with four molecules of a ligand to form the tetrakis complex.

$$\text{"Pd}^{2+}\text{"} + 4L \rightleftharpoons [PdL_4]^{2+}$$

To obtain a quantitative insight into the stability of the compounds, an activation strain analysis (ASA) and energy decomposition analysis (EDA) were performed. As for DMSO, three coordination modes were explored, which are shown in Figure 80: four molecules of DMSO bind the metal via S (A) or via O (B) or two DMSO molecules bind via S and two via O in cis or trans arrangement, respectively. In fact, both coordination via S and via O has been reported.[207]

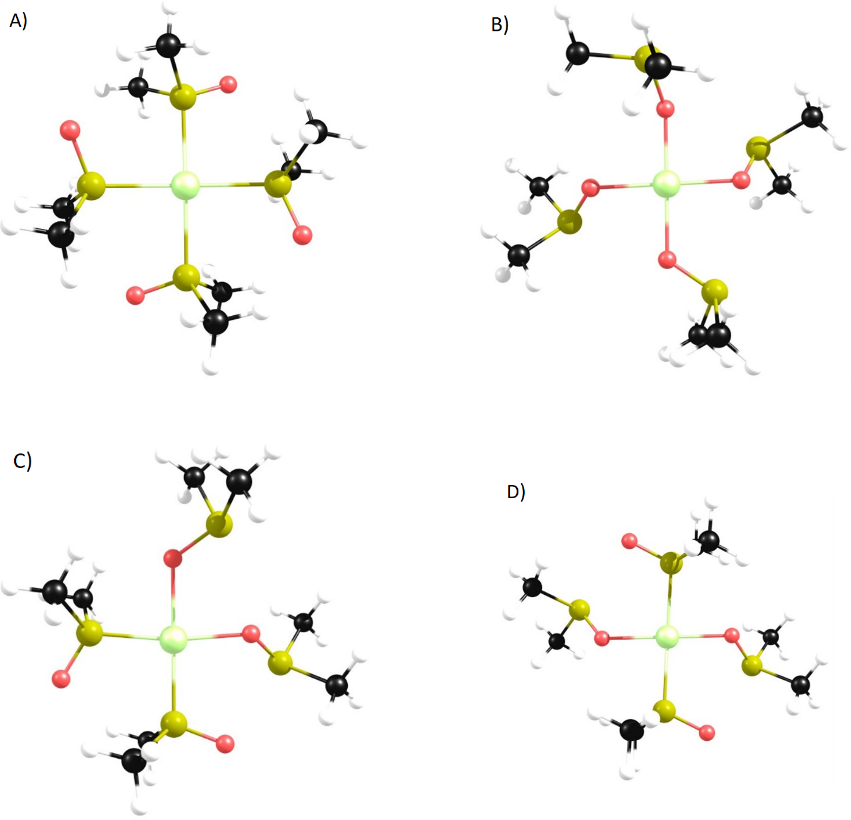

Figure 80: bonding modes of DMSO to Pd(II). Level of theory: ZORA-OPBE/TZ2P.

Table 18: ASA and EDA for the studied complexes; all values are expressed in kcal/mol. Level of theory: ZORA-OPBE/TZ2P. ΔE is given by the sum of ΔE_{int} and ΔE_{strain}. ΔE_{int} is the sum of ΔE_{oi}, ΔV_{elstat} and ΔE_{Pauli} contributions (Paragraph 4.7).

	ΔE_{strain}	ΔE_{int}	ΔE_{oi}	ΔV_{elstat}	ΔE_{Pauli}	ΔE	$\Delta\Delta E^{a}$
DMSO (A)	25.63	-426.02	-493.87	-176.50	244.36	-400.38	0
DMSO (B)	39.37	-456.77	-407.55	-313.21	263.99	-417.40	-16.95
DMSO (C)	30.84	-453.25	-487.69	-261.68	296.12	-422.40	-22.05
DMSO (D)	27.83	-443.84	-464.06	-249.17	269.39	-416.01	-15.62
ACN	35.64	-449.58	-494.77	-365.63	410.82	-413.94	-
DMF	39.72	-465.93	-424.88	-336.57	295.52	-426.21	-
NH_3	33.10	-431.31	-419.15	-344.98	332.82	-398.21	-

[a]: ΔE difference relative to the least stable compound A computed for the $Pd(DMSO)_4^{2+}$ isomers.

From the energy values reported in Table 18, it can be noticed that the most stable complex C bears two DMSO molecules bonded via S and two via O. From ASA, it emerges that bonding via S is associated to a significantly smaller strain: from A to B, ΔE_{strain} increases by 13.74 kcal·mol^{-1}, but the increase (in absolute value) of ΔE_{int} is much larger (30.75 kcal·mol^{-1}), fully accounting for the greater stability of B. When both coordination modes are present, ΔE_{strain} increases as the result of switching the coordination of two DMSO ligands from S to O coordination, but the increment of ΔE_{int} (in absolute value) is almost equal to that observed when moving from A to B, i.e. when switching the coordination of all four ligands. This explains that C is more stable than B. When inspecting the different contributions to ΔE_{int} obtained through EDA, it is clear that moving from A to B the electrostatic interaction strongly increases, the decreased orbital interaction decrease and increased Pauli repulsion do not cancel completely its stabilizing effect. When comparing C to A complexes, the coordination switching from S to O of two ligands modestly affects ΔE_{oi}, which decreases (in absolute value) only by 6.18 kcal·mol^{-1}, as well as Pauli repulsion, which increases by 22.02 kcal·mol^{-1}. The large increase of ΔV_{elstat} is the factor that mainly compensates and overcomes the destabilizing contributions, leading to a strong stabilization of the complex (22.02 kcal·mol^{-1}).

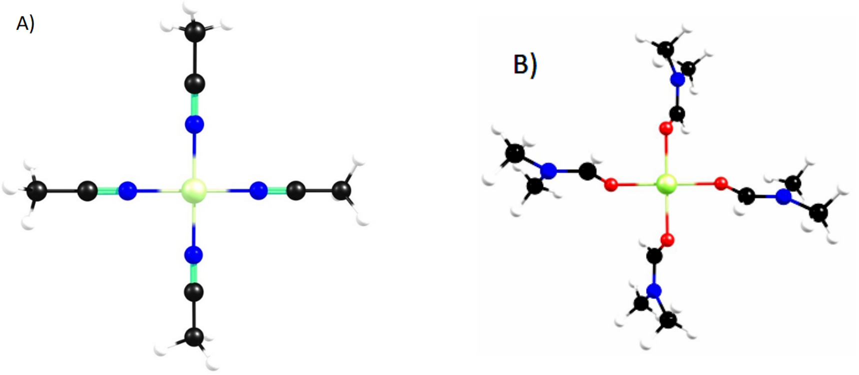

Figure 81: complexes of Pd(II) with ACN (A) and DMF (B) ligands. Level of theory: ZORA-OPBE/TZ2P.

In acetonitrile and in DMF, the predicted complexes are shown in Figure 81. Both complexes have rather significant ΔE_{strain}. Particularly, with DMF, the value is the largest of the whole series, but is counterbalanced by a large negative ΔE_{int}, so that in gas-phase it turns out to be the most stable complex, with an overall ΔE comparable to that of $Pd(DMSO)_4^{2+}$ C. Notably, ΔE_{oi} drastically diminishes when going from this latter to $Pd(DMF)_4^{2+}$, but this is accompanied by a large electrostatic stabilization, while ΔE_{Pauli} is almost unchanged. Conversely, a very large Pauli repulsion is computed for

$Pd(ACN)_4^{2+}$, the destabilizing effect of which is not fully counterbalanced, despite the large negative electrostatic and orbital interaction contributions, thus making the stability of this complex comparable to that of $Pd(DMSO)_4^{2+}$ B and D isomers. The stability trend of the series of DMSO complexes has been estimated also in a polar medium, to obtain a better estimation of the phenomena under conditions more similar to those of the DS. Single point energies have been computed in water and isomer A shows the lowest negative energy, confirming the evidence that the coordination via S leads to the least stabilized complex, while the other isomers follow the stability trend B (-0.75 kcal·mol^{-1}) < D (7.62 kcal·mol^{-1}) < C (-13.20 kcal·mol^{-1}). Notably, the stability of $Pd(DMSO)_4^{2+}$ isomer D is very close to that of isomer B in water; in gas phase, the difference was due mainly to the large electrostatic contribution, which is weakened in water. Thus, in a catalytic test in the presence of DMSO, the complex C is the one which can be formed. This investigation found that the formation of the complex $Pd(DMF)_4^{2+}$ turns out to be the most favourite, while the complex with ACN brings to the lowest energetic gain. However, the comparison between the ΔE related to the formation of the three complex is not straightforward, as the initial "Pd^{2+}" state cannot be properly described, from the computational point of view. Another approach, that allows to avoid this issue, is the evaluation of the relative stability of the Pd complexes, by focusing at the reaction involving the exchange of the ligands.

$$[PdL_4]^{2+} + 4L' \rightleftharpoons [PdL'_4]^{2+} + 4L$$

This calculation is made by using the same molecular structures (of complexes and ligands) used for the previous calculation. This further confirms the lower stability of $[Pd(ACN)_4]^{2+}$, as the substitution with both DMSO or DMF leads to a decrease in the energy of the system. Conversely, the substitution of DMF by another ligand turn out to be always unfavourable (Table 19).

Table 19: ΔE of the reaction of exchange of ligand.

$[PdL_4]^{2+}$	**L'**	***ΔE***
$[Pd(DMSO)_4]^{2+}$ (C)	DMF	-0.006044
	ACN	0.0135869
	NH_3	0.03867224

$[Pd(DMF)_4]^{2+}$	DMSO	0.0060440
	ACN	0.0196310
	NH_3	0.04471627

$[Pd(ACN)_4]^{2+}$	DMSO	-0.0135869
	DMF	-0.0196310
	NH_3	0.02508526

$[Pd(NH_3)_4]^{2+}$	DMSO	-0.03867224
	DMF	-0.04471627
	ACN	-0.02508526

In the mechanism of enhancement of the DS, the formation of a cationic Pd(II) complex is one of the key steps and therefore the easier the complex formation the higher the expected promotion effect. This computational investigation pointed out that with DMSO several coordination geometries are possible, the most stable of which is the complex cis-$[Pd(O\text{-}DMSO)_2(S\text{-}DMSO)_2]^{2+}$ (namely, the complex DMSO (C) of Table 18). As to the stability of the complexes with the three different co-solvents, the complex with DMF turns out to be the most stable, whereas the complex with ACN is the less stable. This modelling was successfully developed with very good agreement with the crystallographic data. Although this is a raw evaluation, this was confirmed by a more elaborated calculation, taking into the account not only the stability of the complexes, but also the energetic gains related to the formation of the complexes starting from the ligands and the Pd(II) atom (Table 18). Interestingly, the most stable complex (that with DMF) is correlated to the most efficient promotion of the formation of HP during the first 4 hours of reaction (in the presence of DMF), avoiding an excessive leaching of the metal. The presence of ACN brings to the formation of the least stable complex and, at the same time, gives the lowest value of Pd leaching (which is almost as the same as the unpromoted catalyst, Table 17). Moreover, in the first hour of reaction the enhancement of the DS reaction is comparable with those obtained with DMSO, but after that time the increase of HP production is kept constant. On the other hand, when DMSO is added to the reaction mixture, the formation of the cis-$[Pd(O\text{-}DMSO)_2(S\text{-}DMSO)_2]^{2+}$ complex leads to the dissolution of the metal. In fact, a leaching higher than 15% is observed with this co-solvent and it is not possible to explain this phenomenon in the presence of this co-solvent. Moreover, at the end of the catalytic test, the HP production is the same of the unpromoted Pd/SpDVB. This can be explained by assuming that part of the metal phase is deactivated once dissolved as complex, since the Pd(II) species in solution are not active toward the DS, as proposed by Priyiadarshini et al.[208] Nevertheless, part of the produced HP can be consumed in the oxidation of DMSO to dimethyl sulfone, leading to an underestimation of the HP formed.

2.5.4 Unreduced Pd catalysts supported on SpDVB

To shade a light on the role of the Pd(II) complexes in the production of HP, two commercially available Pd(II) complexes were tested in the DS, namely $[Pd(NH_3)_4]SO_4$ and $[Pd(ACN)_4]BF_4$. Those complexes are anchored to SpDVB by ion-exchange, with a procedure similar to that used to introduce the Pd precursor into the polymer support, to obtain the heterogeneous catalysts coded as Pd-NH_3/SpDVB and Pd-ACN/SpDVB. The results of the catalytic experiments, along with those of Pd/SpDVB catalyst in methanol and in the presence of ACN, are presented in Figure 82.

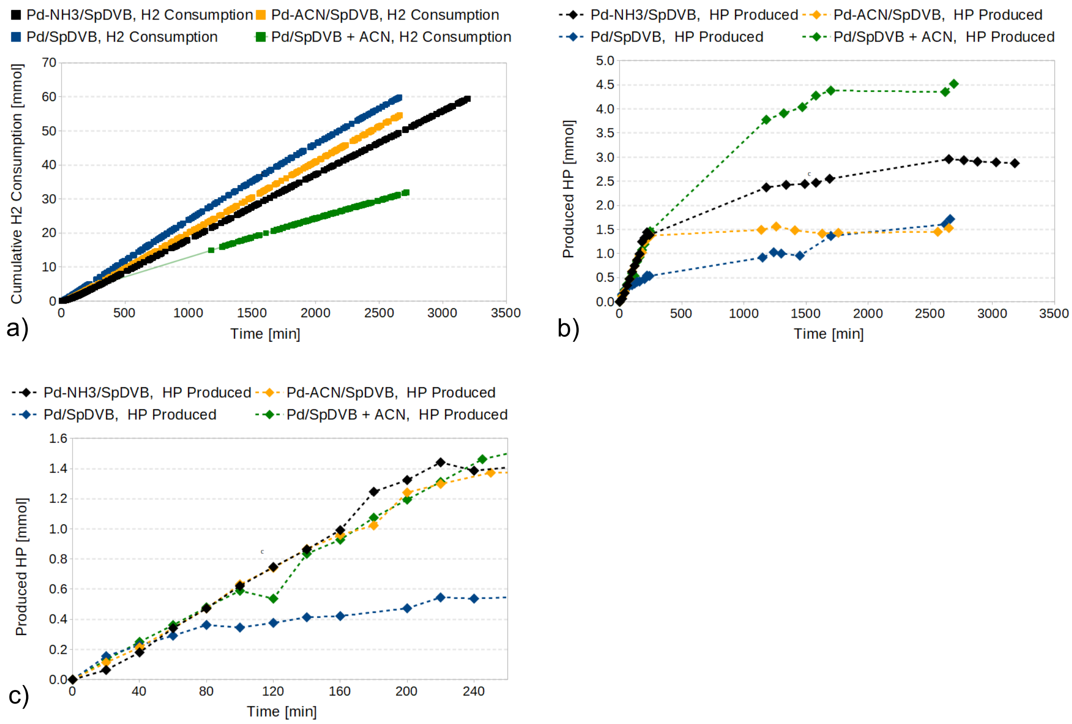

Figure 82: results of catalytic tests with Pd-NH$_3$/SpDVB in methanol (black), of Pd-ACN/SpDVB in methanol (yellow), Pd/SpDVB in methanol (blue) and Pd/SpDVB in methanol (blue), methanol with 10% vol. of ACN (green) In a) the cumulative H$_2$ consumption, in b) the production of HP, with a magnification of the first 250' of the catalytic test in section c).

The H$_2$ consumption of the unreduced catalysts (1.13 mmol/h for Pd-NH$_3$/SpDVB and 1.25 mmol/h for Pd-ACN/SpDVB) is lower than that of Pd/SpDVB (1.37 mmol/h), but almost no deactivation is observed over time, even after more than 2500', differently from the Pd/SpDVB catalyst in the presence of ACN. In the first 240 min of reaction, the HP production is almost the same for the unreduced catalysts, corresponding to the HP production of Pd/SpDVB in the presence of ACN (average production of HP of 0.38 mmol/h, Figure 82c). On the other hand, the behaviour of the catalysts is completely different for longer times. As for Pd-ACN/SpDVB catalyst, the HP production reaches a plateau, which interestingly is equal to the value of HP produced by the unpromoted catalyst at the end of the catalytic experiment. The production of HP of Pd-NH$_3$/SpDVB does not stop after 4 hours, but the rate of production is decreasing over time, until a plateau is reached (2.9 mmol after 2650'). This can be appreciated also from the trend of productivity

(Figure 83c and 83d). In particular, after an induction time, the productivity of both unreduced catalysts and the promoted one are almost the same, with considerable differences only after 4 hours of reaction.

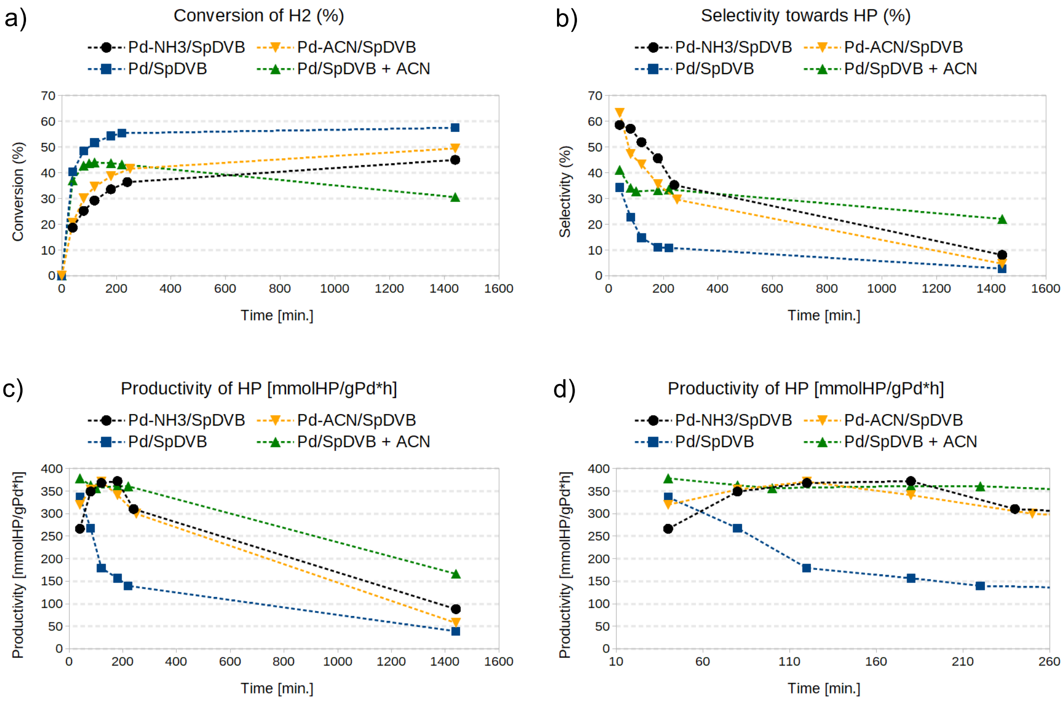

Figure 83: Pd-NH$_3$/SpDVB in methanol (black), Pd-ACN/SpDVB in methanol (yellow), Pd/SpDVB in methanol (blue) and in methanol with 10% vol. of ACN (green). The three sections illustrates; a) conversion of H$_2$; b) selectivity towards HP; c) productivity of HP, with magnification of the first 250' of the catalytic test in section d).

The conversion of the unreduced catalysts is lower than the reduced one, mainly in the first 4 hours of reaction, and is slightly lower for Pd-NH$_3$/SpDVB than for Pd-ACN/SpDVB. Nevertheless, after 24 hours the value increases and reaches a plateau (45 % for Pd-NH$_3$/SpDVB and 50% for Pd-NH$_3$/SpDVB). As to the selectivity, the unreduced catalysts shows the highest value obtained in this Thesis for SpDVB supported catalysts at the beginning of the catalytic test, but despite the productivity is almost constant in the first 240', the increase of conversion causes the selectivity to steadily decrease. In fact, after 24 hours, when also the productivity has decreased, the selectivity of the unreduced catalysts is almost the same of that of the unpromoted one: in particular, the selectivity of Pd-NH_3/SpDVB is only 5 % higher than that of Pd/SpDVB. On the contrary, the presence of ACN keeps the value of selectivity above 22 % after the same time of reaction.

The investigations on Pd-ACN/SpDVB catalyst are particularly interesting, as the initial form of the catalyst is just that supposed to be formed during a catalytic test with Pd/SpDVB catalyst in the presence of ACN. Whenever the Pd(II) is present in the catalyst before the catalytic test or is formed during the reaction in the presence of ACN, under DS conditions both catalysts present palladium species with almost the same activity. This is even more evident by comparing the performance of Pd/SpDVB in the presence of ACN and Pd-ACN/SpDVB. However, the best performances in HP production over time are obtained with Pd/SpDVB in the presence of ACN. These are the best condition, as the metal nanoparticles act as a palladium reservoir, which allows to continuously produce Pd(II) complexes, thanks to the presence of ACN in solution, keeping high the concentration of $[Pd(ACN)_4]^{2+}$ species.

As to Pd-NH_3/SpDVB, the performances in the first 240 min of experiment are almost the same of those of Pd-ACN/SpDVB. However, on longer reaction time Pd-ACN/SpDVB completely stops to produce HP, while Pd-NH_3/SpDVB is still productive. To rationalize this difference, the stability of the palladium complex with ammonia, as well as the energetic contributes involved in its formation were investigated (Tables 18 and 19). On the basis of these results the $[Pd(NH_3)_4]^{2+}$ (Figure 84) complex turns out to be the least stable among all the investigated compounds.

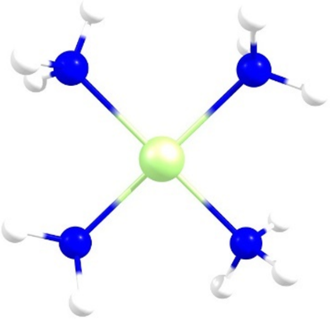

Figure 84: Complex of Pd(II) with NH_3 ligand. Level of theory: ZORA-OPBE/TZ2P.

As this complex is already formed in the Pd-NH_3/SpDVB catalyst, considering the reaction of formation could be misleading. However, the complex appears the least stable also by considering the reaction of ligand exchange. Nevertheless, the correlation between stability of the palladium complex and its activity in the DS in this case could be dependent not only on its formation reaction, but also on its stability towards the reduction to form metal palladium that allegedly aggregates to form metal nanoparticles. Although particularly telling, the formation of the Pd(II) complexes is not fully suitable to describe the activity and the stability of Pd-NH_3/SpDVB and Pd-ACN/SpDVB catalysts, since the Pd(II) complex is already formed inside the catalyst. To better rationalize the activity of Pd-NH_3/SpDVB and Pd-ACN/SpDVB catalysts further investigations aimed to assess the stability of the Pd(II) complexes in the presence of H_2 are needed. These additional investigations are also very important to better define the effect of the coordinating solvents.

2.5.5 Conclusive remarks on the general effect of coordinating solvents

In Chapter 3 acetonitrile is introduced as a novel promoter for the DS reaction when coupled with Pd catalysts supported on ion-exchange resins. In Chapter 4 this promotion effect is extended to zeolite supported catalysts to show that acetonitrile behaves as selectivity enhancer in the presence of palladium catalysts supported on any catalytic support bearing ion-exchange functionalities. In this Chapter the enhancing effect is proved to potentially occur by using any ligand able to form cationic Pd complexes, in the presence of ion-exchange supported palladium catalysts. Initially, the effect was generalized to nitrile compounds, showing that nitriles can probably exert two different kind of interactions towards the metal catalyst. On the one hand they deactivate the catalyst, as the consequence of the coating of the metal nanoparticles by the coordinating moieties, depending on the steric hindrance of the nitrile compound. On the other hand nitriles are able to form Pd(II) species which are more active in the production of HP. Interestingly, the nature of the nitrile ligand seems to poorly affect the promotion effect. The effect of further coordinating solvents such as DMSO and DMF, both able to form cationic Pd complexes, was also investigated. The outcomes show that DMF is the most effective promoter in the enhancement of the production of HP in the first 240 min of reaction, when compared to nitriles or DMSO. Nevertheless, in longer experiments the highest promotion effect is obtained with nitriles. The selectivity enhancement of DMSO not only is lower than of ACN and DMF, but also steadily decreases during the DS experiment. As the consequence, at the end of the catalytic experiment, the amount of produced HP is equal to that produced in pure methanol. Conversely, with respect other coordinating solvent, DMSO promotes a severe leaching of the catalyst (<15%) and is not stable under reaction conditions. DFT calculations shows that the most stable and easily formed Pd(II) complex, by using the different coordinating solvents as ligands, is formed with DMF, whereas ACN forms the least stable. Starting from these findings, a possible correlation between the promotion effect of a co-solvent and its ligand properties was suggested. However, the task is not straightforward, as several additional factors, such as the leaching by DMSO and the passivation of the active metal by nitriles, should be taken into account. As DMF seems the only solvent with no other interaction with the catalyst than the formation of Pd(II) species, that are efficient in the production of HP, it could be concluded that the higher the stability of the complex the higher the promotion effect. On the other hand, nitriles are able to block catalytic sites leading to the cleavage of O–O bonds, thus lowering the catalytic activity of the hydrogenation reaction. Even though the complex formed with ACN is less stable, the partial poisoning of the catalyst allows to reach the highest selectivity and productivity with nitriles. Although the catalytic experiments with supported Pd(II) complexes confirm the highest production of Pd(II) species under DS conditions, the catalysts are likely very little stable, as they can be easily reduced under reaction conditions. By changing the ligand of the Pd precursor (ACN or NH_3) used for the preparation of the catalysts, the initial HP production is the same, but reaching the plateau of the production of hydrogen peroxide takes a different time. Moreover, it is important to underline that the initial production of HP (240 min) is the same observed for the reduced catalyst (Pd/SpDVB) in the presence of ACN. In the case of ACN present in solution, the catalyst produces HP for longer time before to reach a plateau, as the excess of ligand in solution allows to increase the amount catalytic species produced over time. This last investigation opens a new issue about the stability of the Pd(II) species in the presence of a co-solvent. In particular, to better understand the catalytic behaviour of the catalysts, it does not seem enough to evaluate the formation of the Pd(II) complexes and the stability of these species towards the reduction should also be evaluated with DFT calculations. This further investigation is expected to better rationalize the effect of the different co-solvents in the DS and to identify optimized Pd(II) ligands to reach a stronger promotion effect.

Chapter 6: Correlation between amount of co-solvent and promotion effect

2.6 Introduction

In the previous Chapters 3-5 the investigation of the effect of different coordinating solvents in the DS clearly showed that their action is connected to ion-exchange materials as catalytic supports. This represents a preliminary investigation on this phenomenon, unprecedented in literature, and therefore the promotion effect was investigated by taking into the account only one concentration of the co-solvent, that is 10% vol in methanol. In this Chapter the investigation has been extended to reaction mixtures with different co-solvent:methanol ratio. This study was carried out with ACN, as a representative of nitrile compounds, and with DMF. DMSO was excluded from this investigation, due to the extensive leaching of metal, making this co-solvent poorly relevant for potential practical applications. Pd/SpDVB, the most used and promising catalyst, was selected for the experiments along with Pd/C, as the reference catalyst with a support lacking of ion-exchange groups. The aim of this Chapter is to achieve a better understanding of the interaction between the coordinating solvents and the catalyst, by evaluating the performance as a function of amount and nature of the co-solvent. This also set the basis for the optimization of the reaction mixture in order to maximize the production of hydrogen peroxide. However, this investigation is not fully focused on the optimization of the catalytic system, as many parameters, such as temperature, pressure, amount of catalyst and several others, determine the yield of HP. Moreover, a possible approach to further increase the productivity of a catalyst is the exploitation of reaction mixtures containing two or more co-solvents.

2.6.1 Effect of the amount of acetonitrile

The effect on the amount of acetonitrile on the performance of Pd/SpDVB was investigated by using different amount of ACN in methanol, such as 1%, 5%, 10%, 15%, 20%, 25%, 50% and 100% (pure acetonitrile), with a new batch of the Pd/SpDVB catalyst, different from that used for the tests described in Chapter 3. On the basis of previous investigations and the literature reports[161] it is clear that acetonitrile exerts two different kind of interactions with the catalyst. On the one hand, it passivates the metal nanoparticles, reducing the consumption of hydrogen and allegedly decreasing the rate of HP hydrogenation. On the other hand, with palladium catalysts supported on ion-exchangers ACN generates in situ Pd species that are more active in the production of HP. These phenomena have opposite effects on the metal nanoparticles, as the passivation deactivates the catalyst and lowers the hydrogen conversion, whereas the latter effect activates the catalyst towards the production of HP. When the interactions are strong enough, not only an increase in the production of HP, but also in the consumption of hydrogen are observed (see results with Pd/K1221, Paragraph 2.3.2.7). The cumulative consumption of hydrogen and the production of hydrogen peroxide with different amount of ACN are reported in Figure 85-86.

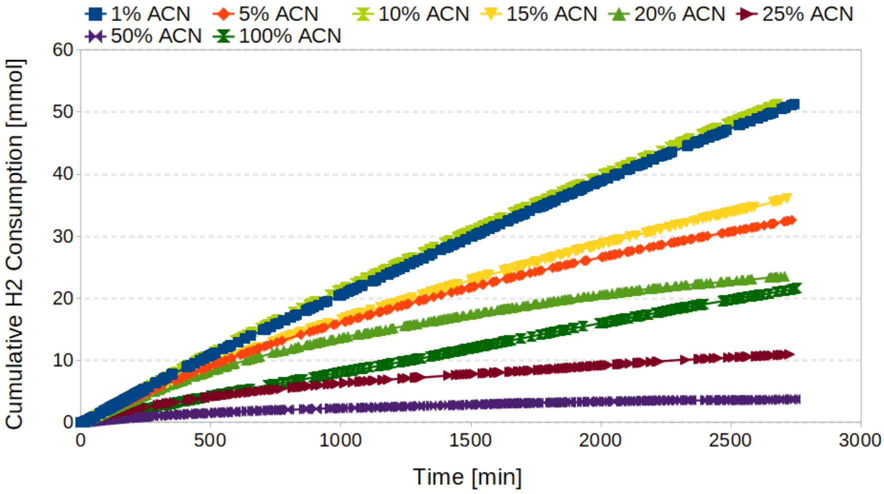

Figure 85: cumulative hydrogen consumption of Pd/SpDVB with different amount of acetonitrile as co-solvent in the reaction mixture.

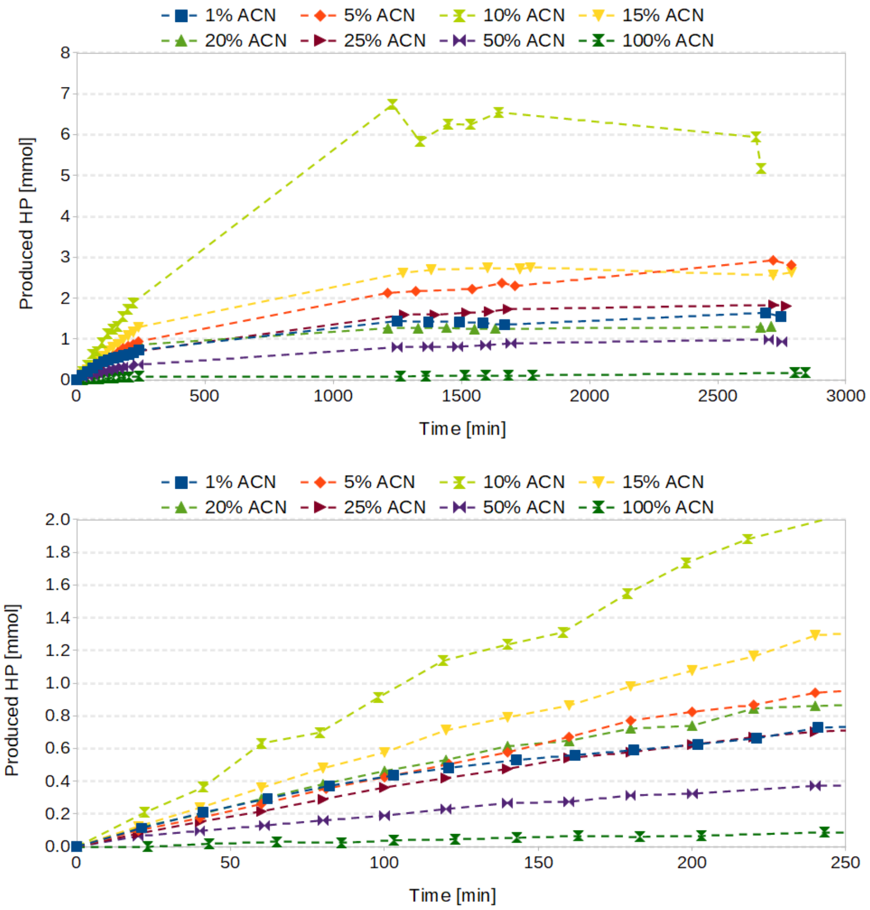

Figure 86: cumulative hydrogen peroxide production of Pd/SpDVB with different amount of acetonitrile as co-solvent in the reaction mixture, at the end of the test (upper panel) and after 240 min (lower panel).

From Figure 86 it is clear that the activity of the catalyst strongly depends on the concentration of ACN. This can be better appreciated from the values of conversion, selectivity and productivity of the catalyst (Figure 87).

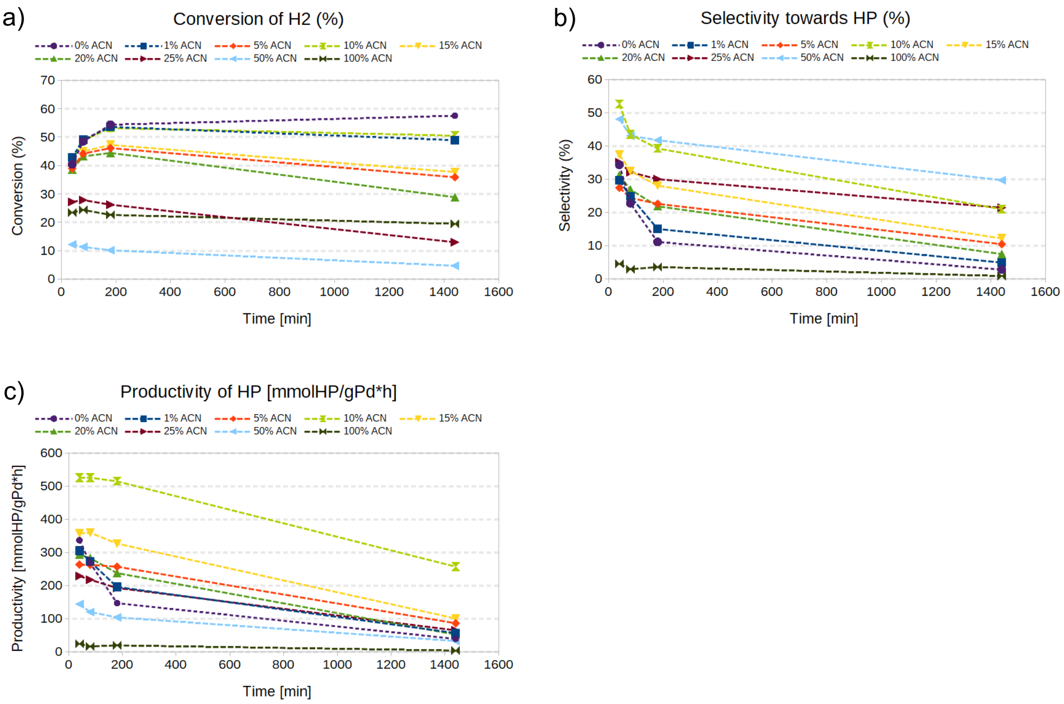

Figure 87: performance of Pd/SpDVB with different amount of acetonitrile as co-solvent in the reaction mixture; a) H_2 conversion, b) selectivity towards HP and c) HP productivity.

The presence of any amount of ACN in the reaction mixture decreases the conversion of the catalyst. With 1% vol ACN a slight deactivation occurs, as the conversion does not change with respect the unpromoted catalyst at the beginning at the experiment and does not change up to 180 min. However, this trend continues and after 1440 min the catalyst in the presence of 1% of ACN the conversion is about 10% lower than the unpromoted catalyst. By changing the concentration of ACN, the higher the amount of acetonitrile in solution the higher the decrease of the conversion of hydrogen. The only case out of this trend is the experiment performed in pure acetonitrile. However, in this case the production of HP is almost zero, reaching at the end of the catalytic experiment, a value of 0.17 mmol. This result is in agreement with the report of Wilson et al.[55] pointing out that a protic solvent is needed to obtain HP and aprotic solvents lead only to the production of water. However, with the SBR setup, the produced water is continuously accumulated in solution and therefore the catalyst produces small amounts of HP thanks to the effect of the protic by-product. In the work of Wilson et al.

the formation of a small amount of HP is not observed, since they were working with a TBR, and therefore the produced water is continuously removed from the reactor. Differently from that of conversion, productivity and selectivity of the catalyst are more complex by changing the concentration of ACN in the reaction mixture. Therefore, for sake of clarity, the performances of the catalyst at 180 min as a function of the amount of acetonitrile in solution are reported in Figure 88.

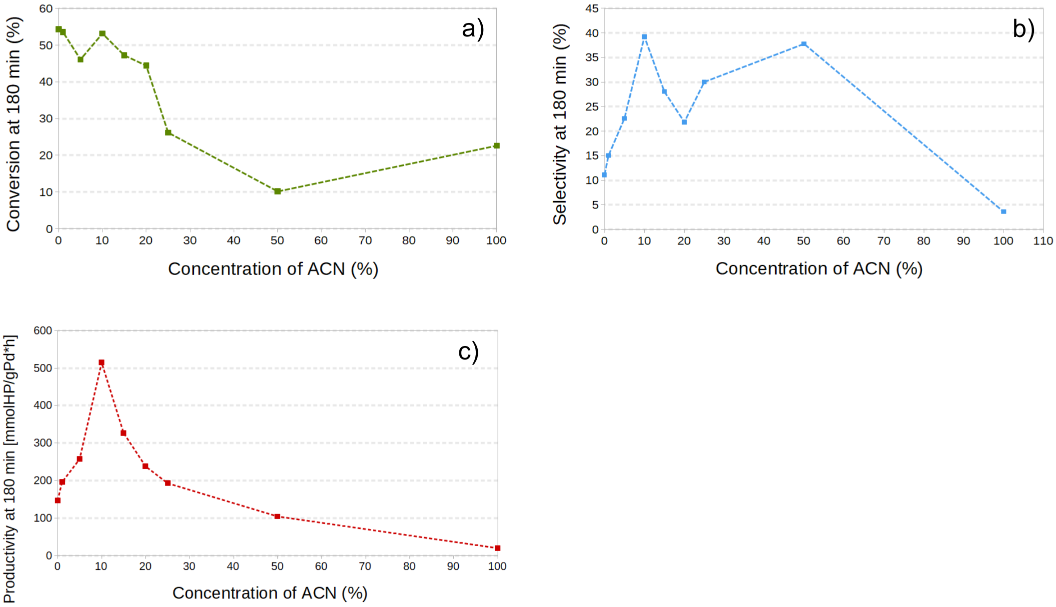

Figure 88: performance of Pd/SpDVB at 180 min as a function of the amount of acetonitrile as co-solvent in the reaction mixture; a) H_2 conversion, b) selectivity towards HP and c) HP productivity.

The results clearly show that the higher the ACN concentration in solution, the lower is the H_2 conversion (except with 100% ACN). The productivity has a peculiar and clear trend, reaching a maximum value of 514 $mmol_{HP}/g_{Pd}·h$ with 10% ACN in solution. The productivity of the unpromoted catalyst is 147 $mmol_{HP}/g_{Pd}·h$ at 180 min, whereas the presence of just 1% and 5% ACN in solution increases this value to 196 $mmol_{HP}/g_{Pd}·h$ and 257 $mmol_{HP}/g_{Pd}·h$, respectively. For ACN concentration higher than 10%, the productivity decreases with an exponential decay. The selectivity follows the trend of the productivity for ACN concentrations lower than 25%. More in details, only 1% ACN in solution is enough to increase the selectivity of the unpromoted catalyst (11%) until 15% and it continuously increases with the amount of ACN reaching the value of 39% with 10% of ACN, to decrease to 22% by further increasing the concentration of ACN to 20% vol. With ACN concentrations of 25% or higher, the selectivity starts to increase again, reaching the top value of 42% with a 50% ACN methanol solution. However, the increase of selectivity at high amount of acetonitrile (>25% vol.) is not due to an increase in the production of HP, as it occurs at lower concentration, but is clearly related to the decrease of the conversion. Even though the productivity decreases, being lower than with pure methanol with 50% ACN, the conversion is less then half of that in pure methanol and the overall consequence is a significant increase of the selectivity. Moving from pure methanol to pure acetonitrile, initially (1%-10% ACN) both selectivity and productivity increase with the ACN concentration. In the range 15%-20% ACN, productivity and selectivity decrease when compared to the maximum value reached with 10% of ACN in solution, although these parameters are higher than in pure methanol. Finally, for ACN concentrations higher than 25% the selectivity increases, but the productivity becomes lower than in pure methanol.

The trend of the productivity is the consequence of the two phenomena promoted by the presence of acetonitrile. In fact, the higher the amount of ACN in solution, the stronger the deactivation of the catalyst by poisoning. The interaction between the metal nanoparticles and the catalytic support are not strong enough to boost the conversion as observed with Pd/K1221. On the other hand, the higher the amount of cationic Pd species interacting with the catalytic support, more productive appears the catalyst. The proposed mechanism of productivity enhancement is schematized in Figure 89. The enhancement effect of acetonitrile actually occurs for concentrations of ACN up to 10%. If the concentration of ACN is further increased the poisoning effect of ACN prevail, thus leading to both the deactivation of the catalyst and the drop of the production of HP.

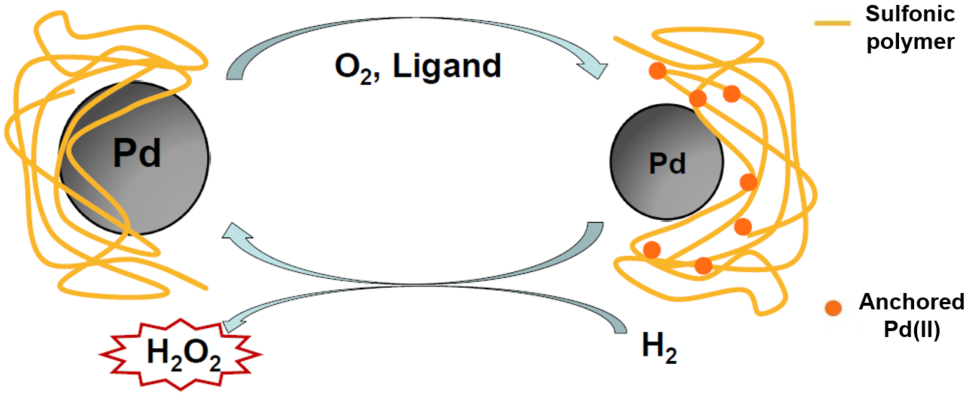

Figure 89: schematization of the proposed mechanism of HP formation by Pd(II) species, by release-and-capture of the metal by the ion-exchange support.

Although in this investigation the best promotion effect is obtained with 10% vol of acetonitrile in solution, by changing the reaction conditions or the experimental setup, the best ratio between methanol and acetonitrile could be different.

The dependence of the performance of Pd/C on the amount of ACN was also evaluated, by using several acetonitrile solutions in methanol (specifically 5%, 10% 25%, 50% and 75% vol). The cumulative consumption of hydrogen and the production of hydrogen peroxide are reported in Figure 90. For this investigation a different batch of the commercial Pd/C was used as the reference. Although the supplier, the Pd content and metal distribution are the same of the batch used for the experiments presented in Chapter 3, this batch of material appears significantly more active. This is likely due to ageing of the batch used in the previous investigation. In any case, this new Pd/C batch is still less active than Pd/SpDVB.

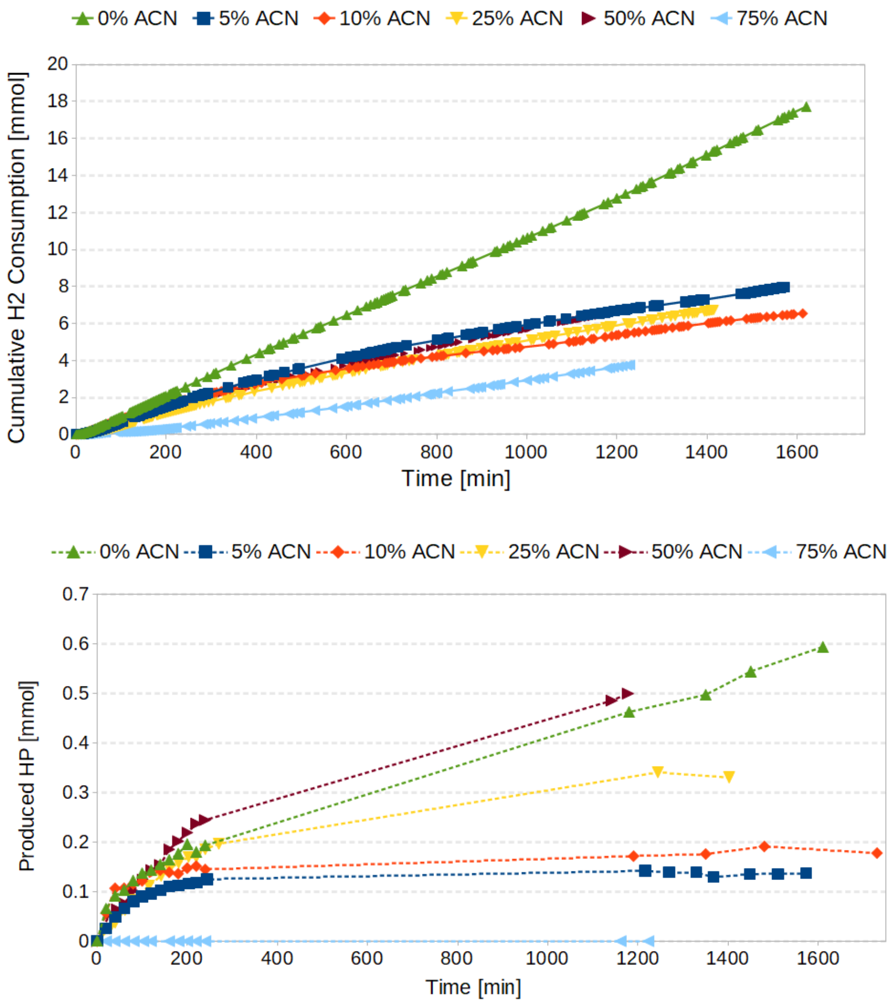

Figure 90: cumulative hydrogen consumption (upper panel) and production of hydrogen peroxide (lower panel) of Pd/C with different amount of acetonitrile as co-solvent in the reaction mixture.

The trend of the conversion observed for Pd/SpDVB is quite similar also for Pd/C, as the presence of acetonitrile reduces the H_2 consumption with respect in pure methanol. However, the deactivation does not linearly increase with the concentration of the co-solvent, with the catalyst in the presence of 10% ACN more active for the first 300 min than with 5% ACN and more active for the first 800 min than with 25% ACN. With 75% of acetonitrile the catalyst is poorly active, with a conversion that is never higher than 5% during the first 240 min of reaction. Conversion, selectivity and productivity determined for the experiments with different amount of ACN are presented in Figure 91.

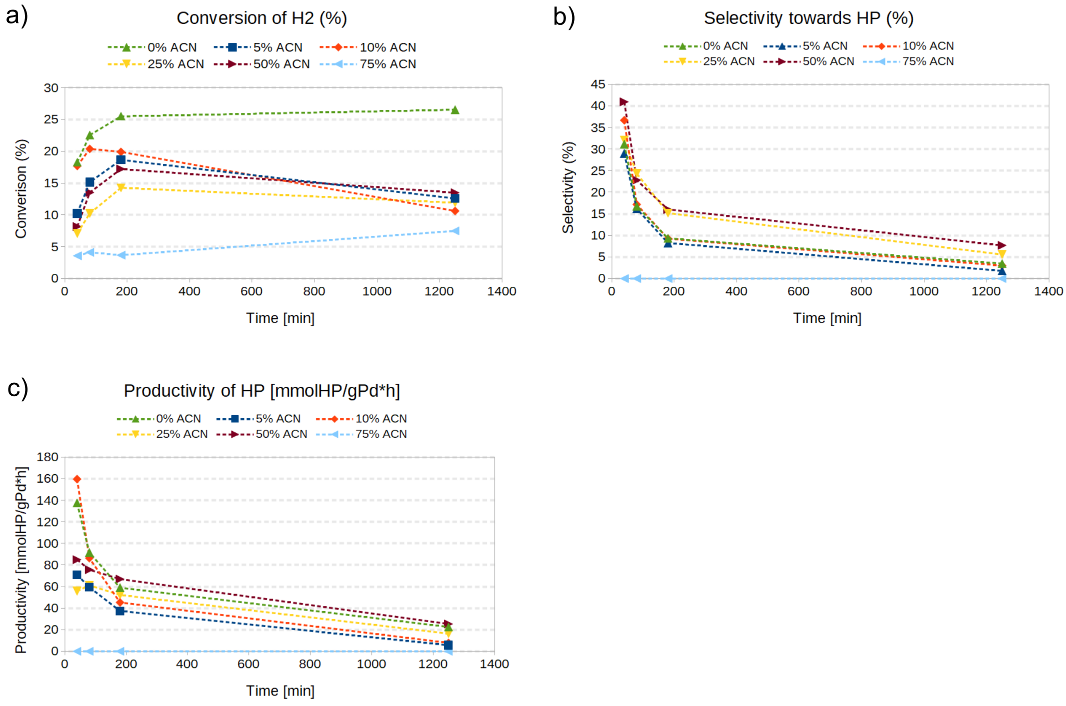

Figure 91: performance of Pd/C with different amount of acetonitrile as co-solvent in the reaction mixture; a) H_2 *conversion, b) selectivity towards HP and c) HP productivity.*

In pure methanol, the amount of produced hydrogen peroxide is higher than with any amount of co-solvent, with the only exception of the experiment with 50% of acetonitrile. In that case, after 120 min of reaction, the production of HP in the presence of 50% of ACN is higher than that in pure methanol. The trend of selectivity is more complex, since with 5% and 10% ACN almost no changes are observed in comparison with the experiment in pure methanol, whereas with 25% and 50% the selectivity at 240 min is about 6% higher than that of the experiment without co-solvent. However, with 50% of acetonitrile in the reaction mixture, for the first time not only a selectivity but also a productivity enhancement is observed on Pd/C by the addition of nitriles. On the other hand, when the concentration of the co-solvent is increased up to 75%, no production of hydrogen peroxide is observed. The trends of the parameters defining the performance of the catalyst as a function of the co-solvent, reported at 180 min, are shown in Figure 92.

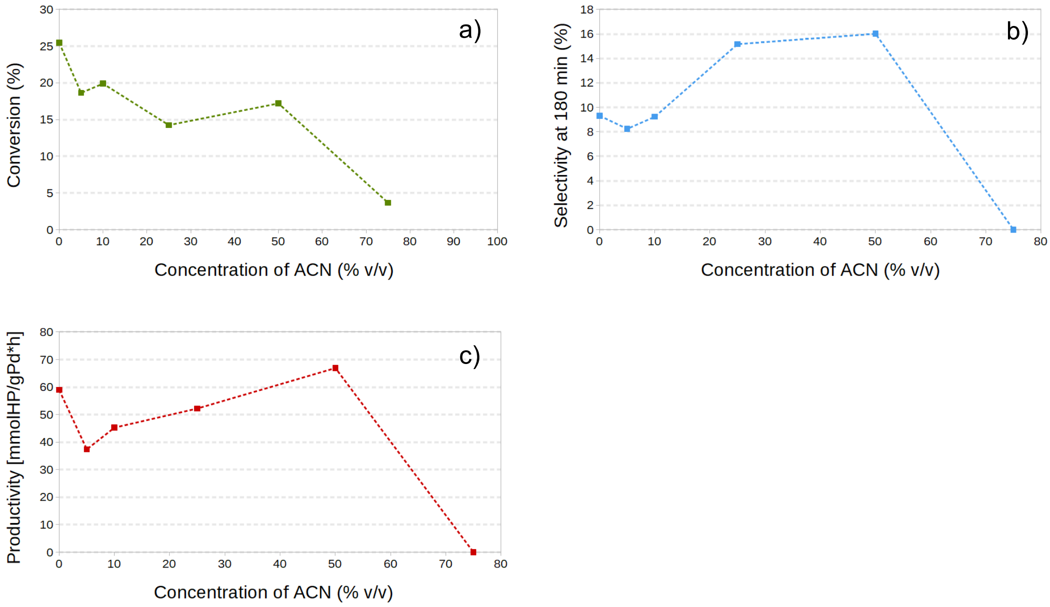

Figure 92: performance of Pd/C at 180 min as a function of the amount of acetonitrile as co-solvent in the reaction mixture; a) H_2 conversion, b) selectivity towards HP and c) HP productivity.

The conversion is constantly, but not linearly, decreasing with the increase of the ACN amount. A minimum of productivity is obtained with a 5% of co-solvent in solution, but the amount of produced HP steadily increases to reach the maximum value, that is higher than in pure methanol, at 50% ACN. However, this promotion effect is poor, as at that considered reaction time the productivity is only 8 $mmol_{HP}/g_{Pd}\cdot h$ higher than in pure methanol and the final amount of produced HP is only 0.04 mmol higher. Therefore, it is not possible to unambiguously state that the productions of HP in pure methanol and in a 50% ACN are significantly different. Moreover, by increasing the ACN concentration, the gradual deactivation of the catalyst is observed. As the consequence, for ACN concentrations higher than 25%, a selectivity enhancement is observed, as discussed for Pd/SpDVB. Similarly to Pd/SpDVB, when the amount of aprotic solvent is large enough, the production of HP is completely suppressed. No experiments were made with Pd/SpDVB in the presence of 75% of acetonitrile, but on the basis of these results, the production of HP is expected to be negligible also in that case. The productivity enhancement observed with Pd/C in the presence of a high concentration of ACN is not fully rationalized, but it can be excluded a mechanism similar to that discussed for Pd catalysts supported on ion-exchangers, as the promotion effect is negligible. In this case, the suppression of the O-O cleavage, that in some ranges of concentrations gives to Pd/C not only a deactivation of the hydrogen consumption, but also a small increase in the productivity, preventing the hydrogenation of the produced hydrogen peroxide.

2.6.2 Effect of the amount of N,N-dimethylformamide

Similarly to the tests with acetonitrile, the performance of the catalysts were evaluated in the presence of different amounts of DMF as the co-solvent. In particular, the performance of the catalyst in methanol solutions with 5%, 10% and 25% of DMF were evaluated. The results of the catalytic experiments are reported on Figure 93.

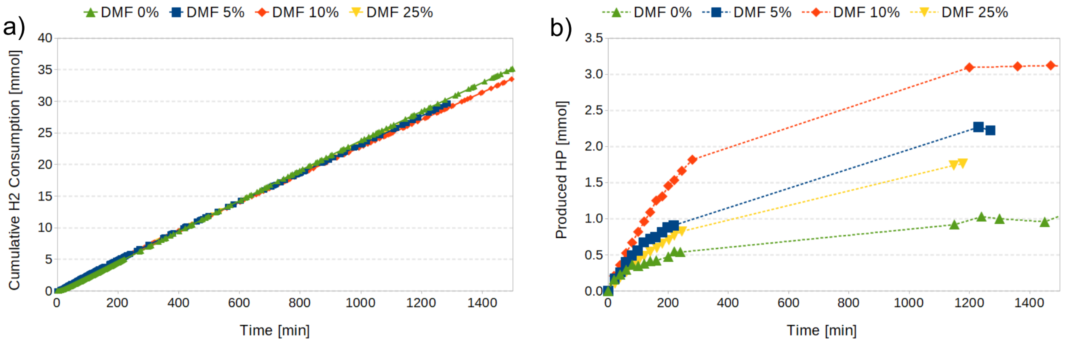

Figure 93: cumulative hydrogen consumption a) and production of hydrogen peroxide b) of Pd/SpDVB with different amount of DMF as co-solvent in the reaction mixture.

Differently from ACN, the consumption of hydrogen is very slightly affected by tuning the amount of DMF in solution. As the experiments with 5% and 25% DMF are 1200 min long, the overall activity is discussed at that reaction time. In particular, in pure methanol the catalyst consumes 28.4 mmol of H_2 at 1200 min, whereas the consumption is slightly lower, but comparable, in the presence of different amounts of DMF. In that case, the catalyst consumes 27.4 mmol, 27.3 mmol and 27.4 mmol with 5%, 10% and 25% of DMF, respectively. The deactivation of the catalyst with DMF is minimal and this is in line with the assumption that this co-solvent does not act as a poison on the metal nanoparticles, contrary to ACN. Furthermore, this can be also appreciated by taking into account the conversion of hydrogen, increasing in the first 240 minutes of reaction, to finally stabilize at about 55% (Figure 94).

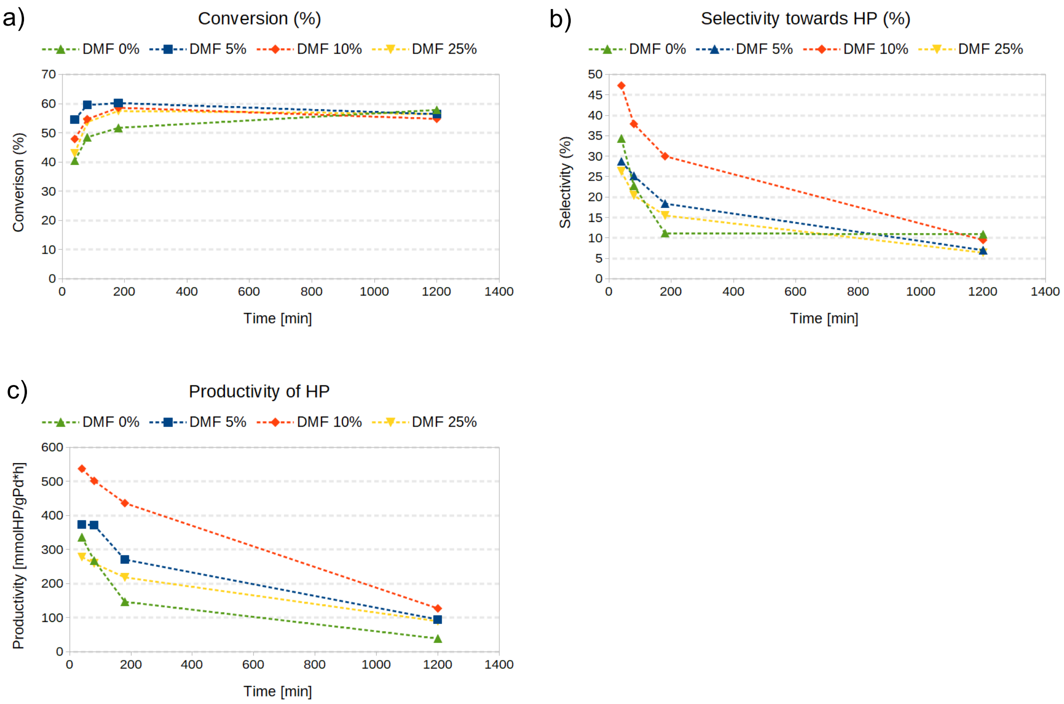

Figure 94: performance of Pd/SpDVB with different amount of DMF as co-solvent in the reaction mixture; a) H_2 conversion, b) selectivity towards HP and c) HP productivity.

As to the productivity, any DMF concentrations investigated gives a promotion effect, with the lowest production of HP obtained for the catalyst in pure methanol. Although for 25% DMF, during the first 80 minutes of reaction, the production of HP is lower than that of the unpromoted catalyst, the promotion effect can be clearly recognized for any other DMF concentration and reaction time. In particular, at 1200 min the production of HP is the highest with 10% DMF (3.10 mmol) and decreases to 2.12 mmol, 1.86 mmol and 1.02 mmol for 5%, 25% of DMF and pure methanol, respectively. A similar trend in the promotion effect can be recognized also for the productivity at lower reaction times (<240 min), whereas at 1200 min the differences flatten (Figure 94c). This trend is qualitatively similar of that of ACN, inducing a higher promotion effect by using 10% of co-solvent, even though the promotion effect is stronger in the case of 10% ACN with respect to the other amounts of acetonitrile when compared to the productivity enhancement obtained with 10% DMF with respect to 5% or 25% DMF. In this investigation, 10% vol turns out to be the DMF concentration providing the highest increase of the production of HP, decreasing steadily for higher promoter concentrations. However, since no deactivation of the catalyst is observed, the decrease of the promotion effect for high concentration of DMF cannot be explained as for ACN and further investigations are ongoing to explain this phenomenon.

With Pd/C, the effect of DMF in the reaction mixture is quite different than with Pd/SpDVB, for which the deactivation is not observed (Chapter 5). The results of the catalytic experiments with with Pd/C in methanol reaction mixtures with 5%, 10% and 25% DMF are presented in Figure 94.

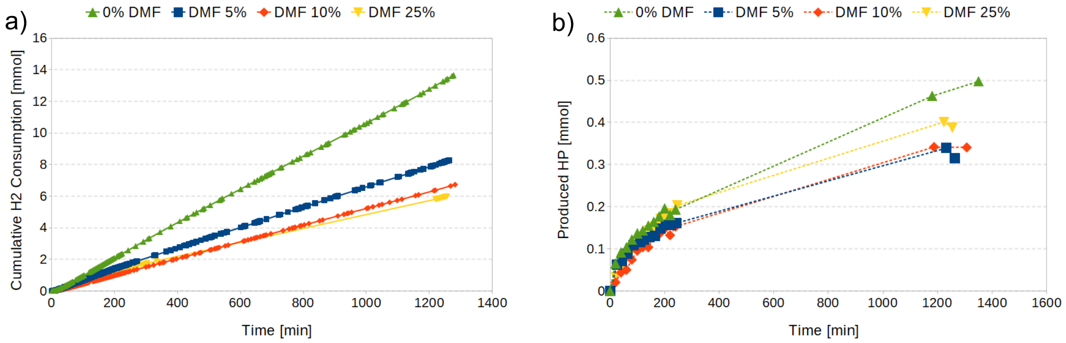

Figure 95: cumulative hydrogen consumption a) and production of hydrogen peroxide b) of Pd/C with different amount of DMF as co-solvent in the reaction mixture.

In this case, the higher the amount of DFM in solution, the higher the decrease in the H_2 consumption. The highest step in the deactivation is between pure methanol and 5% DMF in solution, inducing a decrease of the final consumption of hydrogen (at 1250 min) from 13.4 mmol to 8.6 mmol. By increasing the DMF concentration beyond 5%, a further deactivation occurs, although to a lower extent, with the consumption of 6.6 mmol and 5.9 mmol H_2 with 10% and 25% of DMF, respectively. This trend can be appreciated also for H_2 conversion (Figure 96).

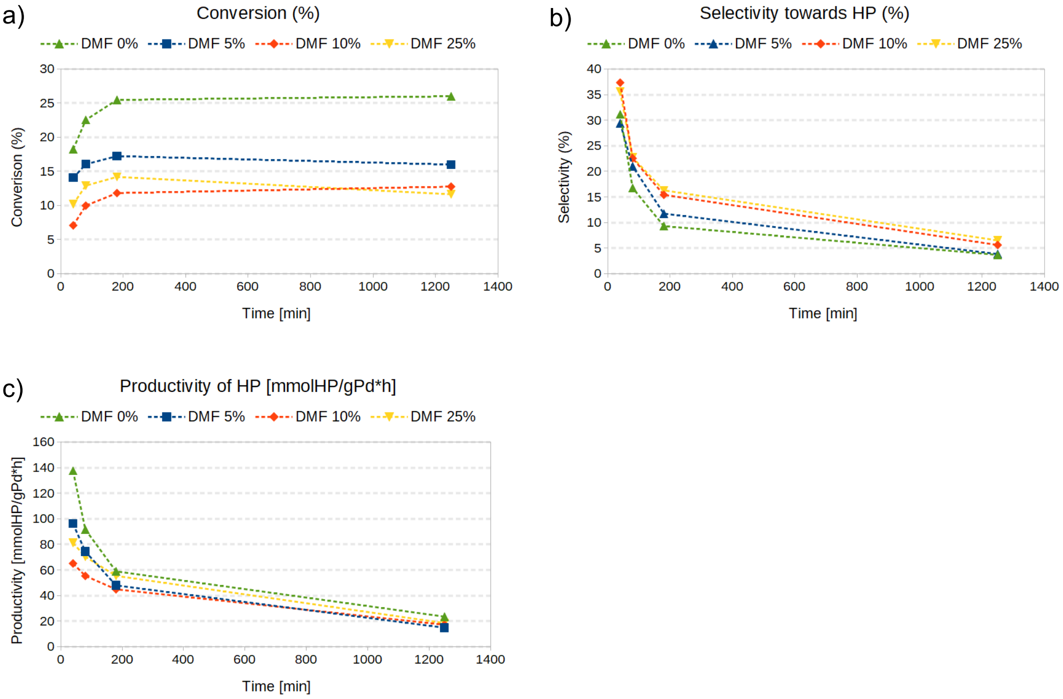

Figure 96: performance of Pd/C with different amount of DMF as co-solvent in the reaction mixture; a) H_2 conversion, b) selectivity towards HP and c) HP productivity.

The presence of 5% DMF in the reaction mixture decreases of about 10% the conversion, when compared to the catalytic experiment in pure methanol. The lower conversion is obtained with 10% DMF, especially in the first 240 min of reaction, while after 1250 min it is almost equal to that obtained with 25% DMF. The productivity is always lowered by adding any amount of co-solvent. In the first 240 min of reaction, the productivity with 5% and 25% DMF is lower than the experiment with pure methanol of about 20 $mmol_{HP}/g_{Pd}\cdot h$ and is further reduced to 10 $mmol_{HP}/g_{Pd}\cdot h$ with 10% of DMF, being the lowest value. The selectivity is enhanced by any DMF concentration with the highest increases with 10% and 25%, showing a superimposable trend over time. In this case, the selectivity enhancement is on average of 6%, while with 5% a lower increase of 2-4% is obtained. As this selectivity boost is not relying on the increase of the production of HP, but rather on the decrease of the hydrogen consumption, it can be concluded that DMF is not acting as a promoter. The reason of this trend, that is substantially different from that obtained with Pd/SpDVB, is not fully rationalized, but it can be reasonably assumed that with ion-exchange catalysts the cationic Pd(II) species interacting with the catalytic support are not only more productive, but also more active in the consumption of hydrogen. This allows the catalyst to have a conversion of hydrogen that is almost the same than in pure methanol. As this phenomenon is not occurring with Pd/C, the addition of DMF to the reaction mixture only leads to the deactivation of the catalyst.

2.6.3 Conclusive remarks on the effect of the co-solvent concentration

In this Chapter are reported the investigations on the dependence of the performance of the Pd/SpDVB and Pd/C catalysts on the concentration of acetonitrile or N,N-dimethylformamide. The use of DMSO was excluded as it leads to an extensive leaching of the metal phase. In the case of Pd/SpDVB, the higher the amount of acetonitrile in solution the stronger the deactivation of the catalyst, particularly for long reaction times (>240 min). The promotion effect, in terms of productivity of the catalyst, increases with the concentration of ACN, reaching the highest enhancement at 10% vol, to continuously decreases for higher concentrations. This is the consequence of the balance between promotion effect of the co-solvent, that consist in the formation of Pd(II) species interacting with the catalytic support, and the well known poisoning effect of acetonitrile towards the metal nanoparticles. As to the selectivity, there are two ranges of co-solvent concentration leading to an enhancement. The first corresponds to the peak of productivity (10% of ACN), the second occurs at higher concentrations of nitrile and is allegedly connected to the severe poisoning of the catalyst, preventing the over-hydrogenation of HP to water. With Pd/C the absence of ion-exchange groups causes the ACN to act as an inhibitor of the catalyst activity at any concentration. The consumption is always lowered in the presence of the co-solvent, even though the promotion effect connected to the inhibition of the hydrogenation of the O-O bond is observed at high concentration of acetonitrile. However, the promotion effect is very limited and the catalyst does not significantly exceeds the performance obtained in pure methanol. When the concentration of acetonitrile is very high (>75%) the production of HP drops, since the amount of protic solvent in solution is not enough to ensure the formation of H_2O_2.

With N,N-dimethylsulfoxide the behaviour of the two investigated catalysts is quite different. With Pd/SpDVB tuning the amount of DMF has a very little influence on the conversion of hydrogen. The production of HP shows also in this case a maximum at 10% of co-solvent concentration. However, since a poisoning effect is not observed in this range of concentrations, it is difficult to rationalize the experimental trend. Once more, with Pd/C in the presence of DMF the behaviour of the catalyst differs from that of the catalyst supported on the ion-exchange resin, as a poisoning occurs with any concentration of the co-solvent. The production of hydrogen peroxide is negatively influenced by the presence of the amide, and becomes lower than in methanol with 10% of DMF. This last part of the investigation, dealing with the effect of DMF on Pd/C and Pd/SpDVB is complex and still unclear, on the basis of the current insight of the catalytic systems.

Chapter 7: Investigation with the Trickle Bed Reactor

2.7 Introduction to the investigation with the Trickle Bed Reactor

In this last Chapter are reported the investigations performed with a continuous Trickle Bed Reactor (TBR) setup, specifically designed for the DS.[97,124,209,210] The investigation with the Trickle Bed reactor (TBR) was carried out in the "Laboratory of Industrial Chemistry and reaction engineering (TKR)", under the supervision of Academy Professor Tapio Salmi, at Åbo Akademi in Turku/Åbo (Finland). This kind of experiment is very important in order to study the catalyst under conditions closer to a possible technological application and to evaluate the modification of the catalyst, particularly its deactivation, under duty.

In this setup, the catalyst is diluted with a small amount of quartz sand (typically 2-3 g) and the powder mixture containing the catalyst is blocked into the column in between of two layers of quartz wool. A thermocouple is inserted from the bottom of the column to reach the middle of the catalyst layer, to directly measure the temperature under duty. Liquid and a gas phases are continuously fed from the top of the column. A stainless steel filter with cut-off of 7 μm is placed at the end of the column, before the back-pressure regulator. The reaction conditions are different from the SBR setup used in the previous Chapters, especially the pressure which is set to 20 bars. Moreover, the column is cooled at 15°C and CO_2 is used as diluent gas. The total flow rate of the reaction gases is 4 mL/min, with a 5:1 vol ratio between oxygen and hydrogen. The flow rate of the liquid phase is 1 mL/min, significantly lower than the gas flow rate, in order to work in the trickle bed regime. Under these conditions, the gas phase is the prevailing one, with the liquid phase dripping into the column while wetting the catalyst. Both gas and liquid phases are analysed, to determine the consumption of hydrogen (with GC), the production of HP (with $TiOSO_4$ method, Paragraph 2.1.4) and the production of water (with Karl-Fisher titration). With the analysis of the consumed hydrogen together with the production of both the possible products (H_2O, H_2O_2), the mass balance of the hydrogen can be defined. The error related to the balance is typically 5% (occasionally 10%) in excess when compared to the amount of fed hydrogen: this derives from the moisture of the air, increasing the amount of water in the liquid samples. As the column is pressurized with CO_2 at the beginning of the catalytic experiment, there are two different methods to start the catalytic experiment:

- *gas first method (GF)*: after reaching the pressure of 20 bars with CO_2 inside the column, the reactor is stabilized for 30', the CO_2 flow is switched off and the reaction gases are fed. After 30', the flow of the solvent is turned on and the moment when the first drops of the solvent comes out from the reactor is considered the start of the catalytic experiment;

- *methanol first method (MF)*: after reaching the pressure of 20 bars of CO_2 inside the column, the reactor is stabilized for 30' and the solvent flow is turned on. When the methanol reaches the liquid-gas separator, further 30' are waited, the CO_2 flow is stopped and the reaction gases are fed to the reactor.

As described in Paragraphs 2.7.2.2 and 2.7.3.2 the two different conditioning methods significantly affect the DS experiment. The MF approach should be considered the method of choice, as it is safer since it avoids the contact between the reaction gases and the dry catalyst. In fact, although it seldom occurs, the contact between the H_2/O_2 mixture and the dry Pd catalyst can lead to a very fast and exothermic production of water. Nevertheless, the GF method had to be necessarily applied for a few catalysts.

With this setup were investigated both catalysts previously studied with the SBR setup, mainly Pd/SpDVB and Pd/C as the reference, beside the catalysts prepared by the hosting research group, which are Pd catalysts supported on inorganic solids. In this Chapter the effect of the catalytic support, the effects of the catalyst loading, of the particle size of the powder catalyst and of the conditioning of the reactor are investigated. Moreover, the effect of the co-solvent was investigated with the aforementioned catalysts, by using methanol reaction mixtures containing different amounts of acetonitrile or N,N-dimethylformamide.

On the basis of the published studies on Pd catalysts supported on K2621 for the DS reaction using a TBR, in the present work the most promising resin catalyst for this reaction, Pd/SpDVB, is investigated. These are therefore preliminary results that set the basis for the exploitation of this catalyst with a TBR setup, opening several questions regarding the kinetic of the reaction.

2.7.1 Investigation on palladium catalysts supported on inorganic materials with the Trickle Bed Reactor

2.7.1.1 General overview on the performances of the catalysts over inorganic supports

The materials used as catalytic supports in this part of the investigation are commercial silica, alumina and zeolites with different ratio Si/Al. All the zeolites employed with the TBR are in the acid form and belong to the Hβ group, with the Si/Al ratios of 25, 38 and 300 (the higher the ratio, the lower the ion-exchange capacity of the material). The palladium content of the catalysts, available in the laboratories of the hosting group by Dr. Christoph Schmidt and Prof. Narendra Kumar, is 1.3% w/w. These catalysts were produced by the evaporation impregnation method according to the reference.[211] This approach is quite similar to the WI method exploited for the preparation of the zeolite supported Pd catalysts used for the investigations reported in Chapter 4. All these catalysts, in the form of very fine powders, were pressed to form a pellet and finally ground and sieved to obtain samples with the desired particles size. With the catalyst supported on inorganic materials, this procedure is fundamental. In fact, when they are used as prepared, the particles are too fine and they are almost completely flushed out from the reactor by the liquid flow. Moreover, even if they are treated with this procedure, with the MF conditioning method these catalysts are flushed out from the reactor in a large extent as soon as the liquid phase reaches the catalytic bed. Therefore, in this part of the investigation only the GF method is used. Initially, a screening of all the catalysts (Table 20) was performed. All the investigations with these catalysts were made by loading into the reactor 150 mg of catalyst, diluted in 2 grams of quartz sand.

Table 20: list of the catalysts supported on inorganic materials.

Label	**Catalytic support**	**Si/Al ratio of the support**	**Pd content (%)**
Pd/SiO_2	Silica	-	1.3
Pd/Al_2O_3	Alumina	-	1.3
Pd/Hβ25	Hβ Zeolite	25	1.3
Pd/Hβ38	Hβ Zeolite	38	1.3
Pd/Hβ300	Hβ Zeolite	300	1.3

In the first trial, catalysts with a diameter of the particles lower than 63 μm were used. The lower size of the particles is not known for these material, but is for sure higher than 7 μm, as no flush-out of the material is detected and only traces of the catalyst are found in the filter at the bottom of the reactor. the results of the catalytic experiments with the catalysts listed in Table 20 are reported in Figure 97. It is important to underline that in this Chapter the parameters are presented as instantaneous values. In a typical catalytic experiment, after an induction time, the conversion of hydrogen and the production of HP are stabilized. Therefore, when the catalyst reaches a steady state, the conversion and productivity become constant over time and, consequently, also the selectivity.

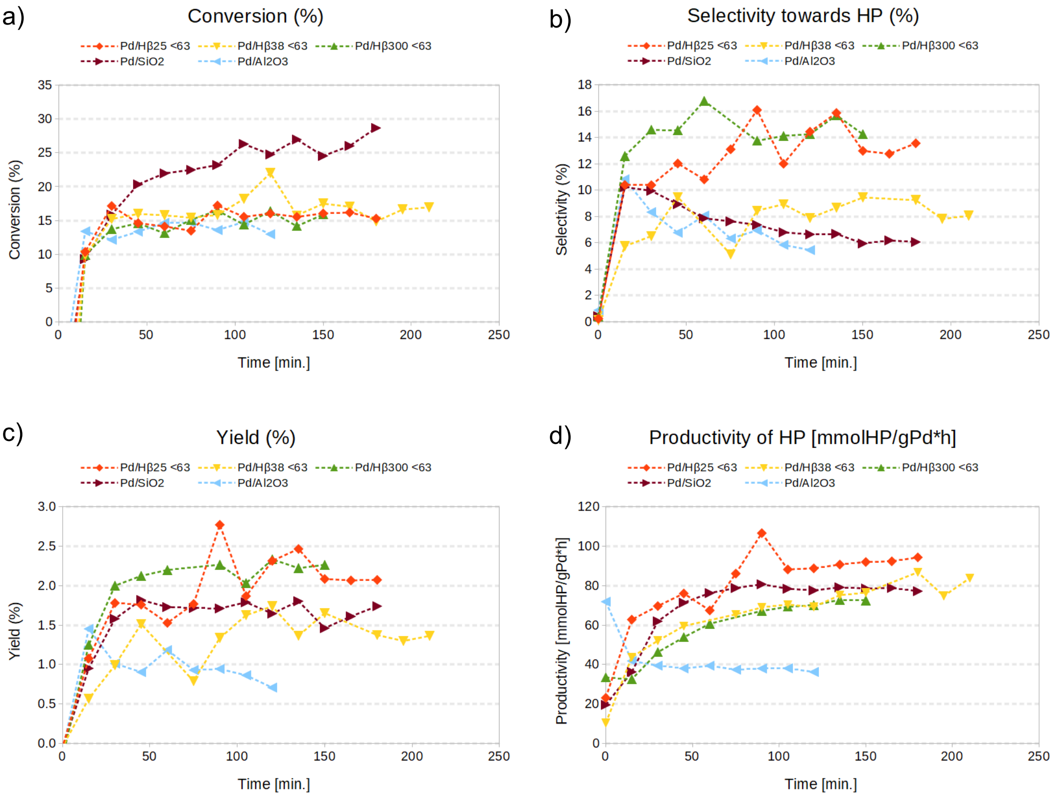

Figure 97: performance of palladium catalysts over inorganic supports, using GF method; a) H_2 conversion, b) selectivity towards HP, c) yield and d) HP productivity.

All catalysts show the same activity, in terms of hydrogen conversion that on average is 12-13%, except Pd/SiO_2, which shows higher conversion, reaching 25%. Excluding Pd/SiO_2, these data point out that the nature of the inorganic support poorly affect the activity of the catalysts. When selectivity is considered, three catalysts (Pd/SiO_2, Pd/Al_2O_3 and Pd/Hβ38) present a lower selectivity at the steady state (6-8%), whereas Pd/Hβ25 and Pd/Hβ300 shows a higher selectivity (12-14%). The presence of acidic functionalities (ion-exchange groups) is expected to produce a selectivity enhancement, when compared to other inorganic supports. However, this occurs only with Pd/Hβ25 and Pd/Hβ300 and a clear correlation between the selectivity of the catalyst and the amount of acidic groups cannot be recognized. Pd/Hβ38 is an outlier, since it behaves more similarly to the catalysts on supports lacking of ion-exchange functionalities. Finally, the productivity of the catalysts is generally similar, except for Pd/Al_2O_3 being less productive and showing a lower yield. A recycle experiment was made with Pd/SiO_2, re-using the catalyst after a first catalytic run. The recycle test showed an increase of the conversion (from 25% to 35%) without any relevant change in selectivity, rising the productivity from 70 mmolHP/gPd·h to 90 mmolHP/gPd·h. Summing up, the results obtained in the TBR with Pd supported on inorganic materials are rather modest, since all catalysts present low conversion and low selectivity, with a yield never higher than 2.5%. The highest concentration of HP at the steady state, obtained with Pd/Hβ25, is only 3.07 mM. Moreover, by considering the low values of conversion, selectivity and HP productivity, it is hard to compare the performance of these catalysts.

2.7.1.2 Effect of the particle size with zeolite supported catalysts

The catalyst Pd/Hβ25 was used to investigate the effect of the size of the grains of catalyst for zeolite supported catalyst. This catalyst was chosen as it show the highest HP productivity among the palladium catalysts supported on inorganic materials. By testing fractions with three different particles size (<63 μm, 63-90 μm, 90-125 μm) conversion appears strongly affected by the grain size (Figure 98).

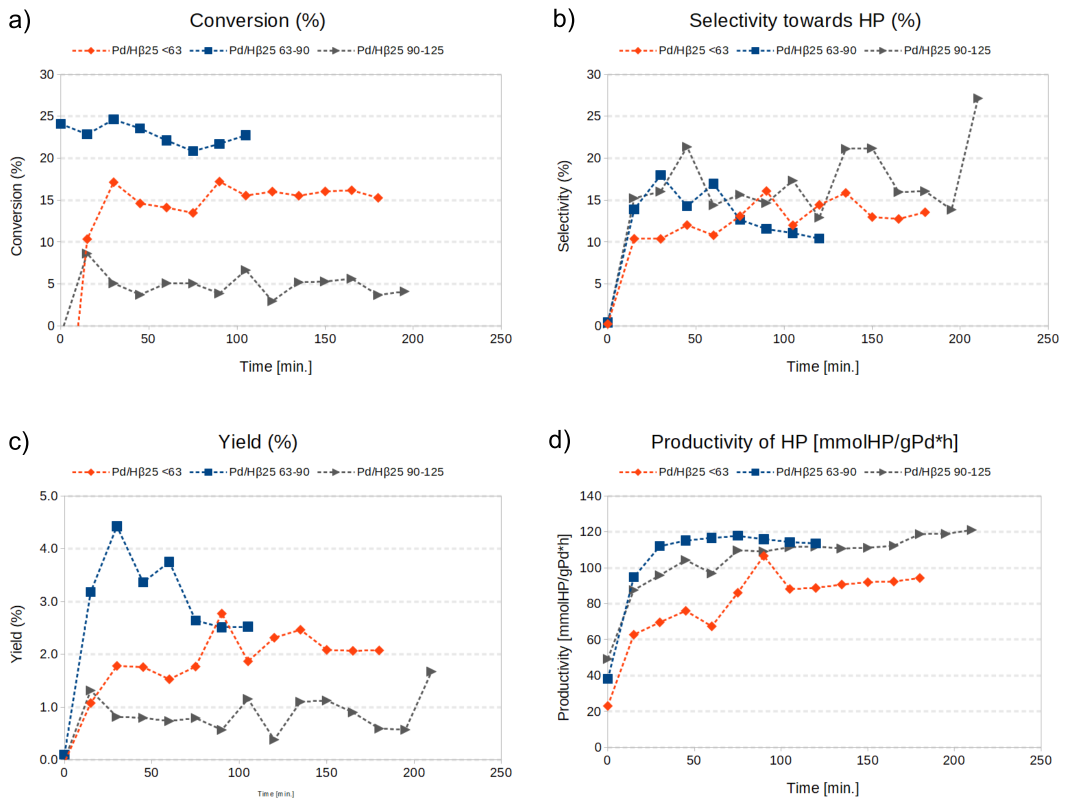

Figure 98: performance of Pd/Hβ25 with different particle size, using GF method; a) H_2 conversion, b) selectivity towards HP, c) yield and d) HP productivity.

On the one hand, the higher the size of the grains, the higher the wetting of the catalyst by methanol and hence the H_2 conversion. On the other hand, by increasing the grain size the diffusion restrictions within the porous system of the catalyst also increase, with the consequent decrease of the conversion. In fact, the steady state conversion for the smallest, intermediate and biggest fraction are 14.5%, 20.8% and 3.7%, respectively. The combination of these two effects makes the fraction of 63-90 μm the most active in terms of H_2 consumption. Interestingly, the selectivity is almost not affected by the grain size. The fraction with particle size in the range 63-90 μm shows a slightly higher productivity (>100 $mmol_{HP}/g_{Pd}\cdot h$), due to its higher conversion. Also the biggest fraction reaches a productivity higher than 100 $mmol_{HP}/g_{Pd}\cdot h$ despite its low conversion, thanks to its slightly higher selectivity. Once more, the yields are very low and the catalysts appear very poorly active and productive, making this comparison hardly relevant.

2.7.1.3 Effect of acetonitrile with zeolite supported catalysts

The effect of ACN was first investigated with Pd/Hβ25, the support of which shows the higher ion-exchange capacity, by using a reaction mixture of ACN 10% vol in methanol. The higher ion-exchange capacity is expected to be beneficial for the enhancement effect of ACN. The results of the catalytic tests with the fraction 63-90 μm of the catalyst are reported in Figure 99.

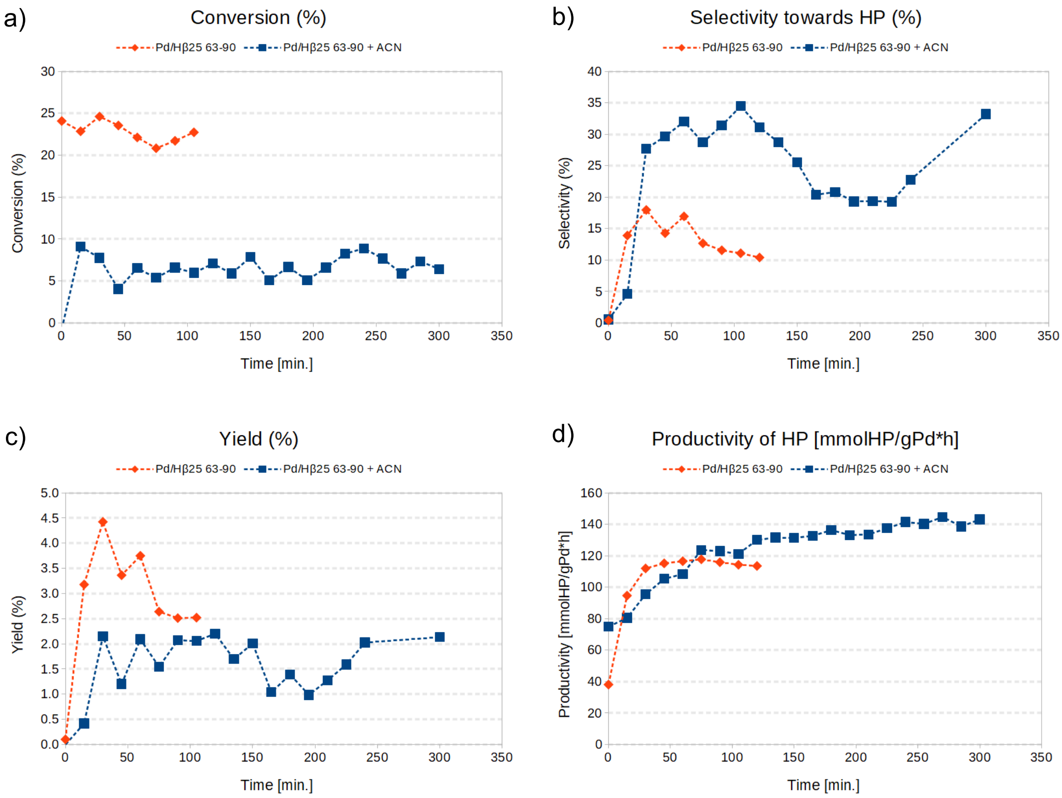

Figure 99: performance of Pd/Hβ25 of the particle size 63-90 μm, in methanol (red) and methanol:acetonitrile 9:1 (blue), using GF method; a) H_2 conversion, b) selectivity towards HP, c) yield and d) HP productivity.

The conversion at the steady state is decreased from about 20% to 5%, while the productivity is almost unchanged: as the consequence, the selectivity is increased in the presence of ACN. However, only a very little increase of the HP productivity is observed (from 110 $mmol_{HP}/g_{Pd}h$ to 130 $mmol_{HP}/g_{Pd}h$). This implies the suppression of the formation of water, rather than the increase of the production of HP, as the effect of ACN in the TBR. The absence of a significant increase of the productivity is quite similar to the effect of ACN on Pd/C with the SBR (Paragraph 2.3.1), based on the suppression of the O-O cleavage and not related to the formation of species more active towards the production of HP. Therefore, from the present data it can be assumed that the promotion effect observed in the SBR, associated to the co-presence of ion-exchange supports and coordinating solvent, does not occur with zeolite supported catalysts in the TBR setup.

The fraction with particle size in the range 90-125 μm is barely active in pure methanol. Accordingly, a small increase in selectivity is detected, but these changes are negligible, as the catalyst is almost inactive and the experiment data are therefore too scattered to be discussed. Interestingly, it was found that the presence of ACN leads to a small leaching of the palladium, that is later reduced under duty to form metal palladium that is stuck on the walls of the metal column. This can be appreciated by running a DS experiment with the column filled only by the inert material after the above mentioned test. When this phenomenon occurs, a small amount of HP is produced. Washing the reactor with a 10% solution of nitric acid allows to remove the residual of palladium. As the experiments with the smallest fraction of the catalyst were affected by the presence of these traces of palladium, they are not comparable with those of the other fractions and are not presented.

2.7.2 Investigation on Pd/C with the Trickle Bed Reactor

The commercial Pd/C catalyst used as the reference for the SBR experiments was investigated also with the TBR setup. This investigation is focused on the effects of the catalyst loading and of its dilution with the quartz sand, as well as those of the conditioning method (GF versus MF) and of ACN as the co-solvent.

2.7.2.1 Investigation on the catalyst loading with Pd/C

Initially, the effect of the dilution of the catalyst with different amounts of quartz sand were considered, in particular by using 150 mg of the catalyst and 2 g or 3 g of inert material. For this preliminary investigation, the GF conditioning method was used. It is important to underline that with Pd/C catalyst no issues related to the mechanical stability of the catalyst occurred and it was not necessary to press the catalyst into a pellet and grind it to obtain fractions with bigger particles size. In Figure 100 are reported the performances of the catalyst with different amounts of quartz sand.

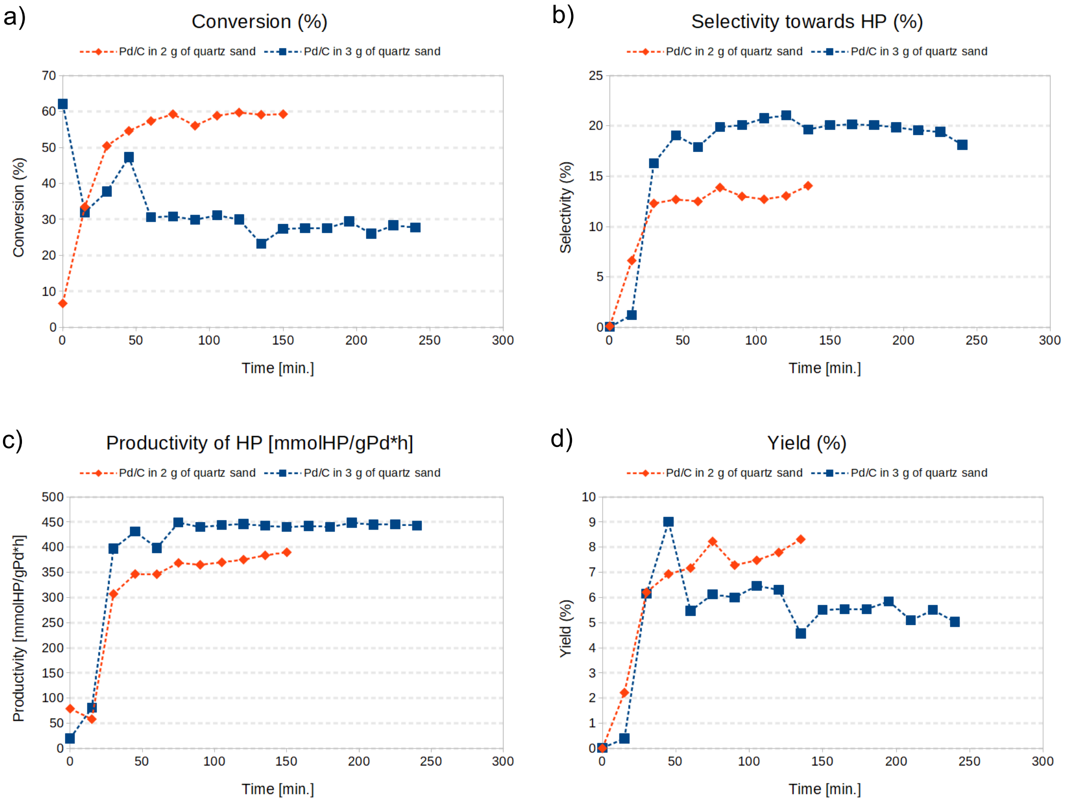

Figure 100: performance of Pd/C (150 mg) in 2 g of quartz sand (red) and 3 g of quartz sand (blue), using GF method; a) H_2 conversion, b) selectivity towards HP, c) yield and d) HP productivity.

The different dilution of the catalyst with the inert material has a remarkable effect on the steady conversion of the catalyst, consistently decreasing from 59% to 28% by increasing the amount of quartz sand from 2 g to 3 g. This suggests that under these liquid flow rate conditions, the catalyst wetting is lowered by increasing the dilution. The efficiency of the catalyst, that is the fraction of sites actually involved in the reaction, does not seem complete and is further reduced by the dilution. However, also the selectivity depends on the dilution of Pd/C. In particular, the higher the dilution the higher the selectivity, experimentally increasing from 13.5% to 20% with 2 g and 3 g of quartz sand, respectively. Moreover, also the productivity is enhanced by increasing the dilution, specifically from 380 $mmol_{HP}/g_{Pd}$·h to 445 $mmol_{HP}$/

g_{Pd}·h with 2 g and 3 g of quartz sand, respectively. This suggests a different interpretation of the results, beside that of the insufficient efficiency of the catalyst. In fact, since the higher the concentration of the catalyst in the layer, the higher its activity, when the activity is sufficiently high there is a higher probability that the reduction of hydrogen peroxide occurs. This leads therefore to an increase of the conversion and a decrease of selectivity and productivity. The excessive activity of Pd/C was further confirmed by repeating the experiment with 2 g of sand as the diluent. In fact, most probably in the second experiment a different distribution of the catalyst within the layer, featured by the presence of large aggregates of catalyst, was achieved. This led to a periodical exponential increase of the temperature of the catalyst layer up to 100° C and the experiment must be stopped for safety reasons. In that case, before quitting the experiment, the catalyst was producing almost only water.

A further way to increase the dilution of the catalyst, with the aim to achieve a higher selectivity, is to decrease the amount of catalyst loading. The result of an experiment with 25 mg of catalyst diluted with 2 g of quartz sand are presented in Figure 101 along with those obtained by diluting 150 mg of catalyst in 2 grams of inert material.

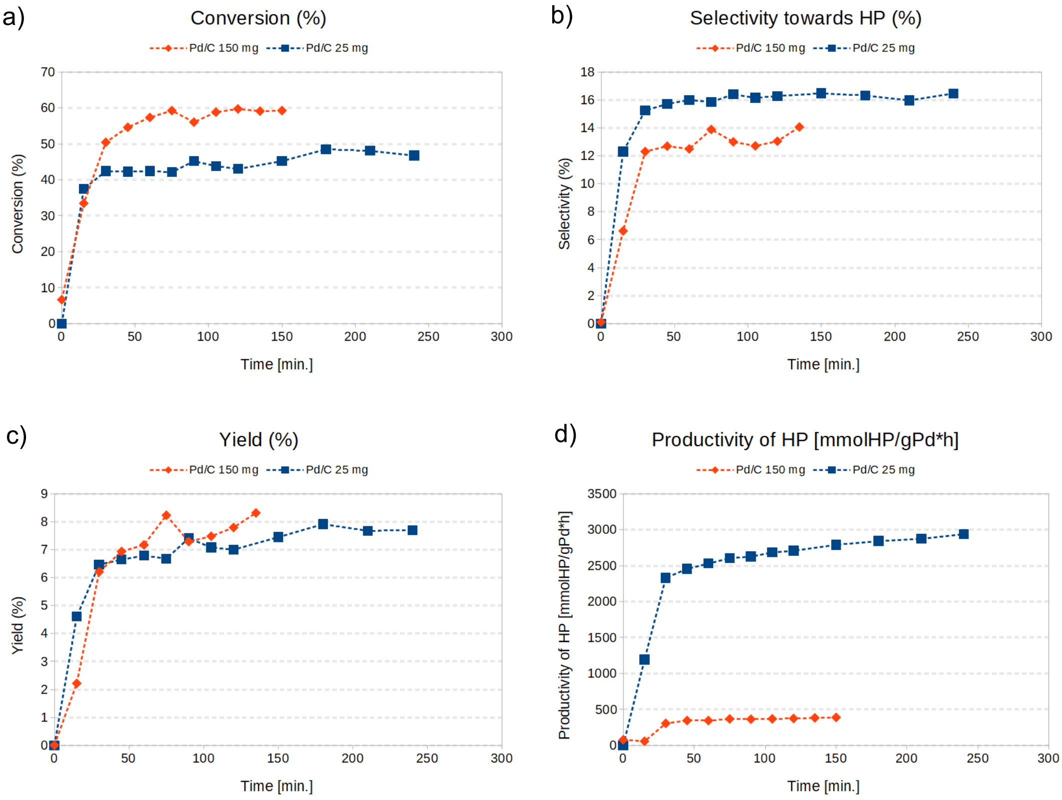

Figure 101: performance of Pd/C with 150 mg of catalyst loading (red) and 25 mg of catalyst loading (blue), using GF method; a) H_2 conversion, b) selectivity towards HP, c) yield and d) HP productivity.

As expected, by decreasing the amount of catalyst from 150 mg to 25 mg the conversion decreases, specifically from 59% to 48%. However, this decrease is not linearly proportional to the amount of catalyst. According to the previous investigation, the higher dilution induces a selectivity enhancement, as the probability of the further reduction of HP to water is lower. The most important outcome of this investigation is the much higher hydrogen consumption for each catalytic site, resulting from the not linear correlation between conversion and catalyst loading. In fact, in the first approximation, by loading 150 mg of catalyst, each mg of the material provides 0.4% of conversion, whereas by loading 25 mg of catalyst, one mg of material contributes for 1.9% of conversion. To explain this outcome, it must be assumed that the efficiency is not complete, when using 150 mg of catalyst and the catalytic results (Figure 101) are the consequence of both an incomplete efficiency of the catalyst and the decrease of the selectivity, due to the high hydrogenation activity. With 25 mg of catalyst its efficiency increases and therefore also the consumption of hydrogen per amount of catalyst. The selectivity is higher with 25 mg of catalyst than with 150 mg (13.5% and 16.5%, respectively), but is lower than that obtained with 150 mg in 3 grams of quartz sand. The quantitative explanation of these trends is not trivial and further experiments with different catalyst loadings and dilution ratios are needed to define a suitable interpretative. Nevertheless, these investigations clearly show that under these reaction conditions it is remarkably more convenient to load 25 mg of catalyst instead 150 mg into the reactor, as 12 mM with respect and 9.5 mM solutions of HP are obtained. This can be better appreciated by evaluating the productivity, reaching a value of 2900 $mmol_{HP}/g_{Pd}\cdot h$, therefore every single catalytic site produces more than seven times the amount of hydrogen peroxide produced with a catalyst loading of 150 mg.

2.7.2.2 Investigation on the effect of the conditioning with Pd/C

The effect of the conditioning method, GF or MF, on the performance of the catalyst was investigated with Pd/C. This was possible as this catalyst is mechanically stable in the catalytic bed under duty without any pretreatment. This investigation was carried out with 25 mg of catalyst dispersed in 2 g of quartz sand, the most promising experimental conditions, according to the previous Paragraph 2.7.2.1. In Figure 102 are reported the results of the catalytic experiments.

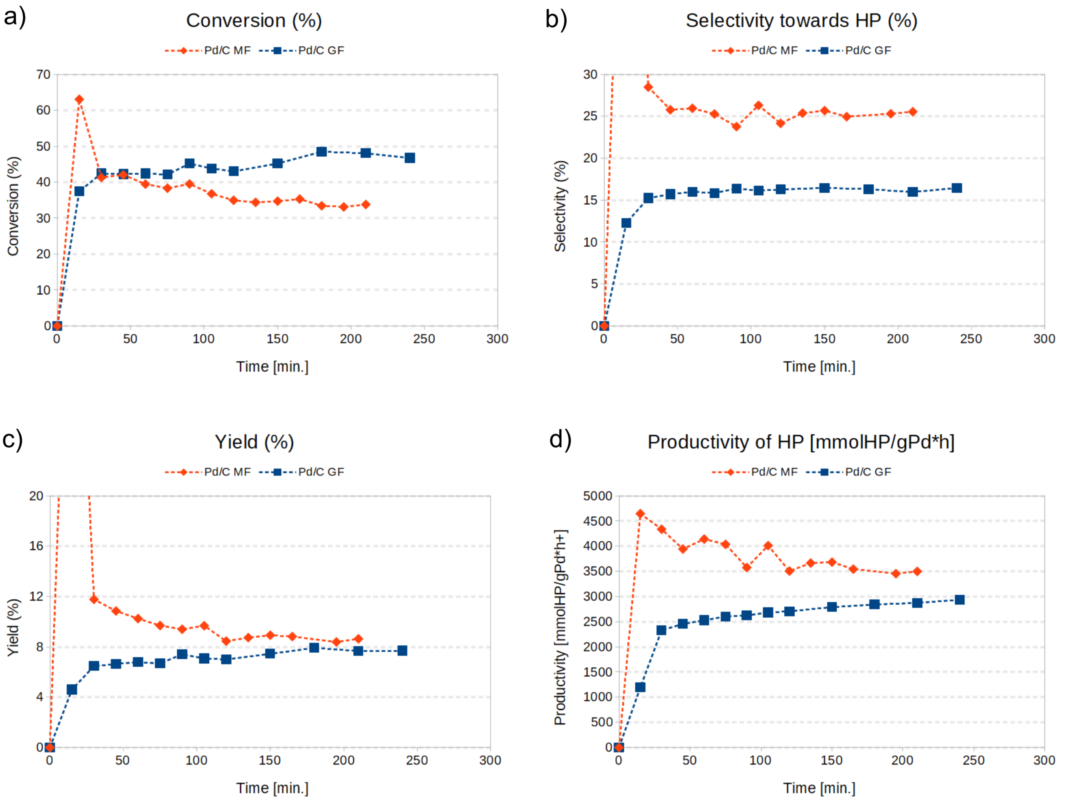

Figure 102: performance of Pd/C with the MF conditioning method (red) and the GF conditioning method (blue); a) H_2 conversion, b) selectivity towards HP, c) yield and d) HP productivity.

Initially, the conversion is similar with the different conditioning methods, whereas after about 50 min the conversion starts to decline and reaches a value at the steady state of 33%. Therefore, the MF method slightly deactivates the catalyst and the explanation of this evidence becomes clear by taking into account the selectivity. In fact, with the MF method the selectivity is increased up to 25% (16.5% with the GF method), hence it can be assumed in this case the activity of the catalyst towards the hydrogenation of HP is less prominent, being the catalyst more selective but at the same time less active. This positive effect can be noticed also for the HP productivity, that at the beginning of the catalytic experiment is higher than 4500 $mmol_{HP}/g_{Pd}\cdot h$, to stabilize at the steady state at the value of 3500 $mmol_{HP}/g_{Pd}\cdot h$, with an improvement of about 600 $mmol_{HP}/g_{Pd}\cdot h$ when compared to the GF conditioning. It is important to underline that with MF method the catalytic run formally starts just when the reaction gases start to feed and therefore after 15-20 minutes of the reaction the gases are starting to exit the reactor. This leads to very large values of conversion and selectivity but these values are ostensible as they are not the consequence of an actual hydrogen consumption. From this investigation is clear that the MF method allows to produce higher amounts of HP with higher selectivity, although the reason is still not fully clarified. However, these findings are suggesting that the dry catalyst in contact with the reaction gases produces only water, as large amount of water is found by Karl-Fisher titration samples of reaction mixture collected at the beginning of the catalytic experiment. Subsequently, the production of HP increases over time, until reaching the steady state. On the contrary, with the MF method the productivity is initially higher and then lowers over time. Experiments with the addition of small amounts of water to the reaction mixture were made and non negative effects on the selectivity were observed. This means that the lower selectivity at the beginning of the experiment with the GF method is not due to the presence of water, produced by the catalyst, but to the contact of the reaction gases with the catalyst in the absence of the liquid phase. This effect is still not clear, but can be related to a change on the oxidation state of the catalyst towards a form that is more active in the combustion reaction.

2.7.2.3 Effect of acetonitrile as co-solvent with Pd/C

The effect of acetonitrile on Pd/C with the TBR setup was investigated by using a 10% vol ACN methanol solution, the MF conditioning and 25 mg of catalyst in 2 grams of sand. According to the result with the SBR, acetonitrile is expected to bear a negative effect on the conversion. The results on the effect of ACN are reported on Figure 103. The results obtained with the TBR setup are quite similar and in line with those achieved with the SBR.

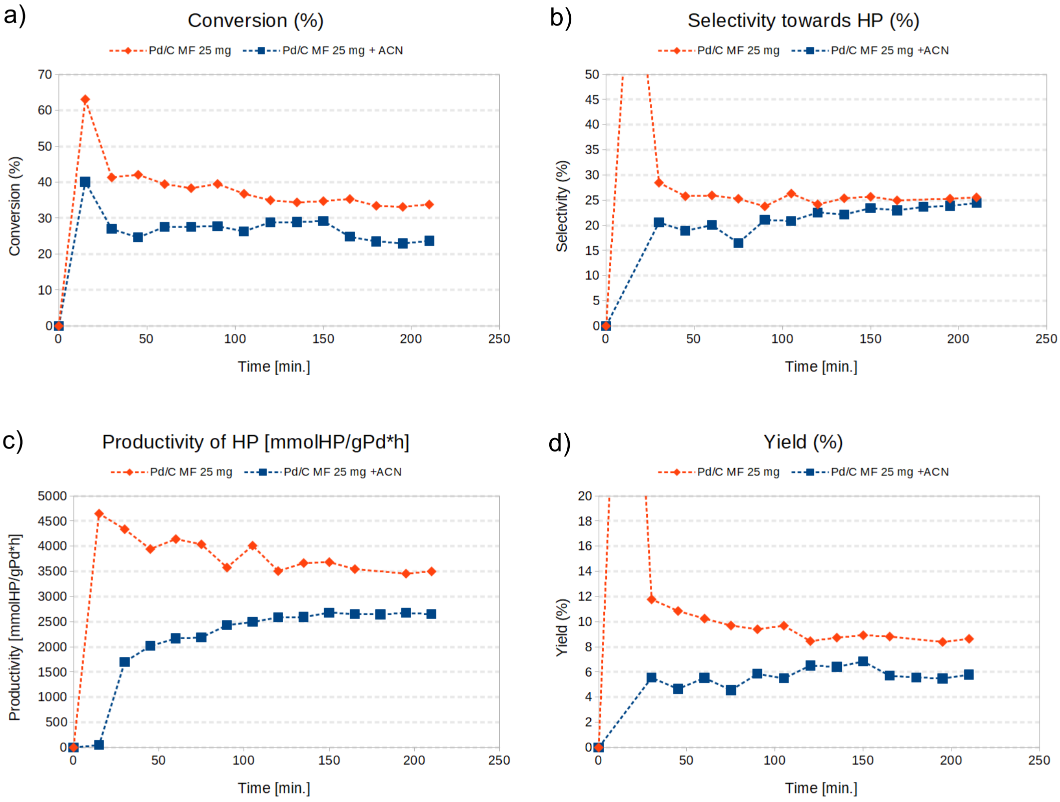

Figure 103: performance of Pd/C in methanol (red) and in methanol:acetonitrile 9:1 (blue), using MF method; a) H_2 conversion, b) selectivity towards HP, c) yield and d) HP productivity.

In fact, a decrease of the conversion is observed in the presence of ACN, from 33% in pure methanol to 24% in the presence of ACN. Although before the steady state, the selectivity is of about 15% lower in the presence of acetonitrile, when compared to pure methanol, at the end of the catalytic experiments the value is almost unchanged by the presence of the co-solvent. As a consequence of the lower activity with ACN, the productivity is lowered up to 2650 $mmol_{HP}/g_{Pd}\cdot h$. As for the experiment in the SBR, described in Chapter 3, with catalysts supported on materials lacking of ion-exchange groups (Pd/C or Pd/pDVB), the presence of ACN leads to the drop of both hydrogen conversion and production of HP, but the overall selectivity is almost unchanged. Therefore, also with the TBR setup, ACN shows a poisoning effect towards Pd/C. Finally, both in pure methanol and in the presence of ACN, the metal leaching is below the limit of detection (<0.6%).

2.7.2.4 Conclusive remarks on the investigations with Pd/C on the Trickle Bed Reactor

The investigations with Pd/C show that the distribution of the catalyst within the catalytic bed is of utmost importance for the performance of a catalyst in a packed continuous reactor. In the case of the DS reaction, this parameter not only affects the overall activity of the catalyst, but also its selectivity. Indeed, as HP can be seen as an intermediated of the formation of water, the higher the activity of the catalyst, thanks to its high concentration in the catalytic layer, the lower its selectivity. When operating under pressure conditions, these findings could have significant consequences also from the point of view of the safety, as a too high activity of the catalyst can can lead to runaway reactions. The best working conditions are obtained with a low amount of catalyst (25 mg on 2 g of inert). When higher amounts of catalyst are loaded, not only a part of the catalyst is not active in the reaction, but the overall process turns out to be less selective. The conditioning method is also influencing the activity of the catalyst: in particular, the contact between the dry catalyst and the reaction gases lead to a lower selectivity all along the experiment. The reaction gases in the absence of the liquid phase can modify the catalyst into a less selective form, but further investigations are needed to understand this phenomenon. As to the effect of acetonitrile, the presence of the co-solvent provides results fully in line with the semi-batch investigations. Hence, the co-solvent is decreasing the consumption of hydrogen as well as the production of hydrogen peroxide, without affecting the selectivity to a significant extent.

As a general overview, Pd/C is a promising catalyst, showing a high production of hydrogen peroxide with a rather satisfying selectivity under suitable experimental conditions, when compared to catalysts supported on inorganic materials. This catalyst is stable over time and allows to produce a 12 mM solution of HP, under the considered experimental conditions, although this value could be probably improved with further extensive studies. These findings clearly suggest that this catalyst is more promising in the DS reaction when compared to all the catalysts supported on inorganic materials, according to the investigations with the SBR setup (Paragraph 2.4.4).

2.7.3 Investigations on polymer supported Palladium catalysts with the Trickle Bed Reactor

2.7.3.1 Preliminary investigation on Pd/pDVB and Pd/SpDVB

In a first moment Pd/pDVB and Pd/SpDVB catalysts were investigate with the TBR setup without any pretreatment, by loading 150 mg of catalyst and 2 g of sand and by using the GF conditioning method. According to the results obtained with the SBR, both the catalysts are expected to be quite active, with Pd/SpDVB being more selective towards the production of HP. The results with Pd/pDVB (Figure 104) are in line with the outcomes carried out with the SBR.

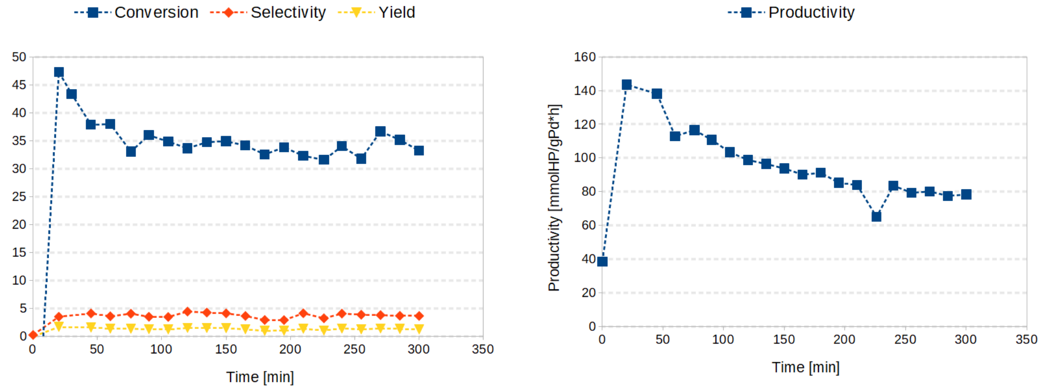

Figure 104: results of the catalytic experiment with Pd/pDVB, using GF method; parameters defining the performance (left) and productivity (right).

The Pd/pDVB catalyst shows a high conversion (about 33% at the steady state), although lower than Pd/C, and a poor selectivity, becoming less than 4% at the end of the DS experiment. In fact, the productivity is close to that of zeolite supported catalysts, although these catalysts are less active. Moreover, the production of HP decreases over time and stabilized to an average value of 78-80 $mmol_{HP}/g_{Pd} \cdot h$: this is quite hard to explain, as no leaching of the palladium is observed (<2.5%), thus the deactivation is not due to a loss of the active metal. This catalyst shows rather unpromising performances and therefore the testing has been interrupted after this preliminary study. As for the Pd/SpDVB catalyst, the experiment under the same reaction conditions shows a very high activity (Figure 105), with a quite high conversion (about 50%) at the beginning of the catalytic experiment. However, the catalyst turns out to be very unstable from a mechanical point of view and is continuously flushed out from the reactor. It is important to underline that the fraction which is flushed out by the liquid flow must smaller than 7 µm.

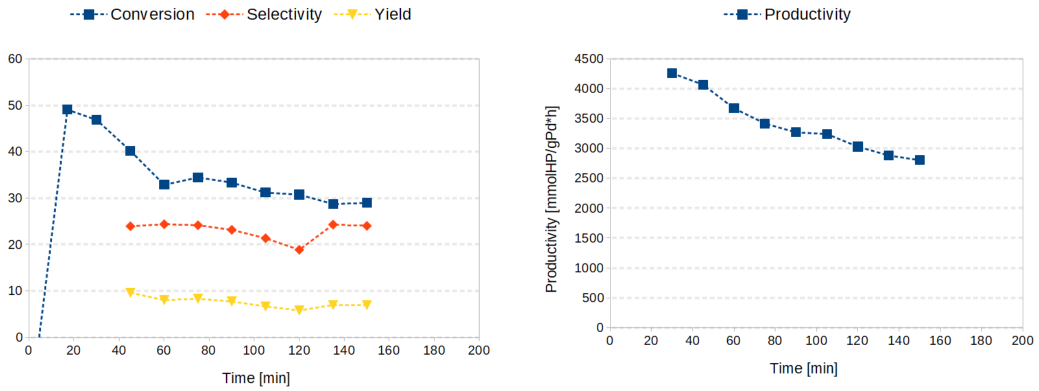

Figure 105: results of the catalytic experiment with Pd/SpDVB, using GF method; parameters defining the performance (left) and productivity (right).

As the consequence, both the consumption of hydrogen and the production of hydrogen peroxide are steadily decreasing over time. During the first 30 minutes of the catalytic experiment, the loss of catalyst is so high that is even impossible to analyse the reaction mixture to determine the production of water and hydrogen peroxide due to the presence of a large amount of suspended solid. Nevertheless, the catalyst shows rather promising results with the production of an 18 mM solution of HP in the first measured samples. To overcome the issue of the mechanical instability, a further experiment was made with a lower amount of catalyst (25 mg), but still part of the solid was flushed out and the results were hardly reproducible. Finally, the catalyst was pressed to form a pellet, ground and sieved with the same protocol developed for catalysts supported on inorganic materials and a remarkable increase of the stability was obtained. This pretreatment was therefore applied to Pd/SpDVB before the catalytic tests reported in Paragraph 2.7.3.22.7.2.5.

2.7.3.2 Effect of the particle size of Pd/SpDVB

The Pd/SpDVB catalyst was pressed, ground and sieved to separate fractions with different diameter. The fractions with the diameters 32-63 µm, 63-90 µm, 90-125 µm, 125-180 µm and 180-250 µm were collected and used for catalytic experiments with the GF conditioning method. The low catalyst loading, i.e. 25 mg in 2 g of inert, was chosen to avoid the excessive production of water. The results of the experiments with fractions with different particles size are reported in Figure 106.

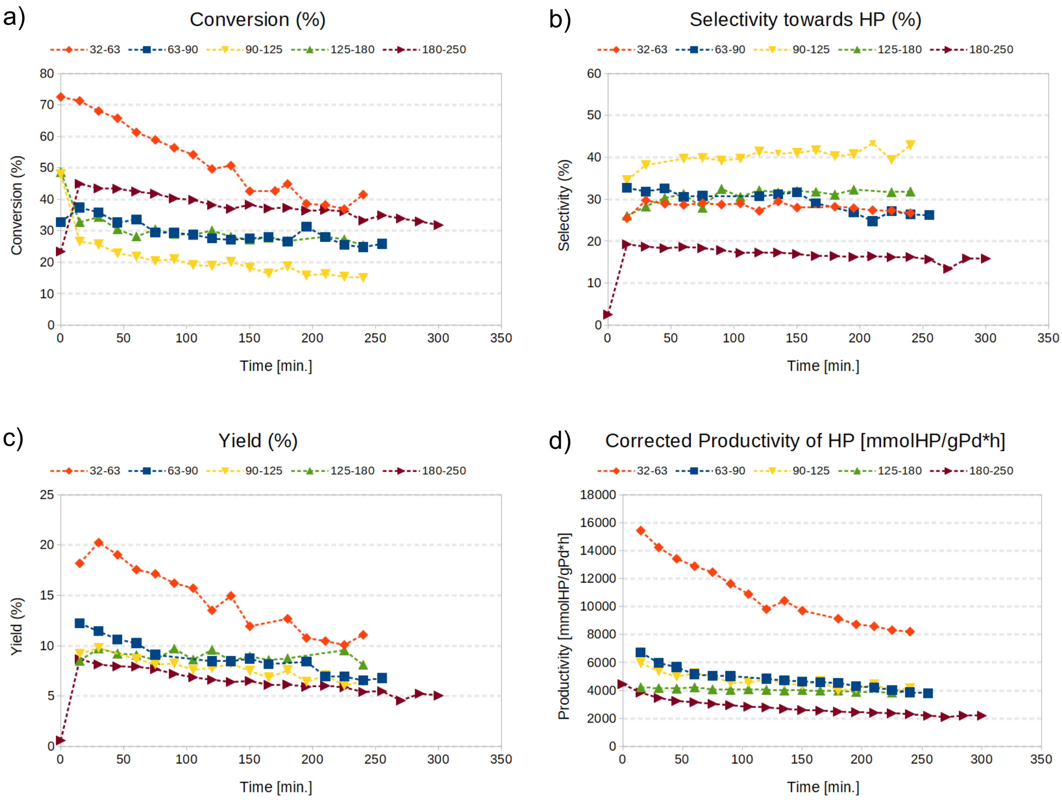

Figure 106: performance of Pd/SpDVB with different particle size, using GF method; a) H_2 conversion, b) selectivity towards HP, c) yield and d) HP productivity.

Also in this case a small flush-out of the catalyst occurs, but to a smaller extent and it stops after 5-10 min of reaction. This small amount of solid was collected and weighted after drying to determine the loss of catalyst from the catalytic bed. The amount of catalyst lost for the different fractions is reported in Figure 107. The productivity was determined by taking into the account the amount of catalyst removed from the reactor by the liquid flow.

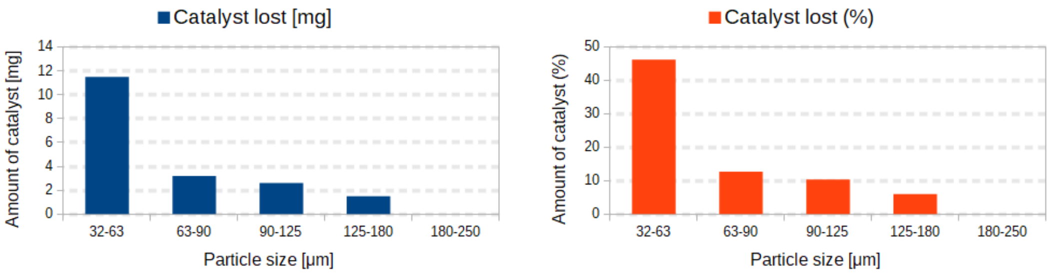

Figure 107: catalyst loss in the DS experiment for the different fractions of Pd/SpDVB.

The conversion of the catalyst depends not only on particles size of the material, but also on the amount of catalyst that is not removed by the liquid flow. Hence, to take into the account the loss of catalyst, the hydrogen consumption over time per mg of catalyst is calculated. In Figure 108 is reported the H_2 consumption at the end of the catalytic experiment, expressed in mmol/h·g_{cat}. As not all the fractions could reach the steady state, the conversion is calculated as the average of the last five values at the end of the test.

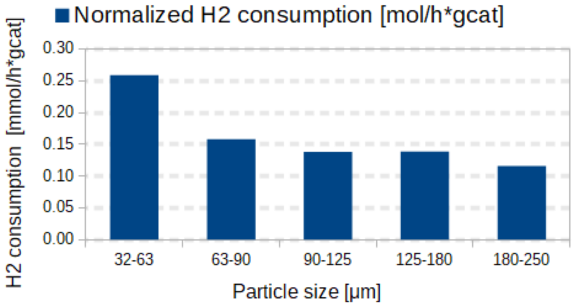

Figure 108: normalized consumption of hydrogen calculated on the effective catalyst loading

The interpretation of these data is giving a more realistic evaluation on the dependence between the activity of the catalyst and the particle size. In fact, if the lowest conversion is reported for the intermediate fraction with 90-125 µm and the second most active fraction is that with the biggest particles (180-250 µm) a very different trend is observed with the normalized consumption of H_2. The consumption of hydrogen is decreasing with the increase of the particle size of the catalyst, with the consumption in the range 0.16-0.12 mmol/h·g_{cat} for all the fraction, except that with diameter in the range 32-63 µm. This last fraction shows a normalized consumption that is 0.26 mmol/h·g_{cat} and is clearly an outlier with respect to all the other fractions. The different trend of the conversion (Figure 106) is the sum of the contributions of the normalized consumption and the amount of catalyst that is flushed out from the column. A trend similar to that of the normalized consumption is observed also for the productivity, with the bigger and the smaller fractions being the least and the most productive, respectively. However, the smallest fraction presents a remarkable deactivation in the production of HP, decreasing from 15400 $mmol_{HP}/g_{Pd}$·h at 15 min to 8200 $mmol_{HP}/g_{Pd}$·h at 240 min. Although these results are still unclear, they suggest that the activity of the catalyst is affected by diffusive restrictions that increase with the particles size. The fraction with particle size in the range 32-63 µm shows catalytic performances that are very different from the other fractions, as it is both more active and more productive. The selectivity of this catalyst is rather high, when compared to that of Pd nanoparticles supported on different catalytic supports, and depends on the particles size. These results suggest that there are no diffusion restrictions for particles smaller than 63 µm and thus the catalyst appears much more active. Moreover, the issue of the wetting affecting the smallest fraction of Pd/Hβ25 is not recognized for Pd/SpDVB. However, the smallest fraction of Pd/SpDVB is less stable from the mechanical point of view, leading to a higher catalyst loss, with the consequent decline of the activity over time. It is important to point out that the release of the catalyst takes place also after the pressing pretreatment and, since the size of the particles flushed-out the reactor is smaller than 7 µm, a degradation of the catalyst particles under reaction conditions has necessarily to occur. This could be reasonably due to the disintegration of the polymer aggregates, obtained by the pressing treatment, promoted by the swelling in the presence of the reaction mixture. The fractions with size 32-63 µm and 63-90 µm show a selectivity of 26.5% at the end of the catalytic experiment, whereas that with diameter 125-180 µm is featured by a slightly higher selectivity of 32%. Finally, the fraction with the biggest size presents the lower selectivity (16%) and the fraction with diameter 90-125 µm shows the highest selectivity, reaching 43%. The overall trend of the selectivity is not fully rationalized, but could be affected by the diffusive restrictions within the catalyst particles.

2.7.3.3 Investigation on the effect of the conditioning with Pd/SpDVB

The effect of the conditioning method was evaluated with Pd/SpDVB, upon using 25 mg of catalyst with 125-180 µm particles size, dispersed in 2 g of quartz sand. This particles size fraction was chosen as it is the most stable from the mechanical point of view. This experiment allows to evaluate the effect of GF and MF conditioning methods on the stability of this fraction, as well as the effect on the performance in the DS. The results of the catalytic experiments with GF and MF conditioning methods are reported in Figure 109.

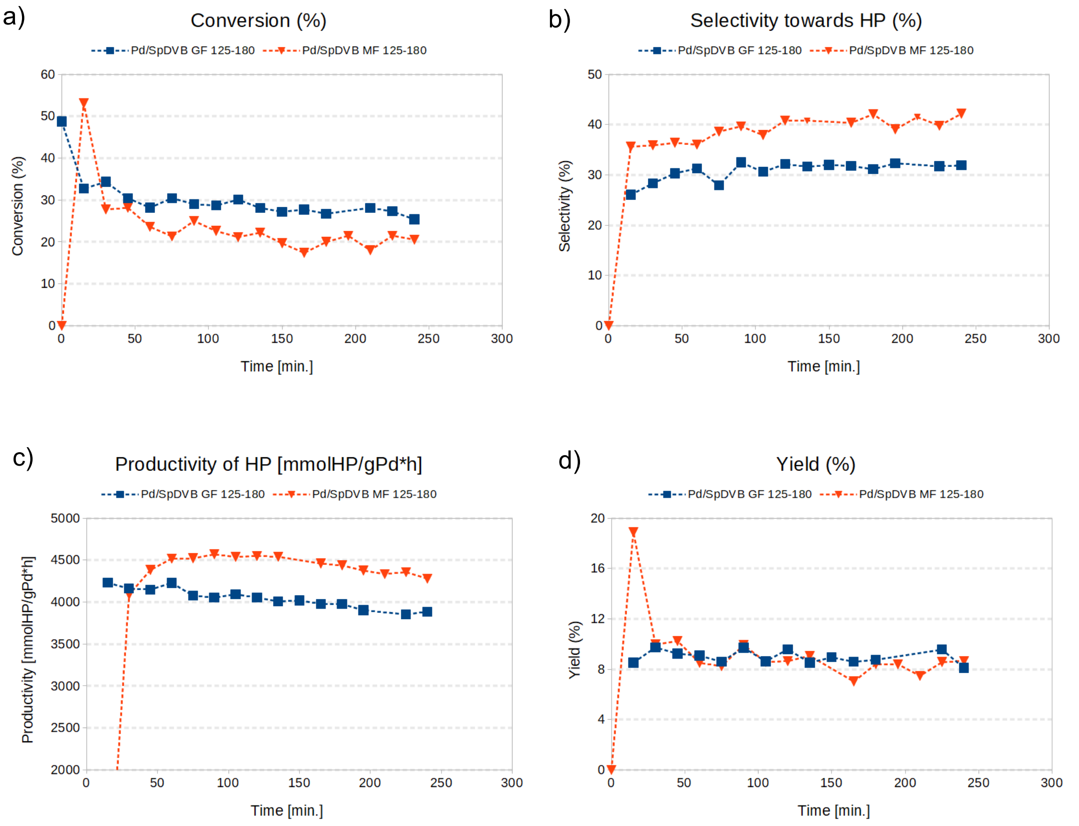

Figure 109: performance of Pd/SpDVB with the MF conditioning method (red) and the GF conditioning method (blue); a) H_2 conversion, b) selectivity towards HP, c) yield and d) HP productivity.

Similarly to Pd/C, by using the MF method the conversion is reduced. However, in this case the difference is smaller and conversion decrease from 27% to 20% for GF and MF respectively. Also in this case, the higher the conversion the lower the selectivity, being the latter parameter 32% and 41% for GF and MF methods respectively. However, these parameters balance each other, leading to the same yield for both catalysts (8.5%). With the GF method, the catalyst is more active, but with a lower HP selectivity, whereas the MF method makes the catalyst less active but more selective towards HP. Therefore, MF pretreatment method increases the productivity from 3650 $mmol_{HP}/g_{Pd} \cdot h$ to 4200 $mmol_{HP}/g_{Pd} \cdot h$, when compared to the GF method. The concentration of HP produced at the steady state is 15.2 mM and 17.5 mM with the GF and MF methods, respectively. Moreover, no differences in the flush-out behaviour were observed with the two conditioning procedures. These findings are in line with those obtained with Pd/C, even though with the reference catalyst the differences in the performance are larger. As for Pd/C, the effect of this condition is still not clear and more investigations are needed to describe these findings. However, this investigation is useful to develop and efficient and safe procedure for testing Pd/SpDVB and, more generally, polymer catalysts in the TBR.

2.7.2.4 Effect of acetonitrile as co-solvent on Pd/SpDVB

The effect of ACN was investigated with Pd/SpDVB, by using 25 mg of catalyst with 125-180 µm particles size, dispersed in 2 g of quartz sand and by using the MF conditioning procedure. The choice of this specific particles size fraction is discussed in the previous Paragraph, whereas the MF method was chosen mainly because is more efficient and safe. The effect of acetonitrile was investigated by using several ACN methanol solutions with different concentration, such as 0.1%, 1%, 5%, 10%, 20% and 50%. According to the results obtained with the SBR setup, the presence of ACN as the co-solvent is expected to enhance the selectivity of the catalyst. The results of the catalytic experiments are presented in Figure 110.

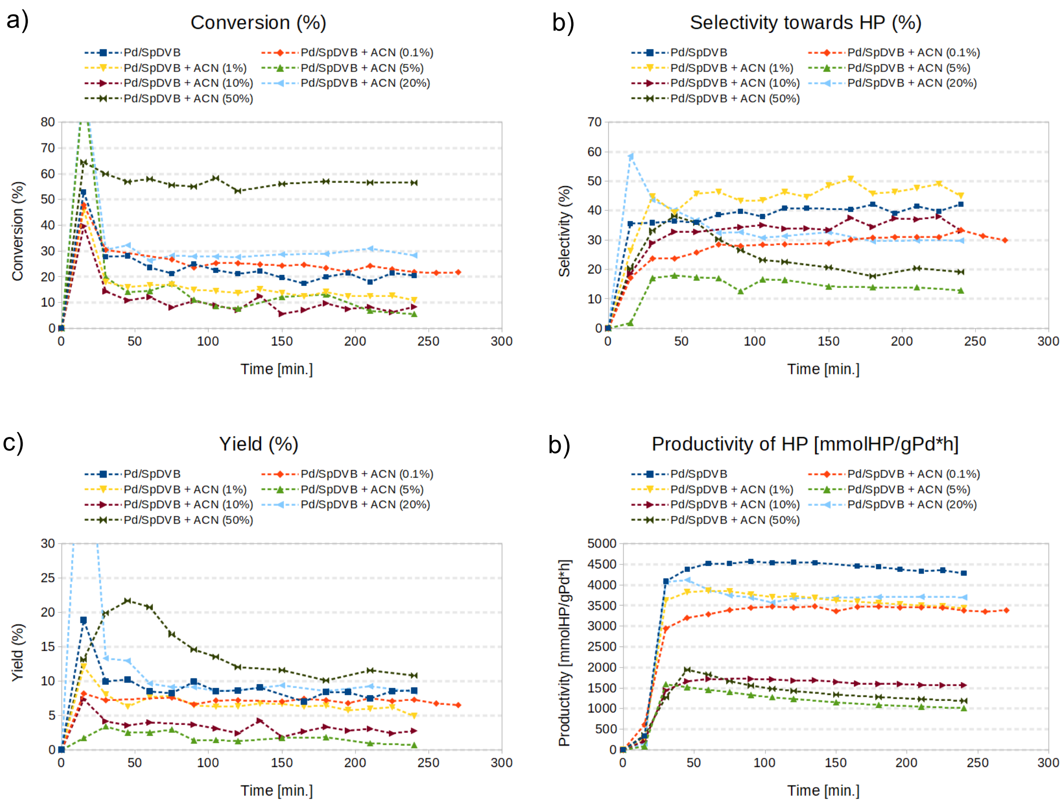

Figure 110: performance of Pd/SpDVB with different amount of acetonitrile as co-solvent in the reaction mixture, using MF method; a) H_2 conversion, b) selectivity towards HP, c) yield and d) HP productivity.

Moreover, to better understand the results of the DS experiments, the values at the steady state of the parameters defining the performance of the catalysts are reported in Figure 111.

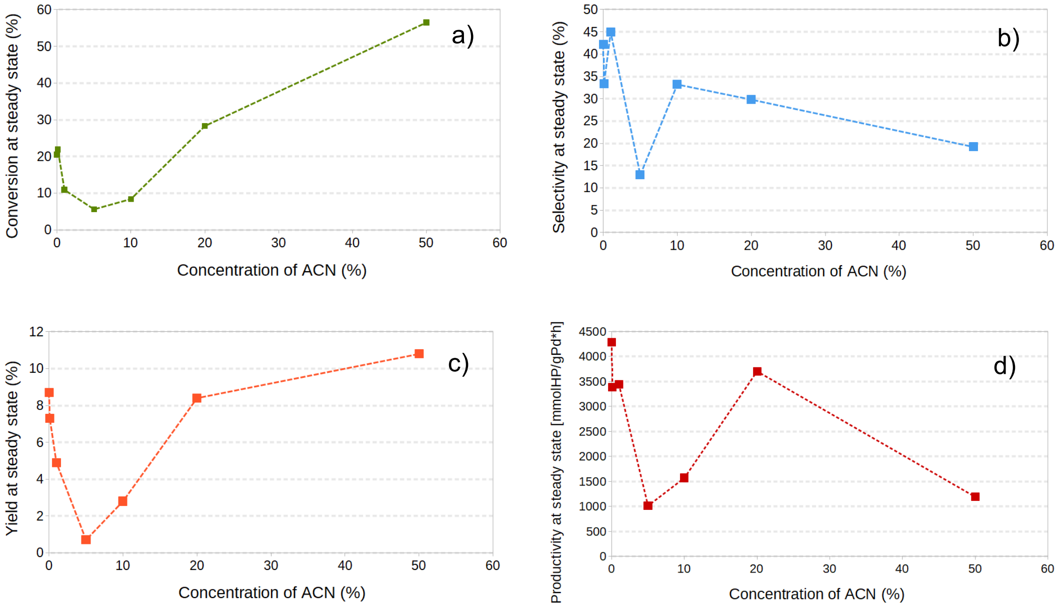

Figure 111: dependence of the performance of Pd/SpDVB at the steady state on the amount of acetonitrile as co-solvent in the reaction mixture; a) H_2 conversion, b) selectivity towards HP, c) yield and d) HP productivity

The results clearly show that all the reaction mixtures with ACN concentration equal or lower than 10% decrease the conversion of hydrogen. Beyond 10% ACN, H_2 conversion increases with the concentration of co-solvent. A small increase of the conversion in the SBR is obtained with pure ACN, when compared to 50% ACN methanol solution (Paragraph 2.6.1). However, the observed phenomenon in the TBR is different, as the enhancement is reached for ACN concentrations equal to 20% or higher. Therefore, it can be concluded that a high amount of ACN promotes the activity of the catalyst in the formation of water. This effect is stronger in the TBR, as a lower amount of ACN is enough to increase H_2 conversion. This is confirmed by the selectivity values, that are the lowest for ACN concentrations higher than 20%, with the exclusion only of the selectivity observed in the experiment with 5% ACN. In this latter experiment the selectivity turns out to be the lowest among all the DS experiments with ACN as the co-solvent.

Nevertheless, a small selectivity enhancement is observed only with a 0.1% of nitrile in solution and the selectivity gain, with respect the unpromoted test, is only about 2-3% at the steady state. For any value of ACN concentration, except for the experiment with 0.1% of co-solvent, the productivity decreases over time before the stabilization to the steady state. Moreover, the lowest productivity values are observed for 50% ACN and in between 5% and 10% of co-solvent, whereas in this same range the maximum enhancement is achieved in the SBR. The conversion of hydrogen also shows a minimum in the 5-10% range of ACN concentration. Finally, it is important to notice that no leaching is found, as the total amount of palladium in the reaction mixture is below the limit of detection, corresponding to a leaching <0.6% w. In summary, contrary to the SBR setup, no selectivity or productivity enhancements are obtained with Pd/SpDVB in the TBR. A high amount of ACN in the reaction mixture (≥20%) leads to an activation of the catalyst, but due to an improved production of water, as the selectivity is decreased. Characterizations of the spent catalysts and kinetic modelling are still ongoing, therefore it is still not possible to support the possible formation of Pd(II) complexes and their role in the DS. These Pd(II) species are proposed to be more active than the metal nanoparticles in the DS in SBR with 5-15% of co-solvent. Conversely, in the TBR setup a decrease of the productivity is observed in that range and it can be supposed that if the cationic species are formed, these are deactivating the catalyst and suppressing the production of HP.

2.7.2.5 Effect of N,N-dimethylformamide as co-solvent with Pd/SpDVB

The effect of DMF was investigated with Pd/SpDVB, by using 25 mg of catalyst with 125-180 µm particles size, dispersed in 2 g of quartz sand and using the MF conditioning procedure. The choice of this specific fraction and conditioning method are discussed in the previous Paragraphs. The effect of the use of DMF as the co-sovent was investigated by using several DMF methanol solutions with different concentrations, such as 0.1%, 1%, and 10%. The results of the catalytic experiments are presented in Figure 112.

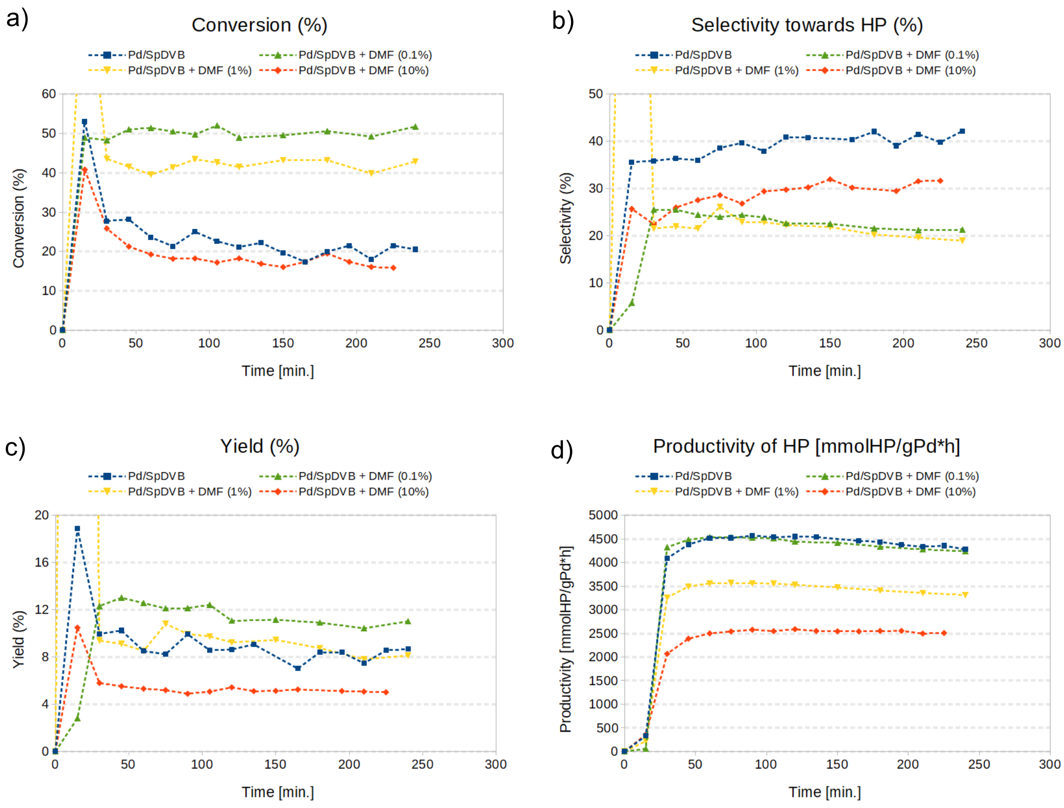

Figure 112: performance of Pd/SpDVB with different amount of DMF as co-solvent in the reaction mixture, using MF method; a) H_2 conversion, b) selectivity towards HP, c) yield and d) HP productivity.

Differently from ACN, only the use of a 10% of DMF in solution reduces the hydrogen consumption, whereas with 0.1% and 1% the conversion increases from 20.5% in pure methanol to 52% and 43%, respectively. Conversely, the presence of a small amount of DMF, such as 0.1-1%, decreases the selectivity from 43% for pure methanol to 18% and 21%, respectively. Accordingly, the productivity is lowered by any amount of DMF added into solution. With 0.1 % the decrease of productivity is less than 50 $mmol_{HP}/g_{Pd}\cdot h$, while using higher amount of DMF this effect is stronger. Generally, the higher the amount of DMF, the higher the decrease of the productivity. Similarly to ACN, in TBR also DMF is not acting as a promoter for the formation of HP, in contrast to SBR. Moreover, when the concentration of the co-solvent is low, a large increase of the hydrogen consumption is also obtained.

2.7.3 Conclusive remarks on the investigations with the Trickle Bed Reactor

This last part of the Thesis represents a preliminary investigation on the DS reaction with a continuous TBR, based on different classes of Pd catalysts studied also with the SBR. In particular, the performances of these catalysts were compared under different reaction conditions to asses the effect of the co-solvent, as well as that of parameters crucial for the TBR, such as the particle size of the catalyst, the catalyst loading and the conditioning method. This kind of experiments suggests that the performance of the catalysts can be further improved, by changing several additional parameters, such as the pressure, the distribution of the catalyst within the catalytic bed and the liquid and gas flow rates. According to the outcomes obtained with the SBR, the catalysts supported on inorganic materials are showing rather unpromising performances in the DS, as these catalysts are poorly active and their selectivity is very low. The presence of acidic groups of the zeolite catalysts does not significantly improve the production of hydrogen peroxide, similarly to Pd/Al_2O_3 and zeolite supported catalysts in the TBR. The commercial Pd/C catalyst appears more promising just in this preliminary investigation. It was demonstrated that the performance of this catalyst can be improved by tuning the catalyst loading and the distribution of Pd/C in the catalytic layer. A promising approach for future investigations could be distributing the catalyst all long the length of the column, to remarkably increase its dilution within the inert filler. This is expected to increase the catalyst loading while keeping high the dilution with the inert material, to reach a higher production of HP. The Pd/SpDVB outperforms once more any other material included in the investigation, as with it reached the highest production of hydrogen peroxide. However, this catalyst suffers from stability issues related to its disaggregation into very fine powder that is flushed out by the liquid flow. The performance of this catalyst both in terms of conversion of hydrogen and production of hydrogen peroxide is strongly affected by the particles size of the catalyst and, in particular, the lower the particle size, the higher its performance. These findings suggest that some diffusion restrictions are present under the experimental condition exploited in this investigation.

Further experiment are needed to model this phenomenon, for example to understand the nature of the diffusion restrictions. The effect of the addition of a coordinating solvent in the reaction mixture are by now rather unpromising in the TBR, as the presence of co-solvents, ACN and DMF, leads to the deactivation of the catalyst. In fact, a decrease of the production of hydrogen peroxide is always achieved by adding any amount of the co-solvent with both Pd/C and Pd/SpDVB. With Pd/C this result is in line with the findings obtained with the SBR, whereas in the case of Pd/SpDVB catalyst these results are quite unexpected. It seems that the promotion effect of the co-solvents cannot be extended to a continuous system, working under pressure, although further investigations are needed to confirm this preliminary result. Only a Pd catalyst supported on zeolite increases the selectivity in the presence of a co-solvent. However, the nature of the promotion effect seems different than that observed with the SBR setup, as it relies on the selective poisoning of catalytic sites responsible of the cleavage of the O-O bond.

Part 3

CONCLUSIONS

In this Thesis palladium catalysts for the direct synthesis of hydrogen peroxide are investigated. The main focus of the work is the investigation of coordinating solvents as novel promoters for the DS reaction. The most investigated material is the novel Pd/SpDVB catalyst, consisting in a nanostructured palladium phase supported on a mesoporous acidic ion-exchange resin. Moreover, palladium catalysts supported on inorganic materials, mainly zeolites, were also studied, along with commercial Pd/C, representing the reference material. These catalysts were used to investigate the effect of the catalytic support as well as its interaction with coordinating solvents, which is at the basis of the promotion effect. In the first part of this Thesis the catalytic experiments were performed with a semi-batch reactor working under very mild conditions. Preliminary investigations pointed out that the catalytic activity of Pd/SpDVB can be improved by conveniently tuning the synthetic procedure of the support. More in details, it was found that the procedure of functionalization of the support with the ion-exchange groups affects the production of hydrogen peroxide of the corresponding Pd catalyst. In particular, a remarkable increase of the production of H_2O_2 is obtained with Pd catalysts supported on ion-exchange resins that underwent to osmotic stress during the functionalization. This part of the investigation led to further peculiar outcomes, such as the self-production of hydrogen peroxide by ion-exchange resins without any active metal and the presence of a stable hydride phase in the Pd catalysts supported over SpDVB.

The exploitation of coordinating solvents as promoters resembles the action of halides, the most established selectivity enhancers for the DS. However, the use of halides is unsuitable for a technological application due to severe corrosion issues induced by these species. Halides are known to be good ligands for Pd(II) to form palladium complexes. On these basis, further ligands should act as promoters, without the drawback of the corrosion. The most straightforward starting point for this investigation is represented by acetonitrile, that is not only an effective ligand towards Pd(II), but also is widely available and non corrosive. The use of acetonitrile as co-solvent was investigated with extensive library of catalysts included in this project. It was found that acetonitrile enhances both the production of hydrogen peroxide and the selectivity of the reaction. Remarkably, this effect is obtained only for catalysts supported on materials bearing ion-exchange functionalities, such as ion-exchange resins and zeolites. An explanation of this effect comes from the characterisation of the spent catalysts, mainly TEM and XPS. In an oxidizing environment, the co-solvent forms Pd(II) cationic complexes that can interact with the ion-exchange groups of the catalytic support, to give rise to a release-and-capture mechanism. The Pd(II) species, grafted to the ion-exchange functions of the support, are much more active in the production of hydrogen peroxide, when compared to the supported metal nanoparticles of the catalyst.

Further coordinating solvents, such as DMF and DMSO, were also considered as possible promoters, with positive results. Once more it was found that the promotion effect can be obtained only with supports able to interact with cations. The extent of the promotion effect depends on the nature and the concentration of the coordinating solvent. Preliminary DFT investigations suggest that the effect of the co-solvents depends on both the mechanism of the formation of the Pd(II) complexes and their stability. DS experiments with Pd(II) catalysts further confirm the highest activity of Pd(II) complexes in the formation of hydrogen peroxide, when compared to the nanostructured metal catalysts, and clearly show that the Pd(II) catalysts are less stable than the corresponding reduced materials under reaction conditions.

Finally, in the last part of this Thesis, the catalysts are investigated with a continuous reactor, operating under harsher conditions. These experiments confirm once more that Pd/SpDVB outperforms not only Pd/C, but also the palladium catalysts supported on zeolites. In fact, it was possible to obtain a quite high productivity with very little refinement of the reaction conditions. On the other hand, with the continuous reactor the presence of co-solvents generally leads to the deactivation of the catalysts. This behaviour is substantially different than that observed under semi-batch conditions and suggests that additional issues affect the catalytic performance. In particular, the results under continuous conditions suggest the presence of diffusion restrictions as well as a low stability of the catalyst from the mechanical point of view. Once these limitations are overcome, the exploitation of coordinating solvent as promoters could be achieved.

In conclusion, the main and novel outcome of this work is the possibility to exploit coordinating solvents as corrosion-free selectivity enhancers. This result paves the way to the development of advanced catalytic systems for the technological application of the direct synthesis of hydrogen peroxide.

Part 4

EXPERIMENTAL PART

4.1 Synthesis and characterization of the polymer supported catalysts

4.1.1 Synthesis of pDVB

According to the reference,[145] 6 g of divinylbenzene, 60 mL of THF, previously purified by peroxides by flushing it through a neutral alumina column, 6 mL of deionized water and 165 mg of AIBN are added into a 100 mL Teflon liner. The mixture is stirred for 4 hours and heated in an autoclave at 100° C for 72 hours, under autogenic pressure (2.1 bars). The resulting polymer, in the form of a white brittle cylinder, is broken into pieces of 1-2 cm with a spatula and dried at air for 14 days.

4.1.2 Sulfonation of pDVB

In the sulfonation procedure 2 g of pDVB are swollen in the proper amount of solvent for two hours (10-30 mL of DCE or DCM), than 100 mL of concentrated sulfuric acid are added and the suspension is heated at 80°C for 3 hours at reflux and under magnetic stirring. When no swelling solvent is used, the pDVB is swollen with 100 mL sulfuric acid, later used for the sulfonation. After the sulfonation the mixture is filtered and the polymer is washed with 20 mL aliquotes of H_2SO_4 water solutions, decreasing the concentrations at every wash (10 M, 5 M, 2.5 M, 1.25 M, 0.65 M), and finally with water until the wastewater is neutral. The polymer is washed with 100 mL of methanol and dried for 24 hours at 110° C. The solid is ground and the 180-400 μm fraction is washed for 24 hours with methanol in Soxlet apparatus. Then the polymer is dried at 110° C for 24 hours.

4.1.3 Evaluation of the ion-exchange capacity of SpDVB

To evaluate the ion-exchange capacity of a resin, 100 mg of the material are swollen into a flask with 10.0 mL of NaOH 0.1 M, and stirred overnight with an orbital plate. Then, the solution is titrated with HCl 0.1 M Normex, and the same amount of basic solution is titrated to evaluate the exact concentration of the NaOH solution. To reduce the error due to the atmospheric CO_2, the NaOH solution is stirred overnight in a flask, together with the samples. The content of acidic ion-exchange group is calculated with the following equation:

$$Ion-exchange\,capacity\,[mmol\,H^{+}/g]=10^{3}\frac{C_{NaOH}V_{NaOH}-C_{HCl}V_{HCl}}{m_{pDVB}}$$

4.1.4 SAV measurement

Figure 113: gooch used for the SAV measurement.

To measure the SAV of a polymer a modified gooch was used, which is adapted to fit in the centrifuge (Figure 113). The upper part is half filled with the dried polymer and filled right below the frosted part. After closing the glassware to avoid the evaporation of the solvent, the polymer is let swell for 5 hours. The excess of solvent is removed by centrifugation and the glassware, together with the swollen polymer is weighted (P_2). The polymer is dried on the glassware with a ventilated oven at 70°C for 24 hours and then is weighted again (P_3). The polymer is remover, and after washing with methanol and drying the glassware, it is weighted again (P_1). The SAV is calculated with the following equation:

$$SAV=\frac{1}{\rho_{solv}}\cdot\frac{(P_2-P_3)}{(P_3-P_1)}$$

With ρ_{solv} the density of the solvent in g/mL.

4.1.5 Synthesis of Pd/SpDVB, Pd/K2621 and Pd/K1221 catalysts – *catalysts supported on sulfonated polydivinylbenzene and commercial ion-exchange resins*

As for SpDVB, the fraction with particles diameters in the range of 180-400 µm is used for the preparation of the catalyst. When a commercial resin is used, the material is washed with methanol using Soxlet apparatus and dried at 110° C. In this case the material is not ground. To produce the catalyst, the sulfonic polymer (up to 1 g per batch) is swollen for two hours with 10 mL of deionized water in a flask. After the swelling of the polymer 5 mL of an aqueous solution of $[Pd(NH_3)_4]SO_4$, containing the exact amount of precursor to obtain a catalyst with a 1% of metal loading, (25.3 mg/g_{SpDVB}). The amount of catalyst precursor is calculated with the following equation:

$$m_{[Pd(NH_3)_4]SO_4} = \frac{m_{POL} \cdot MM_{[Pd(NH_3)_4]SO_4}}{MM_{Pd}}$$

With m_{POL} weight of the polymer in mg and $m_{[Pd(NH_3)_4]SO_4}$ weight of the Pd precursor in mg. The suspension is stirred overnight with a mechanical shaker, is vacuum filtered on a G3 gooch and washed with water (about 200 mL). The wastewater are transferred into a 250 mL volumetric flask that after the addition of 5 mL of aqua regia is filled with water. The exact amount of metal loading is calculated by difference with the palladium of the wastewater, measured by ICP-OES (Ametek Spectro Genesis). The solid product is washed with 50 mL of purified THF and suspended in 50 mL of the same solvent. The slurry is treated with hydrogen using a glass reactor. The pressure of H_2 is set at 5 bars and then the reactor is heated ad 65° for 5 hours under magnetic stirring. The catalyst is recovered by filtration with a G4 gooch, washed with 50 mL THF and dried for 24 h at 70° C.

4.1.6 Synthesis of Pd/pDVB catalysts – *catalyst supported on unsulfonated polyvinilbenzene*

The unfunctionalized pDVB (1 g) is swollen with 8 mL of a $[Pd(acac)_2]$ (28.3 mg) dichloromethane solution. The volume of the solution and the amount of metal precursor exactly correspond to the amount necessary to swell the polymer and the amount of palladium needed to obtain a 1% w/w palladium catalyst. The solid is stored at -20°C for 24 hours. 15 mL of a $NaBH_4$ (0.2525 g) methanol solution are added. After 3 hours, the solid is recovered by vacuum filtration, washed with 250 mL of methanol and dried at 100°C for 24 hours. The exact amount of metal loading is calculated by difference with the palladium of the wastewater, measured by ICP-OES.

4.1.7 Synthesis of Pd/SpDVB(Na) catalyst – *catalyst supported on neutralized sulfonated polydivinylbenzene*

The SpDVB resin (~500 mg) is swollen in 60 mL of an aqueous NaOH 0.1 M solution and stirred with the mechanical shaker for 24 hours. Then the solid is filtrated with G4 gooch and washed with deionized water until neutrality of the wastewater. The solid is washed with 100 mL of methanol and dried at 70°C for 24 hours, hence the synthesis of the metal catalyst using the neutralized support was made with the same procedure involved for the synthesis of the catalysts supported on acidic (not neutralized) ion-exchange resins.

4.1.8 Synthesis of Pd-NH_3/SpDVB and Pd-ACN/SpDVB – *unreduced catalyst supported on sulfonated polydivinylbenzene*

The fraction with particles diameters in the range of 180-400 µm of SpDVB is swollen for two hours with 10 mL of deionized water in a flask. 5 mL of an aqueous solution of $[Pd(NH_3)_4]SO_4$ or $[Pd(ACN)_4]BF_4$ (containing the exact amount of precursor to obtain a catalyst with a 1% of metal loading), are added (the exact amount of precursor is calculated by the equation in paragraph 4.1.5, by using the proper molar mass). The suspension is stirred overnight with a mechanical shaker and filtered on a G4 gooch. The solid product is washed with 50 mL of purified THF and with 50 mL of diethyl ether. The catalyst is dried for 24 h at 40 °C. The exact amount of metal loading is calculated by difference with the palladium of the wastewater, measured by ICP-OES.

4.2 Synthesis of zeolite supported catalysts

The zeolite supported catalysts were prepared by the research group of Prof. Peirong Chen, by Wuwan Xiong. Here is reported a brief overview of the synthesis of the catalysts.

4.2.1 Synthesis of SSZ-13(1Al) and SSZ-13(2Al) zeolites

4.2.1.1 SSZ-13(1Al) synthesis

SSZ-13 zeolites with the isolation of aluminium arrangement in a six-membered ring (6-MR) are synthesized using only N,N,N-trimethyl-1-adamantanammonium hydroxide (TMAdaOH) as structure directing agent. In a typical synthesis, 31.23 g TMAdaOH are added to 28.53 g deionized water and stirred for 15 minutes under ambient condition. Then, 0.29 g of aluminium hydroxide powder are added. After 30’, 11.11 g colloidal silica solution are added and stirred for 2 h under ambient conditions. The resulting mixture is transferred into a stainless-steel autoclave and kept at 160 °C for 6 days with a static oven. Afterwards, the solid is recovered by filtration, washed thoroughly with deionized water, and dried at 100 ℃. Then, the solid is calcined in flowing dry air (200 mL/min) at 580 ℃ for 15 h.

4.2.1.2 SSZ-13(2Al) synthesis

SSZ-13 zeolites with the paired of aluminium arrangement in 6-MR were synthesized by combining sodium hydroxide and TMAdaOH as structure directing agent. More specifically, 4.38 g 5M sodium hydroxide, 15.63 g TMAdaOH and 36.58 g deionized water are mixed and intense stirred. After 15 min, 0.29 g aluminium hydroxide powder is added to this solution under vigorous stirring at room temperature for 30’. Then the synthetic procedure is the same as reported before for SSZ-13(1Al) zeolite.

4.2.2 Synthesis of zeolites in the ammonia form

4.2.2.1 Synthesis of NH_4-SSZ-13

Ammonium ions are introduced on SSZ-13(1Al) or SSZ-13(2Al) by ion-exchange with a 1M $(NH_4)_2SO_4$ solution by suspending the material in the solution at room temperature for 24 h. NH_4-form zeolites are recovered by filtration and dried at 100 ℃ for 24 h.

4.2.2.2 Synthesis of NH_4-LTA

Ammonium ions are introduced on LTA by ion-exchang with a 1M $(NH_4)_2SO_4$ solution by suspending the material in the solution and heating the suspension at 100 ℃ for 6 h under intense stirring and reflux. The solid is filtered and washed with deionized water. This procedure is repeated 4 times using fresh 1 M $(NH_4)_2SO_4$ solution. The solids is dried at 100 °C for 24 h.

4.2.3 Synthesis of 1% wt. Pd-Zeolite catalysts

4.2.3.1 Ion-exchange method (IE)

2 g obtained NH_4-form zeolites are dispersed in 50 mL deionized water, and the desired amount of the $Pd(NO_3)_2 \cdot 2H_2O$ solution (0.1 g/L) is added into the mixture. The mixed solution is stirred at 80 °C for 20 h. Solid is recovered by filtration, washed repeatedly with deionized water, and dried at 100 °C for 24 h. Thereafter, the solids is calcined at 500 °C in flowing dry air (200 mL/min) for 2 h, to obtain the acid form of the zeolite.

4.2.3.2 Wet impregnation method (WI)

2 g obtained NH_4-form zeolites are dispersed in 50 mL deionized water, and the desired amount of the $Pd(NO_3)_2 \cdot 2H_2O$ solution (0.1 g/L) is added into the mixture. After stirred for 10 mins, the mixture was stirred at room temperature for 24 h and then dried at 100 ℃ for 24 h. The solid is calcined at 500 ℃ in flowing dry air (200 mL/min) for 2 h, to obtain the acid form of the zeolite.

4.3 Determination of the concentration of hydrogen peroxide in methanol solutions

This paragraph gives a description of all the analytical methods used for the determination of the HP content in methanol solutions. The efficiency of the methods is checked, as described in Chapter 1, by titrating several HP solutions in methanol. All the titrations were performed with a Brand bottle-top Burette Titrette®, with a nominal volume of 25 mL and an accuracy of 18 µL. Every titration was repeated three times and the concentration of HP was determined from the mean value of the end points of the three titrations.

4.3.1 Preparation of the HP standard solutions

The Stock Solution of HP is obtained by the dilution of 1 mL of concentrated HP (30 % vol) into 1 L of deionized water. The concentration of the Stock Solution is exactly determined by titration with potassium permanganate 0.02 M Normex of 50 mL of HP solution to which 20 mL of H_2SO_4 3.6 M (dil. 1 : 5 in water) have been added;[212] no indicators are needed. The solutions for the titrations (Titr1-Titr5, Table 3) are obtained upon dilution of the stock solution with methanol, with different dilution ratios. After the preparation all the solution are stored at 4 °C.

4.3.2 Titration with potassium permanganate

1 mL of the sample is added to 2.5 mL of H_2SO_4 5 M, and titrated with $KMnO_4$ 0.002 M Normex. After the addition of the first drops of titrating solution a pale pink colour is formed, but differently from the titration of aqueous solutions of HP, it disappears after a few seconds.

4.3.3 Iodometric titration

The iodometric titration of the solutions of HP is performed with either a mildly acidic or a strongly acidic conditions. For both cases, a solution of Na_2MoO_4 0.13 g/L in aqueous H_2SO_4 10^{-3} M (solution A), and a solution of KI 10 g/L (solution B) are prepared by dissolving the solid reagents. For the titration under mildly acidic condition, 2 mL of the solution A and 3 mL of the solution B are added to 1 mL of the sample. The formed I_3^- is titrated with a standard solution of sodium thiosulfate 0.001 M, using starch as the indicator. For iodometric titration under strongly acidic conditions, 1 mL of a sample was treated with 2 mL of solution A, 2.5 mL of 5 M H_2SO_4 and 3 mL of solution B.

4.3.4 Cerimetric titration

1 mL of the sample is titrated with a 0.2 mM $Ce(SO_4)_2$ solution in 0.2 M H_2SO_4, prepared by dilution of a 0.1 M cerium sulfate standard solution. A 0.1 % w/w aqueous solution of ferroin is used as the indicator.

4.3.5 Spectrophotometric detection with titanium oxysulfate

0.5 mL of titanium (IV) oxysulfate solution are added to 1 mL of the sample in a 10 mL volumetric flask and diluted with deionized water. The UV-Vis absorption spectrum was recorded, from 355 nm to 800 nm, with a scan rate of 200 nm/min and using a water solution (0.5 mL of $TiOSO_4$ solution and 1 mL of methanol diluted to 10 mL with deionized water) as the reference. For the analysis of concentrated samples (above 20 mM of HP) the solution can be diluted up to 1 : 5 vol with deionized water without precipitation of TiO_2. For the analysis of sample coming from the reaction mixture containing benzonitrile (insoluble in water), the sample is diluted with 1 mL of methanol prior to the dilution with water in the 10 mL volumetric flask. In this investigation nine samples (Vis1-Vis9, Table 4), are prepared by dilution, from the solutions Titr1-Titr5 and M reported in Table 3, in order to determine the calibration curve.

4.4 Catalytic experiment – *Semi-batch Reactor*

4.4.1 Description of the reactor and the setup

Table 21: components of the SBR

Instrument	**Additional informations**	**Task**
Mass-flow controller	Bronkhorst El-flow select	Flow the gas phase into the TBR
Micro-gaschromathograph (μgc)	Agilent 3000 A	Analysis of reaction gases
UV-Vis spectrophotometer	Varian Cary 100 Bio	Analysis of the amount of HP produced

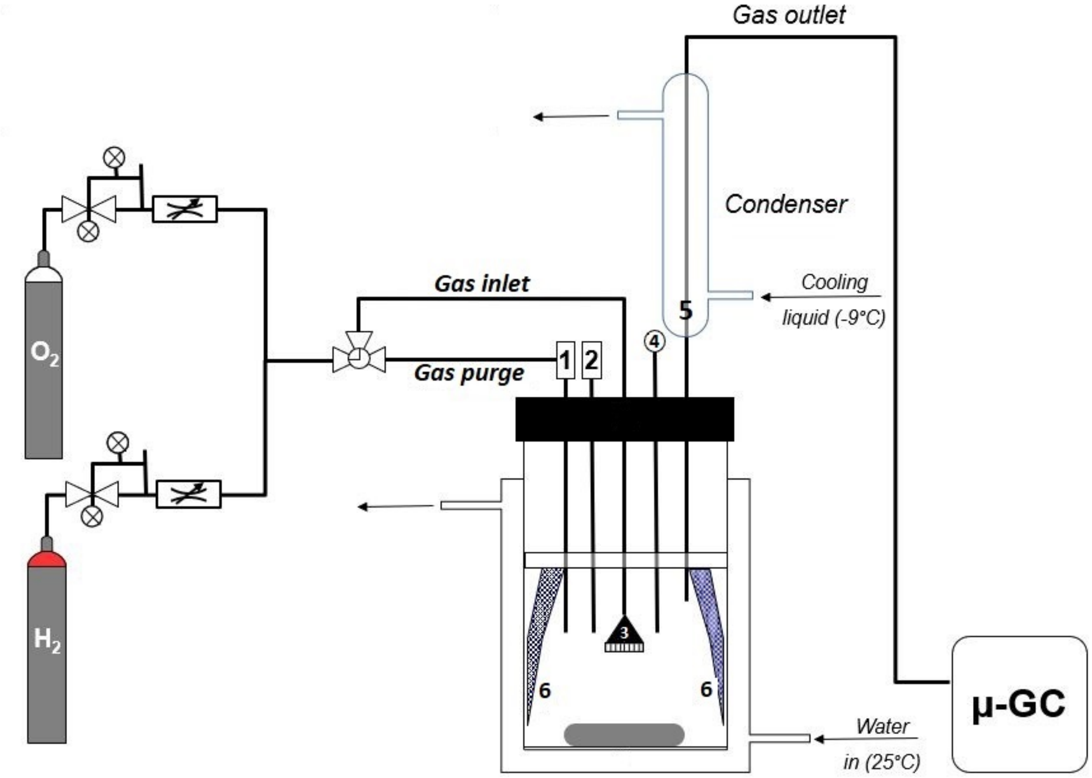

Figure 114: scheme of the SBR.

The SB reactor is composed by a 500 mL glass vessel with an external jacket that allows the thermostating of the internal liquid at 25° C with a water bath. Except when mentioned, all the internal components of the reactor are made of Teflon. The reactor is closed with a cap with five inlets that allow the insertion of several tools. According to Figure 114, there are:

1. a tube connected to a silica membrane through the reaction mixture is sampled with a syringe;
2. a tube to insert the catalyst;
3. a glass tube connected to a silica membrane, to flush the reaction gases in the reaction mixture;
4. a tube, closed on the bottom, that allows the measurement of the internal temperature with a thermocouple;
5. a glass component connected to a refrigerating system cooled at -9° C, through which flows the outgoing gas mixture.

All the pipes internal to the reactor are fixed to a disk, in which are connected four baffles (6), necessary to keep the liquid under stirring on a turbulent motion and enhance the dissolution of the gases in the liquid phase.

The reaction gases are fed to the reactor from two gas bottle, the flows are set by two mass-flow controller and then mixed before reaching the reactor. The line for the outgoing gases is connected (after the cooling system) to a micro-gaschromatograph (μ-gc) with a MS5A column, to periodically sample and analyse the hydrogen consumption. Some more informations on the experimental parameters are give on Table 22.

Table 22: experimental parameters of the method for the analysis of H_2/O_2 mixture

Column	MS5A
Inlet temperature [°C]	60
Inject temperature [°C]	60
Column temperature [°C]	100
Sampling time [s]	15
Inject time [ms]	200
Backflush time [s]	20
Run time [s]	90
Column pressure [psi]	30
Detector	TCD
Carrier gas	Ar

4.4.2 Description of the catalytic experiment with the SBR

4.4.2.1 Preparation of the reactor

300 mL of the reaction mixture (methanol or methanol with a co-solvent) are measured with a volumetric flask. A small amount of the liquid (about 10 mL) are stored into a flask, the remaining is put in the reactor. The reactor is closed and the flow of gases is turned on (1 mL/min of H_2 and 24 mL/min O_2). The reaction gases are flushed in the reactor 2 hours, measuring them with the μ-gc; this to completely remove nitrogen from the reactor and to condition the μ-gc. At the same time the catalyst (100 mg) is swollen with 2 mL of the small amount of solvent that is not put in the reactor. After 2 hours the catalyst is added to the reactor, the tube is washed with the remaining reaction mixture previously stored in the flask, and this is considered as the zero-point of the catalytic experiment.

4.4.2.2 Catalytic experiment

During the first 4 hours of a catalytic experiment the outgoing gases are analysed every 3’, while the liquid phase is sampled every 20’. As for the liquid phase, the reaction mixture (about 1 mL) is sampled with a glass syringe and filtered with the same syringe, by using a Teflon filter with a 0.2 µm cut-off. The sample is weighted, to calculate its exact amount, and the HP concentration is determined by using the spectrophotometric analysis with $TiOSO_4$, as reported in Paragraph 2.1.4. Before the sampling, the reaction gases are flown for 30 seconds through the sampling line, to clean it from residual of the liquid phase from the previous sample. At the end of the catalytic experiment the reaction mixture is filtered with a paper filter and the catalyst is dried overnight under the fume hood.

4.4.2.3 Data analysis

From the chromatograph of the outgoing gas mixture is calculated the molar ratio of H_2 and hence the instantaneous and cumulative H_2 consumption. The outgoing flow Φ_{H_2OUT} of the gases is calculated by the following equation:

$$\Phi_{H_2,OUT}=(\frac{Area_{H_2}-b}{a})\cdot\Phi_{TOT,\mathrm{IN}}$$

with $\Phi_{H_2\mathrm{IN}}$ the total gas flow fed to the reactor, *a* and *b* the slope and intercept of the calibration curve. Knowing the outgoing hydrogen flow, the instantaneous consumption is calculated, by the difference between the fed flow and this value. This value is normalized by the consumption at the beginning of the experiment, assuming its value equal to zero, this to consider small fluctuation that are present in the gc analysis. This consumption is volumetric, then the molar consumption can be calculated by dividing it by the molar volume of the gas at 25° C. The integration of this value gives the consumption of hydrogen, $n_{H_2,cons}$. This value is used to evaluate the conversion and selectivity, as reported on Paragraph 2.2.2.

As for the calibration of the μ-gc in order to evaluate the concentration of hydrogen in the exhausted gases, the reactor is filled with 300 mL of methanol and conditioned with the same procedure of a catalytic experiment. The reaction gases are fed to the reactor with different volumetric ratios between hydrogen and oxygen, and analysed 8 times, after the stabilization of the chromatographic areas. For each concentration a mean value of the area of hydrogen is calculated and this value is plotted against the percentage of hydrogen fed to the reactor. This calibration is repeated at least each 6 months, but it can be necessary to built a new calibration curve more frequently, if the area of hydrogen at the beginning of the catalytic experiment significantly differs from the expected area for a 4% gas mixture (the value in the absence of H_2 consumption). In Figure 115 is represented an example of a calibration curve.

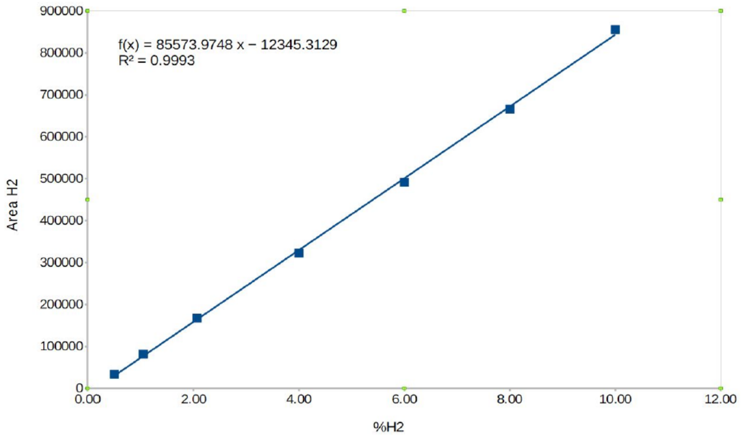

Figure 115: calibration curve of the μ-gc

4.5 Catalytic experiment – *Trickle Bed Reactor*

4.5.1 Description of the reactor and the setup

Table 23: components of the TBR

Instrument	**Additional informations**	**Task**
HPLC pump	Eldex ReciPro Series 2000	Flow the liquid phase into the TBR
Mass-flow controller	Brooks 5866 and 5850 series	Flow the gas phase into the TBR
Back pressure regulator	U3L (ultra low flow back pressure regulator)	Set the pressure into the TBR
Micro-gaschromathograph (*μ-gc*)	Agilent 6890N	Analysis of reaction gases
UV-Vis spectrophotometer	Shimadzu UV-2600i	Analysis of the amount of HP produced
Karl-Fisher titrator (KF)	736 GP Tritino	Analysis of the water content
Thermostat	Grant LT D6G	Cooling of the column

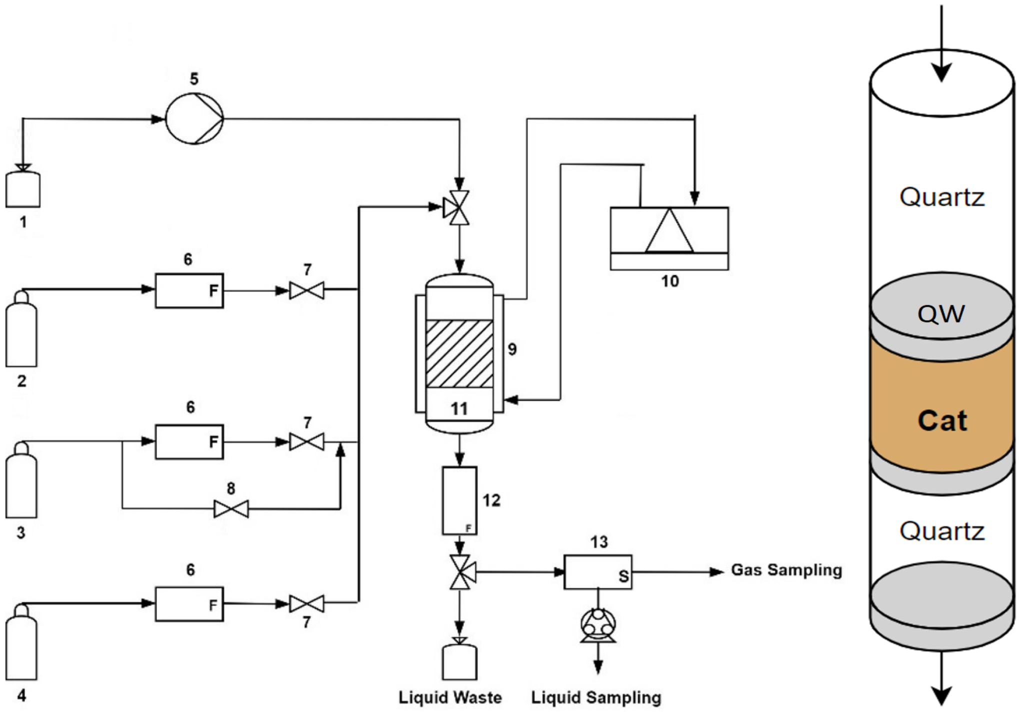

Figure 116: scheme of the TBR.

The TBR (Figure 116) is composed of a AISI 316 stainless steel 30 cm long column with an internal diameter of 12 mm, connected to the setup designed to flow the liquid and gas phases and to collect the outgoing reaction mixture. The liquid phase is stored on a glass bottle (1) connected to an HPLC pump (5) that flows the gas to the TBR at 1 mL/min flow rate. The reaction gases are stored in two gas bottles (pure O_2 and H_2 5% in CO_2, respectively 2 and 4). The inert gas (CO_2), necessary to pressurize the reactor before the catalytic experiment is connected to a third gas line. All the gases are flown to the reactor with mass-flow controllers (6, on 7 a safety valve to close the gas flows). In the case of the inert gas, an additional gas line with a valve (8) allows to skip the mass-flow controller and feed the reactor straight from the bottle, to fast pressurize the reactor if needed. The column (11) is surrounded by a copper serpentine (9) cooled at 15° C with a water bath (10). On the bottom of the column are located a filter with a 7 μm of cut-off and the tool to control the pressure into the column (12). This consist on a membrane, in the lower part flows the reaction mixture, while in the upper part an argon flow (6 mL/min) is flushed. The pressure of the Ar flow is controlled by a back pressure regulator; by controlling the pressure of the Ar flow it is possible to control the pressure of the reaction mixture, that must be at least equal to the Ar pressure to be able to go through the membrane. The outgoing reaction mixture is collected into a glass balloon (13) that allows the separation of the liquid and gas phases. In this way the liquid phase can be collected with a peristaltic pump to analyse the water content and the amount of HP produced, while the gas phase is sampled with a gas syringe through a membrane, to analyse the hydrogen amount. The consumption of hydrogen is calculated differently from the SBR setup. In this case, the diluent (CO_2) is used as the internal standard and the ratio between the area of H_2 and CO_2 is calculated from the chromatographs. From this ratio is possible to determine the amount of hydrogen in the exhausted gases and therefore the conversion.

4.5.2 Description of the catalytic experiment with the TBR reactor

4.5.2.1 Preparation of the reactor

In a typical catalytic experiment the column is filled with quartz sand until almost half of its height, blocked on the bottom of the column with a layer of quartz wool. The catalyst (from 150 mg to 25 mg) is diluted with quartz sand, typically 2 g, and then is put in the column in the middle of two layers of quartz wool. The column is then filled with quartz sand. In the middle of the catalyst layer is located a thermocouple to measure the temperature of the catalyst during the catalytic experiment. After filling it, the column is connected to the setup and is pressurized at 20 bars with CO_2 flow set at 50 mL/min. The conditioning of the reactor can be done with two different modalities:

- “Gas first” method (GF): After 30’-45’ the CO_2 flow is switched off and the flows of the reaction gases are turned on, by setting the oxygen flow at 17.2 mL/min and the H_2/CO_2 flow at 24.5 mL/min, to have an internal flow of 20 bars at 4 mL/min with a ratio of H_2/O_2 of 1:5. After 30’ the liquid flow is turned on (1 mL/min) and when the first drops of liquid are collected in the liquid/gas separator the zero-point of the catalytic experiment is taken;

- “Methanol first” method (MF): After 30’-45’ the CO_2 flow is switched off and the liquid flows is turned on (1 mL/min). After the first drops of liquid are collected in the liquid/gas separator the liquid is flushed into the TBR for 30’ and then gas flow is turned on by setting the gas flows ad mentioned before. This is considered as the zero-point of the catalytic experiment is taken.

4.5.2.2 Catalytic experiment

In the catalytic experiment both liquid and gas phases are sampled every 15’, starting from the zero-point of the experiment. The gas phase is analysed by gas-chromatograph to evaluate the hydrogen consumption, while the liquid sample is divided in two aliquots. 0.5 mL are analysed by KF titration to quantify the amount of water, while about 1 mL (exact amount determined by weighting) is used to calculate the HP produced, with the same method used in the SB reactor (described on Paragraph 2.1.4). The water produced during the DS is obtained by the difference between the water present in the sample and the water content of the liquid phase before the catalytic experiment. With the GF method this is calculated by analysing the water contend of the fresh liquid phase stored on the liquid reserve before the HPLC pump. With the MF method is possible to obtain a more accurate value by calculating the water content of the first sample obtained on the zero-point of the experiment, which is collected in the very same moment the reaction gases are turned on.

4.6 Characterization of the fresh and spent catalysts

4.6.1 Evaluation of Pd leaching with ICP-OES

In the case it is necessary to determine the amount of leached Pd, 200 mL of the reaction mixture are measured with a volumetric flask after the filtration and then are dried with rotating evaporator into a glass balloon. The balloon is washed with 5 mL of *acqua regia* that is transferred into a 250 mL volumetric flask and filled with water. This solution is analysed by ICP-OES (Ametek Spectro Genesis) to determine the amount of palladium in the former 200 mL of reaction mixture; the total amount of palladium leached is 3/2 of the palladium present in that amount of reaction mixture.

4.6.2 TEM characterisation

Samples for (S)TEM analysis are prepared gently grinding the specimen in an agate mortar and depositing them onto a lacey carbon copper TEM grid a drop of the powder dispersed in isopropanol. The liquid suspensions were sonicated for 15 minutes for better homogenization. Prepared TEM grids are inserted in the column of a ZEISS LIBRA200FE electron microscope after overnight drying. TEM microscope is operating both in transmission and scanning-TEM modes.

4.6.3 XRD characterisation

XRD of powder measurements were carried out using a PANalytical X'Pert Pro diffractometer equipped with a Co X-ray tube and a real-time multiple strip (RTMS) detector (X'Celerator). Panalytical High Score Plus software and Panalytical ICSD database were used for phase identification.

4.6.4 XPS characterisation

The samples for XPS analysis are prepared using pristine silicon substrates on which some droplets of a dispersion in methanol of the sample are deposited. Then the substrates are heated at 50°C for about 10 min to dry the dispersion. XPS measurements are performed in ultra-high vacuum conditions (1-2×10-6 mbar) at room temperature, using a VG Scienta XM 650 X-ray source. The X-rays produced are monochromatized using a VG Scienta XM 780 monochromator optimized for Al Kα radiation (1486.7 eV). Photoelectrons are collected at normal emission and analysed with a Scienta SES 100 electron analyser. The calibration of XPS spectra is carried out by placing the C 1s peak at 284.5 eV. XPS spectra are fitted with the XPSpeak 4.1 software. The fit is initially performed by fixing the binding energy (BE) of the different components at the expected values.[213] Moreover, full-width-at-half-maximum (FWHM) and linesHApe (Voigt function) are fixed, in terms of percentage of Lorentzian and Gaussian components, at plausible values (1.0-1.5 eV range for FWHM, 35-65% range for the Lorentzian component in the linesHApe). Then, BE is let free to vary and the fit is carried out again, maintaining the other two parameters fixed. The final result is evaluated by checking the χ2 parameter; if far from 1, (the correct value for an optimum simulation), all the parameters of the peak are tuned and the fit repeated.

4.6.5 DSC/TGA characterisation

Thermogravimetric analyses were performed on a TA Instruments 2960 SDT simultaneous TGA/DSC apparatus. A 10 °C/min heating ramp from 30 to 800 °C was applied, under nitrogen atmosphere. Sample size was approximately 5 mg and alumina crucibles were used.

4.7 Computational investigations

Density Functional Theory (DFT) calculations were carried out with the Amsterdam Density Functional (ADF) software,[214–216] using the OPBE4 functional and employing the zeroth-order regular approximation (ZORA)[217] to take into account scalar relativistic effects, which are mandatory in the presence of heavy nuclei.[218–221] The TZ2P basis set was used for all the elements. It is a large uncontracted set of Slater-type orbitals (STOs), is of triple-ζ quality and is augmented with two sets of polarization functions on each atom. In addition, core electrons were described with the frozen-core approximation: up to 1s for C, O and S, and up to 3d in the case of Pd; the level of theory is denoted in the text ZORA-OPBE/TZ2P. For the numerical integration, the Becke grid was used. [222,223] Frequency calculations were run to assess the nature of the structures located on the potential energy surface: all minima have real frequencies. Solvent effects were included using the Conductor-like Screening Model (COSMO),[224,225] which is implemented in the ADF program. For H_2O, chosen to mimic a polar environment, we used a solvent-excluding surface with an effective radius of 1.93 Å, and a relative dielectric constant of 78.39. The empirical parameter in the scaling function in the COSMO equation was set to 0.0. The radii of the atoms were taken to be MM3 radii,[226] divided by 1.2, giving 1.350 Å for H, 1.700 Å for C, 1.517 for O, 1.792 for S and 1.975 Å for Pd.[227] To gain quantitative insight into the stability of the compounds, an activation strain

(ASA) and energy decomposition analysis (EDA) was performed[228,229] as implemented in ADF. Using this fragment based approach, according to the ASA scheme, we have decomposed the energy relative to the reactants into strain, ΔE_{strain} (i.e. the deformation energy required by the reactants to acquire the structure they have in the compound of interest) and interaction, ΔE_{int} (i.e. the interaction energy between the deformed reactants):

$$\Delta E = \Delta E_{strain} + \Delta E_{\mathrm{int}}$$

Within EDA, ΔE_{int} can be written as the sum of electrostatic interaction (ΔV_{elstat}) the interaction between Coulomb charge densities, Pauli repulsion (ΔE_{Pauli}), related to the repulsive interaction between filled orbitals and orbital interaction (ΔE_{oi}) due to stabilizing interactions such as HOMO-LUMO interaction:

$$\Delta E_{\mathrm{int}} = \Delta V_{elstat} + \Delta E_{Pauli} + \Delta E_{oi}$$

REFERENCES

[1] *Proc. R. Soc. Lond. A* **1934**, *147*, 332–351.

[2] Catherine E. Housecroft, Alan G. Sharpe, *Inorganic Chemistry*, Paerson Education Limited, Edimburg Gate, Harlow, Essex (England), **2005**.

[3] Hydrogen Peroxide; G. Goor, J. Glennberg, S. Jacobi, in *Ullmann's Encyclopedia of Industrial Chemistry*, Wiley-VCH, **2007**.

[4] J. M. Campos-Martin, G. Blanco-Brieva, J. L. G. Fierro, *Angew. Chem. Int. Ed.* **2006**, *45*, 6962–6984.

[5] R. Ciriminna, L. Albanese, F. Meneguzzo, M. Pagliaro, *ChemSusChem* **2016**, *9*, 3374–3381.

[6] R. Hage, A. Lienke, *Angewandte Chemie International Edition* **2006**, *45*, 206–222.

[7] G. Gao, Y. Tian, X. Gong, Z. Pan, K. Yang, B. Zong, *Chinese Journal of Catalysis* **2020**, *41*, 1039–1047.

[8] J. Yu, D. Shao, C. Sun, C. Xu, D. Hinks, *Cellulose* **2017**, *24*, 2647–2655.

[9] D. Yu, M. Wu, J. Lin, *Fibers Polym* **2017**, *18*, 1741–1748.

[10] A. B. Sorokin, E. V. Kudrik, *Catalysis Today* **2011**, *159*, 37–46.

[11] K. Kosaka, H. Yamada, K. Shishida, S. Echigo, R. A. Minear, H. Tsuno, S. Matsui, *Water Research* **2001**, *35*, 3587–3594.

[12] C. Samanta, *Applied Catalysis A: General* **2008**, *350*, 133–149.

[13] S. R. Jennings, D. J. Dollhopf, W. P. Inskeep, *Applied Geochemistry* **2000**, *15*, 235–243.

[14] R. J. Lewis, G. J. Hutchings, *ChemCatChem* **2019**, *11*, 298–308.

[15] Y. Yi, L. Wang, G. Li, H. Guo, *Catal. Sci. Technol.* **2016**, *6*, 1593–1610.

[16] T. Richards, J. H. Harrhy, R. J. Lewis, A. G. R. Howe, G. M. Suldecki, A. Folli, D. J. Morgan, T. E. Davies, E. J. Loveridge, D. A. Crole, J. K. Edwards, P. Gaskin, C. J. Kiely, Q. He, D. M. Murphy, J.-Y. Maillard, S. J. Freakley, G. J. Hutchings, *Nat Catal* **2021**, DOI 10.1038/s41929-021-00642-w.

[17] X. Lu, W.-J. Zhou, H. Wu, A. Liebens, P. Wu, *Applied Catalysis A: General* **2016**, *515*, 51–59.

[18] M. Alvear, M. E. Fortunato, V. Russo, K. Eränen, M. Di Serio, J. Lehtonen, S. Rautiainen, D. Murzin, T. Salmi, *Ind. Eng. Chem. Res.* **2021**, *60*, 9429–9436.

[19] J. Lu, X. Zhang, J. J. Bravo-Suárez, T. Fujitani, S. T. Oyama, *Catalysis Today* **2009**, *147*, 186–195.

[20] V. Russo, R. Tesser, E. Santacesaria, M. Di Serio, *Ind. Eng. Chem. Res.* **2013**, *52*, 1168–1178.

[21] M. Alvear, K. Eränen, D. Yu. Murzin, T. Salmi, *Ind. Eng. Chem. Res.* **2021**, *60*, 2430–2438.

[22] M. Ghanta, D. R. Fahey, D. H. Busch, B. Subramaniam, *ACS Sustainable Chem. Eng.* **2013**, *1*, 268–277.

[23] K. Sato, *Science* **1998**, *281*, 1646–1647.

[24] P. Roffia, M. Padovan, E. Moretti, G. D. Alberti, *Catalytic Process for Preparing Cyclohexanone-Oxime*, **1988**, US4745221A.

[25] L. Xu, J. Ding, Y. Yang, P. Wu, *Journal of Catalysis* **2014**, *309*, 1–10.

[26] L. Balducci, D. Bianchi, R. Bortolo, R. D'Aloisio, M. Ricci, R. Tassinari, R. Ungarelli, *Angew. Chem.* **2003**, *115*, 5087–5090.

[27] Y. Luo, J. Xiong, C. Pang, G. Li, C. Hu, *Catalysts* **2018**, *8*, 49.
[28] D. R. C. Huybrechts, L. D. Bruycker, P. A. Jacobs, *Nature* **1990**, *345*, 240–242.
[29] G. B. Shul'pin, T. Sooknoi, V. B. Romakh, G. Süss-Fink, L. S. Shul'pina, *Tetrahedron Letters* **2006**, *47*, 3071–3075.
[30] P. N. Patil, P. R. Gogate, *Separation and Purification Technology* **2012**, *95*, 172–179.
[31] P. Sun, C. Tyree, C.-H. Huang, *Environ. Sci. Technol.* **2016**, *50*, 4448–4458.
[32] Y. Zhang, Y. Zhuang, J. Geng, H. Ren, K. Xu, L. Ding, *Science of The Total Environment* **2016**, *550*, 184–191.
[33] H. Li, B. Zheng, Z. Pan, B. Zong, M. Qiao, *Front. Chem. Sci. Eng.* **2018**, *12*, 124–131.
[34] Y. Hou, Y. Wang, F. He, S. Han, Z. Mi, W. Wu, E. Min, *Materials Letters* **2004**, *58*, 1267–1271.
[35] D. Vandenberg, J.-P. Ganhy, N. VANLAUTEM, *Process for the Manufacture of Hydrogen Peroxide*, **1999**, WO1999040024A1.
[36] S. Fukuzumi, Y. Yamada, K. D. Karlin, *Electrochimica Acta* **2012**, *82*, 493–511.
[37] M. Mazzucato, G. Daniel, A. Mehmood, T. Kosmala, G. Granozzi, A. Kucernak, C. Durante, *Applied Catalysis B: Environmental* **2021**, *291*, 120068.
[38] M. Mazzucato, C. Durante, *Current Opinion in Electrochemistry* **2022**, *35*, 101051.
[39] H. Henkel, W. Weber, S. O. Henkel, **1914**, US1138520A.
[40] J. S. Campbell, *Process for Producing Hydrogen Peroxide and an Alkali Metal Perborate*, **1969**, US3433582A.
[41] H. G. Wallace, *Catalytic Production of Hydrogen Peroxide from Its Elements*, **1967**, US3336112A.
[42] L. W. Gosser, J.-A. T. Schwartz, *Catalytic Process for Making Hydrogen Peroxide from Hydrogen and Oxygen Employing a Bromide Promoter*, **1988**, US4772458A.
[43] K. T. Chuang, B. Zhou, *Production of Hydrogen Peroxide*, **1994**, US5338531A.
[44] L. W. Gosser, J.-A. T. Schwartz, *Hydrogen Peroxide Production Method Using Platinum/Palladium Catalysts*, **1989**, US4832938A.
[45] L. Kim, G. W. Schoenthal, *Catalytic Production of Hydrogen Peroxide from Its Elements*, **1977**, US4007256A.
[46] R. Meiers, U. Dingerdissen, W. F. Hölderich, *Journal of Catalysis* **1998**, *176*, 376–386.
[47] R. Meiers, W. F. Hölderich, *Catalysis Letters* **1999**, *59*, 161–163.
[48] Sato A., Miyake T., *Production of propylene oxide*, **1992**, JPH04352771A.
[49] G. Li, J. Edwards, A. F. Carley, G. J. Hutchings, *Catalysis Communications* **2007**, *8*, 247–250.
[50] D. Dissanayake, *Journal of Catalysis* **2003**, *214*, 113–120.
[51] D. W. Flaherty, *ACS Catal.* **2018**, *8*, 1520–1527.
[52] J. H. Lunsford, *Journal of Catalysis* **2003**, *216*, 455–460.
[53] R. Todorovic, R. J. Meyer, *Catalysis Today* **2011**, *160*, 242–248.

[54] J. A. Keith, T. Jacob, *Angewandte Chemie International Edition* **2010**, *49*, 9521–9525.
[55] N. M. Wilson, D. W. Flaherty, *J. Am. Chem. Soc.* **2016**, *138*, 574–586.
[56] M. Selinsek, B. J. Deschner, D. E. Doronkin, T. L. Sheppard, J.-D. Grunwaldt, R. Dittmeyer, *ACS Catal.* **2018**, *8*, 2546–2557.
[57] B. J. Deschner, D. E. Doronkin, T. L. Sheppard, A. Zimina, J.-D. Grunwaldt, R. Dittmeyer, *J. Phys. Chem. C* **2021**, *125*, 3451–3462.
[58] L. Chen, J. W. Medlin, H. Grönbeck, *ACS Catal.* **2021**, *11*, 2735–2745.
[59] N. M. Wilson, J. Schröder, P. Priyadarshini, D. T. Bregante, S. Kunz, D. W. Flaherty, *Journal of Catalysis* **2018**, *368*, 261–274.
[60] V. V. Krishnan, A. G. Dokoutchaev, M. E. Thompson, *Journal of Catalysis* **2000**, *196*, 366–374.
[61] S. Chinta, *Journal of Catalysis* **2004**, *225*, 249–255.
[62] Y. Han, J. Lunsford, *Journal of Catalysis* **2005**, *230*, 313–316.
[63] V. Paunovic, V. Ordomsky, M. Fernanda Neira D'Angelo, J. C. Schouten, T. A. Nijhuis, *Journal of Catalysis* **2014**, *309*, 325–332.
[64] P. G. T. Foss, W. gerrard, *Solubililty of Gases in Liquids*, John Wiley, **1990**.
[65] J. S. Adams, A. Chemburkar, P. Priyadarshini, T. Ricciardulli, Y. Lu, V. Maliekkal, A. Sampath, S. Winikoff, A. M. Karim, M. Neurock, D. W. Flaherty, *Science* **2021**, *371*, 626–632.
[66] D. P. Dissanayake, J. H. Lunsford, *Journal of Catalysis* **2002**, *206*, 173–176.
[67] Q. Liu, J. Lunsford, *Journal of Catalysis* **2006**, *239*, 237–243.
[68] A. Biffis, M. Zecca, M. Basato, *Eur. J. Inorg. Chem.* **2001**, *2001*, 1131–1133.
[69] A. Biffis, P. Centomo, A. Del Zotto, M. Zecca, *Chem. Rev.* **2018**, *118*, 2249–2295.
[70] Q. Liu, J. C. Bauer, R. E. Schaak, J. H. Lunsford, *Applied Catalysis A: General* **2008**, *339*, 130–136.
[71] G. Bernardotto, F. Menegazzo, F. Pinna, M. Signoretto, G. Cruciani, G. Strukul, *Applied Catalysis A: General* **2009**, *358*, 129–135.
[72] J. Xu, L. Ouyang, G.-J. Da, Q.-Q. Song, X.-J. Yang, Y.-F. Han, *Journal of Catalysis* **2012**, *285*, 74–82.
[73] J. K. Edwards, G. J. Hutchings, *Angewandte Chemie International Edition* **2008**, *47*, 9192–9198.
[74] P. Landon, P. J. Collier, A. F. Carley, D. Chadwick, A. J. Papworth, A. Burrows, C. J. Kiely, G. J. Hutchings, *Phys. Chem. Chem. Phys.* **2003**, *5*, 1917–1923.
[75] E. Ntainjua N., J. K. Edwards, A. F. Carley, J. A. Lopez-Sanchez, J. A. Moulijn, A. A. Herzing, C. J. Kiely, G. J. Hutchings, *Green Chem.* **2008**, *10*, 1162.
[76] J. K. Edwards, A. Thomas, B. E. Solsona, P. Landon, A. F. Carley, G. J. Hutchings, *Catalysis Today* **2007**, *122*, 397–402.
[77] E. Ntainjua N., M. Piccinini, J. C. Pritchard, J. K. Edwards, A. F. Carley, J. A. Moulijn, G. J. Hutchings, *ChemSusChem* **2009**, *2*, 575–580.
[78] T. Richards, R. J. Lewis, D. J. Morgan, G. J. Hutchings, *Catal Lett* **2022**, DOI 10.1007/s10562-022-03967-8.

[79] J. K. Edwards, J. Pritchard, P. J. Miedziak, M. Piccinini, A. F. Carley, Q. He, C. J. Kiely, G. J. Hutchings, *Catal. Sci. Technol.* **2014**, *4*, 3244–3250.

[80] S. Sterchele, P. Biasi, P. Centomo, P. Canton, S. Campestrini, T. Salmi, M. Zecca, *Applied Catalysis A: General* **2013**, *468*, 160–174.

[81] Y.-F. Han, Z. Zhong, K. Ramesh, F. Chen, L. Chen, T. White, Q. Tay, S. N. Yaakub, Z. Wang, *J. Phys. Chem. C* **2007**, *111*, 8410–8413.

[82] D. Gudarzi, W. Ratchananusorn, I. Turunen, M. Heinonen, T. Salmi, *Catalysis Today* **2015**, *248*, 58–68.

[83] S. Wang, D. E. Doronkin, M. Hähsler, X. Huang, D. Wang, J. Grunwaldt, S. Behrens, *ChemSusChem* **2020**, *13*, 3243–3251.

[84] S. Wang, R. Lewis, D. E. Doronkin, D. Morgan, J.-D. Grunwaldt, G. Hutchings, S. Behrens, *Catal. Sci. Technol.* **2020**, 10.1039.C9CY02210D.

[85] D. E. Doronkin, S. Wang, D. I. Sharapa, B. J. Deschner, T. L. Sheppard, A. Zimina, F. Studt, R. Dittmeyer, S. Behrens, J.-D. Grunwaldt, *Catal. Sci. Technol.* **2020**, *10*, 4726–4742.

[86] S. Wang, K. Gao, W. Li, J. Zhang, *Applied Catalysis A: General* **2017**, *531*, 89–95.

[87] S. J. Freakley, Q. He, J. H. Harrhy, L. Lu, D. A. Crole, D. J. Morgan, E. N. Ntainjua, J. K. Edwards, A. F. Carley, A. Y. Borisevich, C. J. Kiely, G. J. Hutchings, *Science* **2016**, *351*, 965–968.

[88] H. Li, Q. Wan, C. Du, J. Zhao, F. Li, Y. Zhang, Y. Zheng, M. Chen, K. H. L. Zhang, J. Huang, G. Fu, S. Lin, X. Huang, H. Xiong, *Nat Commun* **2022**, *13*, 6072.

[89] P. Tian, F. Xuan, D. Ding, Y. Sun, X. Xu, W. Li, R. Si, J. Xu, Y.-F. Han, *Journal of Catalysis* **2020**, *385*, 21–29.

[90] V. R. Choudhary, C. Samanta, T. V. Choudhary, *Applied Catalysis A: General* **2006**, *308*, 128–133.

[91] F. Menegazzo, M. Signoretto, E. Ghedini, G. Strukul, *Catalysts* **2019**, *9*, 251.

[92] T. Ricciardulli, S. Gorthy, J. S. Adams, C. Thompson, A. M. Karim, M. Neurock, D. W. Flaherty, *J. Am. Chem. Soc.* **2021**, *143*, 5445–5464.

[93] Hydrogenation and Dehydrogenation; P. N. Rylander, in *Ullmann's Encyclopedia of Industrial Chemistry*, Wiley-VCH, **2007**.

[94] G. Gallina, J. García-Serna, T. O. Salmi, P. Canu, P. Biasi, *Ind. Eng. Chem. Res.* **2017**, *56*, 13367–13378.

[95] T. Deguchi, M. Iwamoto, *J. Phys. Chem. C* **2013**, *117*, 18540–18548.

[96] V. Choudhary, C. Samanta, *Journal of Catalysis* **2006**, *238*, 28–38.

[97] I. Huerta, P. Biasi, J. García-Serna, M. J. Cocero, J.-P. Mikkola, T. Salmi, *Green Processing and Synthesis* **2016**, *5*, DOI 10.1515/gps-2016-0001.

[98] S. T. Marshall, J. W. Medlin, *Surface Science Reports* **2011**, *66*, 173–184.

[99] P. Centomo, C. Meneghini, S. Sterchele, A. Trapananti, G. Aquilanti, M. Zecca, *Catalysis Today* **2015**, *248*, 138–141.

[100] P. Centomo, C. Meneghini, S. Sterchele, A. Trapananti, G. Aquilanti, M. Zecca, *ChemCatChem* **2015**, *7*, 3712–3718.

[101] G. Blanco-Brieva, E. Cano-Serrano, J. M. Campos-Martin, J. L. G. Fierro, *Chem. Commun.* **2004**, 1184.

[102] C. Burato, P. Centomo, M. Rizzoli, A. Biffis, S. Campestrini, B. Corain, *Adv. Synth. Catal.* **2006**, *348*, 255–259.

[103] Q. Liu, K. K. Gath, J. C. Bauer, R. E. Schaak, J. H. Lunsford, *Catal Lett* **2009**, *132*, 342–348.

[104] P. Biasi, J.-P. Mikkola, S. Sterchele, T. Salmi, N. Gemo, A. Shchukarev, P. Centomo, M. Zecca, P. Canu, A.-R. Rautio, K. Kordàs, *AIChE J.* **2017**, *63*, 32–42.

[105] V. R. Choudhary, A. G. Gaikwad, S. D. Sansare, *Catalysis Letters* **2002**, *83*, 235–239.

[106] A. G. Gaikwad, S. D. Sansare, V. R. Choudhary, *Journal of Molecular Catalysis A: Chemical* **2002**, *181*, 143–149.

[107] F. Wang, C. Xia, S. P. de Visser, Y. Wang, *J. Am. Chem. Soc.* **2019**, *141*, 901–910.

[108] A. Barnes, R. J. Lewis, D. J. Morgan, T. E. Davies, G. J. Hutchings, *Catal. Sci. Technol.* **2022**, 10.1039.D1CY01962G.

[109] L. Ouyang, P. Tian, G. Da, X.-C. Xu, C. Ao, T. Chen, R. Si, J. Xu, Y.-F. Han, *Journal of Catalysis* **2015**, *321*, 70–80.

[110] C. Ao, P. Tian, L. Ouyang, G. Da, X. Xu, J. Xu, Y.-F. Han, *Catal. Sci. Technol.* **2016**, *6*, 5060–5068.

[111]T. Ishihara, Y. Hata, Y. Nomura, K. Kaneko, H. Matsumoto, *Chem. Lett.* **2007**, *36*, 878–879.

[112] L. Fu, K. T. Chuang, R. Fiedorow, in *Studies in Surface Science and Catalysis*, Elsevier, **1992**, pp. 33–41.

[113] A. Y. Stakheev, L. M. Kustov, *Applied Catalysis A: General* **1999**, *188*, 3–35.

[114] G. Blanco-Brieva, M. P. de Frutos Escrig, J. M. Campos-Martin, J. L. G. Fierro, *Green Chem.* **2010**, *12*, 1163.

[115] A. Rodríguez-Gómez, *Molecular Catalysis* **2018**, 10.

[116] S. Melada, R. Rioda, F. Menegazzo, F. Pinna, G. Strukul, *Journal of Catalysis* **2006**, *239*, 422–430.

[117] J. K. Edwards, B. Solsona, E. N. N, A. F. Carley, A. A. Herzing, C. J. Kiely, G. J. Hutchings, *Science* **2009**, *323*, 1037–1041.

[118] Z. Zhang, T. T. Wong, W. M. H. Sachtler, *Journal of Catalysis* **1991**, *128*, 13–22.

[119] G. Blanco-Brieva, M. Montiel-Argaiz, F. Desmedt, P. Miquel, J. M. Campos-Martin, J. L. G. Fierro, *Top Catal* **2017**, *60*, 1151–1155.

[120] A. Barnes, R. J. Lewis, D. J. Morgan, T. E. Davies, G. J. Hutchings, *Catalysts* **2022**, *12*, 1396.

[121] Z. Jin, Y. Liu, L. Wang, C. Wang, Z. Wu, Q. Zhu, L. Wang, F.-S. Xiao, *ACS Catal.* **2021**, *11*, 1946–1951.

[122] T. Mastren, B. W. Stein, T. G. Parker, V. Radchenko, R. Copping, A. Owens, L. E. Wyant, M. Brugh, S. A. Kozimor, F. M. Nortier, E. R. Birnbaum, K. D. John, M. E. Fassbender, *Anal. Chem.* **2018**, *90*, 7012–7017.

[123] P. Centomo, I. Bonato, L. Hanková, L. Holub, K. Jeřábek, M. Zecca, *Top Catal* **2013**, *56*, 611–617.

[124] P. Biasi, F. Menegazzo, P. Canu, F. Pinna, T. O. Salmi, *Ind. Eng. Chem. Res.* **2013**, *52*, 15472–15480.

[125] J. Kim, Y.-M. Chung, S.-M. Kang, C.-H. Choi, B.-Y. Kim, Y.-T. Kwon, T. J. Kim, S.-H. Oh, C.-S. Lee, *ACS Catal.* **2012**, *2*, 1042–1048.
[126] D. C. Sherrington, *Chem. Commun.* **1998**, 2275–2286.
[127] Ion Exchangers; F. De Darel, T. V. Arden, in *Ullmann's Encyclopedia of Industrial Chemistry*, Wiley-VCH, **2007**.
[128] O. Okay, *Progress in Polymer Science* **2000**, *25*, 711–779.
[129] Heterogeneous Catalysis and Solid Catalysts; H. Knözinger, K. Kochloefl, in *Ullmann's Encyclopedia of Industrial Chemistry*, Wiley-VCH, **2007**.
[130] A. Chakrabarti, M. M. Sharma, *Reactive Polymers* **1993**, *20*, 1–45.
[131] E. Lotero, Y. Liu, D. E. Lopez, K. Suwannakarn, D. A. Bruce, J. G. Goodwin, *Ind. Eng. Chem. Res.* **2005**, *44*, 5353–5363.
[132] N. Özbay, N. Oktar, N. A. Tapan, *Fuel* **2008**, *87*, 1789–1798.
[133] J.-Y. Park, D.-K. Kim, J.-S. Lee, *Bioresource Technology* **2010**, *101*, S62–S65.
[134] P. Centomo, M. Zecca, A. Biffis, *Chemistry – A European Journal* **2020**, *26*, 9243–9260.
[135] B. Corain, K. Jerabek, P. Centomo, P. Canton, *Angew. Chem. Int. Ed.* **2004**, *43*, 959–962.
[136] P. Centomo, M. Zecca, B. Corain, *J Clust Sci* **2007**, *18*, 947–962.
[137] A. Biffis, H. Landes, K. Jeřábek, B. Corain, *Journal of Molecular Catalysis A: Chemical* **2000**, *151*, 283–288.
[138] M. Králik, B. Corain, M. Zecca, **2000**, 11.
[139] H. Miyamura, R. Matsubara, Y. Miyazaki, S. Kobayashi, *Angewandte Chemie International Edition* **2007**, *46*, 4151–4154.
[140] W. Laufer, W. F. Hoelderich, *Chem. Commun.* **2002**, 1684–1685.
[141] F. Frison, C. Dalla Valle, C. Evangelisti, P. Centomo, M. Zecca, *Catalysts* **2019**, *9*, 124.
[142] Y. Zhang, S. Wei, F. Liu, Y. Du, S. Liu, Y. Ji, T. Yokoi, T. Tatsumi, F.-S. Xiao, *Nano Today* **2009**, *4*, 135–142.
[143] S. Wei, D.-X. Lu, J. Sun, Y. He, L. Zhu, Y.-L. Zhang, F.-S. Xiao, *Colloids and Surfaces A: Physicochemical and Engineering Aspects* **2012**, *414*, 327–332.
[144] Karel. Jerabek, *Anal. Chem.* **1985**, *57*, 1598–1602.
[145] S. Sterchele, P. Centomo, M. Zecca, L. Hanková, K. Jeřábek, *Microporous and Mesoporous Materials* **2014**, *185*, 26–29.
[146] L. Hanková, L. Holub, K. Jeřábek, *J. Polym. Sci. Part B: Polym. Phys.* **2015**, *53*, 774–781.
[147] Y.-L. Zhang, J.-N. Wang, Y. He, Y. He, B.-B. Xu, S. Wei, F.-S. Xiao, *Langmuir* **2011**, *27*, 12585–12590.
[148] F. Liu, L. Wang, Q. Sun, L. Zhu, X. Meng, F.-S. Xiao, *J. Am. Chem. Soc.* **2012**, *134*, 16948–16950.
[149] F. Liu, W. Li, Q. Sun, L. Zhu, X. Meng, Y.-H. Guo, F.-S. Xiao, *ChemSusChem* **2011**, *4*, 1059–1062.
[150] F. Liu, W. Kong, C. Qi, L. Zhu, F.-S. Xiao, *ACS Catal.* **2012**, *2*, 565–572.
[151] F. Liu, X. Meng, Y. Zhang, L. Ren, F. Nawaz, F.-S. Xiao, *Journal of Catalysis* **2010**, *271*, 52–58.

[152] J. García-Serna, T. Moreno, P. Biasi, M. J. Cocero, J.-P. Mikkola, T. O. Salmi, *Green Chem.* **2014**, *16*, 2320.

[153] R. Dittmeyer, J.-D. Grunwaldt, A. Pashkova, *Catalysis Today* **2015**, *248*, 149–159.

[154] G. Blanco-Brieva, M. Montiel-Argaiz, F. Desmedt, P. Miquel, J. M. Campos-Martin, J. L. G. Fierro, *RSC Adv.* **2016**, *6*, 99291–99296.

[155] F. A. Cotton, G. Wilkinson, *Advanced Inorganic Chemistry*, Wiley, New York, **1988**.

[156] S. Abate, M. Freni, R. Arrigo, M. E. Schuster, S. Perathoner, G. Centi, *ChemCatChem* **2013**, *5*, 1899–1905.

[157] G. M. Lari, B. Puértolas, M. Shahrokhi, N. López, Javier Pérez-Ramírez, *Angew. Chem.* **2017**, *129*, 1801–1805.

[158] L. F. de L. e Freitas, B. Puértolas, J. Zhang, B. Wang, A. S. Hoffman, S. R. Bare, J. Pérez-Ramírez, J. W. Medlin, E. Nikolla, *ACS Catal.* **2020**, *10*, 5202–5207.

[159] R. J. Lewis, M. Koy, M. Macino, M. Das, J. H. Carter, D. J. Morgan, T. E. Davies, J. B. Ernst, S. J. Freakley, F. Glorius, G. J. Hutchings, *J. Am. Chem. Soc.* **2022**, jacs.2c04828.

[160] R. Burch, P. R. Ellis, *Applied Catalysis B: Environmental* **2003**, *42*, 203–211.

[161] V. Paunovic, V. V. Ordomsky, V. L. Sushkevich, J. C. Schouten, T. A. Nijhuis, *ChemCatChem* **2015**, *7*, 1161–1176.

[162] W. C. Bray, H. A. Liebhafsky, *J. Am. Chem. Soc.* **1931**, *53*, 38–44.

[163] H. A. Liebhafsky, *J. Am. Chem. Soc.* **1932**, *54*, 1792–1806.

[164] H. A. Liebhafsky, *J. Am. Chem. Soc.* **1932**, *54*, 3499–3508.

[165] H. A. Liebhafsky, *J. Am. Chem. Soc.* **1934**, *56*, 2369–2372.

[166] G. H. Jeffery, J. Bassett, J. Mendham, R. C. Denney, *Vogel's Textbook of Quantitative Chemical Analysis*, John Wiley & Sons Inc, Harlow, **1989**.

[167] C. E. Huckaba, F. G. Keyes, *J. Am. Chem. Soc.* **1948**, *70*, 1640–1644.

[168] E. C. Hurdis, Hendrik. Romeyn, *Anal. Chem.* **1954**, *26*, 320–325.

[169] A. Pashkova, K. Svajda, G. Black, R. Dittmeyer, *Review of Scientific Instruments* **2009**, *80*, 055104.

[170] A. Pashkova, K. Svajda, R. Dittmeyer, *Chemical Engineering Journal* **2008**, *139*, 165–171.

[171] G. Eisenberg, *Ind. Eng. Chem.* **1943**, *15*, 327.

[172] W. C. Wolfe, *Anal. Chem.* **1962**, *34*, 1328–1330.

[173] K. P. Reis, V. K. Joshi, M. E. Thompson, *Journal of Catalysis* **1996**, *161*, 62–67.

[174] C. Dalla Valle, M. Zecca, F. Rastrelli, C. Tubaro, P. Centomo, *Polymers* **2020**, *12*, 600.

[175] I. M. Abrams, *Ind. Eng. Chem.* **1956**, *48*, 1469–1472.

[176] W. T. Tysoe, R. M. Ormerod, R. M. Lambert, G. Zgrablich, A. Ramirez-Cuesta, *J. Phys. Chem.* **1993**, *97*, 3365–3370.

[177] A. L. Bugaev, A. A. Guda, A. Lazzarini, K. A. Lomachenko, E. Groppo, R. Pellegrini, A. Piovano, H. Emerich, A. V. Soldatov, L. A. Bugaev, V. P. Dmitriev, J. A. van Bokhoven, C. Lamberti, *Catalysis Today* **2017**, *283*, 119–126.

[178] Z. Zhao, X. Huang, M. Li, G. Wang, C. Lee, E. Zhu, X. Duan, Y. Huang, *J. Am. Chem. Soc.* **2015**, *137*, 15672–15675.

[179] A. L. Bugaev, A. A. Guda, K. A. Lomachenko, V. V. Srabionyan, L. A. Bugaev, A. V. Soldatov, C. Lamberti, V. P. Dmitriev, J. A. van Bokhoven, *J. Phys. Chem. C* **2014**, *118*, 10416–10423.

[180] B. G. Achhammer; M. J. Reiney; F. W Reinhart, *J. Res. Natl. Bur.* **1951**, *47*, 116.

[181] Phenol; M. Weber, M. Weber, M. Kleine-Boymann, in *Ullmann's Encyclopedia of Industrial Chemistry*, Wiley-VCH, **2007**.

[182] L. Gubler, S. M. Dockheer, W. H. Koppenol, *J. Electrochem. Soc.* **2011**, *158*, B755–B769.

[183] G. Scott, *Polymer Degradation and Stability* **1995**, *48*, 315–324.

[184] T. Deguchi, M. Iwamoto, *Journal of Catalysis* **2011**, *280*, 239–246.

[185] J. Brehm, R. J. Lewis, D. J. Morgan, T. E. Davies, G. J. Hutchings, *Catal Lett* **2022**, *152*, 254–262.

[186] X. Ji, D. Chen, L. Peng, F. Frison, C. D. Valle, C. Tubaro, M. Zecca, P. Centomo, D. Ye, P. Chen, *Catalysis Today* **2021**, *376*, 1–8.

[187] R. A. Sheldon, M. Wallau, I. W. C. E. Arends, U. Schuchardt, *Acc. Chem. Res.* **1998**, *31*, 485–493.

[188] N. Gemo, S. Sterchele, P. Biasi, P. Centomo, P. Canu, M. Zecca, A. Shchukarev, K. Kordás, T. O. Salmi, J.-P. Mikkola, *Catal. Sci. Technol.* **2015**, *5*, 3545–3555.

[189] F. Zhao, K. Murakami, M. Shirai, M. Arai, *Journal of Catalysis* **2000**, *194*, 479–483.

[190] J. R. Stahlbush, R. M. Strom, *Reactive Polymers* **1990**, *13*, 233–240.

[191] P. Tian, L. Ouyang, X. Xu, C. Ao, X. Xu, R. Si, X. Shen, M. Lin, J. Xu, Y.-F. Han, *Journal of Catalysis* **2017**, *349*, 30–40.

[192] S. Sterchele, P. Biasi, P. Centomo, A. Shchukarev, K. Kordás, A.-R. Rautio, J.-P. Mikkola, T. Salmi, P. Canton, M. Zecca, *ChemCatChem* **2016**, *8*, 1564–1574.

[193] K. Dorfner, *Ion Exchangers*, De Gruyter, Boston, MA, USA, **2011**.

[194] C. Burato, S. Campestrini, Y.-F. Han, P. Canton, P. Centomo, P. Canu, B. Corain, *Applied Catalysis A: General* **2009**, *358*, 224–231.

[195] S. Sterchele, P. Biasi, P. Centomo, S. Campestrini, A. Shchukarev, A.-R. Rautio, J.-P. Mikkola, T. Salmi, M. Zecca, *Catalysis Today* **2015**, *248*, 40–47.

[196] P. Centomo, K. Jeřábek, D. Canova, A. Zoleo, A. L. Maniero, A. Sassi, P. Canton, B. Corain, M. Zecca, *Chemistry – A European Journal* **2012**, *18*, 6632–6643.

[197] X. Yin, G. S. Zhu, W. Yang, Y. Li, G. Q. Zhu, R. Xu, J. Sun, S. Qiu, R. R. Xu, *Advanced Materials* **2005**, *17*, 2006–2010.

[198] Zeolites; E. Roland, P. Kleinschmit, in *Ullmann's Encyclopedia of Industrial Chemistry*, Wiley-VCH, **2007**.

[199] F. Göltl, R. E. Bulo, J. Hafner, P. Sautet, *J. Phys. Chem. Lett.* **2013**, *4*, 2244–2249.

[200] M. R. Hudson, W. L. Queen, J. A. Mason, D. W. Fickel, R. F. Lobo, C. M. Brown, *J. Am. Chem. Soc.* **2012**, *134*, 1970–1973.

[201] http://www.iza-structure.org/databases/, accessed on 09/01/2023.

[202] A. Wang, K. Lindgren, M. Di, D. Bernin, P.-A. Carlsson, M. Thuvander, L. Olsson, *Applied Catalysis B: Environmental* **2020**, *278*, 119315.

[203] https://www.acsmaterial.com/blog-detail/ssz-13-zeolite.html, accessed on 01/08/2023.

[204] J. Liu, N. Ruffini, P. Pollet, V. Llopis-Mestre, C. Dilek, C. A. Eckert, C. L. Liotta, C. B. Roberts, *Ind. Eng. Chem. Res.* **2010**, *49*, 8174–8179.

[205] J. Ishida, M. Nakatsuji, T. Nagata, H. Kawasaki, T. Suzuki, Y. Obora, *ACS Omega* **2020**, *5*, 9598–9604.

[206] T. Nagata, Y. Obora, *ACS Omega* **2020**, *5*, 98–103.

[207] T. Diao, P. White, I. Guzei, S. S. Stahl, *Inorg. Chem.* **2012**, *51*, 11898–11909.

[208] P. Priyadarshini, D. W. Flaherty, *AIChE J.* **2019**, *65*, e16829.

[209] P. Biasi, F. Menegazzo, F. Pinna, K. Eränen, T. O. Salmi, P. Canu, *Chemical Engineering Journal* **2011**, *176–177*, 172–177.

[210] P. Biasi, P. Canu, F. Menegazzo, F. Pinna, T. O. Salmi, *Ind. Eng. Chem. Res.* **2012**, *51*, 8883–8890.

[211] A. V. Tokarev, E. V. Murzina, P. K. Seelam, N. Kumar, D. Yu. Murzin, *Microporous and Mesoporous Materials* **2008**, *113*, 122–131.

[212] E. Bottari, M. R. Festa, *Laboratorio di Chimica Analitica Quantitativa*, Università “La Sapienza” Roma, Roma, **1993**.

[213] XPSPeak 4.1, https://xpspeak.software.informer.com/4.1/, accessed on 20/05/2021.

[214] E. J. Baerends, D. E. Ellis, P. Ros, *Chemical Physics* **1973**, *2*, 41–51.

[215] G. te Velde, F. M. Bickelhaupt, E. J. Baerends, C. Fonseca Guerra, S. J. A. van Gisbergen, J. G. Snijders, T. Ziegler, *J. Comput. Chem.* **2001**, *22*, 931–967.

[216] A. D. Becke, *Phys. Rev. A* **1988**, *38*, 3098–3100.

[217] E. van Lenthe, E. J. Baerends, J. G. Snijders, *The Journal of Chemical Physics* **1994**, *101*, 9783–9792.

[218] F. Zaccaria, L. P. Wolters, C. Fonseca Guerra, L. Orian, *J. Comput. Chem.* **2016**, *37*, 1672–1680.

[219] M. Dalla Tiezza, F. M. Bickelhaupt, L. Orian, *ChemistryOpen* **2019**, *8*, 143–154.

[220] Ahmad, Dalla Tiezza, Orian, *Catalysts* **2019**, *9*, 679.

[221] L. Orian, F. M. Bickelhaupt, *Synlett* **2021**, *32*, 561–572.

[222] A. D. Becke, *The Journal of Chemical Physics* **1988**, *88*, 2547–2553.

[223] M. Franchini, P. H. T. Philipsen, L. Visscher, *J. Comput. Chem.* **2013**, *34*, 1819–1827.

[224] A. Klamt, *J. Phys. Chem.* **1995**, *99*, 2224–2235.

[225] A. Klamt, G. Schüürmann, *J. Chem. Soc., Perkin Trans. 2* **1993**, 799–805.

[226] C. C. Pye, T. Ziegler, *Theoretical Chemistry Accounts: Theory, Computation, and Modeling (Theoretica Chimica Acta)* **1999**, *101*, 396–408.

[227] N. L. Allinger, X. Zhou, J. Bergsma, *Journal of Molecular Structure: THEOCHEM* **1994**, *312*, 69–83.

[228] F. M. Bickelhaupt, E. J. Baerends, in *Reviews in Computational Chemistry*, John Wiley & Sons, Ltd, **2000**, pp. 1–86.

[229] F. M. Bickelhaupt, K. N. Houk, *Angewandte Chemie International Edition* **2017**, *56*, 10070–10086.